3-23-2021

Energy-Constrained Distinguishability Measures for Assessing Performance in Quantum Information Processing

Kunal Sharma
Louisiana State University at Baton Rouge

ENERGY-CONSTRAINED DISTINGUISHABILITY MEASURES FOR ASSESSING PERFORMANCE IN QUANTUM INFORMATION PROCESSING

A Dissertation

Submitted to the Graduate Faculty of the
Louisiana State University and
Agricultural and Mechanical College
in partial fulfillment of the
requirements for the degree of
Doctor of Philosophy

in

The Department of Physics and Astronomy

by
Kunal Sharma
BS-MS, Indian Institute of Science Education and Research Bhopal, 2016
May 2021

To my parents

Vishnu and Yogita Sharma

ACKNOWLEDGMENTS

The completion of this dissertation could not have been possible without the help and support of countless people.

First and foremost, I thank my Ph.D. supervisor Mark M. Wilde for his support, guidance, and friendship over the last five years. I am grateful to him for devoting many hours to discussions and explanations on several research topics. His broad expertise in quantum information science has immensely helped me learn various research topics during my Ph.D. His perseverance and passion for solving research problems have always inspired me and many others. I am thankful to him for regularly providing constructive feedback, which has helped me grow as a researcher. I will always be indebted to him for his constant support as an advisor and a friend and the opportunities he provided me in the past five years.

I am grateful to the late Jonathan P. Dowling for showing a lot of confidence in me. His ability to connect with students and motivate them irrespective of their background is something I would like to replicate in my life.

I had the privilege to work at the Los Alamos National Lab as a long-term graduate research assistant during my Ph.D. Many thanks to Patrick J. Coles for providing me with such an exciting opportunity and for his support and friendship. I am grateful to him for offering me to lead several research projects and for providing constant feedback. He has also taught me how to conduct research collaboratively by valuing my opinion in every research discussion. I am also thankful to Lukasz Cincio for his support and for teaching me how to be an efficient researcher. I have significantly benefited from his advice on many academic and non-academic challenges.

I am incredibly grateful to Marco Cerezo and Zoë Holmes for always being available whenever I needed them. Discussions on research and random topics with them have made the last two years of my Ph.D. a delightful experience. I could not have asked for better friends and colleagues. Along with them, many thanks to Piotr Czarnik, Gopikrishnan

Muraleedharan, and Burak Şahinoğlu for making my stay in Los Alamos exciting. Special thanks to Samson Wang for discussing science and philosophy from the UK.

I thank Barry C. Sanders for his help and for hosting me at the University of Calgary. Several research discussions with him have helped me develop research ideas and communicate them better. I also thank Kamil Bradler, Daiqin Su, Haoyu Qi, and Christian Weedbrook for their hospitality and many discussions at Xanadu.

I am thankful to several mentors for guiding me over many years. Many thanks to Pankaj Baluja, Lalit K. Banga, Aditi Sen De, Suvankar Dutta, Suresh Dwivedi, Vibhuti Dwivedi, Madhu Gupta, Ambar Jain, Ravi P. Rau, Jeyaraman Sankar, Ruchika Sankar, and Ujjwal Sen. I especially acknowledge Prasun Dutta for asking me fundamental physics questions a countless number of times and for teaching me the joy of living a simple life. A special thanks to Michael Nielsen for writing remarkable essays on "principles of effective research" and "six rules for rewriting," which have helped improve my scientific approach immensely over the past few years.

I thank Ivan Agullo, Li Chen, Ravi P. Rau, and Mark M. Wilde for taking out time to be on my Ph.D. committee and for providing feedback on my work. I am grateful to Mark M. Wilde for his valuable comments on this thesis. Many thanks to Claire R. Bullock, Carol Duran, Arnell Nelson, Paige Whittington, Yao Zeng, and other members of the Department of Physics and Astronomy at LSU for their help during my Ph.D.

I collaborated with many colleagues over the last five years. Many thanks to Sushovit Adhikari, Andrew Arrasmith, Kamil Bradler, Marco Cerezo, Lukasz Cincio, Patrick J. Coles, Ish Dhand, Enrico Fontana, Zoë Holmes, Robert Israel, Eneet Kaur, Sumeet Khatri, Meenu Kumari, Ludovico Lami, Felix Leditzky, Jarrod McClean, Kyungjoo Noh, Haoyu Qi, Barry C. Sanders, Akira Sone, Andrew Sornborger, Daiqin Su, Yuan Su, Masahiro Takeoka, Eyuri Wakakuwa, Samson Wang, Xin Wang, Mark M. Wilde, and Yadong Wu. It has been a pleasure to collaborate with these great researchers.

I have been fortunate to have wonderful friends all around the world. I thank Ja-

cob Beckey, Anthony Brady, Ritwika Chakraborty, Arghya Chattopadhyay, Anirban N. Chowdhury, Siddhartha Das, Sarah Davis, Arundhati Deshmukh, Himadri S. Dhar, Arpit Dua, Enrico Fontana, Isabella Goetting, Girraj Goyal, Pinky Goyal, Wendy K. Hahn, Stav Haldar, Yoshita Holamoge, Samreen Iram, Kevin V. Jacob, Namitha A. James, Geo Jose, Vishal Joshi, Salini Karuvade, Vishal Katariya, Eneet Kaur, Prateek Khandelwal, Sumeet Khatri, Meenu Kumari, Dan W. McCarn, Aby Philip, Prateek Raj, Sayonee Ray, Meghan Ryan, Vinay Sagar, Sahil Saini, Ruchika Shankar, Karunya Shirali, Aliza Siddiqui, Uttam Singh, Alejandra C. Spillari, Sudhanshu Srivastava, Simran Thapa, Justin Yirka, and Chenglong You. I am grateful to Noah Davis, Siddharth Soni, and Haoyu Qi for their great friendship and for supporting me throughout my Ph.D. Special thanks to Divya Rastogi Joshi for the care she put into making me feel at home during the past three years.

Finally, I would like to thank everyone in my family, especially my sister Kanika Sharma and my parents Vishnu P. Sharma and Yogita Sharma. I am indebted to them for everything they have done for me. I would have never completed this thesis without their love, care, and encouragement. I am grateful to them for continually supporting my studies and everything else I do in my life.

TABLE OF CONTENTS

ABSTRACT

The aim of this thesis is to develop a framework for assessing performance in quantum information processing with continuous variables. In particular, we focus on quantifying the fundamental limitations on communication and computation over bosonic Gaussian systems. Due to their infinite-dimensional structure, we make a realistic assumption of energy constraints on the input states of continuous-variable (CV) quantum operations. Our first contribution is to show that energy-constrained distinguishability measures can be used to establish tight upper bounds on the communication capacities of phase-insensitive, bosonic Gaussian channels – thermal, amplifier, and additive-noise channels. We then prove that an optimal Gaussian input state for the energy-constrained, generalized channel divergence of two particular Gaussian channels is the two-mode squeezed vacuum state that saturates the energy constraint. Next, we develop theoretical and numerical tools based on energy-constrained distinguishability measures to quantify the accuracy in implementing Gaussian unitary operations. Finally, we propose an optimal test for the performance of CV quantum teleportation in terms of the energy-constrained channel fidelity between ideal CV teleportation and its experimental implementation. Here we prove that the optimal state for testing CV teleportation is an entangled superposition of twin-Fock states. These results are relevant for experiments that make use of Gaussian unitaries and CV teleportation.

CHAPTER 1

INTRODUCTION

One of the major goals in quantum information science is determining whether quantum properties such as superposition of quantum states and entanglement can lead to some advantage over their classical counterparts in storing, communicating, and processing information. The most common notion of universal quantum computation consists of the manipulation of qubits encoded in discrete quantum systems and the application of a universal set of quantum operations on these qubits [1]. In principle, an ideal quantum computer can provide an exponential speedup for the abelian hidden subgroup problem [2, 3] and a quadratic speedup for search problems [4]. Moreover, quantum computers have the potential to simulate physical systems that are impossible to simulate efficiently classically, including fermionic lattice models [5], quantum chemistry [6], and field theories [7].

Quantum resources also open a window for many communication-based applications that were not possible before. A communication task involves encoding classical or quantum messages into a quantum state, which are then transmitted through a quantum channel. A quantum channel is a model for a communication link between two parties. The properties of a quantum channel and its coupling to an environment govern the evolution of a quantum state that is sent through the channel. Depending on the type of the message (classical or quantum) and the type of the quantum resource (states and channels), several communication tasks are possible, including classical communication, entanglement-assisted classical communication, quantum communication, and private communication [8]. Quantum resources also provide novel ways to generate secret keys. In a quantum key distribution (QKD) protocol, the security of a message is guaranteed due to quantum mechanical properties, which is different from the security due to the complexity-theoretic assumptions required classically [9, 10].

An interesting way to transfer a quantum state from one location to another is by

quantum teleportation – a fundamental protocol in quantum information theory with no classical analog [11]. It allows for the simulation of an ideal quantum channel by making use of entanglement and classical communication. In particular, a quantum state can be transmitted from one place to another if two parties share an entangled state and perform local operations and classical communication. One of the most important features of teleportation is that even a state that is completely *unknown* to the sender and the receiver can be transmitted faithfully. Since its inception, significant advances have been made in experimental implementations of teleportation protocols [12–22]. Moreover, beyond quantum communication, quantum teleportation and techniques inspired from it have found applications in measurement-based quantum computation, quantum error correction, quantum networks, QKD, etc.

The notion of quantum computation, communication, and teleportation can be extended in several ways. For example, discrete-variable (DV) quantum computation can be performed by encoding a finite amount of quantum information into a continuous-variable (CV) system [23–25]. This approach is appealing given that already existing advanced optical technologies can be used for state preparation, manipulation of states, and measurement for the required quantum computational and communication tasks [26]. The notion of quantum computation can be further extended to CV systems, such that the transformations involved are arbitrary polynomial functions of continuous variables [27].

One of the advantages of CV quantum computation could be in simulating bosonic systems, such as electromagnetic fields, trapped atoms, and Bose-Einstein condensates, etc. Moreover, a hybrid of DV and CV quantum computation could be efficient for distributed quantum computing and other related tasks [28–30]. Furthermore, CV resources could also lead to a more practical approach to quantum key distribution [31].

Similarly, quantum teleportation has also been generalized in many ways, such as teleportation of qudits [11], bidirectional teleportation [32–34], and port-based teleportation [35,36]. Other than teleportation of finite-dimensional states, quantum states of fields

(e.g., optical modes, the vibrational modes of trapped ions, etc.) can also be teleported using a protocol called continuous-variable quantum teleportation [37]. In CV teleportation, two distant parties, Alice and Bob, share a resource state – a two-mode squeezed vacuum (TMSV) state, which is a CV analog of a Bell state. After mixing her share of the TMSV state with an unknown state on a balanced beamsplitter, Alice performs homodyne detection of complementary quadratures. Alice then communicates the classical measurement outcomes to Bob, based on which Bob performs displacement operations on his share of the TMSV resource state [37].

The promises of quantum computing, communication, and teleportation, as described above, rely on the ability to control and manipulate quantum systems with ideal (unitary) transformations. In practice, quantum states are fragile and susceptible to noise, and quantum operations are not experimentally realized in their ideal form, which puts strong limitations on the computational and communication power of quantum devices. Thus the characterization of noise in quantum devices is a critical step toward making these systems more precise. The next step is to develop techniques to perform reliable computation and communication even in the presence of noise.

In this thesis, we study the following three problems related to CV quantum communication, computation, and teleportation:

1. What are the ultimate limits to quantum and private communication through phase-insensitive bosonic Gaussian channels?

2. How accurately can ideal Gaussian unitary transformations be simulated by their experimental implementations?

3. How accurately can ideal CV teleportation be simulated by its noisy experimental implementation?

Below we further motivate and describe challenges associated with these problems. We then argue that energy-constrained distinguishability measures serve as an important tool

in answering the aforementioned questions. We also point to corresponding chapters in this thesis while stating our results below.

Energy-constrained quantum and private capacities of phase-insensitive bosonic Gaussian channels. The quantum capacity $Q(\mathcal{N})$ of a quantum channel $\mathcal{N}$ is the maximum rate at which quantum information (qubits) can be reliably transmitted from a sender to a receiver by using the channel many times. The private capacity $P(\mathcal{N})$ of a quantum channel $\mathcal{N}$ is defined to be the maximum rate at which a sender can reliably communicate classical messages to a receiver by using the channel many times, such that the environment of the channel gets negligible information about the transmitted message. In general, the best-known characterization of the quantum or private capacity of a quantum channel is given by the optimization of regularized information quantities over an unbounded number of uses of the channel [38–41]. Since these information quantities are additive for a special class of channels called degradable channels [42, 43] (see Definition 24), the capacities of these channels can be calculated without any regularization. However, for the channels that are not degradable, these information quantities can be superadditive [44–48], and quantum capacities can be superactivated for some of these channels [49, 50]. Hence, it is difficult to determine the quantum or private capacity of channels that are not degradable, and the natural way to characterize such channels is to bound these capacities from above and below.

In this thesis, we focus on an important class of non-degradable channels called phase-insensitive bosonic Gaussian channels. In particular, we extensively study the communication capabilities of the following phase-insensitive Gaussian channels: thermal noise channels, amplifier channels, and additive-noise channels (see Chapter 2.3).

To motivate the thermal channel model, consider that almost all communication systems are affected by thermal noise [51]. Even though the pure-loss channel has relevance in free-space communication [52,53], it represents an ideal situation in which the environment of the channel is prepared in a vacuum state. Instead, consideration of a thermal state with

a fixed mean photon number as the state of the environment is more realistic, and such a channel is called a bosonic Gaussian thermal channel [53, 54]. Hence, quantum thermal channels model free-space communication with background thermal radiation affecting the input state, in addition to transmission loss. Additionally, the dark counts of photon detectors can also be modeled as arising from thermal photons in the environment [53,54]. In the context of private communication, a typical conservative model is to allow an eavesdropper access to the environment of a channel, and in particular, tampering by an eavesdropper can be modeled as the excess noise realized by a thermal channel [55, 56].

Interestingly, quantum amplifier channels model spontaneous parametric down-conversion in a nonlinear optical system [57], along with the dynamical Casimir effect in superconducting circuits [58], the Unruh effect [59], and Hawking radiation [60]. Moreover, an additive-noise channel is ubiquitous in quantum optics due to the fact that the aggregation of many independent random disturbances will typically have a Gaussian distribution [61].

Since, in practice, no communication scheme could ever use infinite energy to transmit information, we employ the notion of energy-constrained quantum and private communication over bosonic Gaussian channels [62]. Previously, formulas for the energy-constrained quantum and private capacities of the single-mode pure-loss channel were conjectured in [63] and proven in [62, 64]. Also, for a single-mode quantum-limited amplifier channel, the energy-constrained quantum and private capacities have been established in [62, 65]. However, unlike pure-loss and quantum-limited amplifier channels, other phase-insensitive Gaussian channels are not degradable, which makes it challenging to fully characterize their communication capacities. Therefore, we establish several bounds on the energy-constrained quantum and private capacities of all phase-insensitive Gaussian channels in Chapter 3.

We summarize our findings for the thermal noise channel and point readers to Chapter 3 for further details. We establish a first upper bound in Section 3.2.1 by using the theorem that any thermal channel can be decomposed as the concatenation of a pure-loss

channel followed by a quantum-limited amplifier channel. In order to establish two other upper bounds, we extend the notion of approximate degradability from [66] to infinite-dimensional quantum channels. In Section 3.1, we then establish general upper bounds on the energy-constrained quantum and private capacities of approximately degradable channels for infinite-dimensional systems. Finally, we apply these general bounds to thermal channels and establish two different upper bounds on its quantum capacity in Sections 3.2.2 and 3.2.3. While establishing these bounds, we solve an interesting optimization problem related to quantum channels, summarized in Remark 79. We establish a fourth upper bound in Section 3.2.4 by proving a theorem that any phase-insensitive single-mode bosonic Gaussian channel can be decomposed as a pure-amplifier channel followed by a pure-loss channel if the original channel is not entanglement breaking.

We then compare these different upper bounds on the energy-constrained quantum capacity of a thermal channel. For a detailed summary of our results, we point to Section 3.3. Interestingly, we find parameter (e.g., the mean-energy value of the channel inputs, thermal noise parameter, etc.) regimes for which the bound based on approximate degradability is closest to a known lower bound in comparison to all other upper bounds. Note that the bounds based on the notion of approximate degradability rely on the energy-constrained diamond distance (see Definition 54) between two quantum channels (see Definitions 61 and 62, and Remark 64). Therefore, tighter bounds on capacities of thermal channels can be established by finding better estimates of the energy-constrained diamond distance.

Similarly, we establish several bounds on energy-constrained capacities of a quantum amplifier channel and an additive-noise channel in Sections 3.6 and 3.7, respectively. Finally, we discuss the optimization of the Gaussian energy-constrained generalized channel divergence in Section 3.8.

Continuous-variable unitary operations. The required operations for universal CV quantum computation can be divided into two primary categories: Gaussian and non-Gaussian operations [27, 67]. Gaussian operations correspond to the evolution of the state

of light under a Hamiltonian that is an arbitrary second-order polynomial in the electromagnetic field operators. In particular, any second-order Hamiltonian can be decomposed as a sequence of phase-space displacements (elements of the Heisenberg–Weyl group) and symplectic transformations (see, e.g., [68] for a review). In general, along with Gaussian unitary operations, access to a Hamiltonian of at least the third power in the quadrature operators is sufficient to approximate any non-Gaussian Hamiltonian that is polynomial in the quadrature operators [27, 69].

These CV Gaussian quantum gates have been extensively investigated both theoretically and experimentally in the context of quantum optics and quantum information processing [70–73]. In general, these quantum gates are not experimentally realized in their ideal form. Rather, one approximates these operations using a sequence of other basic operations. For example, a displacement unitary (see Eq. 2.3.12) on an arbitrary input state is commonly approximated by sending it through a particular beamsplitter along with a highly excited coherent state [70]. Moreover, squeezing and SUM transformations (see Eqs. 2.3.56 and 2.3.58) are generally implemented using strongly pumped nonlinear processes, which are inherently noisy, and their high sensitivity to the coupling of optical fields in a nonlinear medium makes their implementation on an arbitrary quantum state challenging [71]. Rather, one can approximately realize these latter gates by using a sequence of passive transformations, homodyne measurements, and off-line squeezed vacuum states [71–73].

In this thesis, we devise methods for characterizing the performance of several experimental approximations to Gaussian unitaries. In particular, we focus on displacement operators, phase rotations, beamsplitters, single-mode squeezing operators, and the SUM operation, which are sufficient to generate any arbitrary Gaussian unitary operation acting on n modes of the electromagnetic field [74].

In discrete-variable quantum computing, one of the main theoretical tools used for assessing the performance of quantum gates is the diamond distance between the ideal

unitary and its noisy implementation. In the context of CV unitaries and channels, the diamond distance is not the correct metric to use as in the infinite-energy limit, a Gaussian unitary becomes perfectly distinguishable from its experimental implementation. In Sections 4.1–4.5, we explicitly prove this result for all Gaussian operations mentioned above. We then propose the energy-constrained diamond distance as a suitable metric for assessing the performance of continuous-variable quantum gates.

In general, it is computationally challenging to estimate the energy-constrained diamond distance. Therefore, we develop several analytical and numerical tools to bound it. In particular, for assessing the performance of a displacement unitary, we calculate the energy-constrained sine distance between an ideal displacement and its experimental approximation in Section 4.1.3. We then establish a lower bound on the energy-constrained diamond distance by defining a semidefinite (SDP) program on a truncated Hilbert space in Section 4.1.5. Furthermore, we analytically show that for a fixed value of the energy constraint and a sufficiently high value of the truncation parameter, the energy-constrained diamond distance between two quantum channels can be estimated with an arbitrarily high accuracy by using an SDP on a truncated Hilbert space.

Similarly, we quantify the accuracy in implementing a beamsplitter, a phase rotation, a measurement-induced single-mode squeezer, and a measurement-induced SUM gate in Sections 4.2–4.5. The main message of our findings is that simulation of these Gaussian unitaries is more accurate for low values of the energy constraint on input states.

Continuous-variable teleportation. We first note that ideal CV teleportation of an unknown state is only possible in the unrealistic limit of noiseless homodyne detection and infinite squeezing in the shared TMSV state. In such a theoretical setting, CV teleportation simulates an ideal quantum channel. A more practical strategy accounts for finite squeezing and unideal detection, which instead of an identity channel induces an additive-noise channel on input states [37].

Prior to our work, theoretical and experimental proposals assessed the performance of

CV teleportation by estimating the accuracy in teleporting particular quantum states, such as ensembles of coherent states, squeezed states, cat states, etc. [75–85]. Although these states are relevant for several quantum information processing applications, they do not represent the performance of CV teleportation when the goal is to teleport an arbitrary unknown state.

Another contribution of this thesis is to determine an optimal test for benchmarking CV teleportation. In particular, by taking the performance metric to be the energy-constrained channel fidelity between ideal CV teleportation and its experimental implementation, we determine the optimal input state that can be used to assess the performance of an experimental implementation. Mathematically, this problem is equivalent to estimating the energy-constrained channel fidelity between the identity channel and an additive-noise channel. We then develop numerical and analytical techniques to find exact solutions to the optimization involved in estimating the energy-constrained channel fidelity. In particular, we first reduce the problem of estimating the energy-constrained channel fidelity to a quadratic program over an infinite number of variables, as in (5.1.19). We then define a truncated version of this quadratic program in (5.1.30) and solve it numerically. Finally, we provide analytical solutions by invoking the Karush-Kuhn-Tucker (KKT) conditions [86,87], as in (5.1). Our main contribution is that entangled superpositions of twin-Fock states are optimal for assessing the performance of CV teleportation. Furthermore, we believe that our techniques to solve the optimization problem corresponding to the energy-constrained channel fidelity between ideal CV teleportation and its experimental implementation can be applied more generally to other channel discrimination problems.

The necessary background for this thesis is familiarity with the basics of quantum mechanics, quantum information theory, and quantum continuous variables. We point readers to [88] for quantum optics, [8, 68, 89] for quantum information theory, and [1] for quantum computation. In Chapter 2 we summarize definitions and prior results relevant for the rest of the thesis.

This thesis is based on the following papers:

- **Optimal tests for continuous-variable quantum teleportation and photodetectors** [90]
  Kunal Sharma, Barry C. Sanders, and Mark M. Wilde
  arXiv:2012.02754 (2020)
  (Chapter 5)

- **Characterizing the performance of continuous-variable Gaussian quantum gates** [92]
  Kunal Sharma and Mark M. Wilde
  Physical Review Research 2, 013126 (2020), arXiv:1810.12335
  (Chapter 4)

- **Bounding the energy-constrained quantum and private capacities of phase-insensitive bosonic Gaussian channels** [93]
  Kunal Sharma, Mark M. Wilde, Sushovit Adhikari, and Masahiro Takeoka
  New Journal of Physics 20, 063025 (2018), arXiv:1708.07257
  (Chapter 3)

Other papers to which the author contributed during his Ph.D.

- **Connecting ansatz expressibility to gradient magnitudes and barren plateaus** [94]
  Zoë Holmes, Kunal Sharma, Marco Cerezo, Patrick J. Coles
  arXiv:2101.02138 (2021)

- **Error mitigation on a near-term quantum photonic device** [95]
  Daiqin Su, Robert Israel, Kunal Sharma, Haoyu Qi, Ish Dhand, and Kamil Bradler
  arXiv:2008.06670 (2020)

- **Noise-Induced Barren Plateaus in Variational Quantum Algorithms** [96]
  Samson Wang, Enrico Fontana, Marco Cerezo, Kunal Sharma, Akira Sone, Lukasz Cincio, and Patrick J. Coles
  arXiv:2007.14384 (2020)

- **Reformulation of the No-Free-Lunch Theorem for Entangled Data Sets** [97]
  Kunal Sharma, Marco Cerezo, Zoë Holmes, Lukasz Cincio, Andrew Sornborger, and Patrick J. Coles
  arXiv:2007.04900 (2020)

- **Information-theoretic aspects of the generalized amplitude damping channel** [98]
  Sumeet Khatri, Kunal Sharma, and Mark M. Wilde
  Physical Review A 102, 012401 (2020), arXiv:1903.07747

- **Trainability of Dissipative Perceptron-Based Quantum Neural Networks** [99]
  Kunal Sharma, Marco Cerezo, Lukasz Cincio, and Patrick J. Coles
  arXiv:2005.12458 (2020)

- **Noise Resilience of Variational Quantum Compiling** [100]
  Kunal Sharma, Sumeet Khatri, Marco Cerezo, and Patrick J. Coles
  New Journal Physics, 22, 043006 (2020), arXiv:1908.04416

- **Variational Quantum State Eigensolver** [101]
  Marco Cerezo, Kunal Sharma, Andrew Arrasmith, and Patrick J. Coles
  arXiv:2004.01372 (2020)

- **Conditional quantum one-time pad** [102]
  Kunal Sharma, Eyuri Wakakuwa, and Mark M. Wilde

Physical Review Letters 124, 050503 (2020), arXiv:1703.02903

- **Entanglement-assisted private communication over quantum broadcast channels** [103]

  Haoyu Qi, Kunal Sharma, and Mark M. Wilde

  Journal of Physics A, 51, 374001 (2018), arXiv:1803.03976

CHAPTER 2

PRELIMINARIES

In this chapter, we review definitions and prior results relevant for the rest of the thesis. We begin by defining quantum states and channels in Section 2.1. In Section 2.2, we review information quantities employed in this thesis. We define bosonic quantum states and channels in Section 2.3. We then provide background on energy-constrained distance measures in Section 2.4. We summarize several notions of convergence for continuous-variable quantum channels in Section 2.5. In Section 2.6, we review the notion of approximate degradibility of quantum channels. We define the energy-constrained quantum and private capacities of quantum channels in Section 2.7. In Section 2.8, we discuss the continuity of information quantities and channel capacities. Finally, we review the Karush-Kuhn-Tucker conditions in Section 2.9.

2.1 Quantum States and Operations

This section briefly reviews the properties of continuous-variable (CV) quantum systems that we use in this thesis. We point readers to [68, 89] for a detailed treatment of CV systems in the context of information theory. In this thesis, we follow the material in [68, 104, 105].

We begin with general definitions of quantum states, channels, and measurements and later focus on bosonic quantum systems.

Definition 1 (Inner product space) *Let $\mathcal{V}$ be a vector space over the complex numbers $\mathbb{C}$. Let $|\psi\rangle, |\phi\rangle, |\xi\rangle \in \mathcal{V}$ and let $\alpha, \beta \in \mathbb{C}$. Then a function $\langle\cdot|\cdot\rangle : \mathcal{V} \otimes \mathcal{V} \to \mathbb{C}$ that maps an ordered pair of vectors to $\mathbb{C}$ is an inner product if it satisfies the following properties:*

1. *Linearity:* $\langle\xi|(\alpha|\psi\rangle + \beta|\phi\rangle) = \alpha\langle\xi|\psi\rangle + \beta\langle\xi|\phi\rangle$.

2. *Skew symmetry:* $\overline{\langle\xi|\psi\rangle} = \langle\psi|\xi\rangle$.

3. Positivity: $\langle\psi|\psi\rangle \geq 0$. *The inequality is saturated if and only if* $|\psi\rangle = 0$.

Every inner product space is a normed vector space, where the norm is defined as follows.

Definition 2 (Norm induced by inner product) *Let* $\mathcal{V}$ *be an inner product space. Let* $|\psi\rangle \in \mathcal{V}$. *Then a norm over this space can be defined as*

$$\|\psi\| \equiv \sqrt{\langle\psi|\psi\rangle} \ . \tag{2.1.1}$$

Let $|\psi\rangle, |\phi\rangle \in \mathcal{V}$ *and* $c \in \mathbb{C}$. *Then the following properties are satisfied, which follow from the definition of the inner product and the Cauchy-Schwarz inequality:*

- $\|\psi\| \geq 0$. *The inequality is saturated if and only if* $|\psi\rangle = 0$.
- $\|c\psi\| = |c|\|\psi\|$.
- $\|\psi + \phi\| \leq \|\psi\| + \|\phi\|$.

Definition 3 (Complete metric space) *A metric space* $\mathcal{V}$ *is called complete if every Cauchy sequence in* $\mathcal{V}$ *is convergent and has a limit in* $\mathcal{V}$.

Using Definitions 1–3, we now provide a formal definition of an infinite-dimensional Hilbert space.

Definition 4 (Hilbert space) *A Hilbert space is a complete inner product space.*

Let $\mathcal{H}$ be a Hilbert space. If $\mathcal{H}$ has a countable orthonormal basis, then it is called a *separable* Hilbert space. Let $\{|i\rangle : i \in \mathbb{N}\}$ denote an orthonormal basis of $\mathcal{H}$ and let $|\psi\rangle \in \mathcal{H}$. For a separable Hilbert space $\mathcal{H}$, the state $|\psi\rangle$ can be written as $|\psi\rangle = \sum_{i=0}^{\infty} \alpha_i |i\rangle$, where $\alpha_i \in \mathbb{C}$, such that $\sum_{i=0}^{\infty} |\alpha_i|^2 = 1$.

We now provide definitions of linear, isometric, bounded, positive semi-definite, and trace-class operators.

Definition 5 (Linear operator) *An operator $M : \mathcal{H} \to \mathcal{H}$ is linear if for all $|\psi\rangle, |\phi\rangle \in \mathcal{H}$ and $\alpha, \beta \in \mathbb{C}$, the following holds:*

$$M(\alpha |\psi\rangle + \beta |\phi\rangle) = \alpha M(|\psi\rangle) + \beta M(|\phi\rangle) \ . \tag{2.1.2}$$

Let $\mathcal{L}(\mathcal{H})$ denote the set of square operators acting on $\mathcal{H}$ and let $\mathcal{L}(\mathcal{H}, \mathcal{H}')$ denote the set of linear operators taking $\mathcal{H}$ to $\mathcal{H}'$.

Definition 6 (Isometry) *An isometry $V \in \mathcal{L}(\mathcal{H}, \mathcal{H}')$ is a linear, norm-preserving operator such that*

$$\|\psi\| = \|V\psi\| \ , \ \forall |\psi\rangle \in \mathcal{H} \ . \tag{2.1.3}$$

Definition 7 (Bounded operators) *A linear operator M is bounded if there exists $t \geq 0$ such that*

$$\|M\psi\| \leq t\|\psi\| \ , \ \forall \psi \in \mathcal{H} \ . \tag{2.1.4}$$

We denote the set of bounded operators acting on $\mathcal{H}$ as $\mathcal{B}(\mathcal{H})$. We note that the least number t satisfying (2.1.4) is called the operator norm or the spectral norm of M.

Definition 8 (Positive semi-definite operators) *A bounded operator $M \in \mathcal{B}(\mathcal{H})$ is positive semi-definite if*

$$\langle\psi|M|\psi\rangle \geq 0 \ , \ \forall |\psi\rangle \in \mathcal{H} \ . \tag{2.1.5}$$

We denote the set of positive semi-definite operators by $\mathcal{P}(\mathcal{H})$ throughout this thesis.

Definition 9 (Trace norm) *The trace norm of an operator $M \in \mathcal{B}(\mathcal{H})$ is defined as*

$$\|M\|_1 \equiv \mathrm{Tr}(|M|), \tag{2.1.6}$$

where

$$|M| \equiv \sqrt{M^\dagger M} \ . \tag{2.1.7}$$

We will later invoke the following important properties of the trace norm:

- The trace norm of an operator $M \in \mathcal{B}(\mathcal{H})$ is equal to the sum of its singular values.
- **Triangle inequality**: Let $M, N \in \mathcal{B}(\mathcal{H})$. Then the following inequality holds:

$$\|M + N\|_1 \leq \|M\|_1 + \|N\|_1 \ . \tag{2.1.8}$$

- **Isometric invariance**: Let V and W be isometries. The trace norm is invariant under multiplication by isometries:

$$\|VMW^\dagger\|_1 = \|M\|_1 \ . \tag{2.1.9}$$

- **Convexity**: Let $M, N \in \mathcal{B}(\mathcal{H})$ and $\lambda \in [0, 1]$. Then the following inequality holds:

$$\|\lambda M + (1 - \lambda)N\|_1 \leq \lambda\|M\|_1 + (1 - \lambda)\|N\|_1 \ . \tag{2.1.10}$$

Definition 10 (Trace-class operators) *A bounded operator $M \in \mathcal{B}(\mathcal{H})$ is a trace-class operator if*

$$\|M\|_1 < \infty \ . \tag{2.1.11}$$

We denote the set of trace-class operators by $\mathcal{T}(\mathcal{H})$ throughout this thesis.

Below we formally define quantum states, Schmidt decomposition theorem, partial trace, and the purification of a mixed state.

Definition 11 (Quantum states) *The set of quantum states (or density operators) can be defined as the following subset of trace-class operators:*

$$\mathcal{D}(\mathcal{H}) \equiv \{\rho \in \mathcal{T}(\mathcal{H}) : \rho \geq 0, \mathrm{Tr}(\rho) = 1\} \ . \tag{2.1.12}$$

We note that every density operator ρ can be represented in terms of the spectral decomposition as follows:

$$\rho = \sum_i \lambda_i |\psi_i\rangle\langle\psi_i| \ , \tag{2.1.13}$$

where $\{|\psi_i\rangle\}_i$ are eigenstates and $\{\lambda_i\}_i$ is a sequence of non-negative numbers, such that $\sum_i \lambda_i = 1$.

Definition 12 (Pure state) *A density operator $\rho \in \mathcal{D}(\mathcal{H})$ is called a pure state if it can be written as $\rho = |\psi\rangle\langle\psi|$, where $|\psi\rangle$ is a vector in $\mathcal{H}$.*

A quantum state ρ is called a mixed state if it cannot be represented as $\rho = |\psi\rangle\langle\psi|$. In other words, states of the form (2.1.13) are mixed states if at least two eigenvalues in $\{\lambda_i\}_i$ are non zero.

Definition 13 (Composite quantum systems) *Let $\mathcal{H}_A$ and $\mathcal{H}_B$ denote Hilbert spaces corresponding to systems A and B, respectively. Then the Hilbert space of systems A and B combined is given by*

$$\mathcal{H}_{AB} \equiv \mathcal{H}_A \otimes \mathcal{H}_B \ . \tag{2.1.14}$$

We now define the Schmidt decomposition using which any pure state of a bipartite system can be decomposed as a superposition of coordinated orthonormal states.

Definition 14 (Schmidt decomposition) *Let $|\psi\rangle_{AB} \in \mathcal{H}_{AB}$ be a bipartite pure state. Let $\{|\phi_i\rangle_A\}_i$ and $\{|\xi_i\rangle_B\}_i$ denote orthonormal bases for $\mathcal{H}_A$ and $\mathcal{H}_B$, respectively. Then the Schmidt decomposition of $|\psi\rangle_{AB} \in \mathcal{H}_{AB}$ is given by*

$$|\psi\rangle_{AB} \equiv \sum_{i=0}^{d-1} \lambda_i \, |\phi_i\rangle_A \, |\xi_i\rangle_B \ , \tag{2.1.15}$$

where $\lambda_i \in \mathbb{R}_{>0}$ and $\sum_i \lambda_i^2 = 1$, and they are called Schmidt coefficients. The Schmidt rank d satisfies

$$d \leq \min\{\dim(\mathcal{H}_A), \dim(\mathcal{H}_B)\} \ . \tag{2.1.16}$$

For a bipartite system, local density operators can be defined that predicts the outcomes of all local measurements. The general method for determining a local density operator is to employ the partial trace operation, defined as follows.

Definition 15 (Partial trace) *Let $\rho_{AB} \in \mathcal{D}(\mathcal{H}_{AB})$. Then the partial trace with respect to system A is given by*

$$\rho_B = \mathrm{Tr}_A(\rho_{AB}) \equiv \sum_i (\langle i|_A \otimes I_B)\rho_{AB}(|i\rangle_A \otimes I_B) \ , \tag{2.1.17}$$

where I_B is an identity operator on system B.

From the Schmidt decomposition and partial trace, it follows that a mixed state can be obtained by employing the partial trace operation over a bipartite pure state. Similarly, for every mixed state, a purification can be defined as follows.

Definition 16 (Purification) *Let $\rho_A \in \mathcal{D}(\mathcal{H}_A)$. Let $|\psi\rangle_{RA}$ be a pure state in $\mathcal{H}_{RA}$. Then $|\psi\rangle_{RA}$ is a purification of ρ_A, if*

$$\rho_A = \mathrm{Tr}_R(|\psi\rangle\langle\psi|_{RA}) \ . \tag{2.1.18}$$

Let $\rho_A = \sum_i \lambda_i |\psi_i\rangle\langle\psi_i|_A$, where $\{|\psi_i\rangle_A\}_i$ is an orthonormal basis. Then a purification of ρ_A is given by

$$|\psi\rangle_{RA} = \sum_i \sqrt{\lambda_i}\, |\phi_i\rangle_R\, |\psi_i\rangle_A \ , \tag{2.1.19}$$

where $\{|\phi_i\rangle_R\}_i$ is an orthonormal basis for $\mathcal{H}_R$. Moreover, all purifications of a density operator are related by an isometry acting on the purifying system.

We now summarize definitions of positive and completely-positive linear maps.

Definition 17 (Positive map) *A linear map $\mathcal{N}_{A\to B} : \mathcal{B}(\mathcal{H}_A) \to \mathcal{B}(\mathcal{H}_B)$ is positive if $\mathcal{N}_{A\to B}(M_A) \geq 0$, for all $M_A \geq 0$, where $M_A \in \mathcal{B}(\mathcal{H}_A)$.*

Definition 18 (Completely positive map) *A linear map $\mathcal{N}_{A\to B} : \mathcal{B}(\mathcal{H}_A) \to \mathcal{B}(\mathcal{H}_B)$ is completely positive if $\mathcal{I}_R \otimes \mathcal{N}_A$ is a positive map for all possible $\mathcal{H}_R$.*

Definition 19 (Trace-preserving map) *A linear map $\mathcal{N}_{A\to B} : \mathcal{T}(\mathcal{H}_A) \to \mathcal{T}(\mathcal{H}_B)$ is trace preserving if*

$$\mathrm{Tr}(M_A) = \mathrm{Tr}(\mathcal{N}_{A\to B}(M_A)) \ , \tag{2.1.20}$$

for all $M_A \in \mathcal{T}(\mathcal{H}_A)$

Using the definitions above, we now define the notion of a quantum channel. We then review the operator-sum representation and isometric extensions of quantum channels. Finally, we conclude this section by describing a complementary channel of a quantum channel, degradable and measurement channels, and positive operator-valued measures.

Definition 20 (Quantum channel) *A quantum channel $\mathcal{N}_{A\to B} : \mathcal{T}(\mathcal{H}_A) \to \mathcal{T}(\mathcal{H}_B)$ is a completely-positive and trace-preserving linear map.*

Theorem 21 (Operator-sum representation) *A linear map $\mathcal{N}_{A\to B} : \mathcal{T}(\mathcal{H}_A) \to \mathcal{T}(\mathcal{H}_B)$ is a quantum channel if and only if there exists a sequence of bounded operators (also known as Kraus operators) $\{V_l\}_l$ such that*

$$\mathcal{N}(M) = \sum_{l=0}^{d-1} V_l M V_l^\dagger \ , \tag{2.1.21}$$

for all $M \in \mathcal{T}(\mathcal{H}_A)$ and $V_l \in \text{Ł}(\mathcal{H}_A, \mathcal{H}_B)$ satisfies

$$\sum_{l=0}^{d-1} V_l^\dagger V_l = I \ , \tag{2.1.22}$$

where $d \leq \dim(\mathcal{H}_A)\dim(\mathcal{H}_B)$.

Let ρ denote a quantum state. Then from (2.1.21) and (2.1.22), it follows that a unitary operation $\mathcal{U} : \rho \to U\rho U^\dagger$ is a quantum channel with a single Kraus operator U, which satisfies $U^\dagger U = I$.

Similar to quantum states, a quantum channel also admits a purification, defined below.

Definition 22 (Isometric extension) *Let $\mathcal{N}_{A\to B} : \mathcal{T}(\mathcal{H}_A) \to \mathcal{T}(\mathcal{H}_B)$ be a quantum channel. Then an isomteric extension or Stinespring dilation $V : \mathcal{H}_A \to \mathcal{H}_B \otimes \mathcal{H}_E$ of the channel $\mathcal{N}_{A\to B}$ is a linear isometry such that*

$$\mathcal{N}_{A\to B}(M_A) = \mathrm{Tr}_E(VM_AV^\dagger) \ , \tag{2.1.23}$$

for all $M_A \in \mathcal{T}(\mathcal{H}_A)$.

Definition 23 (Complementary channel) *Let V denote a linear isometry $V : \mathcal{H}_A \to \mathcal{H}_B \otimes \mathcal{H}_E$. Then a complementary channel $\hat{\mathcal{N}}_{A\to E} : \mathcal{T}(\mathcal{H}_A) \to \mathcal{T}(\mathcal{H}_E)$ of a quantum channel $\mathcal{N}_{A\to B} : \mathcal{T}(\mathcal{H}_A) \to \mathcal{T}(\mathcal{H}_B)$ is defined as*

$$\hat{\mathcal{N}}_{A\to E}(\omega_A) \equiv \mathrm{Tr}_B(V\omega_AV^\dagger) \ , \tag{2.1.24}$$

for all $\omega_A \in \mathcal{T}(\mathcal{H}_A)$.

Definition 24 (Degradable channel) *A quantum channel $\mathcal{N}_{A\to B} : \mathcal{T}(\mathcal{H}_A) \to \mathcal{T}(\mathcal{H}_B)$ is degradable if there exists a quantum channel $\mathcal{D}_{B\to E} : \mathcal{T}(\mathcal{H}_B) \to \mathcal{T}(\mathcal{H}_E)$ such that*

$$\mathcal{D}_{B\to E}(\mathcal{N}_{A\to B}(\omega_A)) = \hat{\mathcal{N}}_{A\to E}(\omega_A) \ , \tag{2.1.25}$$

for all $\omega_A \in \mathcal{T}(\mathcal{H}_A)$.

Definition 25 (Measurement) *Let $\rho \in \mathcal{D}(\mathcal{H})$ be a density operator. Let $\{M_k\}_k$ denote a set of measurement operators for which $\sum_k M_k^\dagger M_k = I$, where I is the identity operator. Then the probability of obtaining outcome k after the measurement is given by*

$$p_K(k) = \mathrm{Tr}\Big(M_k^\dagger M_k \rho\Big) \ , \tag{2.1.26}$$

and the post-measurement state $\tilde{\rho}_k$ is given by

$$\tilde{\rho}_k = \frac{M_k \rho M_k^\dagger}{p_K(k)} \ . \tag{2.1.27}$$

If measurement operators $\{M_k\}_k$ satisfy $M_k^\dagger = M_k$, $M_j M_k = \delta_{jk} M_k$ and $M_k^2 = M_k$, they are called projective measurement operators.

Definition 26 (POVM) *A positive operator-valued measure (POVM) is a set $\{\Lambda_j\}_j$ of operators that satisfy the following properties:*

$$\Lambda_j \geq 0 \quad \textit{and} \quad \sum_j \Lambda_j = I, \ \forall j \ . \tag{2.1.28}$$

2.2 Quantum Entropies and Information

This section summarizes information quantities and their properties relevant to the rest of the thesis.

Definition 27 (Quantum entropy) *The quantum entropy of a state $\rho \in \mathcal{D}(H)$ is defined as*

$$H(\rho) \equiv -\operatorname{Tr}(\rho \log_2 \rho) \ . \tag{2.2.1}$$

The quantum entropy is a non-negative, concave, lower semicontinuous function [106] and not necessarily finite for a density operator acting on an infinite-dimensional Hilbert space (see e.g., Section 2 [107]).

Definition 28 (Binary entropy function) *The binary entropy function is defined for $x \in [0, 1]$ as*

$$h_2(x) \equiv -x \log_2 x - (1-x) \log_2 (1-x) \ . \tag{2.2.2}$$

Throughout the thesis, we use a function $g(x)$, which is the entropy of a bosonic thermal state (see Section 2.3) with mean photon number $x \geq 0$.

Definition 29 (Entropy of a thermal state) *The entropy of a bosonic thermal state with mean photon number $x \geq 0$ is given by:*

$$g(x) \equiv (x+1)\log_2(x+1) - x\log_2 x. \tag{2.2.3}$$

By continuity, we have that $h_2(0) = \lim_{x\to 0} h_2(x) = 0$ and $g(0) = \lim_{x\to 0} g(x) = 0$.

Definition 30 (Quantum relative entropy) *The quantum relative entropy $D(\rho\|\sigma)$ of $\rho, \sigma \in \mathcal{D}(\mathcal{H})$ is defined as [108, 109]*

$$D(\rho\|\sigma) \equiv \sum_i \langle i|\, \rho\log_2\rho - \rho\log_2\sigma + \sigma - \rho\, |i\rangle\,, \tag{2.2.4}$$

where $\{|i\rangle\}_{i=1}^{\infty}$ is an orthonormal basis of eigenvectors of the state ρ, if $\mathrm{supp}(\rho) \subseteq \mathrm{supp}(\sigma)$ and $D(\rho\|\sigma) = \infty$ otherwise.

The quantum relative entropy $D(\rho\|\sigma)$ is non-negative for $\rho, \sigma \in \mathcal{D}(\mathcal{H})$ and is monotone with respect to a quantum channel [110] $\mathcal{N} : \mathcal{T}(\mathcal{H}_A) \to \mathcal{T}(\mathcal{H}_B)$:

$$D(\rho\|\sigma) \geq D(\mathcal{N}(\rho)\|\mathcal{N}(\sigma)). \tag{2.2.5}$$

Definition 31 (Quantum mutual information) *The quantum mutual information $I(A;B)_\rho$ of a bipartite state $\rho_{AB} \in \mathcal{D}(\mathcal{H}_A \otimes \mathcal{H}_B)$ is defined as [109]*

$$I(A;B)_\rho \equiv D(\rho_{AB}\|\rho_A \otimes \rho_B). \tag{2.2.6}$$

Definition 32 (Coherent information) *The coherent information $I(A\rangle B)_\rho$ of ρ_{AB} is defined as [111–113]*

$$I(A\rangle B)_\rho \equiv I(A;B)_\rho - H(A)_\rho, \tag{2.2.7}$$

when $H(A)_\rho < \infty$. This expression reduces to

$$I(A\rangle B)_\rho = H(B)_\rho - H(AB)_\rho, \tag{2.2.8}$$

if $H(B)_\rho < \infty$.

2.3 Bosonic Quantum States and Channels

We begin by recalling the definition of an energy observable and a Gibbs observable [89, 114]. When defining a Gibbs observable, we follow [89, 114].

Definition 33 (Energy observable) *Let G be a positive semi-definite operator. We assume that it has discrete spectrum and that it is bounded from below. In particular, let $\{|e_k\rangle\}_k$ be an orthonormal basis for a Hilbert space $\mathcal{H}$, and let $\{g_k\}_k$ be a sequence of non-negative real numbers. Then*

$$G = \sum_{k=1}^{\infty} g_k |e_k\rangle\langle e_k| \tag{2.3.1}$$

is a self-adjoint operator that we call an energy observable.

Definition 34 (Extension of energy observable) *The nth extension $\overline{G}_n$ of an energy observable G is defined as*

$$\overline{G}_n = \frac{1}{n}(G \otimes I \otimes \cdots \otimes I + \cdots + I \otimes \cdots \otimes I \otimes G), \tag{2.3.2}$$

where n is the number of factors in each tensor product above.

Definition 35 (Gibbs Observable) *An energy observable G is a Gibbs observable if for all $\beta > 0$, we have $\operatorname{Tr}(\exp(-\beta G)) < \infty$, so that the partition function $Z(\beta) := \operatorname{Tr}(\exp(-\beta G))$ has a finite value and hence $\exp(-\beta G)/\operatorname{Tr}(\exp(-\beta G))$ is a well defined thermal state.*

For a Gibbs observable G, let us consider a quantum state ρ such that $\mathrm{Tr}(G\rho) \leq W$. There exists a unique state that maximizes the entropy $H(\rho)$, and this unique maximizer has the Gibbs form $\gamma(W) = \exp(-\beta(W)G)/Z(\beta(W))$, where $\beta(W)$ is the solution of the equation:

$$\mathrm{Tr}(\exp(-\beta G)(G - W)) = 0. \tag{2.3.3}$$

In particular, for the Gibbs observable $G = \hbar\omega\hat{n}$, where $\hat{n} = \hat{a}^\dagger\hat{a}$ is the photon number operator (see Definition 36 below), a thermal state (mean photon number $\bar{n}$) that saturates the energy constrained inequality $\mathrm{Tr}(G\rho) \leq W$ (i.e., $\bar{n} = W$), gives the maximum value of the entropy $g(\bar{n})$, as defined in (2.2.3).

Here, we have fixed the ground-state energy to be equal to zero. In some parts of this thesis, we take the Gibbs observable to be the number operator, and we use the terminology "mean photon number" and "energy" interchangeably.

Definition 36 (Number operator) *The number operator is defined as*

$$\hat{n} = \sum_{n=0}^{\infty} n|n\rangle\langle n|, \tag{2.3.4}$$

where $|n\rangle$ denotes a photon-number state with n photons. The expectation value of $\hat{n}$ corresponds to the mean number of photons in a single-mode quantum state.

m-bosonic modes: Let us consider a system of m bosons described by the position- and momentum-quadrature operators $\hat{x}_j$ and $\hat{p}_j$, respectively, for $j = 1, \ldots, m$, which satisfy the canonical commutation relations (CCR):

$$[\hat{x}_j, \hat{p}_k] = i\delta_{jk}\hbar, \ \forall j, k \in \{1, \ldots, m\} \ . \tag{2.3.5}$$

Henceforth, we set $\hbar = 1$. Let us introduce a vector of quadrature operators as follows

$$\hat{r} = (\hat{x}_1, \hat{p}_1, \ldots, \hat{x}_m, \hat{p}_m)^T \ . \tag{2.3.6}$$

Then the CCR between quadrature operators can be written compactly as

$$[\hat{r}, \hat{r}^T] = i\Omega \ , \tag{2.3.7}$$

where

$$\Omega = \bigoplus_{j=1}^{m} \Omega_1, \quad \text{with} \quad \Omega_1 = \begin{pmatrix} 0 & 1 \\ -1 & 0 \end{pmatrix} . \tag{2.3.8}$$

Here, Ω is the symplectic form.

Using quadrature operators, the bosonic annihilation and creation operators for each mode can be defined as

$$\hat{a}_j = \frac{\hat{x}_j + i\hat{p}_j}{\sqrt{2}} \ . \tag{2.3.9}$$

Definition 37 (Symplectic matrix) *A real matrix S is called symplectic if the following holds:*

$$S\Omega S^T = \Omega \ . \tag{2.3.10}$$

Definition 38 (Inverse and transpose of a symplectic matrix) *Let S denote a symplectic matrix. Then the inverse of S is also a symplectic matrix and given by*

$$S^{-1} = -\Omega S^T \Omega \ , \tag{2.3.11}$$

which implies that S^T is also a symplectic matrix.

Definition 39 (Displacement operator) *Let $r \in \mathbb{R}^{2m}$, such that $r = (x_1, p_1, \ldots, x_m, p_m)^T$. Then the unitary displacement operator (also known as Weyl operators) is defined as follows:*

$$\hat{D}_r \equiv \exp\Big(ir^T \Omega \hat{r}\Big) \ , \tag{2.3.12}$$

where $\hat{r}$ and Ω are defined in (2.3.6) *and* (2.3.8)*, respectively.*

We summarize some useful properties of displacement operators.

- The displacement operator over m modes can be represented as a tensor product of single-mode displacement operators. That is

$$\hat{D}_r = \hat{D}_{r_1} \otimes \cdots \otimes \hat{D}_{r_m} \ , \tag{2.3.13}$$

  where $r_k = (x_k, p_k)^T$.

- $\hat{D}_r^\dagger = \hat{D}_{-r}$.

- Let $r_1, r_2 \in \mathbb{R}^{2m}$. Then the following equality holds:

$$\hat{D}_{r_1+r_2} = \hat{D}_{r_1}\hat{D}_{r_2}e^{ir_1^T\Omega r_2/2} = \hat{D}_{r_2}\hat{D}_{r_1}e^{-ir_1^T\Omega r_2/2} \ . \tag{2.3.14}$$

- The action of the displacement operator over $\hat{r}$ is given by

$$\hat{D}_r^\dagger \hat{r} \hat{D}_r = \hat{r} - r \ . \tag{2.3.15}$$

- Let $\alpha = (x + ip)/\sqrt{2}$, $r = (x, p)^T$, and $\hat{r} = (\hat{x}, \hat{p})^T$. Then

$$\hat{D}_\alpha \equiv e^{\alpha\hat{a}^\dagger - \alpha^*\hat{a}} = \hat{D}_r^\dagger \tag{2.3.16}$$

- Orthogonality of displacement operators: Let $\alpha, \beta \in \mathbb{C}$. Then

$$\mathrm{Tr}\Big(\hat{D}_\alpha \hat{D}_{-\beta}\Big) = \pi\delta^2(\alpha - \beta) \ . \tag{2.3.17}$$

  Let $r_1, r_2 \in \mathbb{R}^{2m}$. Then a similar relation can be defined for the displacement operator over m modes as follows:

$$\mathrm{Tr}\Big(\hat{D}_{r_1} \hat{D}_{-r_2}\Big) = (2\pi)^n \delta^{2n}(r_1 - r_2) \ . \tag{2.3.18}$$

Definition 40 (Wigner characteristic function) *Let* $r = (x_1, p_1, \ldots, x_m, p_m)^T$. *For an* m*-mode quantum state* $\rho \in \mathcal{D}(\mathcal{H})$*, the corresponding Wigner characteristic function is defined as follows*

$$\chi_\rho(r) \equiv \mathrm{Tr}(\hat{D}_r^\dagger \rho) \ . \tag{2.3.19}$$

Definition 41 (Fourier-Weyl relation) *Let* $r = (x_1, p_1, \ldots, x_m, p_m)^T$. *Then every* m*-mode quantum state can be represented in terms of the Wigner characteristic function as follows*

$$\rho = \frac{1}{(2\pi)^m} \int dr \ \chi_\rho(r) \ \hat{D}_r \ , \tag{2.3.20}$$

where $dr = dx_1 dp_1 \ldots dx_m dp_m$.

Definition 42 (Mean vector) *Let* ρ *be an* m*-mode bosonic state. Then the mean vector of* ρ *is defined as follows:*

$$\bar{r}^\rho \equiv \mathrm{Tr}(\rho \hat{r}) = (\bar{x}_1, \bar{p}_1, \ldots, \bar{x}_m, \bar{p}_m)^T \ , \tag{2.3.21}$$

where $\hat{r}$ *is given by* (2.3.6)*,* $\bar{x}_k = \mathrm{Tr}(\rho \hat{x}_k)$ *and* $\bar{p}_k = \mathrm{Tr}(\rho \hat{p}_k)$.

Thus the mean vector of an m-mode quantum state is a $2m \times 1$-dimensional vector.

Definition 43 (Covariance matrix) *Let* ρ *be an* m*-mode bosonic state. Then the covariance matrix elements are defined as*

$$\sigma_{jk}^\rho \equiv \mathrm{Tr}\Big(\{\hat{r}_j^c, \hat{r}_k^c\}\rho\Big) \tag{2.3.22}$$

where $\{\hat{r}_j^c, \hat{r}_k^c\} = \hat{r}_j^c \hat{r}_k^c + \hat{r}_k^c \hat{r}_j^c$ *and* $\hat{r}_j^c = \hat{r}_j - \mathrm{Tr}(\hat{r}_j \rho)$ *for all* $j, k \in \{1, \ldots, 2m\}$*, and* $\hat{r}$ *is given by* (2.3.6).

Thus the covariance matrix of an m-mode quantum state is a $2m \times 2m$-dimensional matrix.

Properties of a covariance matrix σ^ρ:

- The covariance matrix σ^ρ of a state ρ satisfies

$$\sigma^\rho + i\Omega \geq 0 \ , \tag{2.3.23}$$

  which is a manifestation of the uncertainty principle [115].

- The covariance matrix σ^ρ is positive definite, i.e, $\sigma^\rho > 0$.

Definition 44 (Gaussian state) *A quantum state ρ is Gaussian if its Wigner characteristic function has a Gaussian form as*

$$\chi_\rho(r) = \exp\left(-\frac{1}{4}\left[\Omega r\right]^T \sigma^\rho \Omega r + \left[\Omega \bar{r}^\rho\right]^T r\right) \ , \tag{2.3.24}$$

where $\bar{r}^\rho$ and σ^ρ are given by (2.3.21) *and* (2.3.22)*, respectively.*

Thus a bosonic Gaussian state ρ can be completely characterized by its mean vector $\bar{r}^\rho$ and covariance matrix σ^ρ. We now discuss an alternate representation of faithful Gaussian states.

Let us first define the most general quadratic Hamiltonian for m modes. Let H be $2m \times 2m$ positive definite real matrix:

$$\hat{H} = \frac{1}{2}(\hat{r} - \bar{r})^T H (\hat{r} - \bar{r}) \ , \tag{2.3.25}$$

where $\bar{r} \in \mathbb{R}^{2m}$.

Then a faithful Gaussian state can be defined as the thermal state corresponding to $\hat{H}$, i.e.,

$$\rho = \frac{e^{-\hat{H}}}{\mathrm{Tr}\left(e^{-\hat{H}}\right)} \ . \tag{2.3.26}$$

We now define a faithful Gaussian state ρ in terms of its mean vector and the covariance matrix.

Definition 45 (Faithful Gaussian states) *Let ρ denote an m-mode bosonic Gaussian state. Let $\bar{r}^\rho$ and σ^ρ denote the mean vector and the covariance matrix of ρ, respectively. If ρ is faithful, it can represented as follows:*

$$\rho = \frac{e^{-\frac{1}{2}(\hat{r}-\bar{r}^\rho)^T H'(\hat{r}-\bar{r}^\rho)}}{\sqrt{\mathrm{Det}\left(\frac{\sigma^\rho + i\Omega}{2}\right)}} \ , \tag{2.3.27}$$

where

$$\begin{aligned} H' &= S^T H S \\ H &= \bigoplus_{j=1}^{n} \omega_j \begin{pmatrix} 1 & 0 \\ 0 & 1 \end{pmatrix} \end{aligned} \tag{2.3.28}$$

with $\omega_j > 0, \forall j \in \{1, \ldots, n\}$, and S symplectic.

Thermal state. Let $\hat{H}_m \equiv \sum_{j=1}^m \omega_j \hat{a}_j^\dagger \hat{a}_j$, where $\omega_j > 0, \forall j$. Then a thermal Gaussian state θ_β of m modes with respect to $\hat{H}_m$ and having inverse temperature $\beta > 0$ thus has the following form:

$$\theta_\beta = \frac{e^{-\beta \hat{H}_m}}{\mathrm{Tr}\{e^{-\beta \hat{H}_m}\}} \ , \tag{2.3.29}$$

and has a mean vector equal to zero and a diagonal $2m \times 2m$ covariance matrix. One can calculate that the mean photon number in this state is equal to

$$\sum_j \frac{1}{e^{\beta \omega_j} - 1}. \tag{2.3.30}$$

A single-mode thermal state with mean photon number $\bar{n} = 1/(e^{\beta\omega} - 1)$ has the following representation in the photon number basis:

$$\theta(\bar{n}) \equiv \frac{1}{1+\bar{n}} \sum_{n=0}^{\infty} \left(\frac{\bar{n}}{\bar{n}+1}\right)^n |n\rangle\langle n| \ . \tag{2.3.31}$$

It is also well known that thermal states can be written as a Gaussian mixture of displace-

ment operators acting on the vacuum state:

$$\theta_\beta = \int dr\ p(r)\ \hat{D}_r \left[|0\rangle\langle 0|\right]^{\otimes m} \hat{D}_r^\dagger, \tag{2.3.32}$$

where $p(r)$ is a zero-mean, circularly symmetric Gaussian distribution, $r = (x_1, p_1, \ldots, x_m, p_m)^T$, and $dr = dx_1 dp_1 \ldots dx_m dp_m$.. From this, it also follows that randomly displacing a thermal state in such a way leads to another thermal state of higher temperature:

$$\theta_\beta = \int dr\ q(r)\ \hat{D}_r \theta_{\beta'} \hat{D}_r^\dagger, \tag{2.3.33}$$

where $\beta' \geq \beta$ and $q(r)$ is a particular circularly symmetric Gaussian distribution.

Two-mode squeezed vacuum state. The two-mode squeezed vacuum state with parameter $N \geq 0$, which is equivalent to a purification of the thermal state in (2.3.31), is defined as

$$|\psi_{\text{TMS}}(N)\rangle \equiv \frac{1}{\sqrt{N+1}} \sum_{n=0}^{\infty} \sqrt{\left(\frac{N}{N+1}\right)^n} |n\rangle_R |n\rangle_A \ , \tag{2.3.34}$$

where $|n\rangle$ again denotes a photon-number state with n photons.

It is important to note that even though the state in (2.3.34) is a well-defined quantum state for all $N \in [0, \infty)$, the limiting object, often called "ideal EPR state" $\lim_{\bar{n}\to\infty} |\psi_{\text{TMS}}(N)\rangle$ [116], is not a quantum state, as it is unnormalizable and it is thus not contained in the set of density operators. Similarly, the eigenvectors of the position- and momentum-quadrature operators, denoted as $|x\rangle$ and $|p\rangle$, respectively, are also not quantum states. In spite of this, the notions of uniform and strong convergence involve a supremum over the set of density operators (see Section 2.5), and so these objects can be approached in a suitable limit. We point readers to [117] for more clarification on this topic in the context of uniform and strong convergence.

Coherent states. Let $\alpha \in \mathbb{C}$. Then the coherent state $|\alpha\rangle$ is defined as

$$|\alpha\rangle = \hat{D}_\alpha |0\rangle = e^{-\frac{|\alpha|^2}{2}} \sum_{k=0}^{\infty} \frac{\alpha^k}{\sqrt{k!}} |k\rangle \ , \tag{2.3.35}$$

which is an eigenstate of the annihilation operator $\hat{a}$, i.e.,

$$\hat{a} |\alpha\rangle = \alpha |\alpha\rangle \ . \tag{2.3.36}$$

Overlap between two coherent states. Let $\alpha, \beta \in \mathbb{C}$ and let $|\alpha\rangle, |\beta\rangle$ be coherent states. Then the overlap between $|\alpha\rangle$ and $|\beta\rangle$ is given by

$$\langle\beta|\alpha\rangle = \mathrm{e}^{-\frac{1}{2}|\alpha-\beta|^2} \mathrm{e}^{\frac{1}{2}(\alpha\beta^* - \alpha^*\beta)} \ . \tag{2.3.37}$$

Eq. (2.3.37) implies that coherent states are not orthogonal. Nevertheless, they form an overcomplete basis in the sense that an identity operator can be represented as a weighted integral of projectors on coherent states:

$$\frac{1}{\pi} \int d^2\alpha |\alpha\rangle\langle\alpha| = I \ . \tag{2.3.38}$$

Hilbert-Schmidt product of two Gaussian states. Let ρ and τ be m-mode Gaussian states with mean vectors $\bar{r}^\rho$ and $\bar{r}^\tau$, and the covariance matrices σ^ρ and σ^τ, respectively. Then the Hilbert-Schmidt product of ρ and τ is given by

$$\mathrm{Tr}(\rho\tau) = \frac{2^m}{\sqrt{\mathrm{Det}(\sigma^\rho + \sigma^\tau)}} e^{-(\bar{r}^\rho - \bar{r}^\tau)^T (\sigma^\rho + \sigma^\tau)^{-1} (\bar{r}^\rho - \bar{r}^\tau)} \tag{2.3.39}$$

Entangled superposition of twin-Fock states. In this thesis, we employ entangled

superpositions of twin-Fock states, which we define as

$$|\psi\rangle_{RA} = \sum_{n=0}^{\infty} \lambda_n |n\rangle_R |n\rangle_A , \tag{2.3.40}$$

with $\lambda_n \in \mathbb{R}^+$ and $\sum_{n=0}^{\infty} \lambda_n^2 = 1$.

Gaussian unitary operations. We now review the general form of Gaussian unitaries and their action on the mean vector and the covariance matrix of a quantum state. From (2.3.15) and (2.3.25), we note that the most general quadratic Hamiltonian for m modes can be written as follows

$$\hat{H} = \frac{1}{2} \hat{D}_{-\bar{r}} \hat{r}^T H \hat{r} \hat{D}_{\bar{r}} , \tag{2.3.41}$$

which leads to the following Gaussian unitary operation:

$$e^{i\hat{H}} = \hat{D}_{-\bar{r}} \hat{S} \hat{D}_{\bar{r}} , \tag{2.3.42}$$

where

$$\hat{S} = e^{\frac{i}{2} \hat{r}^T H \hat{r}} , \tag{2.3.43}$$

which is a Gaussian unitary corresponding to a Hamiltonian that is purely quadratic in the quadrature operators.

Let $S = e^{\Omega H}$. Then using

$$\hat{S} \hat{D}_{\bar{r}} = \hat{D}_{S^{-1}\bar{r}} \hat{S} , \tag{2.3.44}$$

we get

$$e^{i\hat{H}} = e^{i\bar{\mathbf{r}}^{\mathrm{T}} \Omega S^{-1} \bar{\mathbf{r}}/2} \hat{D}_{(S^{-1}-I)\bar{\mathbf{r}}} \hat{S} . \tag{2.3.45}$$

From (2.3.45) it follows that an arbitrary Gaussian unitary operation can be decomposed as a sequence of displacement operators generated by linear Hamiltonians and Gaussian unitary operations generated by purely quadratic Hamiltonians.

Displacement unitary transformation. We recall from Definition 39 and (2.3.15), the

mean vector of a state ρ transforms as follows:

$$\mathrm{Tr}\Big(\hat{r}\hat{D}_r^\dagger \rho \hat{D}_r\Big) = \bar{r}^\rho + r \ . \tag{2.3.46}$$

Thus the displacement operator only modifies the mean vector of ρ, and the covariance matrix remains unchanged.

Symplectic transformation. Let $\hat{S}$ denote a Gaussian unitary corresponding to a Hamiltonian that is purely quadratic in the quadrature operators, such that $\hat{S} = e^{\frac{i}{2}\hat{r}^T H \hat{r}}$, where H is a real positive definite matrix. Let us assume that the quantum state ρ transforms under $\hat{S}$ as follows: $\hat{S}^\dagger \rho \hat{S}$. Then the mean vector $\bar{r}^\rho$ and the covariance matrix σ^ρ of the state ρ transforms as follows:

$$\bar{r}^\rho \to S\bar{r}^\rho \ , \tag{2.3.47}$$

$$\sigma^\rho \to S\sigma^\rho S^T \ , \tag{2.3.48}$$

where

$$S = e^{\Omega H} \ . \tag{2.3.49}$$

We now state the singular value decomposition of symplectic matrices, which further simplifies the form of a symplectic matrix and equivalently of a symplectic unitary transformation.

Singular value decomposition of symplectic matrices. Any $2m \times 2m$ symplectic matrix can be decomposed as

$$S = OZ\tilde{O} \ , \tag{2.3.50}$$

where O and $\tilde{O}$ are both symplectic and orthogonal matrices, and Z has the following form:

$$Z = \bigoplus_{j=1}^{m} \begin{bmatrix} z_j & 0 \\ 0 & z_j^{-1} \end{bmatrix} \ , \tag{2.3.51}$$

for $z_j \geq 1$.

Beamsplitter. A beamsplitter consists of a semi-reflective mirror, which both partly reflects and transmits the input radiation. In general the unitary operator corresponding to the beamsplitter transformation is given by [26]

$$U_{\mathrm{BS}}^{\theta,\phi} \equiv \exp\Big[i\theta(e^{i\phi}\hat{a}_{\mathrm{in}}^{\dagger}\hat{b}_{\mathrm{in}} + e^{-i\phi}\hat{a}_{\mathrm{in}}\hat{b}_{\mathrm{in}}^{\dagger})\Big], \tag{2.3.52}$$

where $\hat{a}_{\mathrm{in}}$ and $\hat{b}_{\mathrm{in}}$ denote the two incoming modes on either side of the beamsplitter, and θ depends on the interaction time and coupling strength of semi-reflective mirrors. Moreover, ϕ denotes the relative phase shift parameter. Another representation of a beamsplitter is given in terms of the transmissivity η of the beamsplitter, where $\eta = (\cos\theta)^2$. In this thesis, we parametrize a beamsplitter with respect to η and θ interchangeably.

The symplectic matrix corresponding to the beamsplitter transformation is given by

$$S_{\mathrm{BS}} = \begin{bmatrix} \cos\theta & 0 & \sin\theta\sin\phi & \sin\theta\cos\phi \\ 0 & \cos\theta & -\sin\theta\cos\phi & \sin\theta\sin\phi \\ -\sin\theta\sin\phi & \sin\theta\cos\phi & \cos\theta & 0 \\ -\sin\theta\cos\phi & -\sin\theta\sin\phi & 0 & \cos\theta \end{bmatrix}, \tag{2.3.53}$$

which corresponds to an orthogonal symplectic transformation as in (2.3.50).

Phase rotations. The unitary operator corresponding to the phase rotation is given by

$$U_{\mathrm{PR}}^{\phi} = \exp(i\hat{n}\phi), \tag{2.3.54}$$

where $\hat{n}$ denotes the number operator. Moreover, the symplectic matrix corresponding to

the phase rotation unitary is given by

$$S_\phi = \begin{bmatrix} \cos\phi & \sin\phi \\ -\sin\phi & \cos\phi \end{bmatrix} . \tag{2.3.55}$$

which also corresponds to an orthogonal symplectic transformation as in (2.3.50).

Squeezer. A single-mode squeezer is a unitary operator defined as

$$\hat{S}(\xi) \equiv \exp\Big[(\xi^* \hat{a}^2 - \xi \hat{a}^{\dagger 2})/2\Big] , \tag{2.3.56}$$

where $\xi = re^{i\theta}$, with $r \in [0, \infty)$ and $\theta \in [0, 2\pi]$ (see, e.g., [118] for a review). A squeezing transformation realizes a decrement in the variance of one of the quadratures at the expense of a corresponding increment in the variance of the complementary quadrature, which is helpful for improving the sensitivity of an interferometer [119] and for other quantum metrological tasks [118]. Let $\theta = 0$. Then the symplectic transformation corresponding to $\hat{S}(r)$ is given by

$$S_{\rm SQ} = \begin{bmatrix} e^r & 0 \\ 0 & e^{-r} \end{bmatrix} , \tag{2.3.57}$$

which we described as Z in (2.3.50).

SUM gate. A SUM gate is a quantum nondemolition (QND) interaction between two modes and it is the CV analog of the CNOT gate [74]:

$$\mathrm{SUM}^G \equiv \exp(-i\ G \hat{x}_1 \otimes \hat{p}_2) , \tag{2.3.58}$$

where $\hat{x}_1$ and $\hat{p}_2$ correspond to the position- and momentum-quadrature operators of modes 1 and 2, respectively, and G is the gain of the interaction. Generally, $G = 1$ is sufficient for quantum information processing tasks. This CV entangling quantum gate has applications in CV quantum error correction [120, 121] and CV coherent communication [122, 123].

Let ρ_{12}^{in} denote a two-mode input quantum state. Then the action of the ideal SUM^G gate on the mode operators $\hat{x}_1$, $\hat{x}_2$, $\hat{p}_1$, and $\hat{p}_2$ of ρ_{12}^{in} is given by

$$\hat{x}_1^{\text{in}} \to \hat{x}_1^{\text{in}} \ , \tag{2.3.59}$$

$$\hat{p}_1^{\text{in}} \to \hat{p}_1^{\text{in}} - G\hat{p}_2^{\text{in}} \ , \tag{2.3.60}$$

$$\hat{x}_2^{\text{in}} \to \hat{x}_2^{\text{in}} + G\hat{x}_1^{\text{in}} \ , \tag{2.3.61}$$

$$\hat{p}_2^{\text{in}} \to \hat{p}_2^{\text{in}} \ . \tag{2.3.62}$$

Gaussian channels. Quantum channels that take an arbitrary Gaussian input state to another Gaussian state are called quantum Gaussian channels. Let $\mathcal{N}$ denote a Gaussian channel that takes n modes to m modes. Then $\mathcal{N}$ transforms the Wigner characteristic function $\chi_\rho(r)$ of a state ρ as follows:

$$\chi_\rho(r) \to \chi_{\mathcal{N}(\rho)}(r) = \chi_\rho\Big(\Omega^T X^T \Omega r\Big) \exp\Big(-\frac{1}{4} r^T \Omega^T Y \Omega r + i r^T \Omega^T d\Big) \ , \tag{2.3.63}$$

where X is a real $2m \times 2n$ matrix, Y is a real $2m \times 2m$ positive semi-definite symmetric matrix, and $d \in \mathbb{R}^{2m}$, such that they satisfy the following condition for $\mathcal{N}$ to be a physical channel:

$$Y + i\Omega - iX\Omega X^T \geq 0 \ . \tag{2.3.64}$$

Furthermore, since a Gaussian state ρ can be completely characterized by its mean vector $\bar{r}^\rho$ and covariance matrix σ^ρ, the action of a Gaussian channel on ρ can be described as follows:

$$\begin{aligned} \bar{r}^\rho &\to X\bar{r}^\rho + d \ , \\ \sigma^\rho &\to X\sigma^\rho X^T + Y \ . \end{aligned} \tag{2.3.65}$$

Just as every quantum channel can be implemented as a unitary transformation acting on a larger space followed by a partial trace, so can Gaussian channels be implemented as a Gaussian unitary on a larger space with some extra modes prepared in the vacuum state, followed by a partial trace [124]. Given a Gaussian channel $\mathcal{N}_{X,Y}$ with Z such that $Y = ZZ^T$ we can find two other matrices X_E and Z_E such that there is a symplectic matrix

$$S = \begin{bmatrix} X & Z \\ X_E & Z_E \end{bmatrix}, \tag{2.3.66}$$

which corresponds to a Gaussian unitary transformation on a larger space. The complementary channel $\hat{\mathcal{N}}_{X_E,Y_E}$ from input to the environment then effects the following transformation on mean vectors and covariance matrices:

$$\mu^\rho \longmapsto X_E \mu^\rho, \tag{2.3.67}$$

$$V^\rho \longmapsto X_E V^\rho X_E^T + Y_E, \tag{2.3.68}$$

where $Y_E \equiv Z_E Z_E^T$.

Displacement covariance. All Gaussian channels are covariant with respect to displacement operators. Let $\mathcal{N}_{X,Y}$ denote a Gaussian channel with X and Y matrices. Then the following relation holds

$$\mathcal{N}_{X,Y}(D_r \rho D_r^\dagger) = D_{Xr} \mathcal{N}_{X,Y}(\rho) D_{Xr}^\dagger, \tag{2.3.69}$$

and note that D_{Xr} is a tensor product of local displacement operators.

Phase-insensitive bosonic channels. A channel $\mathcal{N}$ is phase insensitive or phase covariant if

$$\mathcal{N}(e^{-i\hat{n}\phi} \rho e^{i\hat{n}\phi}) = e^{-i\hat{n}\phi} \mathcal{N}(\rho) e^{i\hat{n}\phi} \tag{2.3.70}$$

for all $\phi \in \mathbb{R}$ and input states $\rho \in \mathcal{D}(\mathcal{H})$.

A phase-insensitive, single-mode bosonic Gaussian channel adds an equal amount of

noise to each quadrature of the electromagnetic field, such that

$$X = \mathrm{diag}(\sqrt{\tau}, \sqrt{\tau}), \tag{2.3.71}$$

$$Y = \mathrm{diag}(\nu, \nu), \tag{2.3.72}$$

$$d = 0, \tag{2.3.73}$$

where $\tau \in [0, 1]$ corresponds to attenuation, $\tau \geq 1$ amplification, and ν is the variance of an additive noise. Moreover, the following inequalities should hold

$$\nu \geq 0, \tag{2.3.74}$$

$$\nu^2 \geq (1 - \tau)^2, \tag{2.3.75}$$

in order for the map to be a legitimate completely positive and trace preserving map. The channel is entanglement breaking [125] if the following inequality holds [126]

$$\nu \geq \tau + 1. \tag{2.3.76}$$

We now provide examples of phase-insensitive, bosonic Gaussian channels.

Quantum thermal channel. A quantum thermal channel is a phase-insensitive Gaussian channel that can be characterized by a beamsplitter of transmissivity $\eta \in (0, 1)$, coupling the signal input state with a thermal state with mean photon number $N_B \geq 0$, and followed by a partial trace over the environment. Let $\mathcal{B}^{\eta}_{AE}$ denote a beamsplitter with transmissivity $\eta \in (0, 1)$. Let $\theta(N_B)$ denote a thermal state with mean photon number N_B. Then the action of a thermal channel $\mathcal{L}^{\eta, N_B}_{A \to B}$ with the transmissivity parameter η and the thermal noise parameter N_B is defined as

$$\mathcal{L}^{\eta, N_B}_{A \to B}(\rho_A) \equiv \mathrm{Tr}_E(\mathcal{B}^{\eta}_{AE}(\rho_A \otimes \theta_E(N_B))) \ , \tag{2.3.77}$$

for all input states ρ_A.

In the Heisenberg picture, the beamsplitter transformation is given by the following Bogoliubov transformation:

$$\hat{b} = \sqrt{\eta}\hat{a} - \sqrt{1-\eta}\hat{e}, \tag{2.3.78}$$

$$\hat{e}' = \sqrt{1-\eta}\hat{a} + \sqrt{\eta}\hat{e}, \tag{2.3.79}$$

where $\hat{a}, \hat{b}$, $\hat{e}$, and $\hat{e}'$ are the annihilation operators representing the sender's input mode, the receiver's output mode, an environmental input mode, and an environmental output mode of the channel, respectively. If the mean photon number at the input of a thermal channel is no larger than N_S, then the total number of photons that make it through the channel to the receiver is no larger than $\eta N_S + (1-\eta)N_B$.

Pure-loss channel. A thermal channel is called a pure-loss channel if the thermal state in the environment mode has mean photon number $N_B = 0$. Let $\mathcal{L}^{\eta}_{A\to B}$ with the transmissivity parameter η denote a pure-loss channel. Then from (2.3.77) we get

$$\mathcal{L}^{\eta}_{A\to B}(\rho_A) \equiv \mathrm{Tr}_E(\mathcal{B}^{\eta}_{AE}(\rho_A \otimes |0\rangle\langle 0|_E)), \tag{2.3.80}$$

where $|0\rangle\langle 0|_E$ denotes the vacuum state in the mode E. Throughout this thesis, we denote a pure-loss channel by $\mathcal{L}^{\eta}$ and $\mathcal{L}^{\eta,0}$ interchangeably.

Quantum amplifier channel A quantum amplifier channel is a Gaussian channel that can be characterized by a two-mode squeezer with parameter $G > 1$, coupling the signal input state with a thermal state with mean photon number $N_B \geq 0$, and followed by a partial trace over the environment. Let Ξ^{G}_{AE} denote a two-mode squeezer with $G > 1$. Then the action of a quantum amplifier channel $\mathcal{A}^{G,N_B}$ on a state ρ_A is given by

$$\mathcal{A}^{G,N_B}_{A\to B}(\rho_A) \equiv \mathrm{Tr}_E(\Xi^{G}_{AE}(\rho_A \otimes \theta_E(N_B)), \tag{2.3.81}$$

where again $\theta_E(N_B)$ denotes a thermal state with mean photon number N_B.

In the Heisenberg picture, the two-mode squeezer implementing a quantum amplifier channel has the following Bogoliubov transformation:

$$\hat{b} = \sqrt{G}\hat{a} + \sqrt{G-1}\hat{e}^\dagger, \tag{2.3.82}$$

$$\hat{e}' = \sqrt{G-1}\hat{a}^\dagger + \sqrt{G}\hat{e}\ , \tag{2.3.83}$$

where $\hat{a}, \hat{b}$, $\hat{e}$, and $\hat{e}'$ correspond to the same parties as discussed above.

Quantum limited amplifier. When $N_B = 0$, the quantum amplifier channel is called the quantum limited amplifier channel. In other words, a quantum limited amplifier channel $\mathcal{A}^G_{A\to B}$ with the gain parameter G is defined as

$$\mathcal{A}^G_{A\to B}(\rho_A) \equiv \mathrm{Tr}_E(\Xi^G_{AE}(\rho_A \otimes |0\rangle\langle 0|_E)), \tag{2.3.84}$$

where $|0\rangle\langle 0|_E$ again denotes the vacuum state in the mode E. Throughout this thesis, we denote a quantum-limited amplifier channel by $\mathcal{A}^G$ and $\mathcal{A}^{G,0}$ interchangeably.

Additive-noise channel. An additive-noise channel is specified by the following completely positive and trace preserving map:

$$\mathcal{T}^\xi_{A\to B}(\rho) \equiv \int d^2\alpha\ P_\xi(\alpha) D_\alpha \rho D^\dagger_\alpha, \tag{2.3.85}$$

where $P_\xi = \exp(-|\alpha|^2/\xi)/(\pi\xi)$ and D_α is a displacement operator for the input mode. The variance $\xi > 0$ completely characterizes the channel $\mathcal{T}^\xi$, and it roughly represents the number of noise photons added to the input mode by the channel.

From [127, 128], it follows that an additive-noise channel $\mathcal{T}^\xi_{A\to B}$ can be expressed as a concatenation of a pure-loss channel $\mathcal{L}^\eta_{A\to B'}$ with transmissivity η followed by a quantum-

limited amplifier channel $\mathcal{A}^{1/\eta}_{B'\to B}$ with gain parameter $1/\eta$,

$$\mathcal{T}^{\xi}_{A\to B} = \mathcal{A}^{1/\eta}_{B'\to B} \circ \mathcal{L}^{\eta}_{A\to B'} \tag{2.3.86}$$

with $\xi = (1-\eta)/\eta$.

Joint phase covariance. Let $\mathcal{N}$ and $\mathcal{M}$ be quantum channels that take one input mode to m output modes. Then $\mathcal{N}$ and $\mathcal{M}$ are jointly phase covariant if the following holds:

$$\begin{aligned}
\mathcal{N}_{A\to B}\left(e^{i\hat{n}\phi}\rho e^{-i\hat{n}\phi}\right) &= \left(\bigotimes_{i=1}^{m} e^{i\hat{n}_i(-1)^{a_i}\phi}\right)\mathcal{N}_{A\to B}(\rho)\left(\bigotimes_{i=1}^{m} e^{-i\hat{n}_i(-1)^{a_i}\phi}\right), \\
\mathcal{M}_{A\to B}\left(e^{i\hat{n}\phi}\rho e^{-i\hat{n}\phi}\right) &= \left(\bigotimes_{i=1}^{m} e^{i\hat{n}_i(-1)^{a_i}\phi}\right)\mathcal{M}_{A\to B}(\rho)\left(\bigotimes_{i=1}^{m} e^{-i\hat{n}_i(-1)^{a_i}\phi}\right),
\end{aligned} \tag{2.3.87}$$

where $a_i \in \{0,1\}$ for $i \in \{1,\ldots,m\}$, and $\hat{n}_i$ is the number operator in the ith mode.

Homodyne measurement. A homodyne measurement is a Gaussian channel to measure the quadrature operator

$$\hat{x}_\phi = \cos\phi\hat{x} + \sin\phi\hat{p}\ , \tag{2.3.88}$$

and the corresponding probability of outcome is given by

$$p(x_\phi) = \mathrm{Tr}(|x_\phi\rangle\langle x_\phi|\rho)\ , \tag{2.3.89}$$

where $|x_\phi\rangle$ is an improper eigenvector of $\hat{x}_\phi$.

Photodetection. Let $\mathcal{P}$ denote the channel corresponding to the ideal photodetector, whose action on an input state ρ is defined as follows:

$$\mathcal{P}(\rho) \equiv \sum_{n=0}^{\infty} \langle n|\rho|n\rangle |n\rangle\langle n|\ . \tag{2.3.90}$$

The interpretation of this channel is that it measures the input state in the photon-number basis and then outputs the measured value in a classical register.

Throughout this thesis, we consider only those quantum channels that satisfy the fol-

lowing finite output entropy condition:

Condition 46 (Finite output entropy) *Let G be a Gibbs observable and $W \in [0, \infty)$. A quantum channel $\mathcal{N}$ satisfies the finite-output entropy condition with respect to G and W if*

$$\sup_{\rho\,:\,\mathrm{Tr}\{G\rho\}\leq W} H(\mathcal{N}(\rho)) < \infty, \tag{2.3.91}$$

2.4 Distance Measures for Quantum States and Channels

This section defines several distance measures relevant for the rest of the thesis. We begin by defining the trace distance, the fidelity, and the sine distance between two density operators. We then introduce the distance measures for distinguishing quantum channels. Finally, we present the notion of energy-constrained distance measures.

Definition 47 (Trace distance) *The trace distance between two operators $A, B \in \mathcal{L}(\mathcal{H}, \mathcal{H}')$ is defined as follows:*

$$\|A - B\|_1 \ . \tag{2.4.1}$$

The trace distance between two quantum states $\rho, \sigma \in \mathcal{D}(\mathcal{H})$ is an operationally relevant distance measure. In particular, consider the following hypothesis testing scenario: suppose that Alice prepares one of two quantum states ρ and σ, and suppose that it is equally likely a priori for her to prepare either ρ or σ. Furthermore, suppose that Bob can perform a binary POVM to distinguish ρ and σ. Then the maximum success probability to distinguish is linearly related to the normalized trace distance as follows:

$$p_{\mathrm{succ}} = \frac{1}{2}\left(1 + \frac{1}{2}\|\rho - \sigma\|_1\right) \ . \tag{2.4.2}$$

We will later invoke the following important properties of the trace distance between ρ and σ:

- **Isometric invariance**: Let U denote an isometry. Then the trace distance is invariant with respect to an isometric quantum operation as follows:

$$\|\rho - \sigma\|_1 = \|U\rho U^\dagger - U\sigma U^\dagger\|_1 \ . \tag{2.4.3}$$

- **Triangle inequality**: For any three quantum states $\rho, \sigma, \omega \in \mathcal{D}(\mathcal{H})$, the following inequality holds:

$$\|\rho - \omega\|_1 \leq \|\rho - \sigma\|_1 + \|\sigma - \omega\|_1 \ . \tag{2.4.4}$$

- **Monotonicity**: Let $\mathcal{N}_{A\to B}$ denote a quantum channel. Let $\rho, \sigma \in \mathcal{D}(\mathcal{H}_A)$. Then the trace distance is monotone with respect to the action of the channel $\mathcal{N}$:

$$\|\mathcal{N}(\rho) - \mathcal{N}(\sigma)\|_1 \leq \|\rho - \sigma\|_1 \ . \tag{2.4.5}$$

An alternate measure of the closeness of two quantum states is the fidelity, which we define below.

Definition 48 (Fidelity) *The fidelity between ρ and σ is defined as follows [129]:*

$$F(\rho, \sigma) \equiv \left\|\sqrt{\rho}\sqrt{\sigma}\right\|_1^2 . \tag{2.4.6}$$

Similar to the trace distance, the fidelity between two quantum states satisfies important properties, which we summarize below.

- **Multiplicativity**: The fidelity is multiplicative with respect to tensor products:

$$F(\rho_A \otimes \rho_B, \sigma_A \otimes \sigma_B) = F(\rho_A, \sigma_A)F(\rho_B, \sigma_B), \tag{2.4.7}$$

  where $\rho_A, \sigma_A \in \mathcal{D}(\mathcal{H}_A)$ and $\rho_B, \sigma_B \in \mathcal{D}(\mathcal{H}_B)$.

- **Isometric invariance**: Let U denote an isometry. Let $\rho, \sigma \in \mathcal{D}(\mathcal{H})$. Then the

following holds:

$$F(\rho,\sigma) = F(U\rho U^\dagger, U\sigma U^\dagger) \ . \tag{2.4.8}$$

- **Monotonicity**: Let $\mathcal{N}_{A\to B}$ denote a quantum channel. Let $\rho,\sigma \in \mathcal{D}(\mathcal{H}_A)$. Then the fidelity is monotone with respect to the action of the channel $\mathcal{N}$:

$$F(\rho,\sigma) \leq F(\mathcal{N}(\rho),\mathcal{N}(\sigma)) \ . \tag{2.4.9}$$

- **Joint concavity of the root fidelity**: Let p_X denote a probability distribution. Let $\rho_x,\sigma_x \in \mathcal{D}(\mathcal{H})$ for all x. Then the root fidelity is jointly concave with respect to its input arguments:

$$\sqrt{F}\left(\sum_x p_X(x)\rho_x, \sum_x p_X(x)\sigma_x\right) \geq \sum_x p_X(x)\sqrt{F}(\rho_x,\sigma_x) \ . \tag{2.4.10}$$

Definition 49 (Sine distance) *The sine distance between two density operators $\rho,\sigma \in \mathcal{D}(\mathcal{H})$ is defined as [130–133]*

$$C(\rho,\sigma) \equiv \sqrt{1-F(\rho,\sigma)}. \tag{2.4.11}$$

Definition 50 (Relation between fidelity and trace distance) *The following inequalities relate the fidelity and the trace distance [134]:*

$$1-\sqrt{F(\rho,\sigma)} \leq \frac{1}{2}\left\|\rho-\sigma\right\|_1 \leq \sqrt{1-F(\rho,\sigma)} \ , \tag{2.4.12}$$

with the lower bound following from the Powers-Størmer inequality [135] and the upper bound from Uhlmann's theorem [129]. See also [134].

The notions of trace distance and fidelity can be extended to distinguish two quantum operations. We begin by defining the diamond norm of a Hermiticity preserving linear

map.

Definition 51 (Diamond norm) *Let $\mathcal{S}_{A\to B}$ denote a Hermiticity preserving linear map. Then the diamond norm of $\mathcal{S}$ is defined as*

$$\left\|\mathcal{S}\right\|_{\diamond} \equiv \sup_{\rho_{RA}\in\mathcal{D}(\mathcal{H}_R\otimes\mathcal{H}_A)} \left\|(\mathcal{I}_R\otimes\mathcal{S}_{A\to B})(\rho_{RA})\right\|_1 \ , \tag{2.4.13}$$

where $\mathcal{I}_R$ is the identity map acting on a Hilbert space $\mathcal{H}_R$ corresponding to an arbitrarily large reference system [136].

From the convexity of the trace norm (2.1.10) and the Schmidt decomposition theorem as in Definition 14, it suffices to optimize with respect to input states ρ that are pure. A distance measure to distinguish two quantum operations can be defined as follows based on the diamond norm.

Definition 52 (Diamond distance) *Let $\mathcal{N}_{A\to B}$ and $\mathcal{M}_{A\to B}$ denote quantum channels. Then the diamond distance is defined as*

$$\left\|\mathcal{N}-\mathcal{M}\right\|_{\diamond} \equiv \sup_{\rho_{RA}\in\mathcal{D}(\mathcal{H}_R\otimes\mathcal{H}_A)} \left\|(\mathcal{I}_R\otimes\mathcal{N}_{A\to B})(\rho_{RA}) - (\mathrm{id}_R\otimes\mathcal{M}_{A\to B})(\rho_{RA})\right\|_1 , \tag{2.4.14}$$

where $\mathcal{I}_R$ is the identity map acting on a Hilbert space $\mathcal{H}_R$.

Similar to the trace distance between two quantum states, the diamond distance is an operationally relevant distance measure to distinguish two quantum channels. Consider the following hypothesis testing task: suppose that Alice can implement one of two quantum channels $\mathcal{N}$ and $\mathcal{M}$. Bob prepares a state ρ_{RA} and sends system A to Alice. Then Alice flips a fair coin and, based on the outcome, applies either $\mathcal{N}$ or $\mathcal{M}$, and then sends the output system B to Bob. Finally, Bob measures systems R and B to figure out which channel Alice applied. In such a scenario, the maximum success probability to distinguish $\mathcal{N}$ and $\mathcal{M}$ is linearly related to the normalized diamond-norm distance between $\mathcal{N}$ and $\mathcal{M}$

as follows:

$$p_{\text{succ}} = \frac{1}{2}\left(1 + \frac{1}{2}\|\mathcal{N} - \mathcal{M}\|_{\diamond}\right) \tag{2.4.15}$$

Definition 53 (Channel fidelity) *Let $\mathcal{N}_{A\to B}$ and $\mathcal{M}_{A\to B}$ denote quantum channels. The channel fidelity between $\mathcal{N}$ and $\mathcal{M}$ is defined as*

$$F(\mathcal{N}, \mathcal{M}) \equiv \inf_{\rho_{RA} \in \mathcal{D}(\mathcal{H}_R \otimes \mathcal{H}_A)} F((\mathcal{I}_R \otimes \mathcal{N}_{A\to B})(\rho_{RA}), (\mathcal{I}_R \otimes \mathcal{M}_{A\to B})(\rho_{RA})), \tag{2.4.16}$$

where $\mathcal{I}_R$ is the identity map acting on a Hilbert space $\mathcal{H}_R$.

From joint concavity of root fidelity and monotonicity of the square function, the optimization in (2.4.16) can be reduced to pure states in $\mathcal{H}_{RA}$.

Definition 54 (Energy-constrained diamond distance) *Let H_A denote a Hamiltonian corresponding to the quantum system A. Let $\mathcal{N}_{A\to B}$ and $\mathcal{M}_{A\to B}$ be two quantum channels. Let R denote a reference system. Then the energy-constrained diamond distance between $\mathcal{N}_{A\to B}$ and $\mathcal{M}_{A\to B}$ is defined for $E \in [0, \infty)$ as [137, 138]*

$$\|\mathcal{N}_{A\to B} - \mathcal{M}_{A\to B}\|_{\diamond E} \equiv \sup_{\rho_{RA}:\text{Tr}(H_A \rho_A) \leq E} \|\mathcal{N}_{A\to B}(\rho_{RA}) - \mathcal{M}_{A\to B}(\rho_{RA})\|_1 \ , \tag{2.4.17}$$

where $\rho_{RA} \in \mathcal{D}(\mathcal{H}_{RA})$, and it is implicit that the identity channel $\mathcal{I}_R$ acts on system R.

From the convexity of the trace norm and the Schmidt decomposition theorem, it suffices to optimize (2.4.17) with respect to input states ρ_{RA} that are pure and satisfy the energy constraint $\text{Tr}(H_A \rho_A) \leq E$. Moreover, we note that due to the supremum being taken, the diamond norm might only be achieved in the limit (for example, for a sequence of two-mode squeezed vacuum states with squeezing strength becoming arbitrarily large, as discussed in [117]).

Definition 55 (Energy-constrained channel fidelity) *The energy-constrained channel fidelity between two quantum channels $\mathcal{N}_{A\to B}$ and $\mathcal{M}_{A\to B}$ for $E \in [0, \infty)$ is defined as*

[93, 139]

$$F_E(\mathcal{N}_{A\to B}, \mathcal{M}_{A\to B}) \equiv \inf_{\rho_{RA}:\mathrm{Tr}(H_A\rho_A)\leq E} F(\mathcal{N}_{A\to B}(\rho_{RA}), \mathcal{M}_{A\to B}(\rho_{RA})), \tag{2.4.18}$$

$\rho_{RA} \in \mathcal{D}(\mathcal{H}_R \otimes \mathcal{H}_A)$, and again it is implicit that the identity channel $\mathcal{I}_R$ acts on system R.

Definition 56 (Energy-constrained sine distance) *The energy-constrained sine distance between two quantum channels $\mathcal{N}_{A\to B}$ and $\mathcal{M}_{A\to B}$ for $E \in [0, \infty)$ is defined as [93, 139]*

$$C_E(\mathcal{N}_{A\to B}, \mathcal{M}_{A\to B}) \equiv \sup_{\rho_{RA}:\mathrm{Tr}(H_A\rho_A)\leq E} \sqrt{1 - F(\mathcal{N}_{A\to B}(\rho_{RA}), \mathcal{M}_{A\to B}(\rho_{RA}))}. \tag{2.4.19}$$

For both the energy-constrained channel fidelity and the energy-constrained sine distance between two quantum channels $\mathcal{N}$ and $\mathcal{M}$, it is sufficient to optimize over pure input states $\rho_{RA} \in \mathcal{D}(\mathcal{H}_{RA})$ satisfying the energy constraint.

Definition 57 (Relation between (2.4.17) **and** (2.4.18)**)** *Similar to Definition 50, we have the following relation between the energy-constrained channel fidelity and the energy-constrained diamond distance:*

$$1 - \sqrt{F_E(\mathcal{N}_{A\to B}, \mathcal{M}_{A\to B})} \leq \frac{1}{2}\|\mathcal{N}_{A\to B} - \mathcal{M}_{A\to B}\|_{\diamond E} \leq C_E(\mathcal{N}_{A\to B}, \mathcal{M}_{A\to B}) \ , \tag{2.4.20}$$

where $\mathcal{N}_{A\to B}$ and $\mathcal{M}_{A\to B}$ are quantum channels, $E \in [0, \infty)$, and $C_E(\mathcal{N}_{A\to B}, \mathcal{M}_{A\to B})$ is given by (2.4.19).

2.5 Notions of Convergence for Quantum Channels

In this section, we briefly summarize three different notions of convergence for quantum channels: uniform and strong convergence (as presented in [140]), and uniform convergence on the set of density operators whose marginals on the channel input have bounded energy

(as presented in [137, 138]). Uniform and strong convergence in the context of infinite-dimensional quantum channels were studied in [140]. A connection between the notion of strong convergence and the notion of uniform convergence over energy-bounded states was established in [137]. Later, these different topologies of convergence were studied in the context of linear bosonic channels and Gaussian dilatable channels in [141]. Furthermore, topologies of convergence in the context of teleportation simulation of physically relevant phase-insensitive bosonic Gaussian channels have been investigated in [117].

We first recall the notion of uniform convergence for quantum channels.

Definition 58 (Uniform convergence) *Let $\{\mathcal{M}^k_{A\to B}\}_k$ denote a sequence of quantum channels, where each channel takes a trace-class operator acting on a separable Hilbert space $\mathcal{H}_A$ to a trace-class operator acting on a separable Hilbert space $\mathcal{H}_B$. Then the channel sequence $\{\mathcal{M}^k_{A\to B}\}_k$ converges uniformly to another quantum channel $\mathcal{N}_{A\to B}$ if the following holds:*

$$\lim_{k\to\infty} \left\| \mathcal{M}^k_{A\to B} - \mathcal{N}_{A\to B} \right\|_\diamond = 0 \ . \tag{2.5.1}$$

Qualitatively, the uniform convergence of a sequence of quantum channels to another quantum channel implies that the convergence is independent of the input state.

Definition 59 (Strong convergence) *Let $\{\mathcal{M}^k_{A\to B}\}_k$ denote a sequence of quantum channels, where each channel takes a trace-class operator acting on a separable Hilbert space $\mathcal{H}_A$ to a trace-class operator acting on a separable Hilbert space $\mathcal{H}_B$. Then the channel sequence $\{\mathcal{M}^k_{A\to B}\}_k$ converges to another quantum channel $\mathcal{N}_{A\to B}$ in the strong sense if for all $\psi_{RA} \in \mathcal{D}(\mathcal{H}_R \otimes \mathcal{H}_A)$, the following holds:*

$$\lim_{k\to\infty} \left\| \mathcal{M}^k_{A\to B}(\psi_{RA}) - \mathcal{N}_{A\to B}(\psi_{RA}) \right\|_1 = 0 \ , \tag{2.5.2}$$

which can be summarized more compactly as

$$\sup_{\psi_{RA}\in\mathcal{D}(\mathcal{H}_{RA})} \lim_{k\to\infty} \left\| \mathcal{M}^k_{A\to B}(\psi_{RA}) - \mathcal{N}_{A\to B}(\psi_{RA}) \right\|_1 = 0 \ . \tag{2.5.3}$$

Here, it is implicit that the identity channel acts on the reference system R.

Therefore, convergence in the strong sense is the statement that, for each fixed input quantum state ψ_{RA}, the sequence $\{\mathcal{M}^k_{A\to B}(\psi_{RA})\}_k$ of states converges to the state $\mathcal{N}_{A\to B}(\psi_{RA})$ in trace norm. It is important to note that the different orders in which the limits and suprema are taken in (2.5.1) and (2.5.3) lead to physically distinct situations, as discussed in [117]. Moreover, one can infer from the definitions of strong and uniform convergence that the notion of strong convergence is a weaker notion of convergence, in fact implied by uniform convergence.

Definition 60 (Bounded energy uniform convergence) *Let H_A denote an energy observable corresponding to the quantum system A. Then the channel sequence $\{\mathcal{M}^k_{A\to B}\}_k$ converges uniformly (on the set of density operators whose marginals on the channel input have bounded energy) to another quantum channel $\mathcal{N}_{A\to B}$ if the following holds for some $E \in [0,\infty)$:*

$$\lim_{k\to\infty} \left\| \mathcal{M}^k_{A\to B} - \mathcal{N}_{A\to B} \right\|_{\diamond E} = 0 \ . \tag{2.5.4}$$

We note that the strong convergence of a sequence of infinite-dimensional channels is equivalent to uniform convergence on the set of energy-bounded density operators [137].

2.6 Approximate Degradability of Quantum Channels

The concept of approximate degradability was introduced in [66]. The following two definitions of approximate degradability will be useful in our thesis.

Definition 61 (ε-degradable [66]) *A channel $\mathcal{N}_{A\to B}$ is ε-degradable if there exists a channel $\mathcal{D}_{B\to E}$ such that*

$$\frac{1}{2} \left\| \hat{\mathcal{N}} - \mathcal{D} \circ \mathcal{N} \right\|_{\diamond} \leq \varepsilon \ , \tag{2.6.1}$$

where $\hat{\mathcal{N}}$ denotes a complementary channel of $\mathcal{N}$.

Definition 62 (ε-close-degradable [66]) *A channel $\mathcal{N}_{A\to B}$ is ε-close-degradable if there exists a degradable channel $\mathcal{M}_{A\to B}$ such that*

$$\frac{1}{2}\left\|\mathcal{N}-\mathcal{M}\right\|_{\diamond}\leq\varepsilon\ . \tag{2.6.2}$$

Remark 63 *Let $\mathcal{N}_{A\to B}$ be a quantum channel that is ε-close-degradable. Then $\mathcal{N}_{A\to B}$ is $\varepsilon+2\sqrt{\varepsilon}$-degradable by [66, Proposition A.5]. A converse implication is not known to hold.*

Remark 64 *The notion of ε-degradable and ε-close degradable quantum channels was defined in [66] for finite-dimensional channels. In this thesis, we generalize it to infinite-dimensional channels by replacing the diamond norm in* (2.6.1) *and* (2.6.2) *with the energy-constrained diamond norm.*

2.7 Quantum Channel Capacities

The energy-constrained quantum and private capacities of quantum channels have been defined in [62, Section III]. In what follows, we review the definition of quantum communication and private communication codes, achievable rates, and regularized formulas for energy-constrained quantum and private capacities.

Energy-constrained quantum capacity: An (n,M,G,W,ε) code for energy-constrained quantum communication consists of an encoding channel $\mathcal{E}^n:\mathcal{T}(\mathcal{H}_S)\to\mathcal{T}(\mathcal{H}_A^{\otimes n})$ and a decoding channel $\mathcal{D}^n:\mathcal{T}(\mathcal{H}_B^{\otimes n})\to\mathcal{T}(\mathcal{H}_S)$, where $M=\dim(\mathcal{H}_S)$. The energy constraint is such that the following bound holds for all states resulting from the output of the encoding channel $\mathcal{E}^n$:

$$\operatorname{Tr}\{\overline{G}_n\mathcal{E}^n(\rho_S)\}\leq W\ , \tag{2.7.1}$$

where $\rho_S\in\mathcal{D}(\mathcal{H}_S)$. Note that

$$\operatorname{Tr}\left\{\overline{G}_n\mathcal{E}^n(\rho_S)\right\}=\operatorname{Tr}\left\{G\overline{\rho}_n\right\}, \tag{2.7.2}$$

where

$$\overline{\rho}_n \equiv \frac{1}{n}\sum_{i=1}^{n} \mathrm{Tr}_{A^n\setminus A_i}\{\mathcal{E}^n(\rho_S)\}. \tag{2.7.3}$$

due to the i.i.d. nature of the observable $\overline{G}_n$. Furthermore, the quantum communication code satisfies the following reliability condition such that for all pure states $\phi_{RS} \in \mathcal{D}(\mathcal{H}_R \otimes \mathcal{H}_S)$,

$$F(\phi_{RS}, (\mathrm{id}_R \otimes [\mathcal{D}^n \circ \mathcal{N}^{\otimes n} \circ \mathcal{E}^n])(\phi_{RS})) \geq 1 - \varepsilon \ , \tag{2.7.4}$$

where $\mathcal{H}_R$ is isomorphic to $\mathcal{H}_S$. A rate R is achievable for quantum communication over $\mathcal{N}$ subject to the energy constraint W if for all $\varepsilon \in (0,1)$, $\delta > 0$, and sufficiently large n, there exists an $(n, 2^{n[R-\delta]}, G, W, \varepsilon)$ energy-constrained quantum communication code. The energy-constrained quantum capacity $Q(\mathcal{N}, G, W)$ of $\mathcal{N}$ is equal to the supremum of all achievable rates.

If the channel $\mathcal{N}$ satisfies Condition 46 and G is a Gibbs observable, then the quantum capacity $Q(\mathcal{N}, G, W)$ is equal to the regularized energy-constrained coherent information of the channel $\mathcal{N}$ [62]

$$Q(\mathcal{N}, G, W) = \lim_{n\to\infty} \frac{1}{n} I_c(\mathcal{N}^{\otimes n}, \overline{G}_n, W), \tag{2.7.5}$$

where the energy-constrained coherent information of the channel is defined as [62]

$$I_c(\mathcal{N}, G, W) \equiv \sup_{\rho : \mathrm{Tr}\{\rho G\} \leq W} H(\mathcal{N}(\rho)) - H(\hat{\mathcal{N}}(\rho)), \tag{2.7.6}$$

and $\hat{\mathcal{N}}$ denotes a complementary channel of $\mathcal{N}$. Note that another definition of energy-constrained quantum communication is possible, but it leads to the same value for the capacity in the asymptotic limit of many channel uses [62].

Energy-constrained private capacity. An $(n, M, G, W, \varepsilon)$ code for private communication consists of a set $\{\rho^m_{A^n}\}_{m=1}^M$ of quantum states, each in $\mathcal{D}(\mathcal{H}_A^{\otimes n})$, and a POVM $\{\Lambda^m_{B^n}\}_{m=1}^M$

such that

$$\mathrm{Tr}\left\{\overline{G}_n \rho_{A^n}^m\right\} \leq W, \tag{2.7.7}$$

$$\mathrm{Tr}\{\Lambda_{B^n}^m \mathcal{N}^{\otimes n}(\rho_{A^n}^m)\} \geq 1-\varepsilon, \tag{2.7.8}$$

$$\frac{1}{2}\left\|\hat{\mathcal{N}}^{\otimes n}(\rho_{A^n}^m) - \omega_{E^n}\right\|_1 \leq \varepsilon, \tag{2.7.9}$$

for all $m \in \{1,\ldots,M\}$, with ω_{E^n} some fixed state in $\mathcal{D}(\mathcal{H}_E^{\otimes n})$. In the above, $\hat{\mathcal{N}}$ is a channel complementary to $\mathcal{N}$. A rate R is achievable for private communication over $\mathcal{N}$ subject to energy constraint W if for all $\varepsilon \in (0,1)$, $\delta > 0$, and sufficiently large n, there exists an $(n, 2^{n[R-\delta]}, G, W, \varepsilon)$ private communication code. The energy-constrained private capacity $P(\mathcal{N}, G, W)$ of $\mathcal{N}$ is equal to the supremum of all achievable rates.

An upper bound on the energy-constrained private capacity of a channel has been established in [62], but the lower bound still needs a detailed proof. However, the results in [62] suggest the validity of the following form. If the channel $\mathcal{N}$ satisfies Condition 46 and G is a Gibbs observable, then the energy-constrained private capacity $P(\mathcal{N}, G, W)$ is given by the regularized energy-constrained private information of the channel:

$$P(\mathcal{N}, G, W) = \lim_{n\to\infty} \frac{1}{n} P^{(1)}(\mathcal{N}^{\otimes n}, \overline{G}_n, W), \tag{2.7.10}$$

where the energy-constrained private information is defined as

$$P^{(1)}(\mathcal{N}, G, W) \equiv \sup_{\bar{\rho}_{\mathcal{E}_A} : \mathrm{Tr}\{G\bar{\rho}_{\mathcal{E}_A}\} \leq W} \int dx\ p_X(x)[D(\mathcal{N}(\rho_A^x)\|\mathcal{N}(\bar{\rho}_{\mathcal{E}_A})) - D(\hat{\mathcal{N}}(\rho_A^x)\|\hat{\mathcal{N}}(\bar{\rho}_{\mathcal{E}_A}))], \tag{2.7.11}$$

$\bar{\rho}_{\mathcal{E}_A} \equiv \int dx\ p_X(x)\rho_A^x$ is an average state of the ensemble

$$\mathcal{E}_A \equiv \{p_X(x), \rho_A^x\}, \tag{2.7.12}$$

and $\hat{\mathcal{N}}$ denotes a complementary channel of $\mathcal{N}$. Note that another definition of energy-

constrained private communication is possible, but it leads to the same value for the capacity in the asymptotic limit of many channel uses [62].

Remark 65 *The unconstrained quantum and private capacities of a quantum channel $\mathcal{N}$ are defined in the same way as above, but without the energy constraints demanded in* (2.7.1) *and* (2.7.7)*. As a consequence of these definitions and the fact that the set of states with finite but arbitrarily large energy is dense in the set of all states, for channels satisfying the finite output-entropy condition for every energy $W \geq 0$, the unconstrained quantum and private capacities are respectively given by*

$$\sup_{W\geq 0} Q(\mathcal{N}, G, W), \qquad \sup_{W\geq 0} P(\mathcal{N}, G, W). \tag{2.7.13}$$

2.8 Continuity of Information Quantities and Channel Capacities

In this section, we recall continuity bounds for the conditional quantum entropy with energy constraints and for capacities of quantum channels. We also derive a theorem on the continuity of output entropy for infinite-dimensional systems with finite average energy constraints.

2.8.1 Continuity of Conditional Quantum Entropy

The following lemma is a uniform continuity bound for the conditional quantum entropy with energy constraints [114]:

Lemma 1 (Meta-Lemma 17, [114]) *For a Gibbs observable $G \in \mathcal{P}(\mathcal{H}_A)$, and states $\omega_{AB}, \tau_{AB} \in \mathcal{D}(\mathcal{H}_A \otimes \mathcal{H}_B)$, such that $\frac{1}{2}\left\|\omega_{AB} - \tau_{AB}\right\|_1 \leq \varepsilon < \varepsilon' \leq 1$, $\operatorname{Tr}\{(G \otimes I_B)\omega_{AB}\}$, $\operatorname{Tr}\{(G \otimes I_B)\tau_{AB}\} \leq W$, where $W \in [0, \infty)$ and $\delta = (\varepsilon' - \varepsilon)/(1 + \varepsilon')$, the following inequality holds*

$$|H(A|B)_\omega - H(A|B)_\tau| \leq (2\varepsilon' + 4\delta) H(\gamma(W/\delta)) + g(\varepsilon') + 2h_2(\delta)\ . \tag{2.8.1}$$

2.8.2 Continuity of Output Entropy

The following theorem on continuity of output entropy for infinite-dimensional systems with finite average energy constraints is a direct consequence of [142, Theorem 11] and Lemma 1.

Theorem 66 *Let $\mathcal{N}_{A\to B}$ and $\mathcal{M}_{A\to B}$ be quantum channels, $G \in \mathcal{P}(\mathcal{H}_B)$ be a Gibbs observable, such that*

$$\mathrm{Tr}\{\overline{G}_n \mathcal{N}^{\otimes n}(\rho_{A^n})\},\ \mathrm{Tr}\{\overline{G}_n \mathcal{M}^{\otimes n}(\rho_{A^n})\} \leq W\ , \tag{2.8.2}$$

where $W \in [0,\infty)$ and $\rho_{RA^n} \in \mathcal{D}(\mathcal{H}_R \otimes \mathcal{H}_A^{\otimes n})$. If $\frac{1}{2}\left\|\mathcal{N}-\mathcal{M}\right\|_\diamond \leq \varepsilon < \varepsilon' \leq 1$ and $\delta = (\varepsilon'-\varepsilon)/(1+\varepsilon')$, then the following inequality holds

$$\begin{aligned}\left|H((\mathrm{id}_R \otimes \mathcal{N}_{A\to B}^{\otimes n})(\rho_{RA^n})) - H((\mathrm{id}_R \otimes \mathcal{M}_{A\to B}^{\otimes n})(\rho_{RA^n}))\right| \\ \leq n[(2\varepsilon'+4\delta)H(\gamma(W/\delta)) + g(\varepsilon') + 2h_2(\delta)].\end{aligned} \tag{2.8.3}$$

Proof. Let

$$\rho^j = (\mathrm{id}_R \otimes \mathcal{M}_{A\to B}^{\otimes j} \otimes \mathcal{N}_{A\to B}^{\otimes (n-j)})(\rho_{RA^n})\ , \tag{2.8.4}$$

and consider the following chain of inequalities:

$$
\begin{aligned}
&|H(RB^n)_{\rho^0} - H(RB^n)_{\rho^n}| \\
&= \left| \sum_{j=1}^{n} H(RB^n)_{\rho^{j-1}} - H(RB^n)_{\rho^j} \right| && (2.8.5) \\
&\leq \sum_{j=1}^{n} \left| H(RB^n)_{\rho^{j-1}} - H(RB^n)_{\rho^j} \right| && (2.8.6) \\
&= \sum_{j=1}^{n} \left| H(B_j|RB_1 \cdots B_{j-1}B_{j+1} \cdots B_n)_{\rho^{j-1}} - H(B_j|RB_1 \cdots B_{j-1}B_{j+1} \cdots B_n)_{\rho^j} \right| && (2.8.7) \\
&\leq n[(2\varepsilon' + 4\delta) \left(\sum_{j=1}^{n} \frac{1}{n} H(\gamma(W_j/\delta)) \right) + g(\varepsilon') + 2h_2(\delta)] && (2.8.8) \\
&\leq n[(2\varepsilon' + 4\delta) H \left(\frac{1}{n} \sum_{j=1}^{n} \gamma(W_j/\delta) \right) + g(\varepsilon') + 2h_2(\delta)] && (2.8.9) \\
&\leq n[(2\varepsilon' + 4\delta) H \left(\gamma(W/\delta) \right) + g(\varepsilon') + 2h_2(\delta)] \ . && (2.8.10)
\end{aligned}
$$

The first inequality follows from the triangle inequality. The second equality follows from the fact that the states ρ^j and ρ^{j-1} are the same except for the jth output system. Let W_j denote an energy constraint on the jth output state of both the channels $\mathcal{N}$ and $\mathcal{M}$, i.e., $\mathrm{Tr}\{G\mathcal{N}(\rho_{A_j})\}$, $\mathrm{Tr}\{G\mathcal{M}(\rho_{A_j})\} \leq W_j$ and $\frac{1}{n}\sum_j W_j \leq W$. Then the second inequality follows because $\frac{1}{2}\|\rho^j - \rho^{j-1}\|_1 \leq \varepsilon$ for the given channels, and we use Lemma 1 for the jth output system. The third inequality follows from concavity of entropy. The final inequality follows because

$$
\mathrm{Tr}\left\{ \frac{1}{n} \sum_{j=1}^{n} G \ \gamma(W_j/\delta) \right\} = \frac{1}{n} \sum_{j=1}^{n} \mathrm{Tr}\{G \ \gamma(W_j/\delta)\} \leq W/\delta, \tag{2.8.11}
$$

and $\gamma(W/\delta)$ is the Gibbs state that maximizes the entropy corresponding to the energy W/δ. ■

2.8.3 Continuity of Capacities for Channels

The continuity of various capacities of quantum channels has been discussed in [142, Lemma 12]. The general form for the classical, quantum, or private capacity of a channel $\mathcal{N}$ can be defined as $F(\mathcal{N}) = \lim_{n\to\infty} \frac{1}{n} \sup_{P^{(n)}} f_n(\mathcal{N}^{\otimes n}, P^{(n)})$, where $\{f_n\}_n$ denotes a family of functions, and $P^{(n)}$ represents states or parameters over which an optimization is performed. Then the following lemma holds [142].

Lemma 2 (Lemma 12, [142]) *If $F(\mathcal{N}) = \lim_{n\to\infty} \frac{1}{n} \sup_{P^{(n)}} f_n(\mathcal{N}^{\otimes n}, P^{(n)})$ for a channel $\mathcal{N}$ and $\forall\ n, P^{(n)}$, $\left|f_n(\mathcal{N}^{\otimes n}, P^{(n)}) - f_n(\mathcal{M}^{\otimes n}, P^{(n)})\right| \leq nc$, then $|F(\mathcal{N}) - F(\mathcal{M})| \leq c$.*

2.9 Karush-Kuhn-Tucker (KKT) Conditions

In this section, we review the Karush-Kuhn-Tucker (KKT) conditions used in solving convex optimization problems with inequality constraints. We will invoke these conditions in Chapter 5 to solve quadratic programs.

Let $x \in \mathbb{R}^n$ and let $f : \mathbb{R}^n \to \mathbb{R}$. Consider the following primal optimization problem:

$$\begin{aligned} \min_{x\in\mathbb{R}^n} \quad & f(x) \\ \text{subject to} \quad & u_i(x) \leq 0,\ \forall i \in \{1,\ldots,k\} \\ & v_j(x) = 0,\ \forall j \in \{1,\ldots,l\} \end{aligned} \tag{2.9.1}$$

Let $L(x, a, b)$ denote a Lagrangian with the following form:

$$L(x, a, b) \equiv f(x) + \sum_{i=1}^{k} a_i u_i(x) + \sum_{j=1}^{l} b_j v_j(x), \tag{2.9.2}$$

where $a \equiv (a_1, \ldots, a_k)$ and $b \equiv (b_1, \ldots, b_l)$, and $a_i, b_i \in \mathbb{R}$.

Using the Lagrange dual function:

$$g(a, b) \equiv \min_{x\in\mathbb{R}^n} L(x, a, b)\ , \tag{2.9.3}$$

the dual problem corresponding to the optimization in (2.9.1) can be defined as follows

(see [143] for a review):

$$\begin{aligned} \max_{a,b} \quad & g(a,b) \\ \text{subject to} \quad & a_i \geq 0,\ \forall i \in \{1,\ldots,k\}, \end{aligned} \tag{2.9.4}$$

where $b \in \mathbb{R}^l$.

Let $\tilde{x}$ denote a primal feasible point and let $(\tilde{a}, \tilde{b})$ denote a dual feasible point. Then it is easy to show that $f(\tilde{x}) \geq g(\tilde{a}, \tilde{b})$, which is the weak duality condition. To see this, consider the following chain of inequalities:

$$g(\tilde{a}, \tilde{b}) = \min_{x \in \mathbb{R}^n} f(x) + \sum_{i=1}^{k} \tilde{a}_i u_i(x) + \sum_{j=1}^{l} \tilde{b}_j v_j(x) \tag{2.9.5}$$

$$\leq f(\tilde{x}) + \sum_{i=1}^{k} \tilde{a}_i u_i(\tilde{x}) + \sum_{j=1}^{l} \tilde{b}_j v_j(\tilde{x}) \tag{2.9.6}$$

$$\leq f(\tilde{x})\ . \tag{2.9.7}$$

The first equality follows from (2.9.2) and (2.9.3). The first inequality follows due to the minimization over all $x \in \mathbb{R}^n$ in (2.9.5). Since $\tilde{x}$ is a primal feasible point, it satisfies $v_j(\tilde{x}) = 0, \forall j$ and $u_i(\tilde{x}) \leq 0, \forall i$. Moreover, since $\tilde{a}$ is a dual feasible point, $\tilde{a}_i \geq 0, \forall i$. Collectively, these conditions imply that $\sum_{i=1}^{k} \tilde{a}_i u_i(\tilde{x}) \leq 0$ and $\sum_{j=1}^{l} \tilde{b}_j v_j(\tilde{x}) = 0$, which leads to the last inequality.

The duality gap $f(\tilde{x}) - g(\tilde{a}, \tilde{b})$ provides a way to bound how suboptimal primal and dual feasible points are. Let f^* denote the primal optimal value and g^* the dual optimal value. Then the following inequalities hold:

$$f(\tilde{x}) - f^* \leq f(\tilde{x}) - g^* \leq f(\tilde{x}) - g(\tilde{a}, \tilde{b}), \tag{2.9.8}$$

which follow from the weak duality condition in (2.9.7) and from the definitions of the

primal and dual optimal values. Thus we get

$$f^* \in [f(\tilde{x}), g(\tilde{a}, \tilde{b})] \quad \text{and} \quad g^* \in [f(\tilde{x}), g(\tilde{a}, \tilde{b})] \ , \tag{2.9.9}$$

which implies that the optimality of $f(\tilde{x})$ and $g(\tilde{a}, \tilde{b})$ depend on the the duality gap. In other words, if the duality gap is zero, $\tilde{x}$ is a primal optimal point and $(\tilde{a}, \tilde{b})$ is a dual optimal point.

We now describe the KKT conditions for the aforementioned optimization problem, which are necessary conditions in the sense that if a primal optimal point x^* and a dual optimal point (a^*, b^*) with zero duality gap exist, they satisfy the KKT conditions. We later will argue when the KKT conditions are also sufficient for the optimality of a solution. The KKT conditions are given by

$$\begin{aligned}
\text{Stationarity condition} \quad & \partial_x L(x, a, b)|_{x^*} = 0 \\
\text{Complementary slackness} \quad & a_i^* u_i(x^*) = 0, \forall i \in \{1, \ldots, k\} \\
\text{Primal feasibility} \quad & u_i(x^*) \leq 0, \ \forall i \in \{1, \ldots, k\} \\
& v_j(x^*) = 0, \forall j \in \{1, \ldots, l\} \\
\text{Dual feasibility} \quad & a_i^* \geq 0, \forall i \in \{1, \ldots, k\}
\end{aligned} \tag{2.9.10}$$

We provide a brief proof for why primal and dual optimal points with zero duality gap satisfy the KKT conditions. First note that if x^* is a primal optimal solution, then it satisfies the primal feasibility conditions, as a consequence of (2.9.1). Similarly, if (a^*, b^*) is a dual optimal solution, then as a consequence of (2.9.4), it satisfies the dual feasibility condition. Moreover, the zero duality gap implies that inequalities in (2.9.5)–(2.9.7) should be saturated. Therefore, the primal optimal point x^* minimizes $L(x, a^*, b^*)$, which implies that the partial derivative of $L(x, a^*, b^*)$ at $x = x^*$ is equal to zero. In other words, the

stationarity condition is satisfied. Finally, the zero duality gap further implies that

$$\sum_i a_i^* u_i(x^*) = 0. \tag{2.9.11}$$

Since $a_i^* u_i(x^*) \leq 0$, $\forall i \in \{1, \ldots, k\}$, from (2.9.11) we get that $a_i^* u_i(x^*) = 0$, $\forall i$. Thus the complementary slackness is satisfied. This completes the proof.

In our work, we solve an optimization problem in which $f(x)$ is a convex quadratic function in x, and $u_i(x)$ and $v_j(x)$ are linear in x. Thus the Lagrangian in (2.9.2) is a convex function in x. We now argue that for such optimization problems, the KKT conditions are both necessary and sufficient. Suppose that $\bar{x}$ and $(\bar{a}, \bar{b})$ satisfy the KKT conditions. Then from the stationarity condition in (2.9), we get $\partial_x L(x, \bar{a}, \bar{b})|_{\bar{x}} = 0$. Since $L(x, \bar{a}, \bar{b})$ is convex in x, we get $\min_x L(x, \bar{a}, \bar{b}) = L(\bar{x}, \bar{a}, \bar{b})$. Therefore, from (2.9.3), it follows that

$$g(\bar{a}, \bar{b}) = f(\bar{x}) + \sum_{i=1}^{k} \bar{a}_i u_i(\bar{x}) + \sum_{j=1}^{l} \bar{b}_j v_j(\bar{x}) = f(\bar{x}) \ , \tag{2.9.12}$$

where the last equality follows from KKT conditions, i.e., $\bar{a}_i u_i(\bar{x}) = 0, \forall i$ and $v_j(\bar{x}) = 0, \forall j$. Thus the zero duality gap in (2.9.12) implies that $\bar{x}$ and $(\bar{a}, \bar{b})$ are respectively primal and dual optimal solutions, as argued in (2.9.9).

CHAPTER 3

BOUNDING THE ENERGY-CONSTRAINED QUANTUM AND PRIVATE CAPACITIES OF PHASE-INSENSITIVE BOSONIC GAUSSIAN CHANNELS

In this chapter we motivate the importance of energy-constrained distinguishability measures in estimating the ultimate communication capabilities of bosonic Gaussian quantum channels. In particular, we focus on particular phase-insensitive Gaussian channels: thermal, amplifier, and additive-noise channels. In general, these channels are non-degradable bosonic Gaussian channels and hence getting a good estimate of quantum and private capacities is a computationally challenging problem.

Before providing a detailed summary of our results, let us motivate why our results imply that the energy-constrained distinguishability measures can help in establishing tight upper bounds on the quantum and private capacities of bosonic channels. One of the bounds on the capacities of a thermal channel, as established in this chapter, is based on the notion of an ε-degradable quantum channel, as in Definition 61. In particular, this bound relies on the energy-constrained diamond distance between two particular Gaussian channels. We find that for certain parameter (e.g., mean-energy value of the channel inputs, thermal noise parameter, etc.) regimes, in comparison to all other upper bounds established in this chapter, the bound based on the ε-degradability is closest to a known lower bound. Thus, better estimates of the energy-constrained diamond distance can further improve our understanding of quantum and private capacities of thermal channels.

Inspired from these findings, we will develop numerical and analytical tools to estimate energy-constrained distance measures between Gaussian channels in Chapters 4 and 5.

We now provide a detailed summary of the results presented in this chapter.

Summary of results. We start by summarizing our upper bounds on the energy-constrained quantum capacity of thermal channels. A first upper bound is established

by decomposing a thermal channel as a pure-loss channel followed by a quantum-limited amplifier channel [127, 128] and using a data-processing argument. We note that the same method was employed in [144], in order to establish an upper bound on the classical capacity of the thermal channel (note that the general idea for the data-processing argument comes from the earlier work in [145, 146]). Throughout, we call this first upper bound the "data-processing bound." We also prove that this upper bound can be at most 1.45 bits larger than a known lower bound [64, 147] on the energy-constrained quantum and private capacity of a thermal channel. Moreover, the data-processing bound is very near to a known lower bound for the case of low thermal noise and both low and high transmissivity.

The notion of approximate degradability of quantum channels was developed in [66], and upper bounds on the quantum and private capacities of approximately degradable channels were established for quantum channels with finite-dimensional input and output systems. In this dissertation, we establish general upper bounds on the energy-constrained quantum and private capacities of approximately degradable channels for infinite-dimensional systems. These general upper bounds can be applied to any quantum channel that is approximately degradable with energy constraints on the input and output states of the channels. In particular, we apply these general upper bounds to bosonic Gaussian thermal and amplifier channels. In Chapter 5, we summarize how these general upper bounds can be applied to bosonic additive-noise channels.

Our second upper bound is based on the notion of ε-degradability of thermal channels, and we call this bound the "ε-degradable bound." In this method, we first construct a degrading channel, such that a complementary channel of the thermal channel is close in diamond distance [136] to the serial concatenation of the thermal channel followed by this degrading channel. In general, it seems to be computationally hard to determine the diamond distance between two quantum channels if the optimization is over input density operators acting on an infinite-dimensional Hilbert space. However, in our setup, we address this difficulty by constructing a simulating channel, which simulates the serial

concatenation of the thermal channel and the aforementioned degrading channel. Using this technique, an upper bound on the diamond distance reduces to the calculation of the quantum fidelity between the environmental states of the thermal channel and the simulating channel. Based on the fact that, for certain parameter regimes, the resulting capacity upper bound is better than all other upper bounds reported here, we believe that our aforementioned choice of a degrading channel is a good choice.

A third upper bound on the energy-constrained quantum capacity of thermal channels is established using the concept of ε-close-degradability of a thermal channel, and we call this bound the "ε-close-degradable bound." In particular, we show that a low-noise thermal channel is ε-close degradable, given that it is close in diamond distance to a pure-loss channel. We find that the ε-close-degradable bound is very near to the data-processing bound for the case of low thermal noise.

We then prove that any phase-insensitive channel that is not entanglement-breaking [125] can be decomposed as the concatenation of a quantum-limited amplifier channel followed by a pure-loss channel. This theorem was independently proven in [148, 149] (see also [150]). It has been used to bound the unconstrained quantum capacity of a thermal channel in [148], via a data-processing argument. We use this technique to prove an upper bound on the energy-constrained quantum and private capacities of a thermal channel. This technique has also been used most recently in [149] in similar contexts, as well as in [151]. In particular, we find that this upper bound is very near to a known lower bound for the case of low thermal noise and both low and high transmissivity. We call this bound the "bottleneck bound." We find that the bottleneck bound and the data-processing bound are incomparable, as one is better than the other for certain parameter regimes.

We compare these different upper bounds with a known lower bound on the quantum capacity of a thermal channel [64,147]. We find that the data-processing and the bottleneck bounds are very near to a known capacity lower bound for low thermal noise and for both medium and high transmissivity. Moreover, we show that the maximum difference between

the data-processing bound and a known lower bound never exceeds $1/\ln 2 \approx 1.45$ bits for all possible values of parameters, and this maximum difference is attained in the limit of infinite input mean photon number. This result places a strong limitation on any possible superadditivity of coherent information of the thermal channel. We note here that this kind of result was suggested without proof by the heuristic developments in [152]. Next, we plot these upper bounds as well as a known lower bound versus input mean photon number for different values of the channel transmissivity η and thermal noise N_B. In particular, we find that the ε-close-degradable bound is very near to the data-processing bound for low thermal noise and for both medium and high transmissivity. Moreover, all of these upper bounds are very near to a known lower bound for low thermal noise and high transmissivity. We also examine different parameter regimes where the ε-close-degradable bound is tighter than the ε-degradable bound and vice versa. In particular, we find that the ε-degradable bound is tighter than the ε-close degradable bound for the case of high thermal noise.

We find an interesting parameter regime where the ε-degradable bound is tighter than all other upper bounds, as it becomes closest to a known lower bound for the case of high noise and high input mean photon number. However, for the same parameter regime, if the input mean photon number is low, then the data-processing bound is tighter than the ε-degradable bound. This suggests that the upper bounds based on the notion of approximate degradability are good for the case of high input mean photon number. We suspect that these bounds could be further improved for the case of low input mean photon number if it were possible to compute or tightly bound the energy-constrained diamond norm [137, 138] (see also Section 3.8 for some developments in this direction). In Chapter 4 we develop techniques to estimate the energy-constrained diamond distance between quantum channels. In particular, we introduce the notion of energy-constrained diamond distance on a truncated input Hilbert space in (4.1.38), which can be calculated using a semi-definite program, as described in (4.1.67). This serves as a numerical tool to approximate the energy-constrained diamond norm with an arbitrarily high accuracy (see Proposition 116

for more details).

Similar to our bounds on the energy-constrained quantum capacity, we establish several upper bounds on the energy-constrained *private* capacity of bosonic thermal channels. We also develop an improved lower bound on the energy-constrained private capacity of a bosonic thermal channel. In particular, we find that for certain values of the channel transmissivity, a higher private communication rate can be achieved by using displaced thermal states as information carriers instead of coherent states.

Related to our bounds on energy-constrained quantum and private capacities of thermal channels, we establish several upper bounds on the same capacities of quantum amplifier channels. We also establish upper bounds on the energy-constrained quantum and private capacities of an additive-noise channel.

As one of the last technical developments of this chapter, we address the question of computing energy-constrained channel distances in a very broad sense, by considering the energy-constrained, generalized channel divergence of two quantum channels, as an extension of the generalized channel divergence developed in [153]. In particular, we prove that an optimal Gaussian input state for the energy-constrained, generalized channel divergence of two particular Gaussian channels is the two-mode squeezed vacuum state that saturates the energy constraint. It is an interesting open question to determine whether the two-mode squeezed vacuum is optimal among all input states, but we leave this for future work, simply noting for now that an answer would lead to improved upper bounds on the energy-constrained quantum and private capacities of the thermal and amplifier channels. At the least, we have proven that the optimal input state for the particular Gaussian channels is such that its reduction to the channel input system is diagonal in the photon number basis. Moreover, in Chapter 5 we prove that two-mode squeezed vacuum state is not optimal among all input states if one compares an additive-noise channel to an identity channel with respect to energy-constrained channel fidelity.

The rest of the chapter is structured as follows. We provide general upper bounds

on the energy-constrained quantum and private capacities of approximately degradable channels in Section 3.1. We use these tools to establish several upper bounds on the energy-constrained quantum and private capacities of a thermal channel in Sections 3.2 and 3.4, respectively. A comparision of these different upper bounds on energy-constrained quantum capacity of a thermal channel is discussed in Section 3.3. We present an improvement on the achievable rate of private communication through thermal channels, in Section 3.5. We establish bounds on energy-constrained capacities of a quantum amplifier channel and an additive-noise channel in Sections 3.6 and 3.7, respectively. We discuss the optimization of the Gaussian energy-constrained generalized channel divergence in Section 3.8. Finally, we summarize our results and conclude in Section 3.9.

3.1 Bounds on Energy-Constrained Quantum and Private Capacities of Approximately degradable channels

In this section, we derive upper bounds on the energy-constrained quantum and private capacities of approximately degradable channels. We derive these bounds for both ε-degradable (Definition 61) and ε-close-degradable (Definition 62) channels. This general form for the upper bounds on the energy-constrained quantum and private capacities of approximately degradable channels will be directly used in establishing bounds on the capacities of quantum thermal channels and amplifier channels. We also briefly summarize how to obtain the ε-close-degradable bound for an additive-noise channel.

We begin by defining the *conditional entropy of degradation*, which will be useful for finding upper bounds on the energy-constrained quantum and private capacities of an ε-degradable channel. A similar quantity has been defined for the finite-dimensional case in [66].

Definition 67 (Conditional entropy of degradation) *Let $\mathcal{N}_{A\to B}$ and $\mathcal{D}_{B\to E}$ be quantum channels, and let $G \in \mathcal{P}(\mathcal{H}_A)$ be a Gibbs observable. We define the conditional entropy*

of degradation as follows:

$$U_{\mathcal{D}}(\mathcal{N}, G, W) = \sup_{\rho\,:\,\mathrm{Tr}\{G\rho\}\leq W} [H(\mathcal{N}(\rho)) - H(\mathcal{D}\circ\mathcal{N}(\rho))] \ , \tag{3.1.1}$$

where $W \in [0,\infty)$. *For a Stinespring dilation* $\mathcal{V} : \mathcal{T}(B) \to \mathcal{T}(EF)$ *of the channel* $\mathcal{D}$,

$$U_{\mathcal{D}}(\mathcal{N}, G, W) = \sup_{\rho\,:\,\mathrm{Tr}\{G\rho\}\leq W} [H(F|E)_{\mathcal{V}\circ\mathcal{N}(\rho)}] \ . \tag{3.1.2}$$

We note that the conditional entropy of degradation can be understood as the negative entropy gain of the channel $\mathcal{D}_{B\to E}$ [154–157], with the optimization over input states $\mathcal{N}(\rho)$ restricted to the image of $\mathcal{N}$ and obeying the energy constraint $\mathrm{Tr}\{G\rho\} \leq W$. Next, we show that the conditional entropy of degradation in (3.1.2) is additive.

Lemma 3 *Let* $\mathcal{N}_{A\to B}$ *and* $\mathcal{D}_{B\to E}$ *be quantum channels, let* $G \in \mathcal{P}(\mathcal{H}_A)$ *be a Gibbs observable, and let* $W \in [0,\infty)$. *Then for all integer* $n \geq 1$,

$$U_{\mathcal{D}^{\otimes n}}(\mathcal{N}^{\otimes n}, \overline{G}_n, W) = n[U_{\mathcal{D}}(\mathcal{N}, G, W)] \ . \tag{3.1.3}$$

Proof. The following inequality

$$U_{\mathcal{D}^{\otimes n}}(\mathcal{N}^{\otimes n}, \overline{G}_n, W) \geq n[U_{\mathcal{D}}(\mathcal{N}, G, W)] \tag{3.1.4}$$

follows trivially because a product input state is a particular state of the form required in the optimization of $U_{\mathcal{D}^{\otimes n}}(\mathcal{N}^{\otimes n}, \overline{G}_n, W)$. We now prove the less trivial inequality

$$U_{\mathcal{D}^{\otimes n}}(\mathcal{N}^{\otimes n}, \overline{G}_n, W) \leq n[U_{\mathcal{D}}(\mathcal{N}, G, W)] \ . \tag{3.1.5}$$

Consider the following chain of inequalities:

$$H(F^n|E^n)_{(\mathcal{V}^{\otimes n}\circ\mathcal{N}^{\otimes n})(\rho_{A^n})} \leq \sum_{i=1}^{n} H(F_i|E_i)_{(\mathcal{V}\circ\mathcal{N})(\rho_{A_i})} \tag{3.1.6}$$

$$\leq n[H(F|E)_{(\mathcal{V}\circ\mathcal{N})(\bar{\rho}_n)}] \tag{3.1.7}$$

$$\leq n[U_{\mathcal{D}}(\mathcal{N}, G, W)] \ , \tag{3.1.8}$$

where $\bar{\rho}_n = \frac{1}{n}\sum_{i=1}^{n} \rho_{A_i}$. The first inequality follows from several applications of strong subadditivity [158, 159]. The second inequality follows from concavity of conditional entropy [158, 159]. The last inequality follows because $\mathrm{Tr}\{\overline{G}_n \rho_{A^n}\} = \mathrm{Tr}\{G\bar{\rho}_n\} \leq W$ and the conditional entropy of degradation $U_{\mathcal{D}}(\mathcal{N}, G, W)$ involves an optimization over all input states obeying this energy constraint. Since the chain of inequalities is true for all input states ρ_{A^n} satisfying the input energy constraint, the desired result follows. ■

3.1.1 Bound on the Energy-Constrained Quantum Capacity of an ε-Degradable Channel

An upper bound on the quantum capacity of an ε-degradable channel was established as [66, Theorem 3.1(ii)] for the finite-dimensional case. Here, we prove a related bound for the infinite-dimensional case with finite average energy constraints on the input and output states of the channels.

Theorem 68 *Let $\mathcal{N}_{A\to B}$ be an ε-degradable channel with a degrading channel $\mathcal{D}_{B\to E'}$, and let $G \in \mathcal{P}(\mathcal{H}_A)$ and $G' \in \mathcal{P}(\mathcal{H}_{E'})$ be Gibbs observables, such that for all input states $\rho_{A^n} \in \mathcal{D}(H_A^{\otimes n})$ satisfying input average energy constraints $\mathrm{Tr}\{\overline{G}_n \rho_{A^n}\} \leq W$, the following output average energy constraints are satisfied:*

$$\mathrm{Tr}\{\overline{G}'_n \hat{\mathcal{N}}^{\otimes n}(\rho_{A^n})\}, \quad \mathrm{Tr}\{\overline{G}'_n (\mathcal{D}^{\otimes n}\circ\mathcal{N}^{\otimes n})(\rho_{A^n})\} \leq W' \ , \tag{3.1.9}$$

where $\hat{\mathcal{N}}_{A\to E}$ is a complementary channel of $\mathcal{N}$ and $E' \simeq E$. Then the energy-constrained

quantum capacity $Q(\mathcal{N}, G, W)$ is bounded from above as

$$Q(\mathcal{N}, G, W) \leq U_{\mathcal{D}}(\mathcal{N}, G, W) + (2\varepsilon' + 4\delta)H(\gamma(W'/\delta)) + g(\varepsilon') + 2h_2(\delta) \ , \tag{3.1.10}$$

with $\varepsilon' \in (\varepsilon, 1]$, $W, W' \in [0, \infty)$, and $\delta = (\varepsilon' - \varepsilon)/(1 + \varepsilon')$.

Proof. Let

$$\begin{aligned} \sigma_{B^n} &= \mathcal{N}^{\otimes n}(\rho_{A^n}) \ , \\ \rho^j_{E'^j E^{(n-j)}} &= (\mathcal{D}^{\otimes j} \circ \mathcal{N}^{\otimes j}) \otimes \hat{\mathcal{N}}^{\otimes (n-j)}(\rho_{A^n}) \ , \end{aligned}$$

and consider the following chain of inequalities:

$$\begin{aligned} & H(B^n)_\sigma - H(E^n)_{\rho^0} \\ &= H(B^n)_\sigma - H(E'^n)_{\rho^n} + H(E'^n)_{\rho^n} - H(E^n)_{\rho^0} && (3.1.11) \\ &\leq U_{\mathcal{D}^{\otimes n}}(\mathcal{N}^{\otimes n}, \overline{G}_n, W) + H(E'^n)_{\rho^n} - H(E^n)_{\rho^0} && (3.1.12) \\ &= n\ U_{\mathcal{D}}(\mathcal{N}, G, W) \\ &\quad + \sum_{j=1}^{n} [H(E'_j | E'_1 \ldots E'_{j-1} E_{j+1} \ldots E_n)_{\rho^j} - H(E_j | E'_1 \ldots E'_{j-1} E_{j+1} \ldots E_n)_{\rho^{j-1}}] && (3.1.13) \\ &\leq n[U_{\mathcal{D}}(\mathcal{N}, G, W) + (2\varepsilon' + 4\delta) \left(\sum_{j=1}^{n} \frac{1}{n} H(\gamma(W'_j/\delta)) \right) + g(\varepsilon') + 2h_2(\delta)] && (3.1.14) \\ &\leq n[U_{\mathcal{D}}(\mathcal{N}, G, W) + (2\varepsilon' + 4\delta) H \left(\frac{1}{n} \sum_{j=1}^{n} \gamma(W'_j/\delta) \right) + g(\varepsilon') + 2h_2(\delta)] && (3.1.15) \\ &\leq n[U_{\mathcal{D}}(\mathcal{N}, G, W) + (2\varepsilon' + 4\delta) H \left(\gamma(W'/\delta) \right) + g(\varepsilon') + 2h_2(\delta)] \ , && (3.1.16) \end{aligned}$$

The first inequality follows from the definition in (3.1.1). The second equality follows from Lemma 3 and the telescoping technique. Let W'_j denote the energy constraint on the jth output state of both the channels $\mathcal{D} \circ \mathcal{N}$ and $\hat{\mathcal{N}}$, i.e.,

$$\mathrm{Tr}\{G'(\mathcal{D} \circ \mathcal{N})(\rho_{A_j})\}, \mathrm{Tr}\{G' \hat{\mathcal{N}}(\rho_{A_j})\} \leq W'_j \ , \tag{3.1.17}$$

where $\frac{1}{n}\sum_j W'_j \leq W'$. Then the second inequality holds because $\frac{1}{2}\|\rho^j - \rho^{j-1}\|_1 \leq \varepsilon$ for the given channels, and we use Lemma 1 for the jth output system. The third inequality follows from concavity of entropy. The last inequality follows because

$$\mathrm{Tr}\left\{\frac{1}{n}\sum_{j=1}^{n} G\gamma(W'_j/\delta)\right\} = \frac{1}{n}\sum_{j=1}^{n}\mathrm{Tr}\{G\gamma(W'_j/\delta)\} \leq W'/\delta \ , \tag{3.1.18}$$

and $\gamma(W'/\delta)$ is the Gibbs state that maximizes the entropy corresponding to the energy W'/δ. Since the chain of inequalities is true for all ρ_{A^n} satisfying the input average energy constraint, from (2.7.6) and the above, we get that

$$\frac{1}{n} I_c(\mathcal{N}^{\otimes n}, \overline{G}_n, W) \leq U_{\mathcal{D}}(\mathcal{N}, G, W) + (2\varepsilon' + 4\delta) H\left(\gamma(W'/\delta)\right) + g(\varepsilon') + 2h_2(\delta) \ . \tag{3.1.19}$$

Since the last inequality holds for all n, we obtain the desired result by taking the limit $n \to \infty$ and applying (2.7.5). ■

3.1.2 Bound on the Energy-Constrained Quantum Capacity of an ε-Close-Degradable Channel

An upper bound on the quantum capacity of an ε-close-degradable channel was established as [66, Proposition A.2(i)] for the finite-dimensional case. Here, we provide a bound for the infinite-dimensional case with finite average energy constraints on the input and output states of the channels.

Theorem 69 *Let $\mathcal{N}_{A\to B}$ be an ε-close-degradable channel, i.e., $\frac{1}{2}\|\mathcal{N} - \mathcal{M}\|_\diamond \leq \varepsilon < \varepsilon' \leq 1$, where $\mathcal{M}_{A\to B}$ is a degradable channel. Let $G \in \mathcal{P}(\mathcal{H}_A)$, $G' \in \mathcal{P}(\mathcal{H}_B)$ be Gibbs observables, such that for all input states $\rho_{RA^n} \in \mathcal{D}(\mathcal{H}_R \otimes \mathcal{H}_A^{\otimes n})$ satisfying the input average energy constraint $\mathrm{Tr}\{\overline{G}_n \rho_{A^n}\} \leq W$, the following output average energy constraints are satisfied:*

$$\mathrm{Tr}\{\overline{G}'_n \mathcal{N}^{\otimes n}(\rho_{A^n})\},\ \mathrm{Tr}\{\overline{G}'_n \mathcal{M}^{\otimes n}(\rho_{A^n})\} \leq W' \ , \tag{3.1.20}$$

where $W, W' \in [0, \infty)$. Then the energy-constrained quantum capacity $Q(\mathcal{N}, G, W)$ is

bounded from above as

$$Q(\mathcal{N}, G, W) \leq I_c(\mathcal{M}, G, W) + (4\varepsilon' + 8\delta)H(\gamma(W'/\delta)) + 2g(\varepsilon') + 4h_2(\delta) \ , \tag{3.1.21}$$

with $\varepsilon' \in (\varepsilon, 1]$ *and* $\delta = (\varepsilon' - \varepsilon)/(1 + \varepsilon')$.

Proof. Let $\omega_{RB^n} = (\mathrm{id}_R \otimes \mathcal{N}^{\otimes n})(\rho_{RA^n})$ and $\tau_{RB^n} = (\mathrm{id}_R \otimes \mathcal{M}^{\otimes n})(\rho_{RA^n})$, and consider the following chain of inequalities:

$$\begin{aligned} & H(B^n)_\omega - H(RB^n)_\omega - H(B^n)_\tau + H(RB^n)_\tau \\ & = H(B^n)_\omega - H(B^n)_\tau + H(RB^n)_\tau - H(RB^n)_\omega \qquad (3.1.22) \\ & \leq 2n[(2\varepsilon' + 4\delta)H(\gamma(W/\delta)) + g(\varepsilon') + 2h_2(\delta)] \ , \qquad (3.1.23) \end{aligned}$$

The first inequality follows from applying Theorem 66 twice. Then from Lemma 2,

$$Q(\mathcal{N}, G, W) \leq Q(\mathcal{M}, G, W) + (4\varepsilon' + 8\delta)H(\gamma(W'/\delta)) + 2g(\varepsilon') + 4h_2(\delta). \tag{3.1.24}$$

The desired result follows from the fact that the energy-constrained quantum capacity of a degradable channel is equal to the energy-constrained coherent information of the channel [62]. ■

3.1.3 Bound on the Energy-Constrained Private Capacity of an ε-Degradable Channel

In this section, we first derive an upper bound on the private capacity of an ε-degradable channel for the finite-dimensional case, which is different from any of the bounds presented in [66]. Then, we generalize this bound to the infinite-dimensional case with finite average energy constraints on the input and output states of the channels.

Theorem 70 *Let* $\mathcal{N}_{A\to B}$ *be a finite-dimensional* ε*-degradable channel with a degrading channel* $\mathcal{D}_{B\to E'}$*, and let* $\hat{\mathcal{N}} : \mathcal{T}(A) \to \mathcal{T}(E)$ *be a complementary channel of* $\mathcal{N}$*, such that*

$E' \simeq E$. *If*

$$U_{\mathcal{D}}(\mathcal{N}) = \max_{\rho \in \mathcal{D}(\mathcal{H}_A)} [H(\mathcal{N}(\rho)) - H((\mathcal{D} \circ \mathcal{N})(\rho))], \tag{3.1.25}$$

then the private capacity $P(\mathcal{N})$ *of* $\mathcal{N}$ *is bounded from above as*

$$P(\mathcal{N}) \leq U_{\mathcal{D}}(\mathcal{N}) + 6\varepsilon \log_2 \dim(\mathcal{H}_E) + 3g(\varepsilon) \ . \tag{3.1.26}$$

Proof. Consider Stinespring dilations $\mathcal{U} : \mathcal{T}(A) \to \mathcal{T}(BE)$ and $\mathcal{V} : \mathcal{T}(B) \to \mathcal{T}(E'F)$ of the channel $\mathcal{N}$ and the degrading channel $\mathcal{D}$, respectively. Let ρ_{XA^n} be a classical–quantum state in correspondence with an ensemble $\{p_X(x), \rho^x_{A^n}\}$:

$$\rho_{XA^n} = \sum_x p_X(x) |x\rangle\langle x|_X \otimes \rho^x_{A^n} \ , \tag{3.1.27}$$

and let

$$\omega_{XE^nE'^nF^n} = \sum_x p_X(x) |x\rangle\langle x|_X \otimes (\mathrm{id}_E^{\otimes n} \otimes \mathcal{V}^{\otimes n}) \circ \mathcal{U}^{\otimes n}(\rho^x_{A^n}) \ . \tag{3.1.28}$$

Consider the following extension of $\omega_{XE^nE'^nF^n}$:

$$\sigma_{XYE^nE'^nF^n} = \sum_{x,y} p_X(x) p_{Y|X}(y|x) |x\rangle\langle x|_X \otimes |y\rangle\langle y|_Y \otimes (\mathrm{id}_E^{\otimes n} \otimes \mathcal{V}^{\otimes n}) \circ \mathcal{U}^{\otimes n}(\psi^{x,y}_{A^n}) \ , \tag{3.1.29}$$

where $\psi^{x,y}_{A^n}$ is a pure state, and let $\sigma^{x,y}_{E^n E'^n F^n} = (\mathrm{id}_E^{\otimes n} \otimes \mathcal{V}^{\otimes n}) \circ \mathcal{U}^{\otimes n}(\psi^{x,y}_{A^n})$. Consider the following chain of inequalities:

$$I(X;B^n)_\omega - I(X;E^n)_\omega = I(X;F^n|E'^n)_\omega + I(X;E'^n)_\omega - I(X;E^n)_\omega \tag{3.1.30}$$

$$= I(X;F^n|E'^n)_\omega + H(E'^n)_\omega - H(E^n)_\omega + H(E^n|X)_\omega - H(E'^n|X)_\omega \tag{3.1.31}$$

$$\leq I(X;F^n|E'^n)_\omega + 2n[2\varepsilon \log_2 \dim(\mathcal{H}_E) + g(\varepsilon)] \tag{3.1.32}$$

$$\leq I(XY;F^n|E'^n)_\sigma + n[4\varepsilon \log_2 \dim(\mathcal{H}_E) + 2g(\varepsilon)] \tag{3.1.33}$$

$$= H(F^n|E'^n)_\sigma - H(F^n E'^n|XY)_\sigma + H(E'^n|XY)_\sigma + n[4\varepsilon \log_2 \dim(\mathcal{H}_E) + 2g(\varepsilon)] \tag{3.1.34}$$

$$= H(F^n|E'^n)_\sigma - H(E^n|XY)_\sigma + H(E'^n|XY)_\sigma + n[4\varepsilon \log_2 \dim(\mathcal{H}_E) + 2g(\varepsilon)] \tag{3.1.35}$$

$$\leq n[U_{\mathcal{D}}(\mathcal{N}) + 6\varepsilon \log_2 \dim(\mathcal{H}_E) + 3g(\varepsilon)]. \tag{3.1.36}$$

The first two equalities follow from entropy identities. The first inequality follows by applying the telescoping technique twice and using the continuity result of the conditional quantum entropy for finite-dimensional quantum systems [114]. The second inequality follows from the quantum data processing inequality for conditional quantum mutual information. The last two equalities follow from entropy identities and by using that $\sigma^{x,y}_{E^n E'^n F^n}$ is a pure state, so that $H(F^n E'^n)_{\sigma^{x,y}} = H(E^n)_{\sigma^{x,y}}$. The last inequality follows from the definition in (3.1.25), and additivity of $U_{\mathcal{D}}(\mathcal{N})$ [66]. Also, we applied the telescoping technique for each $\sigma^{x,y}$ in the summation, and used the continuity result of the conditional quantum entropy for finite-dimensional systems [114]. Since the chain of inequalities is true for any ensemble $\{p_X(x), \rho^x_{A^n}\}$, the final result follows from the definition of private information of the channel, dividing by n, taking the limit $n \to \infty$, and noting that the regularized private information is equal to the private capacity of any channel. ■

Next, we derive an upper bound on the energy-constrained private capacity of an ε-degradable channel.

Theorem 71 *Let $\mathcal{N}_{A\to B}$ be an ε-degradable channel with a degrading channel $\mathcal{D}_{B\to E'}$, and let $G \in \mathcal{P}(\mathcal{H}_A)$, $G' \in \mathcal{P}(\mathcal{H}_{E'})$ be Gibbs observables, such that for all input states $\rho_{A^n} \in \mathcal{D}(H_A^{\otimes n})$ satisfying input average energy constraints $\operatorname{Tr}\{\overline{G}_n \rho_{A^n}\} \leq W$, the following output average energy constraints are satisfied:*

$$\operatorname{Tr}\{\overline{G}'_n \hat{\mathcal{N}}^{\otimes n}(\rho_{A^n})\},\ \operatorname{Tr}\{\overline{G}'_n (\mathcal{D}^{\otimes n} \circ \mathcal{N}^{\otimes n})(\rho_{A^n})\} \leq W' \ , \tag{3.1.37}$$

where $\hat{\mathcal{N}}_{A\to E}$ is a complementary channel of $\mathcal{N}$, and $E' \simeq E$. Then the energy-constrained private capacity is bounded from above as

$$P(\mathcal{N}, G, W) \leq U_{\mathcal{D}}(\mathcal{N}, G, W) + (6\varepsilon' + 12\delta) H(\gamma(W'/\delta)) + 3g(\varepsilon') + 6h_2(\delta) \ , \tag{3.1.38}$$

with $\varepsilon' \in (\varepsilon, 1]$, $W, W' \in [0, \infty)$, and $\delta = (\varepsilon' - \varepsilon)/(1 + \varepsilon')$.

Proof. Since the proof is similar to the above one and previous ones, we just summarize it briefly below. Consider Stinespring dilations $\mathcal{U} : \mathcal{T}(A) \to \mathcal{T}(BE)$ and $\mathcal{V} : \mathcal{T}(B) \to \mathcal{T}(E'F)$ of the channel $\mathcal{N}$ and the degrading channel $\mathcal{D}$, respectively. Then the action of $\mathcal{U}^{\otimes n}$ followed by $\mathcal{V}^{\otimes n}$ on the ensemble $\{p_X(x), \rho^x_{A^n}\}$ leads to the following ensemble:

$$\{p_X(x), \omega^x_{E^n E'^n F^n} \equiv (\mathrm{id}_E^{\otimes n} \otimes \mathcal{V}^{\otimes n}) \circ \mathcal{U}^{\otimes n}(\rho^x_{A^n})\}. \tag{3.1.39}$$

Similar to the above proof, from applying the telescoping technique three times and using Lemma 1, concavity of entropy, and Lemma 3, we get the following bound:

$$I(X; B^n)_\omega - I(X; E^n)_\omega \leq n[U_{\mathcal{D}}(\mathcal{N}, G, W) + (6\varepsilon' + 12\delta) H(\gamma(W'/\delta)) + 3g(\varepsilon') + 6h_2(\delta)] \ . \tag{3.1.40}$$

The desired result follows from dividing by n, taking the limit $n \to \infty$, the definition of the

energy-constrained private information of the channel, and using the fact that the regularized energy-constrained private information is an upper bound on the energy-constrained private capacity of a quantum channel [62]. ■

3.1.4 Bound on The Energy-Constrained Private Capacity of an ε-Close-Degradable Channel

An upper bound on the private capacity of an ε-close-degradable channel was established as [66, Proposition A.2(ii)] for the finite-dimensional case. Here, we provide a bound for the infinite-dimensional case with finite average energy constraints on the input and output states of the channels.

Theorem 72 *Let $\mathcal{N}_{A\to B}$ be an ε-close-degradable channel, i.e., $\frac{1}{2}\left\|\mathcal{N}-\mathcal{M}\right\|_{\diamond} \leq \varepsilon < \varepsilon' \leq 1$, where $\mathcal{M}_{A\to B}$ is a degradable channel. Let $G \in \mathcal{P}(\mathcal{H}_A)$, $G' \in \mathcal{P}(\mathcal{H}_B)$ be Gibbs observables, such that for all input states $\rho_{A^n} \in \mathcal{D}(\mathcal{H}_A^{\otimes n})$ satisfying input average energy constraints $\operatorname{Tr}\{\overline{G}_n \rho_{A^n}\} \leq W$, the following output average energy constraints are satisfied:*

$$\operatorname{Tr}\{\overline{G}'_n \mathcal{N}^{\otimes n}(\rho_{A^n})\},\ \operatorname{Tr}\{\overline{G}'_n \mathcal{M}^{\otimes n}(\rho_{A^n})\} \leq W' \ , \tag{3.1.41}$$

where $W, W' \in [0,\infty)$. Then

$$P(\mathcal{N}, G, W) \leq I_c(\mathcal{M}, G, W) + (8\varepsilon' + 16\delta) H(\gamma(W'/\delta)) + 4g(\varepsilon') + 8h_2(\delta) \ , \tag{3.1.42}$$

with $\varepsilon' \in (\varepsilon, 1]$, and $\delta = (\varepsilon' - \varepsilon)/(1+\varepsilon')$.

Proof. We follow the proof of [142, Corollary 15] closely, but incorporate energy constraints. Consider Stinespring dilations $\mathcal{U} : \mathcal{T}(A) \to \mathcal{T}(BE)$ and $\mathcal{V} : \mathcal{T}(A) \to \mathcal{T}(BE)$ of the channels $\mathcal{N}$ and $\mathcal{M}$, respectively. Consider an input ensemble $\{p_X(x), \rho^x_{A^n}\}$, which

leads to the output ensembles

$$\{p_X(x), \omega^x \equiv \mathcal{U}^{\otimes n}(\rho^x_{A^n})\}, \tag{3.1.43}$$

$$\{p_X(x), \tau^x \equiv \mathcal{V}^{\otimes n}(\rho^x_{A^n})\}. \tag{3.1.44}$$

Supposing at first that the index x is discrete, from four times applying Theorem 66 and employing the same expansions as in the proof of [142, Corollary 15] , we get

$$I(X;B^n)_\omega - I(X;E^n)_\omega - [I(X;B^n)_\tau - I(X;E^n)_\tau] \leq 4n[(2\varepsilon' + 4\delta)H\left(\gamma(W/\delta)\right) + g(\varepsilon') + 2h_2(\delta)]. \tag{3.1.45}$$

The upper bound is uniform and has no dependence on the particular ensemble except via the energy constraints. Thus, by approximation, the same bound applies to ensembles for which the index x is continuous. Then from Lemma 2, we find that

$$P(\mathcal{N}, G, W) \leq P(\mathcal{M}, G, W) + (8\varepsilon' + 16\delta)H(\gamma(W'/\delta)) + 4g(\varepsilon') + 8h_2(\delta) \tag{3.1.46}$$

$$= I_c(\mathcal{M}, G, W) + (8\varepsilon' + 16\delta)H(\gamma(W'/\delta)) + 4g(\varepsilon') + 8h_2(\delta). \tag{3.1.47}$$

The equality in the last line follows from the fact that the energy-constrained private capacity of a degradable channel is equal to the energy-constrained coherent information of the channel [62]. ■

3.2 Upper Bounds on Energy-Constrained Quantum Capacity of Bosonic Thermal Channels

In this section, we establish four different upper bounds on the energy-constrained quantum capacity of a thermal channel:

1. We establish a first upper bound using the theorem that any thermal channel can be decomposed as the concatenation of a pure-loss channel followed by a quantum-limited amplifier channel [127, 128]. We call this bound the data-processing bound and denote it by Q_{U_1}.

2. Next, we show that a thermal channel is an ε-degradable channel for a particular choice of degrading channel. Then an upper bound on the energy-constrained quantum capacity of a thermal channel directly follows from Theorem 68. We call this bound the ε-degradable bound and denote it by Q_{U_2}.

3. We establish a third upper bound on the energy-constrained quantum capacity of a thermal channel using the idea of ε-close-degradability. We show that the thermal channel is ε-close to a pure-loss bosonic channel for a particular choice of ε. Since a pure-loss bosonic channel is a degradable channel [160], the bound on the energy-constrained quantum capacity of a thermal channel follows directly from Theorem 69. We call this bound the ε-close-degradable bound and denote it by Q_{U_3}.

4. We then establish a fourth upper bound by first proving the theorem that any phase-insensitive single-mode bosonic Gaussian channel can be decomposed as a pure amplifier channel followed by a pure-loss channel, if the original channel is not entanglement breaking. We then invoke the bottleneck inequality to bound the energy-constrained quantum capacity of a thermal channel. We call this bound the bottleneck bound and denote it by Q_{U_4}.

In Section 3.3, we compare, for different parameter regimes, the closeness of these upper bounds with a known lower bound on the quantum capacity of thermal channels.

3.2.1 Data-Processing Bound on the Energy-Constrained Quantum Capacity of Bosonic Thermal Channels

In this section, we provide an upper bound using the theorem that any thermal channel $\mathcal{L}^{\eta,N_B}$ can be decomposed as the concatenation of a pure-loss channel $\mathcal{L}^{\eta',0}$ with transmissivity η' followed by a quantum-limited amplifier channel $\mathcal{A}^{G,0}$ with gain G [127, 128], i.e.,

$$\mathcal{L}^{\eta,N_B} = \mathcal{A}^{G,0} \circ \mathcal{L}^{\eta',0}, \tag{3.2.1}$$

where $G = (1-\eta)N_B + 1$, and $\eta' = \eta/G$. In Theorem 87, we prove that the data-processing bound can be at most 1.45 bits larger than a known lower bound.

Theorem 73 *An upper bound on the quantum capacity of a thermal channel $\mathcal{L}^{\eta,N_B}$ with transmissivity $\eta \in [1/2, 1]$, environment photon number N_B, and input mean photon number constraint N_S is given by*

$$Q(\mathcal{L}^{\eta,N_B}, N_S) \leq \max\{0, Q_{U_1}(\mathcal{L}^{\eta,N_B}, N_S)\} \ , \tag{3.2.2}$$

$$Q_{U_1}(\mathcal{L}^{\eta,N_B}, N_S) \equiv g(\eta' N_S) - g[(1-\eta')N_S], \tag{3.2.3}$$

with $\eta' = \eta/((1-\eta)N_B + 1)$.

Proof. An upper bound on the energy-constrained quantum capacity can be established by using (3.2.1) and a data-processing argument. We find that

$$Q(\mathcal{L}^{\eta,N_B}, N_S) = Q(\mathcal{A}^{G,0} \circ \mathcal{L}^{\eta',0}, N_S) \tag{3.2.4}$$

$$\leq Q(\mathcal{L}^{\eta',0}, N_S) \tag{3.2.5}$$

$$= \max\{0, g(\eta' N_S) - g[(1-\eta')N_S]\} \ . \tag{3.2.6}$$

The first inequality follows from definitions and data processing—the energy-constrained capacity of $\mathcal{A}^{G,0} \circ \mathcal{L}^{\eta',0}$ cannot exceed that of $\mathcal{L}^{\eta',0}$. The second equality follows from the formula for the energy-constrained quantum capacity of a pure-loss bosonic channel with transmissivity η' and input mean photon number N_S [62, 64]. ■

Remark 74 *Applying Remark 65, we find the following data-processing bound $Q_{U_1}(\mathcal{L}^{\eta,N_B})$*

on the unconstrained quantum capacity of bosonic thermal channels:

$$Q(\mathcal{L}^{\eta,N_B}) \leq Q_{U_1}(\mathcal{L}^{\eta,N_B}) = \sup_{N_S:N_S\in[0,\infty]} Q_{U_1}(\mathcal{L}^{\eta,N_B},N_S) \tag{3.2.7}$$

$$= \lim_{N_S\to\infty} Q_{U_1}(\mathcal{L}^{\eta,N_B},N_S) \tag{3.2.8}$$

$$= \log_2(\eta/(1-\eta)) - \log_2(N_B+1), \tag{3.2.9}$$

where the second equality follows from the monotonicity of $g(\eta N_S) - g[(1-\eta)N_S]$ *with respect to* N_S *for* $\eta \geq 1/2$ *[63].*

The bound

$$Q(\mathcal{L}^{\eta,N_B},N_S) \leq -\log_2([1-\eta]\eta^{N_B}) - g(N_B) \tag{3.2.10}$$

was found in [161, 162]. Moreover, the following bound was established in [148, Eq. (40)]:

$$Q(\mathcal{L}^{\eta,N_B},N_S) \leq \max\left\{0, \log_2 \frac{\eta - N(1-\eta)}{(1+N)(1-\eta)}\right\} . \tag{3.2.11}$$

As discussed in [148], a comparison of (3.2.9) *with the bounds from* (3.2.10) *and* (3.2.11) *leads to the conclusion that the bound given in* (3.2.11) *is always tighter than* (3.2.9)*. However,* (3.2.9) *and the bound in* (3.2.10) *are incomparable as one is better than the other for certain parameter regimes. Also,* (3.2.10) *is tighter than* (3.2.11) *for certain parameter regimes.*

We note that the upper bound in (3.2.11) *was indepedently established in [149].*

Remark 75 *The data-processing bound* $Q_{U_1}(\mathcal{L}^{\eta,N_B},N_S)$ *on the energy-constrained quantum capacity* $Q(\mathcal{L}^{\eta,N_B},N_S)$ *places a strong restriction on the channel parameters* η *and* N_B*. Since the quantum capacity of a pure-loss channel with transmissivity* η' *is non-zero only for* $\eta' > 1/2$*, the energy-constrained quantum capacity* $Q(\mathcal{L}^{\eta,N_B},N_S)$ *is non-zero only for*

$$1 \geq \eta > \frac{N_B+1}{N_B+2}. \tag{3.2.12}$$

However, [127, Section 4] provides a stronger restriction on η and N_B than (3.2.12) *does.*

3.2.2 ε-Degradable Bound on the Energy-Constrained Quantum Capacity of Bosonic Thermal Channels

In this section, we provide an upper bound on the energy-constrained quantum capacity of a thermal channel using the idea of ε-degradability. In Theorem 68, we established a general upper bound on the energy-constrained quantum capacity of an ε-degradable channel. Hence, our first step is to construct the degrading channel $\mathcal{D}$ given in (3.2.20), such that the concatenation of a thermal channel $\mathcal{L}^{\eta,N_B}$ followed by $\mathcal{D}$ is close in diamond distance to the complementary channel $\hat{\mathcal{L}}^{\eta,N_B}$ of the thermal channel $\mathcal{L}^{\eta,N_B}$.

We start by motivating the reason for choosing the particular degrading channel in (3.2.20), which is depicted in Figure 3.1, and then we find an upper bound on the diamond distance between $\mathcal{D}\circ\mathcal{L}^{\eta,N_B}$ and $\hat{\mathcal{L}}^{\eta,N_B}$. In general, it is computationally hard to perform the optimization over an infinite dimensional space required in the calculation of the diamond distance between Gaussian channels. However, we address this problem in this particular case by introducing a channel that simulates the serial concatenation of the thermal channel and the degrading channel, and we call it the simulating channel, as given in (3.2.24). This allows us to bound the diamond distance between the channels from above by the trace distance between the environment states of the complementary channel and the simulating channel (Theorem 76). Next, we argue that, for a given input mean photon-number constraint N_S, a thermal state with mean photon number N_S maximizes the conditional entropy of degradation defined in (3.1.2), which also appears in the general upper bound established in Theorem 68. We finally provide an upper bound on the energy-constrained quantum capacity of a thermal channel by using all these tools and invoking Theorem 68.

We now establish an upper bound on the diamond distance between the complementary channel of the thermal channel and the concatenation of the thermal channel followed by a particular degrading channel. Let $\mathcal{B}$ and $\mathcal{B}'$ represent beamsplitter transformations with transmissivity η and $(1-\eta)/\eta$, respectively. In the Heisenberg picture, the beamsplitter

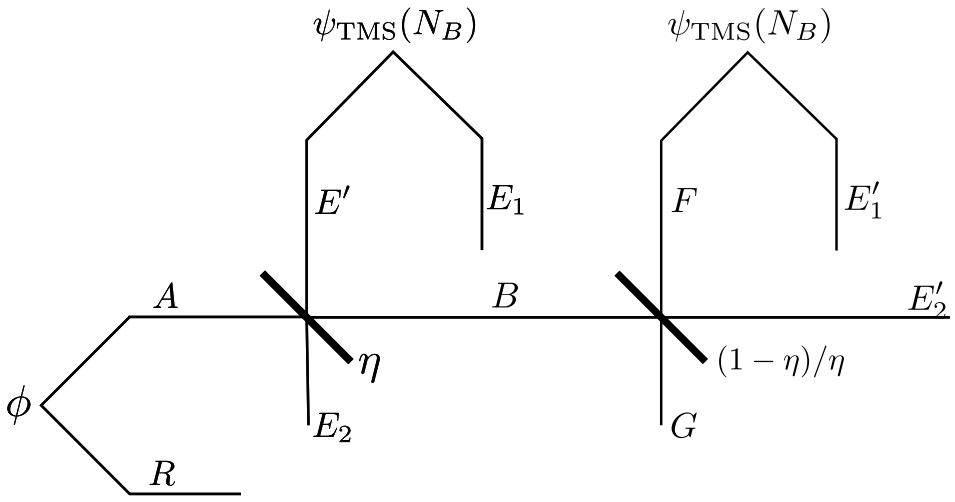

Figure 3.1: The figure plots a thermal channel with transmissivity $\eta \in [1/2, 1]$ and a degrading channel as described in (3.2.20). ϕ_{RA} is an input state to the beamsplitter $\mathcal{B}$ with transmissivity η and $\psi_{\text{TMS}}(N_B)$ represents a two-mode squeezed vacuum state with parameter N_B. System B is the output of the thermal channel, and systems E_1E_2 are the outputs of the complementary channel. The second beamsplitter $\mathcal{B}'$ has transmissivity $(1-\eta)/\eta$, and system B acts as an input to $\mathcal{B}'$. Systems $E_1'E_2'$ represent the output systems of the degrading channel, whose action is to tensor in the state $\psi_{\text{TMS}}(N_B)_{FE_1'}$, interact the input system B with F according to $\mathcal{B}'$, and then trace over system G.

transformation $\mathcal{B}_{C_1D_1\to C_2D_2}$ is given by

$$\hat{c}_2 = \sqrt{\eta}\hat{c}_1 - \sqrt{1-\eta}\hat{d}_1, \tag{3.2.13}$$

$$\hat{d}_2 = \sqrt{1-\eta}\hat{c}_1 + \sqrt{\eta}\hat{d}_1 \ . \tag{3.2.14}$$

Similarly, the beamsplitter transformation $\mathcal{B}'_{C_1D_1\to C_2D_2}$ is given by

$$\hat{c}_2 = \sqrt{(1-\eta)/\eta}\hat{c}_1 + \sqrt{(2\eta-1)/\eta}\hat{d}_1, \tag{3.2.15}$$

$$\hat{d}_2 = -\sqrt{(2\eta-1)/\eta}\hat{c}_1 + \sqrt{(1-\eta)/\eta}\hat{d}_1 \ , \tag{3.2.16}$$

where $\hat{c}_1, \hat{c}_2$, $\hat{d}_1$, and $\hat{d}_2$ are annihilation operators representing various modes involved in the beamsplitter transformations. Here, $\eta \in [1/2, 1]$. It is important to stress that there is a difference in phase between the $\mathcal{B}$ and $\mathcal{B}'$ beamsplitter transformations, which is crucial in our development.

Consider the following action of the thermal channel $\mathcal{L}^{\eta,N_B}$ on an input state ϕ_{RA}:

$$(\mathrm{id}_R \otimes \mathcal{L}^{\eta,N_B})(\phi_{RA}) = \mathrm{Tr}_{E_1E_2}\{\mathcal{B}_{AE'\to BE_2}(\phi_{RA} \otimes \psi_{\mathrm{TMS}}(N_B)_{E'E_1})\} , \tag{3.2.17}$$

where R is a reference system and $\psi_{\mathrm{TMS}}(N_B)_{E'E_1}$ is a two-mode squeezed vacuum state with parameter N_B, as defined in (2.3.34).

Here and what remains in the proof, we consider the action of various transformations on the covariance matrices of the states involved, and we furthermore track only the submatrices corresponding to the position-quadrature operators of the covariance matrices. It suffices to do so because all channels involved in our discussion are phase-insensitive Gaussian channels.

The submatrix corresponding to the position-quadrature operators of the covariance matrix of $\psi_{\mathrm{TMS}}(N_B)_{E'E_1}$ has the following form:

$$V = \begin{bmatrix} 2N_B + 1 & 2\sqrt{N_B(1+N_B)} \\ 2\sqrt{N_B(1+N_B)} & 2N_B + 1 \end{bmatrix} . \tag{3.2.18}$$

The action of a complementary channel $\hat{\mathcal{L}}^{\eta,N_B}$ on an input state ϕ_{RA} is given by

$$(\mathrm{id}_R \otimes \hat{\mathcal{L}}^{\eta,N_B})(\phi_{RA}) = \mathrm{Tr}_B\{\mathcal{B}_{AE'\to BE_2}(\phi_{RA} \otimes \psi_{\mathrm{TMS}}(N_B)_{E'E_1})\} . \tag{3.2.19}$$

It can be understood from Figure 3.1 that the system R is correlated with the input system A for the channel, and the system E' is the environment's input. The beamsplitter transformation $\mathcal{B}$ then leads to systems B and E_2. Hence, the output of the thermal channel $\mathcal{L}^{\eta,N_B}$ is system B, and the outputs of the complementary channel $\hat{\mathcal{L}}^{\eta,N_B}$ are systems E_1 and E_2.

Our aim is to introduce a degrading channel $\mathcal{D}$, such that the combined state of R and the output of $\mathcal{D} \circ \mathcal{L}^{\eta,N_B}$ emulate the combined state of R, E_1, and E_2, to an extent. This

will then allow us to bound the diamond distance between $\mathcal{D} \circ \mathcal{L}^{\eta,N_B}$ and $\hat{\mathcal{L}}^{\eta,N_B}$ from above. For the case when there is no thermal noise, i.e., $N_B = 0$, a thermal channel reduces to a pure-loss channel. Moreover, we know that a pure-loss channel is a degradable channel and the corresponding degrading channel can be realized by a beamsplitter with transmissivity $(1-\eta)/\eta$ [63]. Hence, we consider a degrading channel, such that it also satisfies the conditions for the above described special case.

Consider a beamsplitter with transmissivity $(1-\eta)/\eta$ and the beamsplitter transformation $\mathcal{B}'$ from (3.2.15)-(3.2.16). As described in Figure 3.1, the output B of the thermal channel $\mathcal{L}^{\eta,N_B}$ becomes an input to the beamsplitter $\mathcal{B}'$. We consider one mode (F in Figure 3.1) of the two-mode squeezed vacuum state $\psi_{\text{TMS}}(N_B)_{FE_1'}$ as an environmental input for $\mathcal{B}'$, so that the subsystem E_1' mimics E_1. Hence, our choice of degrading channel seems reasonable, as the combined state of system R and output systems E_1', E_2' of $\mathcal{D} \circ \mathcal{L}^{\eta,N_B}$ emulates the combined state of R, E_1, and E_2, to an extent. We suspect that our choice of degrading channel is a good choice because an upper bound on the energy-constrained quantum capacity of a thermal channel using this technique outperforms all other upper bounds for certain parameter regimes. We denote our choice of degrading channel by $\mathcal{D}_{(1-\eta)/\eta,N_B} : \mathcal{T}(B) \to \mathcal{T}(E_1'E_2')$. More formally, $\mathcal{D}_{(1-\eta)/\eta,N_B}$ has the following action on the output state $\mathcal{L}^{\eta,N_B}(\phi_{RA})$:

$$(\text{id}_R \otimes [\mathcal{D}_{(1-\eta)/\eta,N_B} \circ \mathcal{L}^{\eta,N_B}])(\phi_{RA}) = \text{Tr}_G\{\mathcal{B}'_{BF\to E_2'G}(\mathcal{L}^{\eta,N_B}(\phi_{RA}) \otimes \psi_{\text{TMS}}(N_B)_{FE_1'})\}\,. \quad (3.2.20)$$

Next, we provide a strategy to bound the diamond distance between $\mathcal{D}_{(1-\eta)/\eta,N_B} \circ \mathcal{L}^{\eta,N_B}$ and $\hat{\mathcal{L}}^{\eta,N_B}$. Consider the following submatrix corresponding to the position-quadrature operators of the covariance matrix of an input state ϕ_{RA}:

$$\gamma = \begin{bmatrix} a & c \\ c & b \end{bmatrix}. \quad (3.2.21)$$

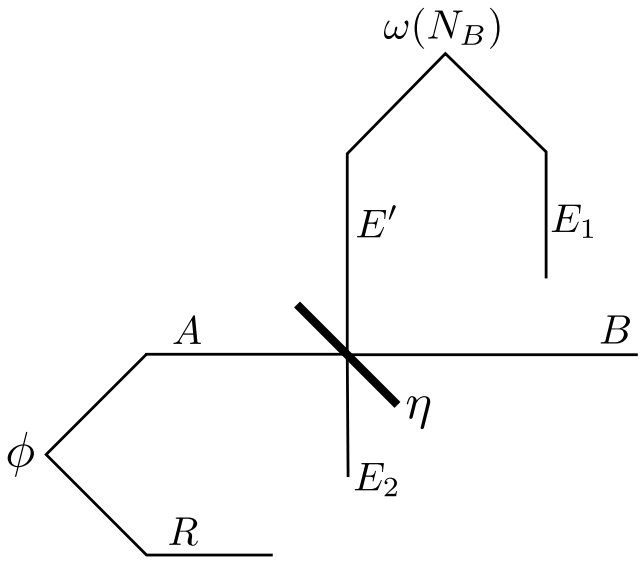

Figure 3.2: The figure plots the simulating channel Ξ described in (3.2.24). ϕ_{RA} is an input state to a beamsplitter $\mathcal{B}$ with transmissivity η and $\omega(N_B)$ represents a noisy version of a two-mode squeezed vacuum state with parameter N_B (see (3.2.25)), one mode of which is an input to the environment mode of the beamsplitter. The simulating channel is such that system B is traced over, so that the channel outputs are E_1 and E_2. Finally, the simulating channel is exactly the same as the channel from system A to systems $E_1'E_2'$ in Figure 3.1.

where $a, b, c \in \mathbb{R}$ are such that the above is the position-quadrature part of a legitimate covariance matrix. Let $\xi_{RE_2'E_2E_1GE_1'}$ denote the state after the beamsplitter transformations act on an input state ϕ_{RA}:

$$\xi_{RE_2'E_2E_1GE_1'} = \mathcal{B}'_{BF\to E_2'G}[\mathcal{B}_{AE'\to BE_2}[\phi_{RA}\otimes\psi_{\text{TMS}}(N_B)_{E'E_1}]\otimes\psi_{\text{TMS}}(N_B)_{FE_1'})] \ . \tag{3.2.22}$$

Then the submatrix corresponding to the position-quadrature operators of the covariance matrix of the output state in (3.2.20) is given by [163]:

$$\gamma' = \begin{bmatrix} a & c\sqrt{1-\eta} & 0 \\ c\sqrt{1-\eta} & b+\eta(1-b+2N_B) & 2\sqrt{N_B(1+N_B)(2-1/\eta)} \\ 0 & 2\sqrt{N_B(1+N_B)(2-1/\eta)} & 2N_B+1 \end{bmatrix} \ . \tag{3.2.23}$$

Now, we introduce a particular channel that simulates the action of $\mathcal{D}_{(1-\eta)/\eta,N_B} \circ \mathcal{L}^{\eta,N_B}$ on an input state ϕ_{RA}. We denote this channel by Ξ, and it has the following action on an input state ϕ_{RA}:

$$(\mathrm{id}_R \otimes \Xi)(\phi_{RA}) = \mathrm{Tr}_B\{\mathcal{B}_{AE' \to BE_2}(\phi_{RA} \otimes \omega(N_B)_{E'E_1})\} , \tag{3.2.24}$$

where $\omega(N_B)_{E'E_1}$ represents a noisy version of a two-mode squeezed vacuum state with parameter N_B and has the following submatrix corresponding to the position-quadrature operators of the covariance matrix:

$$V' = \begin{bmatrix} 2N_B + 1 & 2\sqrt{[N_B(1+N_B)(2\eta-1)]/\eta^2} \\ 2\sqrt{[N_B(1+N_B)(2\eta-1)]/\eta^2} & 2N_B + 1 \end{bmatrix} . \tag{3.2.25}$$

The matrix V' in (3.2.25) is a well defined submatrix of the covariance matrix for the noisy version of a two-mode squeezed vacuum state, because $(2\eta - 1)/\eta^2 \in [0, 1]$ for $\eta \in [1/2, 1]$. The submatrix of the covariance matrix corresponding to the state in (3.2.24) is the same as the submatrix in (3.2.23) [163]. In other words, the covariance matrix for the sytems R, E_1', and E_2' in Figure 3.1 is exactly the same as the covariance matrix for the systems R, E_1, and E_2 in Figure 3.2. This equality of covariance matrices is sufficient to conclude that the following equivalence holds for an quantum input state ϕ_{RA} (see [68, Chapter 5] for a proof):

$$(\mathrm{id}_R \otimes [\mathcal{D}_{(1-\eta)/\eta,N_B} \circ \mathcal{L}^{\eta,N_B}])(\phi_{RA}) = (\mathrm{id}_R \otimes \Xi)(\phi_{RA}) . \tag{3.2.26}$$

Thus, the channels $\mathcal{D}_{(1-\eta)/\eta,N_B} \circ \mathcal{L}^{\eta,N_B}$ and Ξ are indeed the same.

From (3.2.19), (3.2.24), and (3.2.26), the action of both $\hat{\mathcal{L}}^{\eta,N_B}$ and Ξ can be understood as tensoring the state of the environment with the input state of the channel, performing the beamsplitter transformation $\mathcal{B}$, and then tracing out the output of the channels. Using these techniques, we now establish an upper bound on the diamond distance between the complementary channel in (3.2.19) and the concatenation of the thermal channel followed

by the degrading channel in (3.2.20).

Theorem 76 *Fix $\eta \in [1/2, 1]$. Let $\mathcal{L}^{\eta,N_B}$ be a thermal channel with transmissivity η, and let $\mathcal{D}_{(1-\eta)/\eta,N_B}$ be a degrading channel as defined in* (3.2.20)*. Then*

$$\frac{1}{2}\left\|\hat{\mathcal{L}}^{\eta,N_B} - \mathcal{D}_{(1-\eta)/\eta,N_B} \circ \mathcal{L}^{\eta,N_B}\right\|_\diamond \leq \sqrt{1-\eta^2/\kappa(\eta,N_B)}\ , \tag{3.2.27}$$

with

$$\kappa(\eta,N_B) = \eta^2 + N_B(N_B+1)[1+3\eta^2 - 2\eta(1+\sqrt{2\eta-1})]\ . \tag{3.2.28}$$

Proof. Consider the following chain of inequalities:

$$\begin{aligned}
&\left\|(\mathrm{id}_R \otimes \hat{\mathcal{L}}^{\eta,N_B})(\phi_{RA}) - (\mathrm{id}_R \otimes [\mathcal{D}_{(1-\eta)/\eta,N_B} \circ \mathcal{L}^{\eta,N_B}])(\phi_{RA})\right\|_1 \\
&= \left\|(\mathrm{id}_R \otimes \hat{\mathcal{L}}^{\eta,N_B})(\phi_{RA}) - (\mathrm{id}_R \otimes \Xi)(\phi_{RA})\right\|_1 && (3.2.29)\\
&= \|\mathrm{Tr}_B\{\mathcal{B}_{AE'\to BE_2}(\phi_{RA} \otimes \psi_{\mathrm{TMS}}(N_B)_{E'E_1}) - \mathcal{B}_{AE'\to BE_2}(\phi_{RA} \otimes \omega(N_B)_{E'E_1})\}\|_1 && (3.2.30)\\
&\leq \|\mathcal{B}_{AE'\to BE_2}(\phi_{RA} \otimes \psi_{\mathrm{TMS}}(N_B)_{E'E_1}) - \mathcal{B}_{AE'\to BE_2}(\phi_{RA} \otimes \omega(N_B)_{E'E_1})\|_1 && (3.2.31)\\
&= \|\phi_{RA} \otimes \psi_{\mathrm{TMS}}(N_B)_{E'E_1} - \phi_{RA} \otimes \omega(N_B)_{E'E_1}\|_1 && (3.2.32)\\
&= \|\psi_{\mathrm{TMS}}(N_B)_{E'E_1} - \omega(N_B)_{E'E_1}\|_1 && (3.2.33)\\
&\leq 2\sqrt{1 - F(\psi_{\mathrm{TMS}}(N_B)_{E'E_1}, \omega(N_B)_{E'E_1})} && (3.2.34)
\end{aligned}$$

The first equality follows from (3.2.26). The second equality follows from (3.2.19) and (3.2.24). The first inequality follows from monotonicity of the trace distance. The third equality follows from invariance of the trace distance under a unitary transformation (beam-splitter). The last inequality follows from the Powers-Stormer inequality [135].

Next, we compute the fidelity between $\psi_{\mathrm{TMS}}(N_B)_{E'E_1}$ and $\omega(N_B)_{E'E_1}$ by using their respective covariance matrices in (3.2.18) and (3.2.25), in the Uhlmann fidelity formula for

two-mode Gaussian states [166]. We find [163]

$$F(\psi_{\mathrm{TMS}}(N_B)_{E'E_1}, \omega(N_B)_{E'E_1}) = \frac{\eta^2}{\eta^2 + N_B(N_B+1)[1+3\eta^2 - 2\eta(1+\sqrt{2\eta-1})]} \ . \quad (3.2.35)$$

Since these inequalities hold for any input state ϕ_{RA}, the final result follows from the definition of the diamond norm. ■

Theorem 77 *An upper bound on the quantum capacity of a thermal channel $\mathcal{L}^{\eta,N_B}$ with transmissivity $\eta \in [1/2, 1]$, environment photon number N_B, and input mean photon-number constraint N_S is given by*

$$\begin{aligned} Q(\mathcal{L}^{\eta,N_B}, N_S) \leq Q_{U_2}(\mathcal{L}^{\eta,N_B}, N_S) &\equiv g(\eta N_S + (1-\eta)N_B) - g(\zeta_+) - g(\zeta_-) \\ &+ (2\varepsilon' + 4\delta) g([(1-\eta)N_S + (1+\eta)N_B]/\delta) + g(\varepsilon') + 2h_2(\delta) \ , \quad (3.2.36) \end{aligned}$$

with

$$\varepsilon = \sqrt{1 - \eta^2 / \left(\eta^2 + N_B(N_B+1)[1+3\eta^2 - 2\eta(1+\sqrt{2\eta-1})]\right)} \ , \quad (3.2.37)$$

$$\zeta_\pm = \frac{1}{2}\left(-1 + \sqrt{[(1+2N_B)^2 - 2\varrho + (1+2\vartheta)^2 \pm 4(\vartheta - N_B)\sqrt{[1+N_B+\vartheta]^2 - \varrho}]/2}\right) \ , \quad (3.2.38)$$

$$\varrho = 4N_B(N_B+1)(2\eta-1)/\eta \ , \quad (3.2.39)$$

$$\vartheta = \eta N_B + (1-\eta)N_S \ , \quad (3.2.40)$$

$\varepsilon' \in (\varepsilon, 1]$, and $\delta = (\varepsilon' - \varepsilon)/(1+\varepsilon')$.

Proof. From Theorem 76, we have an upper bound on the diamond distance between the complementary channel of the thermal channel and the concatenation of the thermal

channel followed by the degrading channel, i.e.,

$$\frac{1}{2}\left\|\hat{\mathcal{L}}^{\eta,N_B} - \mathcal{D}_{(1-\eta)/\eta,N_B} \circ \mathcal{L}^{\eta,N_B}\right\|_\diamond \leq \sqrt{1-\eta^2/\left(\eta^2 + N_B(N_B+1)[1+3\eta^2-2\eta(1+\sqrt{2\eta-1})]\right)} < \varepsilon' \leq 1. \quad (3.2.41)$$

Due to the input mean photon number constraint N_S, and environment photon number N_B for both $\mathcal{L}^{\eta,N_B}$ and $\mathcal{D}_{(1-\eta)/\eta,N_B}$, there is a total photon number constraint $(1-\eta)N_S + (1+\eta)N_B$ for the average output of n channel uses of both $\hat{\mathcal{L}}^{\eta,N_B}$ and $\mathcal{D}_{(1-\eta)/\eta,N_B} \circ \mathcal{L}^{\eta,N_B}$. Using these results in Theorem 68, we find the following upper bound on the energy-constrained quantum capacity of a thermal channel:

$$Q(\mathcal{L}^{\eta,N_B}, N_S) \leq U_{\mathcal{D}_{(1-\eta)/\eta,N_B}}(\mathcal{L}^{\eta,N_B}, N_S) + (2\varepsilon'+4\delta)g([(1-\eta)N_S+(1+\eta)N_B]/\delta) + g(\varepsilon') + 2h_2(\delta)\,. \quad (3.2.42)$$

Using Proposition 78, we find that the thermal state with mean photon number N_S optimizes the conditional entropy of degradation $U_{\mathcal{D}_{(1-\eta)/\eta,N_B}}(\mathcal{L}^{\eta,N_B}, N_S)$. For the given thermal channel in (3.2.17) and the degrading channel in (3.2.20), we find the following analytical expression [163]:

$$U_{\mathcal{D}_{(1-\eta)/\eta,N_B}}(\mathcal{L}^{\eta,N_B}, N_S) = g(\eta N_S + (1-\eta)N_B) - g(\zeta_+) - g(\zeta_-)\,, \quad (3.2.43)$$

with $\zeta_\pm$ defined as in the theorem statement. ■

Proposition 78 *Let $\mathcal{L}^{\eta,N_B}$ be a thermal channel with transmissivity $\eta \in [1/2, 1]$, environment photon number N_B, and input mean photon number constraint N_S. Let $\mathcal{D}_{(1-\eta)/\eta,N_B}$ be the degrading channel from* (3.2.20)*. Then the thermal state with mean photon number N_S optimizes the conditional entropy of degradation $U_{\mathcal{D}_{(1-\eta)/\eta,N_B}}(\mathcal{L}^{\eta,N_B}, N_S)$, defined from* (3.1.2)*.*

Proof. Consider the Stinespring dilation in (3.2.22) of the degrading channel $\mathcal{D}_{(1-\eta)/\eta,N_B}$

from (3.2.20), and denote it by $\mathcal{W}$. Then according to (3.1.2),

$$U_{\mathcal{D}_{(1-\eta)/\eta,N_B}}(\mathcal{L}^{\eta,N_B},N_S)=\sup_{\rho\,:\,\mathrm{Tr}\{\hat{n}\rho\}\leq N_S} H(G|E_1'E_2')_{(\mathcal{W}\circ\mathcal{L}^{\eta,N_B})(\rho)}\ . \tag{3.2.44}$$

Our aim is to find an input state ρ with a certain photon number $N_t \leq N_S$, such that it maximizes the conditional entropy in (3.2.44). From the extremality of Gaussian states applied to the conditional entropy [167], it suffices to perform the optimization in (3.2.44) over only Gaussian states.

Now, we argue that for a given input mean photon number N_t, a thermal state is the optimal state for the conditional output entropy in (3.2.44). For a thermal channel and our choice of a degrading channel, a phase rotation on the input state is equivalent to a product of local phase rotations on the outputs. Let us denote the state after the local phase rotations on the outputs by

$$\sigma_{E_2'GE_1'}(\phi)=(e^{i\phi\hat{n}}\otimes e^{i\phi\hat{n}}\otimes e^{-i\phi\hat{n}})(\mathcal{W}\circ\mathcal{L}^{\eta,N_B})(\rho)(e^{-i\phi\hat{n}}\otimes e^{-i\phi\hat{n}}\otimes e^{i\phi\hat{n}}), \tag{3.2.45}$$

and let

$$\xi_{E_2'GE_1'}=\frac{1}{2\pi}\int_0^{2\pi} d\phi\ (\mathcal{W}\circ\mathcal{L}^{\eta,N_B})(e^{i\phi\hat{n}}\rho e^{-i\phi\hat{n}})\ . \tag{3.2.46}$$

Note that the phase covariance property mentioned above is the statement that the following equality holds for all $\phi\in[0,2\pi)$ [163]:

$$\sigma_{E_2'GE_1'}(\phi)=(\mathcal{W}\circ\mathcal{L}^{\eta,N_B})(e^{i\phi\hat{n}}\rho e^{-i\phi\hat{n}}). \tag{3.2.47}$$

Consider the following chain of inequalities for a Gaussian input state ρ:

$$H(G|E_1'E_2')_{(\mathcal{W}\circ\mathcal{L}^{\eta,N_B})(\rho)} = \frac{1}{2\pi}\int_0^{2\pi} d\phi\ H(G|E_1'E_2')_{\sigma(\phi)} \tag{3.2.48}$$

$$= \frac{1}{2\pi}\int_0^{2\pi} d\phi\ H(G|E_1'E_2')_{(\mathcal{W}\circ\mathcal{L}^{\eta,N_B})(e^{i\phi\hat{n}}\rho e^{-i\phi\hat{n}})} \tag{3.2.49}$$

$$\leq H(G|E_1'E_2')_{\xi} \tag{3.2.50}$$

$$= H(G|E_1'E_2')_{(\mathcal{W}\circ\mathcal{L}^{\eta,N_B})(\theta(N_t))}\ , \tag{3.2.51}$$

The first equality follows from invariance of the conditional entropy under local unitaries. The second equality follows from the phase covariance property of the channel. The inequality follows from concavity of conditional entropy. The last equality follows from linearity of the channel, and the following identity:

$$\theta(N_t) = \frac{1}{2\pi}\int_0^{2\pi} d\phi\ e^{i\phi\hat{n}}\rho e^{-i\phi\hat{n}}\ . \tag{3.2.52}$$

In (3.2.52), the state after the phase averaging is diagonal in the number basis, and furthermore, the resulting state has the same photon number N_t as the Gaussian state ρ. The thermal state $\theta(N_t)$ is the only Gaussian state of a single mode that is diagonal in the number basis with photon number equal to N_t.

Next, we argue that, for a given photon number constraint, a thermal state that saturates the constraint is the optimal state for the conditional output entropy. Let

$$\tau_{E_2'GE_1'}(\alpha) =$$
$$[D(\sqrt{1-\eta}\alpha)\otimes D(\sqrt{2\eta-1}\alpha)\otimes I][(\mathcal{W}\circ\mathcal{L}^{\eta,N_B})(\theta(N_t))][D^\dagger(\sqrt{1-\eta}\alpha)\otimes D^\dagger(\sqrt{2\eta-1}\alpha)\otimes I]\ . \tag{3.2.53}$$

Consider the following chain of inequalities:

$$H(G|E_1'E_2')_{(\mathcal{W}\circ\mathcal{L}^{\eta,N_B})(\theta(N_t))} = \int d^2\alpha \; q_{(N_S-N_t)}(\alpha) \; H(G|E_1'E_2')_{(\mathcal{W}\circ\mathcal{L}^{\eta,N_B})(\theta(N_t))} \tag{3.2.54}$$

$$= \int d^2\alpha \; q_{(N_S-N_t)}(\alpha) \; H(G|E_1'E_2')_{\tau(\alpha)} \tag{3.2.55}$$

$$= \int d^2\alpha \; q_{(N_S-N_t)}(\alpha) \; H(G|E_1'E_2')_{(\mathcal{W}\circ\mathcal{L}^{\eta,N_B})(D(\alpha)\theta(N_t)D^\dagger(\alpha))} \tag{3.2.56}$$

$$\leq H(G|E_1'E_2')_{(\mathcal{W}\circ\mathcal{L}^{\eta,N_B})\theta(N_S)} \; , \tag{3.2.57}$$

where $q_N(\alpha) = \exp\{-|\alpha|^2/N\}/\pi N$ is a complex-centered Gaussian distribution with variance $N \geq 0$. The first equality follows by placing a probability distribution in front, and the second follows from invariance of the conditional entropy under local unitaries. The third equality follows because the channel is covariant with respect to displacement operators, as reviewed in (2.3.69). The last inequality follows from concavity of conditional entropy, and from the fact that a thermal state with a higher mean photon number can be realized by random Gaussian displacements of a thermal state with a lower mean photon number, as reviewed in (2.3.33). Hence, for a given input mean photon number constraint N_S, a thermal state with mean photon number N_S optimizes the conditional entropy of degradation defined from (3.1.2). ■

Remark 79 *The arguments used in the proof of Proposition 78 can be employed in more general situations beyond that which is discussed there. The main properties that we need are the following, when the channel involved takes a single-mode input to a multi-mode output:*

- *The channel should be phase covariant, such that a phase rotation on the input state is equivalent to a product of local phase rotations on the output.*
- *The channel should be covariant with respect to displacement operators, such that a displacement operator acting on the input state is equivalent to a product of local*

displacement operators on the output.

- *The function being optimized should be invariant with respect to local unitaries and concave in the input state.*

If all of the above hold, then we can conclude that the thermal-state input saturating the energy constraint is an optimal input state. We employ this reasoning again in the proof of Theorem 87. It has also been used in [151].

3.2.3 ε-Close-Degradable Bound on the Energy-Constrained Quantum Capacity of Bosonic Thermal Channels

In this section, we first establish an upper bound on the diamond distance between a thermal channel and a pure-loss channel. Since a pure-loss channel is a degradable channel, an upper bound on the energy-constrained quantum capacity of a thermal channel directly follows from Theorem 69.

Theorem 80 *If a thermal channel $\mathcal{L}^{\eta,N_B}$ and a pure-loss bosonic channel $\mathcal{L}^{\eta,0}$ have the same transmissivity parameter $\eta \in [0,1]$, then*

$$\frac{1}{2}\left\|\mathcal{L}^{\eta,N_B} - \mathcal{L}^{\eta,0}\right\|_\diamond \leq \frac{N_B}{N_B+1} \ . \tag{3.2.58}$$

Proof. Let $\mathcal{B}$ represent the beamsplitter transformation, and let $\theta_E(N_B)$ and $\theta'_E(0)$ denote the states of the environment for the thermal channel and pure-loss channel, respectively. For every input state ψ_{RA} to both thermal and pure-loss channels, the following inequalities

hold:

$$\begin{aligned}
&\left\|(\mathrm{id}_R \otimes \mathcal{L}^{\eta,N_B})(\psi_{RA}) - (\mathrm{id}_R \otimes \mathcal{L}^{\eta,0})(\psi_{RA})\right\|_1 \\
&= \|\mathrm{Tr}_{E'}\{\mathcal{B}_{AE\to BE'}(\psi_{RA} \otimes \theta_E(N_B)) - \mathcal{B}_{AE\to BE'}(\psi_{RA} \otimes \theta'_E(0))\}\|_1 && (3.2.59)\\
&\leq \|\mathcal{B}_{AE\to BE'}(\psi_{RA} \otimes \theta_E(N_B)) - \mathcal{B}_{AE\to BE'}(\psi_{RA} \otimes \theta'_E(0))\|_1 && (3.2.60)\\
&= \|\psi_{RA} \otimes \theta_E(N_B) - \psi_{RA} \otimes \theta'_E(0)\|_1 && (3.2.61)\\
&= \|\theta_E(N_B) - \theta'_E(0)\|_1 && (3.2.62)\\
&= \left\|\sum_{n=0}^{\infty} \frac{(N_B)^n}{(N_B+1)^{n+1}}\ |n\rangle\langle n| - |0\rangle\langle 0|\right\|_1 && (3.2.63)\\
&= \frac{2N_B}{N_B+1}\ . && (3.2.64)
\end{aligned}$$

The first equality follows from the definition of the channel in terms of its environment and a unitary interaction (beam splitter). The first inequality follows from monotonicity of the trace distance. The second equality follows from invariance of the trace distance under a unitary operator (beamsplitter). The last equality follows from basic algebra. Since these inequalities hold for every state ψ_{RA}, the final result follows from the definition of the diamond norm. ■

Remark 81 *In [168], it has been shown that the optimal strategy to distinguish two quantum thermal channels $\mathcal{L}^{\eta,N_B^1}$ and $\mathcal{L}^{\eta,N_B^2}$, each having the same transmissivity parameter η, and thermal noises N_B^1 and N_B^2, respectively, is to use a highly squeezed, two-mode squeezed vacuum state $\psi_{\mathrm{TMS}}(N_S)_{RA}$ as input to the channels. According to [168, Eq. (35)],*

$$\lim_{N_S\to\infty} F(\sigma_{N_B^1}, \sigma_{N_B^2}) = F(\theta(N_B^1), \theta(N_B^2)), \tag{3.2.65}$$

where $\sigma_{N_B^i} \equiv (\mathrm{id}_R \otimes \mathcal{L}^{\eta,N_B^i})(\psi_{\mathrm{TMS}}(N_S)_{RA})$, and $\theta(N_B^i)$ is a thermal state with mean photon

number N_B^i. Hence, a lower bound on the diamond distance in Theorem 80 is given by

$$\frac{1}{2}\left\|\mathcal{L}^{\eta,N_B}-\mathcal{L}^{\eta,0}\right\|_\diamond \geq 1-\sqrt{F(\theta(N_B),\theta(0))}=1-1/\sqrt{N_B+1}, \tag{3.2.66}$$

where the inequality follows from the Powers-Stormer inequality [135]. We also suspect that the upper bound in Theorem 80 is achievable, but we are not aware of a method for computing the trace distance of general quantum Gaussian states, which is what it seems would be needed to verify this suspicion.

Theorem 82 *An upper bound on the quantum capacity of a thermal channel $\mathcal{L}^{\eta,N_B}$ with transmissivity $\eta \in [1/2,1]$, environment photon number N_B, and input mean photon number constraint N_S is given by*

$$\begin{aligned} Q(\mathcal{L}^{\eta,N_B},N_S) \leq Q_{U_3}(\mathcal{L}^{\eta,N_B},N_S) &\equiv g(\eta N_S)-g[(1-\eta)N_S] \\ &+(4\varepsilon'+8\delta)g[(\eta N_S+(1-\eta)N_B)/\delta]+2g(\varepsilon')+4h_2(\delta)\ , \end{aligned} \tag{3.2.67}$$

with $\varepsilon = N_B/(N_B+1)$, $\varepsilon' \in (\varepsilon,1]$ and $\delta=(\varepsilon'-\varepsilon)/(1+\varepsilon')$.

Proof. From Theorem 80, we have that $\frac{1}{2}\left\|\mathcal{L}^{\eta,N_B}-\mathcal{L}^{\eta,0}\right\|_\diamond \leq \frac{N_B}{N_B+1} < \varepsilon' \leq 1$. Due to the input mean photon number constraint N_S for n channel uses, the output mean photon number cannot exceed $\eta N_S+(1-\eta)N_B$ for the thermal channel and ηN_S for the pure-loss channel. Hence, there is a photon number constraint $\eta N_S+(1-\eta)N_B$ for the output of both the thermal and pure-loss channels. Since the pure-loss channel is a degradable channel for $\eta \in [1/2,1]$ [63, 160], the final result follows directly from Theorem 69. ■

3.2.4 Bottleneck Bound on the Energy-Constrained Quantum Capacity of Bosonic Thermal Channels

In this section we establish an upper bound on the quantum capacity of a thermal channel using Theorem 83 below, which states that any phase-insensitive single-mode bosonic

Gaussian channel can be decomposed as a pure-amplifier channel followed by a pure-loss channel, if the original channel is not entanglement breaking. This theorem was independently proven in [148, 149] (see also [150] in this context).

Before we state the theorem, let us recall that the action of a phase-insensitive channel $\mathcal{N}$ on the covariance matrix Γ of a single-mode, bosonic quantum state is given by

$$\Gamma \longmapsto \tau\ \Gamma + \nu I_2, \tag{3.2.68}$$

where ν is the variance of an additive noise, I_2 is the 2×2 identity matrix, and τ and ν satisfy the conditions in (2.3.74)–(2.3.75). Moreover, as mentioned previously, a phase-insensitive channel $\mathcal{N}$ is entanglement-breaking [125, 126] if

$$\tau + 1 \leq \nu\ . \tag{3.2.69}$$

Theorem 83 *Any single-mode, phase-insensitive bosonic Gaussian channel $\mathcal{N}$ that is not entanglement-breaking (i.e., satisfies $\tau + 1 > \nu$) can be decomposed as the concatenation of a quantum-limited amplifier channel $\mathcal{A}^{G,0}$ with gain $G > 1$ followed by a pure-loss channel $\mathcal{L}^{\eta,0}$ with transmissivity $\eta \in (0, 1]$, i.e.,*

$$\mathcal{N} = \mathcal{L}^{\eta,0} \circ \mathcal{A}^{G,0}, \tag{3.2.70}$$

where $\eta = (\tau + 1 - \nu)/2$ and $G = \tau/\eta$.

Proof. The action of a quantum-limited amplifier channel $\mathcal{A}^{G,0}$ with gain G followed by a pure-loss channel $\mathcal{L}^{\eta,0}$ with transmissivity η, on convariance matrix Γ is given by

$$\eta(G\ \Gamma + [G-1]I_2) + [1-\eta]I_2. \tag{3.2.71}$$

By comparing (3.2.68) and (3.2.71), we find that it is necessary for the following equalities

to hold

$$\eta G = \tau, \tag{3.2.72}$$

$$\eta(G-1) + 1 - \eta = \nu. \tag{3.2.73}$$

Solving these equations for η and G in terms of τ and ν then gives $\eta = (\tau + 1 - \nu)/2$ and $G = \tau/\eta$. By the assumption that $\mathcal{N}$ is not entanglement breaking, which is that $\tau + 1 > \nu$, we find that

$$\eta = (\tau + 1 - \nu)/2 > 0. \tag{3.2.74}$$

Now applying the conditions in (2.3.74) and (2.3.75) for the channel $\mathcal{N}$ to be a CPTP map, we find that

$$\eta = (\tau + 1 - \nu)/2 \leq (\tau + 1 - |1 - \tau|)/2 = \begin{cases} \tau & \text{for } \tau \in [0, 1) \\ 1 & \text{for } \tau \geq 1 \end{cases} \tag{3.2.75}$$

By the fact that $G = \tau/\eta$, the above implies that $G > 1$, so that the decomposition in (3.2.70) is valid under the stated conditions. ■

We now introduce an upper bound on the energy-constrained quantum capacity of thermal channels in the following theorem (independently discovered in [149] as well):

Theorem 84 *An upper bound on the energy-constrained quantum capacity of a thermal channel $\mathcal{L}^{\eta,N_B}$ with transmissivity $\eta \in [1/2, 1]$, environment photon number $N_B \geq 0$, such that $\eta > (1-\eta)N_B$, and input mean photon number constraint $N_S \geq 0$ is given by*

$$Q(\mathcal{L}^{\eta,N_B}, N_S) \leq \max\{0, Q_{U_4}(\mathcal{L}^{\eta,N_B}, N_S)\}, \tag{3.2.76}$$

where

$$Q_{U_4}(\mathcal{L}^{\eta,N_B}, N_S) \equiv g(\eta N_S + (1-\eta)N_B) - g[(1/\eta' - 1)(\eta N_S + (1-\eta)N_B)], \tag{3.2.77}$$

and $\eta' = \eta - (1-\eta)N_B$.

Proof. Using Theorem 83, a thermal channel $\mathcal{L}^{\eta,N_B}$ satisfying $\eta > (1-\eta)N_B$ can be decomposed as the concatenation of a quantum-limited amplifier channel $\mathcal{A}^{G,0}$ followed by a pure-loss channel $\mathcal{L}^{\eta',0}$, such that

$$G = \eta/\eta', \tag{3.2.78}$$

$$\eta' = \eta - (1-\eta)N_B \ . \tag{3.2.79}$$

Consider the following chain of inequalities:

$$\begin{aligned} Q(\mathcal{L}^{\eta,N_B}, N_S) &= Q(\mathcal{L}^{\eta',0} \circ \mathcal{A}^{G,0}, N_S) && (3.2.80)\\ &\leq Q(\mathcal{L}^{\eta',0}, GN_S + G - 1) && (3.2.81)\\ &= g(\eta'[GN_S + G - 1]) - g[(1-\eta')(GN_S + G - 1)] && (3.2.82)\\ &= g(\eta N_S + (1-\eta)N_B) - g[(1/\eta' - 1)(\eta N_S + (1-\eta)N_B)] \ . && (3.2.83) \end{aligned}$$

The first inequality is a consequence of the following argument: consider an arbitrary encoding and decoding scheme for energy-constrained quantum communication over the thermal channel $\mathcal{L}^{\eta,N_B}$, which satisfies the mean input photon number constraint $N_S \geq 0$. Due to the decomposition of $\mathcal{L}^{\eta,N_B}$ as $\mathcal{L}^{\eta',0} \circ \mathcal{A}^{G,0}$, this encoding, followed by many uses of the pure-amplifier channel $\mathcal{A}^{G,0}$ can be considered as an encoding for the channel $\mathcal{L}^{\eta',0}$, which also satisfies the mean photon number constraint $GN_S + G - 1$, due to the fact that the pure-amplifier channel $\mathcal{A}^{G,0}$ introduces a gain. Since the energy-constrained quantum capacity of the channel $\mathcal{L}^{\eta',0}$ involves an optimization over all such encodings that satisfies the mean photon number constraint $GN_S + G - 1$, we arrive at the desired inequality. The second equality follows from the formula for the energy-constrained quantum capacity of a pure-loss bosonic channel with transmissivity η' and input mean photon number $GN_S + G - 1$ [62,64].

■

Remark 85 *Applying Remark 65, we find the following bottleneck bound $Q_{U_4}(\mathcal{L}^{\eta,N_B})$ on the unconstrained quantum capacity of bosonic thermal channels for which $\eta > (1-\eta)N_B$:*

$$Q(\mathcal{L}^{\eta,N_B}) \leq Q_{U_4}(\mathcal{L}^{\eta,N_B}) = \sup_{N_S : N_S \in [0,\infty]} Q_{U_4}(\mathcal{L}^{\eta,N_B}, N_S) \tag{3.2.84}$$

$$= \lim_{N_S \to \infty} Q_{U_4}(\mathcal{L}^{\eta,N_B}, N_S) \tag{3.2.85}$$

$$= \max\left\{0, \log_2\left(\frac{\eta - (1-\eta)N_B}{(1-\eta)(N_B+1)}\right)\right\} . \tag{3.2.86}$$

The aforementioned bound on the unconstrained quantum capacity of a thermal channel was also established independently in [148]. Note that (3.2.86) is slightly tighter than (3.2.9) for all parameter regimes. These findings were independently discovered in [149].

Remark 86 *The upper bound $Q_{U_4}(\mathcal{L}^{\eta,N_B}, N_S)$ on the energy-constrained quantum and private capacities of thermal channels places a strong restriction on the channel parameters η and N_B. Since the quantum and private capacities of a pure-loss channel with η' are non-zero only for $\eta' > 1/2$, the energy-constrained quantum and private capacities of a thermal channel will be non-zero only for*

$$1 \geq \eta > \frac{1+2N_B}{2(1+N_B)}, \tag{3.2.87}$$

which is the same as the condition given in [127, Section 4].

3.3 Comparison of Upper Bounds on the Energy-Constrained Quantum Capacity of Bosonic Thermal Channels

In this section, we study the closeness of the four different upper bounds when compared to a known lower bound. In particular, we use the following lower bound on the quantum

capacity of a thermal channel [64, 147] and denote it by Q_L:

$$Q(\mathcal{L}^{\eta,N_B}, N_S) \geq Q_L(\mathcal{L}^{\eta,N_B}, N_S) \equiv g(\eta N_S + (1-\eta)N_B) \\ - g([D + (1-\eta)N_S - (1-\eta)N_B - 1]/2) - g([D - (1-\eta)N_S + (1-\eta)N_B - 1]/2), \tag{3.3.1}$$

where

$$D^2 \equiv [(1+\eta)N_S + (1-\eta)N_B + 1]^2 - 4\eta N_S(N_S+1). \tag{3.3.2}$$

We start by discussing how close the data-processing bound Q_{U_1} is to the aforementioned lower bound. In particular, we show that the data-processing bound Q_{U_1} can be at most 1.45 bits larger than Q_L.

Theorem 87 *Let $\mathcal{L}^{\eta,N_B}$ be a thermal channel with transmissivity $\eta \in [1/2, 1]$, environment photon number N_B, and input mean photon number constraint N_S. Then the following relation holds between the data-processing bound $Q_{U_1}(\mathcal{L}^{\eta,N_B}, N_S)$ in (3.2.3) and the lower bound $Q_L(\mathcal{L}^{\eta,N_B}, N_S)$ in (3.3.1) on the energy-constrained quantum capacity of a thermal channel:*

$$Q_L(\mathcal{L}^{\eta,N_B}, N_S) \leq Q_{U_1}(\mathcal{L}^{\eta,N_B}, N_S) \leq Q_L(\mathcal{L}^{\eta,N_B}, N_S) + 1/\ln 2 \ . \tag{3.3.3}$$

Proof. To prove this result, we first compute the difference between the data-processing bound in (3.2.3) and the lower bound in (3.3.1) and show that it is equal to $1/\ln 2$ as $N_S \to \infty$. Next, we prove that the difference is a monotone increasing function with respect to input mean photon number $N_S \geq 0$. Hence, the difference $Q_{U_1}(\mathcal{L}^{\eta,N_B}, N_S) - Q_L(\mathcal{L}^{\eta,N_B}, N_S)$ attains its maximum value in the limit $N_S \to \infty$. We note that a similar statement has been given in [144] to bound the classical capacity of a thermal channel, but the details of the approach we develop here are different and are likely to be more broadly applicable to related future questions.

For simplicity, we denote $(1-\eta)N_B$ as Y, employ the natural logarithm for $g(x)$, and

omit the prefactor $1/\ln 2$ from all instances of $g(x)$. We use the following property of the function $g(x)$: For large x,

$$g(x) = \ln(x+1) + 1 + O(1/x), \tag{3.3.4}$$

so that as $x \to \infty$, the approximation $g(x) \approx \ln(x+1) + 1$ holds. Using (3.3.4), the data-processing bound in (3.2.3) can be expressed as follows for large N_S:

$$\ln(Y + 1 + \eta N_S) - \ln(Y + 1 + (Y + 1 - \eta)N_S) + O(1/N_S)\ . \tag{3.3.5}$$

Similarly, the lower bound Q_L in (3.3.1) can be expressed as

$$\ln(1 + \eta N_S + Y) - \ln([1 + D + (1-\eta)N_S - Y]/2) - \ln([1 + D - (1-\eta)N_S + Y]/2) + O(1/N_S) - 1\ . \tag{3.3.6}$$

Let us denote the difference between Q_{U_1} and Q_L by $\Delta(\mathcal{L}^{\eta,N_B}, N_S)$.

$$\Delta(\mathcal{L}^{\eta,N_B}, N_S) = Q_{U_1}(\mathcal{L}^{\eta,N_B}, N_S) - Q_L(\mathcal{L}^{\eta,N_B}, N_S). \tag{3.3.7}$$

Then the difference simplifies as

$$\begin{aligned}
&\Delta(\mathcal{L}^{\eta,N_B}, N_S) \\
&= 1 - \ln(Y + 1 + (Y + 1 - \eta)N_S) + \ln\Big([(1+D)^2 - ((1-\eta)N_S - Y)^2]/4\Big) + O(1/N_S)\ . \qquad (3.3.8)\\
&= 1 - \ln(Y + 1 + (Y + 1 - \eta)N_S) + \ln([1 + N_S(1 - \eta + 2Y) + Y + D]/2) + O(1/N_S) \qquad (3.3.9)\\
&= 1 + \ln([1 + N_S(1 - \eta + 2Y) + Y + D]/[2(Y + 1 + (Y + 1 - \eta)N_S)]) + O(1/N_S). \qquad (3.3.10)
\end{aligned}$$

The second equality follows from the definition of D^2. Next, we show that

$$\ln([1 + N_S(1 - \eta + 2Y) + Y + D]/[2(Y + 1 + (Y + 1 - \eta)N_S)]) \to 0 \tag{3.3.11}$$

as $N_S \to \infty$, and hence we get the desired result. Consider the following expression and take the limit $N_S \to \infty$:

$$\lim_{N_S \to \infty} \frac{1 + N_S(1 - \eta + 2Y) + Y + D}{2(Y + 1 + (Y + 1 - \eta)N_S)} \tag{3.3.12}$$

$$= \lim_{N_S \to \infty} \frac{1/N_S + (1 - \eta + 2Y) + Y/N_S + \sqrt{((1 + \eta) + (Y + 1)/N_S)^2 - 4\eta - 4\eta/N_S}}{2((Y + 1)/N_S + (Y + 1 - \eta))} \tag{3.3.13}$$

$$\to \frac{(1 - \eta + 2Y) + 1 - \eta}{2(Y + 1 - \eta)} = 1 \ . \tag{3.3.14}$$

Hence, $\lim_{N_S \to \infty} \Delta(\mathcal{L}^{\eta, N_B}, N_S) = 1$. After incorporating the $1/\ln 2$ factor, which was omitted earlier for simplicity, we find that the difference between the upper and lower bounds approaches $1/\ln 2$ (≈ 1.45 bits) as $N_S \to \infty$.

Now, we show that the difference $\Delta(\mathcal{L}^{\eta, N_B}, N_S)$ is a monotone increasing function with respect to the input mean photon number $N_S \geq 0$. Let $\mathcal{U}^{\eta'}_{A \to B_1 E_1}$ and $\mathcal{V}^{G}_{B_1 \to B_2 E_2}$ denote Stinespring dilations of a pure-loss channel $\mathcal{L}^{\eta', 0} : A \to B_1$ and a quantum limited amplifier channel $\mathcal{A}^{G,0} : B_1 \to B_2$, respectively. For the energy-constrained quantum capacity of a pure-loss channel, the thermal state as an input is optimal for any fixed energy or input mean photon number constraint N_S [64]. Moreover, the lower bound in (3.3.1) is obtained for a thermal state with mean photon number N_S as input to the channel. Then the action of a thermal channel $\mathcal{L}^{\eta, N_B}$ on an input state $\theta(N_S)$ can be expressed as

$$\mathcal{L}^{\eta, N_B}(\theta(N_S)) = \mathrm{Tr}_{E_1 E_2}\{(\mathrm{id}_{E_1} \otimes \mathcal{V}^{G}_{B_1 \to B_2 E_2}) \circ \mathcal{U}^{\eta'}_{A \to B_1 E_1}(\theta(N_S))\} \ . \tag{3.3.15}$$

Consider the following state:

$$\omega_{B_2E_1E_2} = (\mathrm{id}_{E_1} \otimes \mathcal{V}^G_{B_1\to B_2E_2}) \circ \mathcal{U}^{\eta'}_{A\to B_1E_1}(\theta(N_S)) \ . \tag{3.3.16}$$

Since the data-processing bound $Q_{U_1}(\mathcal{L}^{\eta,N_B}, N_S)$ is equal to the quantum capacity of a pure-loss channel with transmissivity η', which in turn is equal to the coherent information for this case, (3.2.3) can also be represented as

$$Q_{U_1}(\mathcal{L}^{\eta,N_B}, N_S) = H(B_2E_2)_\omega - H(E_1)_\omega \ . \tag{3.3.17}$$

Similarly, the lower bound can be expressed as

$$Q_L(\mathcal{L}^{\eta,N_B}, N_S) = H(B_2)_\omega - H(E_1E_2)_\omega. \tag{3.3.18}$$

Hence the difference between (3.3.17) and (3.3.18) is given by

$$\Delta(\mathcal{L}^{\eta,N_B}, N_S) = H(E_2|B_2)_\omega + H(E_2|E_1)_\omega \ . \tag{3.3.19}$$

Now, our aim is to show that the conditional entropies in (3.3.19) are monotone increasing functions of N_S. We employ displacement covariance of the channels, and note that this argument is similar to that used in the proof of Proposition 78. Let

$$\begin{aligned}\sigma_{B_2E_1E_2}(\alpha) = [D(\sqrt{\eta G}\alpha) \otimes I \otimes D(\sqrt{\eta(G-1)}\alpha)]\ \omega_{B_2E_1E_2} \\ \times [D^\dagger(\sqrt{\eta G}\alpha) \otimes I \otimes D^\dagger(\sqrt{\eta(G-1)}\alpha)],\end{aligned} \tag{3.3.20}$$

$$\begin{aligned}\tau_{B_2E_1E_2}(\alpha) = [I \otimes D(\sqrt{1-\eta}\alpha) \otimes D(\sqrt{\eta(G-1)}\alpha)]\ \omega_{B_2E_1E_2} \\ \times [I \otimes D^\dagger(\sqrt{1-\eta}\alpha) \otimes D^\dagger(\sqrt{\eta(G-1)}\alpha)] \ .\end{aligned} \tag{3.3.21}$$

Let $N_S' - N_S \geq 0$, and consider the following chain of inequalities:

$$H(E_2|B_2)_\omega + H(E_2|E_1)_\omega = \int d^2\alpha \; q_{(N_S'-N_S)}(\alpha) \; [H(E_2|B_2)_\omega + H(E_2|E_1)_\omega] \tag{3.3.22}$$

$$= \int d^2\alpha \; q_{(N_S'-N_S)}(\alpha) \; [H(E_2|B_2)_{\sigma(\alpha)} + H(E_2|E_1)_{\tau(\alpha)}] \tag{3.3.23}$$

$$= \int d^2\alpha \; q_{(N_S'-N_S)}(\alpha) \; [H(E_2|B_2)_{(\mathcal{V}^G \circ \mathcal{U}^{\eta'})(D(\alpha)\theta(N_S)D^\dagger(\alpha))}] + \int d^2\alpha \; q_{(N_S'-N_S)}(\alpha) \; [H(E_2|E_1)_{(\mathcal{V}^G \circ \mathcal{U}^{\eta'})(D(\alpha)\theta(N_S)D^\dagger(\alpha))}] \tag{3.3.24}$$

$$\leq H(E_2|B_2)_{(\mathcal{V}^G \circ \mathcal{U}^{\eta'})(\theta(N_S'))} + H(E_2|E_1)_{(\mathcal{V}^G \circ \mathcal{U}^{\eta'})(\theta(N_S'))} \; . \tag{3.3.25}$$

The first equality follows by placing a probability distribution in front, and the second follows from invariance of the conditional entropy under local unitaries. The third equality follows because the channel is covariant with respect to displacement operators, as reviewed in (2.3.69). The last inequality follows from concavity of conditional entropy, and from the fact that a thermal state with a higher mean photon number can be realized by random Gaussian displacements of a thermal state with a lower mean photon number, as reviewed in (2.3.33).

Hence, the difference between the data-processing bound in (3.2.3) and the lower bound in (3.3.1) attains its maximum value in the limit $N_S \to \infty$. ■

Next, we perform numerical evaluations to see how close the four different upper bounds are to the lower bound Q_L in (3.3.1). Since there is a free parameter ε' in both the ε-degradable bound in (3.2.36) and the ε-close-degradable bound in (3.2.67), we optimize these bounds with respect to ε' [163]. In Figure 3.3, we plot the data-processing bound Q_{U_1}, the ε-degradable bound Q_{U_2}, the ε-close-degradable bound Q_{U_3}, the bottleneck bound Q_{U_4}, and the lower bound Q_L versus N_S for certain values of the transmissivity η and thermal noise N_B. In particular, we find that both the data-processing bound and the bottleneck bound are close to the lower bound Q_L for both low and high thermal noise. In

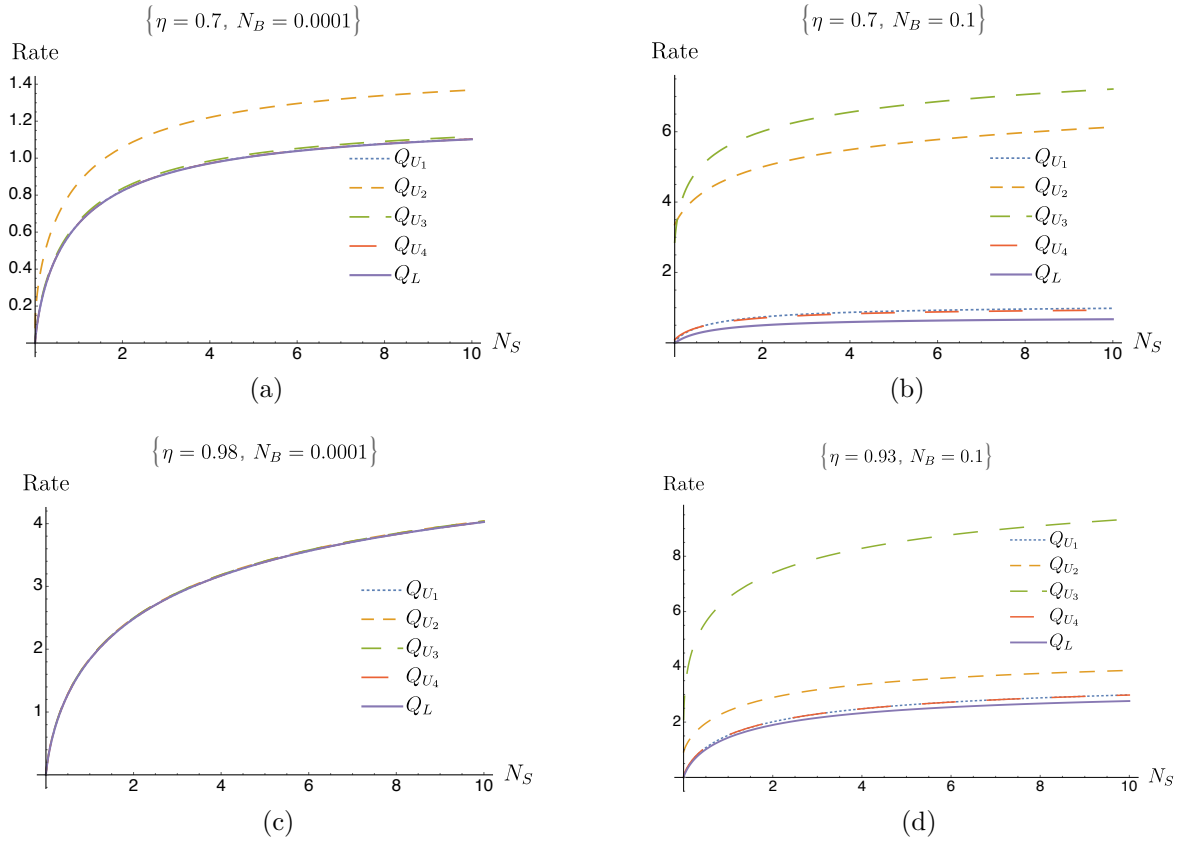

Figure 3.3: The figures plot the data-processing bound (Q_{U_1}), the ε-degradable bound (Q_{U_2}), the ε-close-degradable bound (Q_{U_3}), the bottleneck bound Q_{U_4}, and the lower bound (Q_L) on energy-constrained quantum capacity of thermal channels. In each figure, we select certain values of η and N_B, with the choices indicated above each figure. In all the cases, both the data-processing bound Q_{U_1} and the bottleneck bound Q_{U_4} are close to the lower bound Q_{U_L}. In (a), for medium transmissivity and low thermal noise, the ε-close-degradable bound is close to the data-processing bound and the bottleneck bound, and they are tighter than the ε-degradable bound. In (b), for medium transmissivity and high thermal noise, only the data-processing bound and the bottleneck bound are close to the lower bound. Also the ε-degradable bound is tighter than the ε-close-degradable bound. In (c), for high transmissivity and low thermal noise, all upper bounds are very near to the lower bound. In (d), for high transmissivity and high noise, the ε-degradable bound is tighter than the ε-close-degradable bound.

particular, for the data-processing bound Q_{U_1}, this is related to Theorem 87, as Q_{U_1} can be at most 1.45 bits larger than the lower bound Q_L. In Figure 3.3(a), we plot for medium transmissivity and low thermal noise. We find that the ε-close-degradable bound is very near to the data-processing bound and is tighter than the ε-degradable bound. Moreover, Q_{U_4} is slightly tighter than Q_{U_1} for some parameter regimes. In Figure 3.3(b), we plot for medium transmissivity and high thermal noise. We find that the ε-degradable bound is tighter than the ε-close degradable bound. In Figure 3.3(d), we plot for high transmissivity and high thermal noise. In Figure 3.3(c), we plot for high transmissivity and low thermal noise. We find that all upper bounds are very near to the lower bound Q_L. From Figures 3.3(a) and 3.3(c), it is evident that in the low-noise regime, there is a strong limitation on any potential super-additivity of coherent information of a thermal channel. Similar results were obtained on quantum and private capacities of low-noise quantum channels in [169]. It is important to stress that the upper bound Q_{U_3} can serve as a good bound only for low values of the thermal noise N_B, as the technique to calculate this bound requires the closeness of a thermal channel with a pure-loss channel (discussed in Theorem 80), and the closeness parameter is equal to $N_B/(N_B+1)$.

In Figure 3.4, we plot all the upper bounds and the lower bound Q_L versus N_S, for high transmissivity and high thermal noise. In Figure 3.4(a), we find that the ε-degradable bound is tighter than all other bounds for high values of N_S. In Figure 3.4(b), we plot for the same parameter values, but for low values of N_S. It is evident that for low input mean photon number, both the data-processing bound and the bottleneck bound are tighter than the ε-degradable bound.

The plots suggest that our upper bounds based on the notion of approximate degradability are good for the case of high input mean photon number. We suspect that these bounds can be further improved for the case of low input mean photon number by considering the energy-constrained diamond norm [137, 138]. To address this question, we consider the generalized channel divergences of quantum Gaussian channels in Section 3.8 and argue

about their optimization.

3.4 Upper Bounds on Energy-Constrained Private Capacity of Bosonic Thermal Channels

In this section, we provide four different upper bounds on the energy-constrained private capacity of a thermal channel. These upper bounds are derived very similarly as in Section 3.2. We call these different bounds the data-processing bound, the ε-degradable bound, the ε-close-degradable bound, and the bottleneck bound, and denote them by P_{U_1}, P_{U_2}, P_{U_3}, and P_{U_4}, respectively.

3.4.1 Data-Processing Bound on the Energy-Constrained Private Capacity of Bosonic Thermal Channels

Theorem 88 *An upper bound on the private capacity of a thermal channel $\mathcal{L}^{\eta,N_B}$ with transmissivity $\eta \in [1/2, 1]$, environment photon number $N_B \geq 0$, and input mean photon number constraint $N_S \geq 0$ is given by*

$$P(\mathcal{L}^{\eta,N_B}, N_S) \leq \max\{0, P_{U_1}(\mathcal{L}^{\eta,N_B}, N_S)\} \tag{3.4.1}$$

$$P_{U_1}(\mathcal{L}^{\eta,N_B}, N_S) \equiv g(\eta' N_S) - g[(1-\eta')N_S] \ , \tag{3.4.2}$$

with $\eta' = \eta/((1-\eta)N_B + 1)$.

Proof. A proof follows from arguments similar to those in the proof of Theorem 73. Since a pure-loss channel is a degradable channel [63,160], its energy-constrained private capacity is the same as its energy-constrained quantum capacity [62]. ■

Remark 89 *Applying Remarks 65 and 74, we find the following data-processing bound $P_{U_1}(\mathcal{L}^{\eta,N_B})$ on the unconstrained private capacity $P(\mathcal{L}^{\eta,N_B})$ of a thermal channel $\mathcal{L}^{\eta,N_B}$:*

$$P(\mathcal{L}^{\eta,N_B}) \leq P_{U_1}(\mathcal{L}^{\eta,N_B}) = \log_2(\eta/(1-\eta)) - \log_2(N_B + 1) \ . \tag{3.4.3}$$

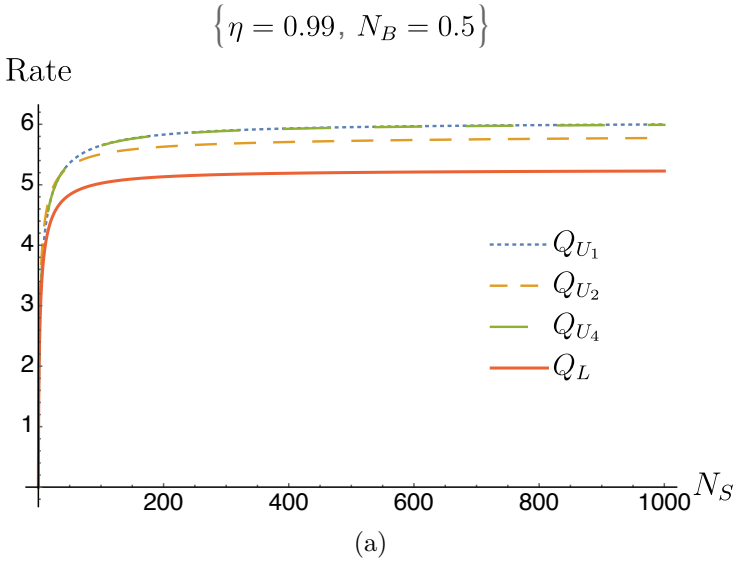

(a)

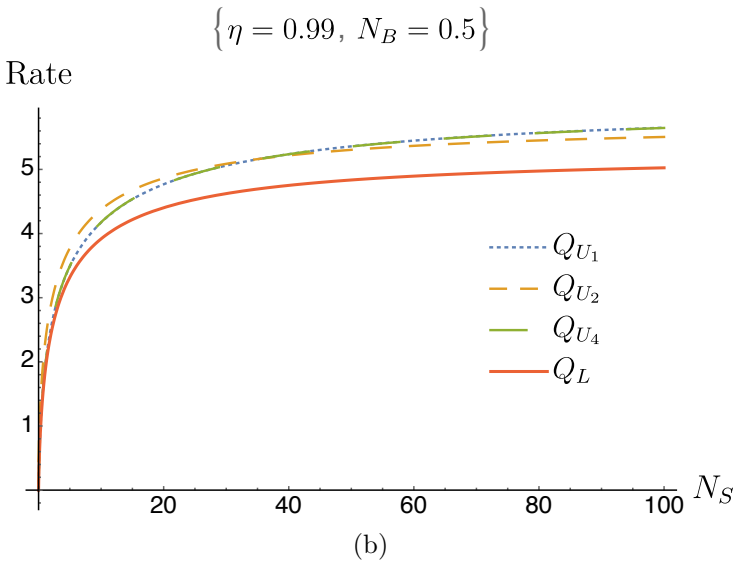

(b)

Figure 3.4: The figures plot the data-processing bound (Q_{U_1}), the ε-degradable bound (Q_{U_2}), and the lower bound (Q_L) on energy-constrained quantum capacity of thermal channels (the ε-close-degradable bound (Q_{U_3}) is not plotted because it is much higher than the other bounds for all parameter values considered). In each figure, we select $\eta = 0.99$ and $N_B = 0.5$. In (a), the ε-degradable upper bound is tighter than all other upper bounds. In (b), for low values of N_S, the data-processing bound is tighter than the ε-degradable bound.

3.4.2 ε-Degradable Bound on the Energy-Constrained Private Capacity of Bosonic Thermal Channels

Theorem 90 *An upper bound on the private capacity of a thermal channel $\mathcal{L}^{\eta,N_B}$ with transmissivity $\eta \in [1/2, 1]$, environment photon number $N_B \geq 0$, and input mean photon number constraint $N_S \geq 0$ is given by*

$$P(\mathcal{L}^{\eta,N_B}, N_S) \leq P_{U_2}(\mathcal{L}^{\eta,N_B}, N_S) \equiv g(\eta N_S + (1-\eta)N_B) - g(\zeta_+) - g(\zeta_-) + (6\varepsilon' + 12\delta) g([(1-\eta)N_S + (1+\eta)N_B]/\delta) + 3g(\varepsilon') + 6h_2(\delta) \ , \quad (3.4.4)$$

with

$$\varepsilon = \sqrt{1 - \eta^2 / \left(\eta^2 + N_B(N_B+1)[1 + 3\eta^2 - 2\eta(1+\sqrt{2\eta-1})]\right)} \ , \quad (3.4.5)$$

$$\zeta_\pm = \frac{1}{2}\left(-1 + \sqrt{[(1+2N_B)^2 - 2\varrho + (1+2\vartheta)^2 \pm 4(\vartheta - N_B)\sqrt{[1+N_B+\vartheta]^2 - \varrho}]/2}\right) \ , \quad (3.4.6)$$

$$\varrho = 4N_B(N_B+1)(2 - 1/\eta) \ , \quad (3.4.7)$$

$$\vartheta = \eta N_B + (1-\eta)N_S \ , \quad (3.4.8)$$

$\varepsilon' \in (\varepsilon, 1]$, and $\delta = (\varepsilon' - \varepsilon)/(1+\varepsilon')$.

Proof. A proof follows from arguments similar to those in the proof of Theorem 77. The final result is obtained using Theorem 71. ■

3.4.3 ε-Close-Degradable Bound on the Energy-Constrained Private Capacity of Bosonic Thermal Channels

Theorem 91 *An upper bound on the private capacity of a thermal channel $\mathcal{L}^{\eta,N_B}$ with transmissivity $\eta \in [1/2, 1]$, environment photon number $N_B \geq 0$, and input mean photon*

number constraint $N_S \geq 0$ is given by

$$P(\mathcal{L}^{\eta,N_B}, N_S) \leq P_{U_3}(\mathcal{L}^{\eta,N_B}, N_S) \equiv g(\eta N_S) - g[(1-\eta)N_S] + (8\varepsilon' + 16\delta) g[(\eta N_S + (1-\eta)N_B)/\delta] + 4g(\varepsilon') + 8h_2(\delta) \ , \quad (3.4.9)$$

with $\varepsilon = N_B/(N_B+1)$, $\varepsilon' \in (\varepsilon, 1]$, and $\delta = (\varepsilon' - \varepsilon)/(1+\varepsilon')$.

Proof. A proof follows from arguments similar to those in the proof of Theorem 82. The final result is obtained using Theorem 72. ■

3.4.4 Bottleneck Bound on the Energy-Constrained Private Capacity of Bosonic Thermal Channels

Theorem 92 *An upper bound on the private capacity of a thermal channel $\mathcal{L}^{\eta,N_B}$ with transmissivity $\eta \in [1/2, 1]$, environment photon number $N_B \geq 0$, such that $\eta > (1-\eta)N_B$, and input mean photon number constraint $N_S \geq 0$ is given by*

$$P(\mathcal{L}^{\eta,N_B}, N_S) \leq \max\{0, P_{U_4}(\mathcal{L}^{\eta,N_B}, N_S)\} \quad (3.4.10)$$

$$P_{U_4}(\mathcal{L}^{\eta,N_B}, N_S) \equiv g(\eta N_S + (1-\eta)N_B) - g[(1/\eta' - 1)(\eta N_S + (1-\eta)N_B)] \ , \quad (3.4.11)$$

and $\eta' = \eta - (1-\eta)N_B$.

Proof. A proof follows from arguments similar to those in the proof of Theorem 84. Since a pure-loss channel is a degradable channel [63,160], its energy-constrained private capacity is the same as its energy-constrained quantum capacity [62]. ■

3.5 Lower Bound on Energy-Constrained Private Capacity of Bosonic Thermal Channels

In this section, we establish an improvement on the best known lower bound [64] on the energy-constrained private capacity of bosonic thermal channels, by using displaced thermal states as input to the channel. We note that a similar effect has been observed in [170] for the finite-dimensional case.

The energy-constrained private information of a channel $\mathcal{N}$, as defined in (2.7.11), can also be written as

$$P^{(1)}(\mathcal{N}, G, W) \equiv \sup_{\bar{\rho}_{\mathcal{E}_A}:\mathrm{Tr}\{G\bar{\rho}_{\mathcal{E}_A}\}\leq W} [H(\mathcal{N}(\bar{\rho}_{\mathcal{E}_A})) - H(\hat{\mathcal{N}}(\bar{\rho}_{\mathcal{E}_A})) - \int dx\ p_X(x)[H(\mathcal{N}(\rho_A^x)) - H(\hat{\mathcal{N}}(\rho_A^x))]] \ , \tag{3.5.1}$$

where $\bar{\rho}_{\mathcal{E}_A} \equiv \int dx\ p_X(x)\rho_A^x$ is an average state of the ensemble $\mathcal{E}_A \equiv \{p_X(x), \rho_A^x\}$ and $\hat{\mathcal{N}}$ denotes a complementary channel of $\mathcal{N}$. If the energy-constrained private information is calculated for coherent-state inputs, then for each element of the ensemble, the following equality holds $H(\mathcal{N}(\rho_A^x)) = H(\hat{\mathcal{N}}(\rho_A^x))$. Hence, the entropy difference $H(\mathcal{N}(\bar{\rho}_{\mathcal{E}_A})) - H(\hat{\mathcal{N}}(\bar{\rho}_{\mathcal{E}_A}))$ is an achievable rate, which is the same as the energy-constrained coherent information.

However, we show that displaced thermal-state inputs provide an improved lower bound for certain values of the transmissivity η, low thermal noise N_B, and both low and high input mean photon number N_S. We start with the following ensemble of displaced thermal states,

$$\mathcal{E} \equiv \{p_{N_S^1}(\alpha), D(\alpha)\ \theta(N_S^2)\ D(-\alpha)\}, \tag{3.5.2}$$

chosen according to the Gaussian probability distribution

$$p_{N_S^1}(\alpha) = \frac{1}{\pi N_S^1} \exp\Big(-|\alpha|^2/N_S^1\Big), \tag{3.5.3}$$

where $D(\alpha)$ denotes the displacement operator, $\theta(N_S^2)$ denotes the thermal state with mean photon number N_S^2, and N_S^1 and N_S^2 are chosen such that $N_S^1 + N_S^2 = N_S$, which is the mean number of photons input to the channel. By employing (2.3.33), the average of this ensemble is a thermal state with mean photon number N_S, i.e.,

$$\bar{\rho}_{\mathcal{E}} = \int d^2\alpha\ p_{N_S^1}(\alpha)\ D(\alpha)\ \theta(N_S^2)\ D(-\alpha) = \theta(N_S)\ . \tag{3.5.4}$$

Hence, this ensemble meets the constraint that the average number of photons input to the channel is equal to N_S.

After the action of the channel on one of the states in the ensemble, the entropy of the output state is given by

$$H(\mathcal{L}^{\eta,N_B}(D(\alpha)\ \theta(N_S^2)\ D(-\alpha))) = H(D(\sqrt{\eta}\alpha)\mathcal{L}^{\eta,N_B}(\theta(N_S^2))D(-\sqrt{\eta}\alpha)) \tag{3.5.5}$$

$$= H(\mathcal{L}^{\eta,N_B}(\theta(N_S^2)))\ , \tag{3.5.6}$$

where the first equality follows because the thermal channel is covariant with respect to displacement operators, as reviewed in (2.3.69). The second equality follows because $D(\sqrt{\eta}\alpha)$ is a unitary operator and entropy is invariant under the action of a unitary operator. Since $H(\mathcal{L}^{\eta,N_B}(\theta(N_S^2)))$ is independent of the Gaussian probability distribution in (3.5.3), we have that

$$\int d^2\alpha\ p_{N_S^1}(\alpha) H(\mathcal{L}^{\eta,N_B}(\theta(N_S^2))) = H(\mathcal{L}^{\eta,N_B}(\theta(N_S^2))). \tag{3.5.7}$$

Similar arguments can be made for the output states at the environment mode.

Hence, a lower bound on the energy-constrained private information in (3.5.1) for the bosonic thermal channel is as follows:

$$\begin{aligned} &P^{(1)}(\mathcal{L}^{\eta,N_B}, N_S) \\ &\geq H(\mathcal{L}^{\eta,N_B}(\theta(N_S))) - H(\hat{\mathcal{L}}^{\eta,N_B}(\theta(N_S))) - [H(\mathcal{L}^{\eta,N_B}(\theta(N_S^2))) - H(\hat{\mathcal{L}}^{\eta,N_B}(\theta(N_S^2)))] \end{aligned} \tag{3.5.8}$$

$$= I_c(\mathcal{L}^{\eta,N_B}, N_S) - I_c(\mathcal{L}^{\eta,N_B}, N_S^2) \equiv P_L(\mathcal{L}^{\eta,N_B}, N_S)\ , \tag{3.5.9}$$

where $\hat{\mathcal{L}}^{\eta,N_B}$ denotes the complementary channel of $\mathcal{L}^{\eta,N_B}$, and we denote the lower bound in (3.5.9) on the private information by $P_L(\mathcal{L}^{\eta,N_B}, N_S)$. The first inequality follows from (2.7.11). Here, $I_c(\mathcal{L}^{\eta,N_B}, N_S)$ denotes the coherent information of the channel for the thermal state with mean photon number N_S as input to the channel. $I_c(\mathcal{L}^{\eta,N_B}, N_S)$ has the

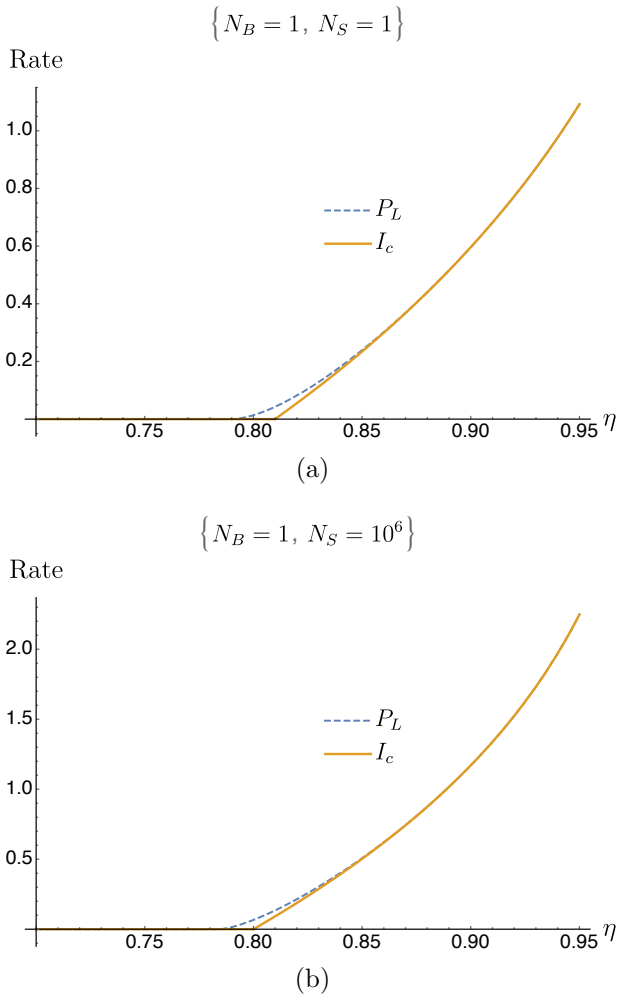

Figure 3.5: The figures plot the optimized value of the lower bound on the private information $P_L(\mathcal{L}^{\eta,N_B}, N_S)$ (dashed line) and coherent information $I_c(\mathcal{L}^{\eta,N_B}, N_S)$ (solid line) of a thermal channel versus transmissivity parameter η. In each figure, we select certain values of the thermal noise N_B and input mean photon number N_S, with the choices indicated above each figure. In all the cases, there is an improvement in the achievable rate of private communication for certain values of the transmissivity η.

same form as (3.3.1), i.e.,

$$I_c(\mathcal{L}^{\eta,N_B}, N_S) = g(\eta N_S + (1-\eta)N_B) - g([D + (1-\eta)N_S - (1-\eta)N_B - 1]/2) \\ - g([D - (1-\eta)N_S + (1-\eta)N_B - 1]/2) \ , \quad (3.5.10)$$

where $D^2 \equiv [(1+\eta)N_S + (1-\eta)N_B + 1]^2 - 4\eta N_S(N_S+1)$. Similarly, $I_c(\mathcal{L}^{\eta,N_B}, N_S^2)$ is defined by replacing N_S in (3.5.10) with N_S^2.

We optimize the lower bound in (3.5.9) on the private information $P_L(\mathcal{L}^{\eta,N_B}, N_S)$ with respect to N_S^2 for a fixed value of N_S [163]. In Figure 3.5, we plot the optimized value of the lower bound in (3.5.9) on the private information $P_L(\mathcal{L}^{\eta,N_B}, N_S)$ (dashed line) and the coherent information in (3.5.10) $I_c(\mathcal{L}^{\eta,N_B}, N_S)$ (solid line) of the thermal channel versus the transmissivity parameter η, for low thermal noise N_B and for both low and high input mean number of photons N_S. We find that a larger rate for private communication can be achieved by using displaced thermal states as input to the channel instead of coherent states, for certain values of the transmissivity η.

3.6 Upper Bounds on Energy-Constrained Quantum and Private Capacities of Quantum Amplifier Channels

Using methods similar to those from Sections 3.2 and 3.4, we now establish three different upper bounds on the energy-constrained quantum and private capacities of a noisy amplifier channel.

3.6.1 Data-Processing Bound on Energy-Constrained Quantum and Private Capacities of Quantum Amplifier Channels

In this section, we establish an upper bound on the energy-constrained quantum and private capacities by invoking Theorem 83 and a data-processing argument to a noisy amplifier channel $\mathcal{A}^{G,N_B}$ with gain $G > 1$, environment photon number $N_B \geq 0$, for which $\tau = G$ and $\nu = (G-1)(2N_B+1)$. This channel is entanglement-breaking when $(G-1)N_B \geq 1$ [126].

Theorem 93 *An upper bound on the energy-constrained quantum and private capacities of a noisy amplifier channel $\mathcal{A}^{G,N_B}$ with gain $G > 1$ and environment photon number $N_B \geq 0$, such that $(G-1)N_B < 1$, and input photon number constraint $N_S \geq 0$, is given by*

$$Q(\mathcal{A}^{G,N_B}, N_S), P(\mathcal{A}^{G,N_B}, N_S) \leq \max\{0, Q_{U_1}(\mathcal{A}^{G,N_B}, N_S)\}, \tag{3.6.1}$$

where

$$Q_{U_1}(\mathcal{A}^{G,N_B}, N_S) \equiv g(G'N_S + G' - 1) - g[(G'-1)(N_S+1)], \tag{3.6.2}$$

$$G' = G/(1 + N_B(1-G)). \tag{3.6.3}$$

Proof. An upper bound on the energy-constrained quantum and private capacities can be established by using (3.2.70) and a data-processing argument. We find that

$$Q(\mathcal{A}^{G,N_B}, N_S) = Q(\mathcal{L}^{\eta,0} \circ \mathcal{A}^{G',0}, N_S) \tag{3.6.4}$$

$$\leq Q(\mathcal{A}^{G',0}, N_S) \tag{3.6.5}$$

$$= \max\{0, g(G'\ N_S + G' - 1) - g[(G'-1)(N_S+1)]\}\ . \tag{3.6.6}$$

The first inequality follows from the definition and data processing—the energy-constrained capacity of $\mathcal{L}^{\eta,0} \circ \mathcal{A}^{G',0}$ cannot exceed that of $\mathcal{A}^{G',0}$. The second equality follows from the formula for the energy-constrained quantum capacity of a quantum-limited amplifier channel with gain G' and input mean photon number N_S [65]. Since a quantum-limited amplifier channel is a degradable channel [160,171], its energy-constrained private capacity is the same as its energy-constrained quantum capacity. ■

Remark 94 *Applying Remark 65, we find the following data-processing bound $Q_{U_1}(\mathcal{A}^{G,N_B})$ on the unconstrained quantum and private capacities of amplifier channels for which $(G-$*

1)$N_B < 1$*:*

$$Q(\mathcal{A}^{G,N_B}), P(\mathcal{A}^{G,N_B}) \leq Q_{U_1}(\mathcal{A}^{G,N_B}) = \sup_{N_S : N_S \in [0,\infty]} Q_{U_1}(\mathcal{A}^{G,N_B}, N_S) \tag{3.6.7}$$

$$= \lim_{N_S \to \infty} Q_{U_1}(\mathcal{A}^{G,N_B}, N_S) \tag{3.6.8}$$

$$= \log_2(G/(G-1)) - \log_2(N_B + 1) \ . \tag{3.6.9}$$

The second equality follows from the monotonicity of $Q_{U_1}(\mathcal{A}^{G,N_B}, N_S)$ *with respect to* N_S*, which in turn follows from the fact that the first derivative of* $Q_{U_1}(\mathcal{A}^{G,N_B}, N_S)$ *with respect to* N_S *goes to zero as* $N_S \to \infty$*, and the second derivative is always negative.*

The bound

$$Q(\mathcal{A}^{G,N_B}), P(\mathcal{A}^{G,N_B}) \leq \log_2\left(\frac{G^{N_B+1}}{G-1}\right) - g(N_B) \tag{3.6.10}$$

was given in [161, 162]. From a comparison of (3.6.9) *with* (3.6.10)*, we find that the bound given in* (3.6.10) *is always tighter than* (3.6.9)*. Both the bounds in* (3.6.9) *and* (3.6.10) *converge to the true unconstrained quantum and private capacity in the limit as* $N_B \to 0$*, but* (3.6.10) *is tighter for* $N_B > 0$*.*

Remark 95 *The data-processing bound* $Q_{U_1}(\mathcal{A}^{G,N_B}, N_S)$ *on the energy-constrained quantum capacity of amplifier channels places a strong restriction on the channel parameters* G *and* N_B*. Since the quantum capacity of a quantum-limited amplifier channel with gain* G' *is non-zero only for* $G' \neq \infty$*, the energy-constrained quantum capacity of an amplifier channel will be non-zero only for*

$$1 \leq G < (1 + N_B)/N_B \ , \tag{3.6.11}$$

which is same as the condition given in [127] and is equivalent to the condition $(G-1)N_B < 1$*, that the channel is not entanglement breaking.*

We now study the closeness of the data-proccessing bound $Q_{U_1}(\mathcal{A}^{G,N_B}, N_S)$ when compared

to a known lower bound. In particular, we use the following lower bound on the energy-constrained quantum and private capacities of an amplifier channel [62, 147] and denote it by $Q_L(\mathcal{A}^{G,N_B}, N_S)$:

$$\begin{aligned} Q(\mathcal{A}^{G,N_B}, N_S) \geq Q_L(\mathcal{A}^{G,N_B}, N_S) &\equiv g(GN_S + (G-1)(N_B+1)) \\ &- g([D + (G-1)(N_S + N_B + 1) - 1]/2) - g([D - (G-1)(N_S + N_B + 1) - 1]/2), \end{aligned} \tag{3.6.12}$$

where

$$D^2 \equiv [(1+G)N_S + (G-1)(N_B+1) + 1]^2 - 4GN_S(N_S+1). \tag{3.6.13}$$

Theorem 96 *Let $\mathcal{A}^{G,N_B}$ be an amplifier channel with gain $G > 1$ and environment photon number $N_B \geq 0$, such that $(G-1)N_B < 1$, and input photon number constraint $N_S \geq 0$. Then the following relation holds between the data-processing bound $Q_{U_1}(\mathcal{A}^{G,N_B}, N_S)$ in* (3.6.1) *and the lower bound $Q_L(\mathcal{A}^{G,N_B}, N_S)$ in* (3.6.12) *on the energy-constrained quantum and private capacities of an amplifier channel:*

$$Q_L(\mathcal{A}^{G,N_B}, N_S) \leq Q_{U_1}(\mathcal{A}^{G,N_B}, N_S) \leq Q_L(\mathcal{A}^{G,N_B}, N_S) + 1/\ln 2\ . \tag{3.6.14}$$

Proof. A proof follows from arguments similar to those in the proof of Theorem 87. ■

3.6.2 ε-Degradable Bound on Energy-Constrained Quantum and Private Capacities of Amplifier Channels

In this section, we provide an upper bound on the energy-constrained quantum and private capacities of a quantum amplifier channel $\mathcal{A}^{G,N_B}$ using the idea of ε-degradability. We first construct an approximate degrading channel $\mathcal{D}$ by following arguments similar

to those in Section 3.2.2. Furthermore, we introduce a particular channel that simulates the serial concatenation of the amplifier channel $\mathcal{A}^{G,N_B}$ and the approximate degrading channel $\mathcal{D}$. We finally provide an upper bound on the energy-constrained quantum and private capacities of an amplifier channel by using all these tools and invoking Theorem 68.

Similar to Section 3.2.2, we first establish an upper bound on the diamond distance between the complementary channel of the amplifier channel and the concatenation of the amplifier channel followed by a particular approximate degrading channel. Let $\mathcal{T}$ and $\mathcal{T}'$ represent transformations of two-mode squeezers with parameter G and $(2G-1)/G$, respectively. In the Heisenberg picture, the unitary transformation corresponding to $\mathcal{T}$ and $\mathcal{T}'$ follow from (2.3.82).

Consider the following action of the noisy amplifier channel $\mathcal{A}^{G,N_B}$ on an input state ϕ_{RA}:

$$(\mathrm{id}_R \otimes \mathcal{A}^{G,N_B})(\phi_{RA}) = \mathrm{Tr}_{E_1E_2}\{\mathcal{T}_{AE'\to BE_2}(\phi_{RA} \otimes \psi_{\mathrm{TMS}}(N_B)_{E'E_1})\}\ , \tag{3.6.15}$$

where R is a reference system and $\psi_{\mathrm{TMS}}(N_B)_{E'E_1}$ is a two-mode squeezed vacuum state with parameter N_B, as defined in (2.3.34). It is evident from (3.6.15) that the output of the noisy amplifier channel $\mathcal{A}^{G,N_B}$ is system B, and the outputs of the complementary channel $\hat{\mathcal{A}}_{G,N_B}$ are systems E_1 and E_2.

Consider a two-mode squeezer $\mathcal{T}'$ with parameter $(2G-1)/G$, such that the output of the amplifier channel $\mathcal{A}^{G,N_B}$ becomes an environmental input for $\mathcal{T}'$. We consider one mode of the two-mode squeezed vacuum state $\psi_{\mathrm{TMS}}(N_B)_{FE_1'}$ as an input for $\mathcal{T}'$, so that the subsystem E_1' mimics E_1. We denote our choice of degrading channel by $\mathcal{D}_{(2G-1)/G,N_B}$: $\mathcal{T}(B) \to \mathcal{T}(E_1'E_2')$. More formally, $\mathcal{D}_{(2G-1)/G,N_B}$ has the following action on the output state $\mathcal{A}^{G,N_B}(\phi_{RA})$:

$$(\mathrm{id}_R \otimes [\mathcal{D}_{(2G-1)/G,N_B} \circ \mathcal{A}^{G,N_B}])(\phi_{RA}) = \mathrm{Tr}_G\{\mathcal{T}'_{BF\to E_2'G}(\mathcal{A}^{G,N_B}(\phi_{RA}) \otimes \psi_{\mathrm{TMS}}(N_B)_{FE_1'}))\}\ . \tag{3.6.16}$$

Now, similar to Section 3.2.2, we introduce a particular channel that simulates the action of $\mathcal{D}_{(2G-1)/G} \circ \mathcal{A}^{G,N_B}$ on an input state ϕ_{RA}. We denote this channel by Λ, and it has the following action on an input state ϕ_{RA}:

$$(\mathrm{id}_R \otimes \Lambda)(\phi_{RA}) = \mathrm{Tr}_B\{\mathcal{T}_{AE' \to BE_2}(\phi_{RA} \otimes \omega(N_B)_{E'E_1})\} , \tag{3.6.17}$$

where $\omega(N_B)_{E'E_1}$ represents a noisy version of a two-mode squeezed vacuum state with parameter N_B, and is the same as (3.2.25), except η is replaced by G. Similar to (3.2.26), the following equivalence holds for any quantum input state ϕ_{RA}:

$$(\mathrm{id}_R \otimes [\mathcal{D}_{(2G-1)/G,N_B} \circ \mathcal{A}^{G,N_B}])(\phi_{RA}) = (\mathrm{id}_R \otimes \Lambda)(\phi_{RA}) . \tag{3.6.18}$$

Thus, the channels $\mathcal{D}_{(2G-1)/G,N_B} \circ \mathcal{A}^{G,N_B}$ and Λ are indeed the same.

Similar to Theorem 76, we now establish an upper bound on the diamond distance between the complementary channel of a noisy amplifier channel and the concatenation of the amplifier channel followed by the degrading channel in (3.6.16).

Theorem 97 *Fix $G > 1$. Let $\mathcal{A}^{G,N_B}$ be an amplifier channel with gain G, and let $\mathcal{D}_{(2G-1)/G,N_B}$ be a degrading channel as defined in* (3.6.16)*. Then*

$$\frac{1}{2}\|\hat{\mathcal{A}}_{G,N_B} - \mathcal{D}_{(2G-1)/G,N_B} \circ \mathcal{A}^{G,N_B}\|_\diamond \leq \sqrt{1 - G^2/\kappa(G,N_B)}, \tag{3.6.19}$$

with

$$\kappa(G,N_B) = G^2 + N_B(N_B+1)[1 + 3G^2 - 2G(1+\sqrt{2G-1})]. \tag{3.6.20}$$

Proof. A proof follows from arguments similar to those in the proof of Theorem 76. ■

Theorem 98 *An upper bound on the energy-constrained quantum capacity of a noisy amplifier channel $\mathcal{A}^{G,N_B}$ with gain $G > 1$, environment photon number N_B, such that*

$(G-1)N_B < 1$, *and input mean photon-number constraint* $N_S \geq 0$ *is given by*

$$Q(\mathcal{A}^{G,N_B}, N_S) \leq Q_{U_2}(\mathcal{A}^{G,N_B}, N_S) \equiv g(GN_S + (G-1)N_B) - g(\zeta_+) - g(\zeta_-) \\ + (2\varepsilon' + 4\delta) g([(G-1)N_S + (1+G)N_B]/\delta) + g(\varepsilon') + 2h_2(\delta) \ , \quad (3.6.21)$$

with

$$\varepsilon = \sqrt{1 - G^2 / \left(G^2 + N_B(N_B+1)[1 + 3G^2 - 2G(1+\sqrt{2G-1})] \right)} \ , \quad (3.6.22)$$

$$\zeta_\pm = \frac{1}{2}\left(-1 + \sqrt{[(1+2N_B)^2 - 2\varrho + (2\vartheta - 1)^2 \pm 4(\vartheta - N_B - 1)\sqrt{[N_B+\vartheta]^2 - \varrho}]/2} \right) \ , \quad (3.6.23)$$

$$\varrho = 4N_B(N_B+1)(2G-1)/G \ , \quad (3.6.24)$$

$$\vartheta = G(1+N_B) + (G-1)N_S \ , \quad (3.6.25)$$

$\varepsilon' \in (\varepsilon, 1]$, *and* $\delta = (\varepsilon' - \varepsilon)/(1+\varepsilon')$.

Proof. A proof follows from arguments similar to those in the proof of Theorem 77. ■

Theorem 99 *An upper bound on the energy-constrained private capacity of a noisy amplifier channel* $\mathcal{A}^{G,N_B}$ *with gain* $G > 1$, *environment photon number* N_B, *such that* $(G-1)N_B < 1$, *and input mean photon-number constraint* $N_S \geq 0$ *is given by*

$$P(\mathcal{A}^{G,N_B}, N_S) \leq P_{U_2}(\mathcal{A}^{G,N_B}, N_S) \equiv g(GN_S + (G-1)N_B) - g(\zeta_+) - g(\zeta_-) \\ + (6\varepsilon' + 12\delta) g([(G-1)N_S + (1+G)N_B]/\delta) + 3g(\varepsilon') + 6h_2(\delta) \ , \quad (3.6.26)$$

with

$$\varepsilon = \sqrt{1 - G^2 / \left(G^2 + N_B(N_B+1)[1 + 3G^2 - 2G(1+\sqrt{2G-1})] \right)} \ , \tag{3.6.27}$$

$$\zeta_{\pm} = \frac{1}{2}\left(-1 + \sqrt{[(1+2N_B)^2 - 2\varrho + (2\vartheta - 1)^2 \pm 4(\vartheta - N_B - 1)\sqrt{[N_B+\vartheta]^2 - \varrho}]/2} \right) \ , \tag{3.6.28}$$

$$\varrho = 4N_B(N_B+1)(2G-1)/G \ , \tag{3.6.29}$$

$$\vartheta = G(1+N_B) + (G-1)N_S \ , \tag{3.6.30}$$

$\varepsilon' \in (\varepsilon, 1]$, *and* $\delta = (\varepsilon' - \varepsilon)/(1+\varepsilon')$.

Proof. A proof follows from arguments similar to those in the proof of Theorem 77. The final result is obtained using Theorem 71. ■

3.6.3 ε-Close-Degradable Bound on Energy-Constrained Quantum and Private Capacities of Amplifier Channels

In this section, we first establish an upper bound on the diamond distance between a noisy amplifier channel and a quantum-limited amplifier channel. Since a quantum-limited amplifier channel is a degradable channel, an upper bound on the energy-constrained quantum capacity of a noisy amplifier channel directly follows from Theorem 69.

Theorem 100 *If a noisy amplifier channel* $\mathcal{A}^{G,N_B}$ *and a quantum-limited amplifier channel* $\mathcal{A}^{G,0}$ *have the same gain* $G > 1$, *then*

$$\frac{1}{2}\left\| \mathcal{A}^{G,N_B} - \mathcal{A}^{G,0} \right\|_{\diamond} \leq \frac{N_B}{N_B+1} \ . \tag{3.6.31}$$

Proof. A proof follows from arguments similar to those in the proof of Theorem 80. ■

Theorem 101 *An upper bound on the energy-constrained quantum capacity of a noisy amplifier channel* $\mathcal{A}^{G,N_B}$ *with gain* $G > 1$, *environment photon number* N_B, *such that*

$(G-1)N_B < 1$, *and input mean photon-number constraint* $N_S \geq 0$ *is given by*

$$Q(\mathcal{A}^{G,N_B}, N_S) \leq Q_{U_3}(\mathcal{A}^{G,N_B}, N_S) \equiv g(GN_S + G - 1) - g[(G-1)(N_S+1)] \\ + (4\varepsilon' + 8\delta)g[(GN_S + (G-1)N_B)/\delta] + 2g(\varepsilon') + 4h_2(\delta) \ , \quad (3.6.32)$$

with $\varepsilon = N_B/(N_B+1)$, $\varepsilon' \in (\varepsilon, 1]$ *and* $\delta = (\varepsilon' - \varepsilon)/(1+\varepsilon')$.

Proof. A proof follows from arguments similar to those in the proof of Theorem 82. ■

Theorem 102 *An upper bound on the energy-constrained private capacity of a noisy amplifier channel* $\mathcal{A}^{G,N_B}$ *with gain* $G > 1$, *environment photon number* N_B, *such that* $(G-1)N_B < 1$, *and input mean photon-number constraint* $N_S \geq 0$ *is given by*

$$P(\mathcal{A}^{G,N_B}, N_S) \leq P_{U_3}(\mathcal{A}^{G,N_B}, N_S) \equiv g(GN_S + G - 1) - g[(G-1)(N_S+1)] \\ + (8\varepsilon' + 16\delta)g[(GN_S + (G-1)N_B)/\delta] + 4g(\varepsilon') + 8h_2(\delta) \ , \quad (3.6.33)$$

with $\varepsilon = N_B/(N_B+1)$, $\varepsilon' \in (\varepsilon, 1]$ *and* $\delta = (\varepsilon' - \varepsilon)/(1+\varepsilon')$.

Proof. A proof follows from arguments similar to those in the proof of Theorem 82. The final result is obtained using Theorem 72. ■

3.7 Upper Bounds on Energy-Constrained Quantum and Private Capacities of Additive-Noise Channels

In this section, we provide upper bounds on the energy-constrained quantum and private capacities of an additive-noise channel using Theorems 73 and 84. Note that we only consider $\xi \in (0,1)$ because the additive-noise channel is not entanglement breaking in this interval [126]. The additive-noise channel with noise paramter ξ was defined in (2.3.85).

Theorem 103 *An upper bound on the energy-constrained quantum and private capacities of an additive-noise channel* $\mathcal{T}^{\xi}$ *with noise parameter* $\xi \in (0,1)$, *and input mean photon*

number constraint N_S is given by

$$Q(\mathcal{T}^{\xi}, N_S), P(\mathcal{T}^{\xi}, N_S) \leq \max\{0, Q_{U_1}(\mathcal{T}^{\xi}, N_S)\}, \tag{3.7.1}$$

where

$$Q_{U_1}(\mathcal{T}^{\xi}, N_S) \equiv g(N_S/(\xi+1)) - g(\xi N_S/(\xi+1)). \tag{3.7.2}$$

Proof. A proof follows from the fact that an additive noise channel can be obtained from a thermal noise channel in the limit $\eta \to 1$ and $N_B \to \infty$, with $(1-\eta)N_B \to \xi$ [172], as well by applying the continuity results for these capacities from [173, Theorem 3] (see also [138]). By taking these limits in (3.2.3), we obtain the desired result. ■

Remark 104 *Applying Remarks 65 and 74, and Theorem 103, we find the following data-processing bound $Q_{U_1}(\mathcal{T}^{\xi})$ on the unconstrained quantum and private capacities of additive-noise channels for $\xi \in (0,1)$:*

$$Q_{U_1}(\mathcal{T}^{\xi}) = \log_2(1/\xi) \ . \tag{3.7.3}$$

Remark 105 *From Theorem 87, it follows that the data-processing upper bound $Q(\mathcal{T}^{\xi}, N_S)$ can be at most 1.45 bits larger than a known lower bound on the energy-constrained quantum and private capacities of an additive-noise channel.*

Remark 106 *The following bound was given in [161, 162] for $\xi \in (0,1)$:*

$$Q(\mathcal{T}^{\xi}), P(\mathcal{T}^{\xi}) \leq \frac{\xi - 1}{\ln 2} + \log_2(1/\xi). \tag{3.7.4}$$

From a comparison of (3.7.3) *with the bound in* (3.7.4)*, we find that the bound in* (3.7.4) *is always tighter than* (3.7.3)*.*

We now establish another upper bound on the energy-constrained quantum and private capacities of an additive-noise channel, by using Theorem 84.

Theorem 107 *An upper bound on the energy-constrained quantum and private capacities of an additive-noise channel $\mathcal{T}^{\xi}$ with noise parameter $\xi \in (0,1)$, and input photon number constraint $N_S \geq 0$ is given by*

$$Q(\mathcal{T}^{\xi}, N_S), P(\mathcal{T}^{\xi}, N_S) \leq \max\{0, Q_{U_4}(\mathcal{T}^{\xi}, N_S)\}, \tag{3.7.5}$$

where

$$Q_{U_4}(\mathcal{T}^{\xi}, N_S) \equiv g(N_S + \xi) - g[\xi(N_S + \xi)/(1-\xi)]. \tag{3.7.6}$$

Proof. A proof follows from arguments similar to those in the proof of Theorem 103. The final result is obtained using Theorem 84. ■

Remark 108 *From a comparision of* (3.7.6) *and* (3.7.2)*, we find that $Q_{U_1}(\mathcal{T}^{\xi}, N_S)$ is tighter than $Q_{U_4}(\mathcal{T}^{\xi}, N_S)$ only for low noise and low input mean photon number. The bound $Q_{U_4}(\mathcal{T}^{\xi}, N_S)$ is tighter than $Q_{U_1}(\mathcal{T}^{\xi}, N_S)$ for all other parameter regimes.*

Remark 109 *Applying Remarks 65 and 74, and Theorem 107, we find the following data-processing bound $Q_{U_4}(\mathcal{T}^{\xi})$ on the unconstrained quantum and private capacities of additive-noise channels:*

$$Q_{U_4}(\mathcal{T}^{\xi}) = \log_2[(1-\xi)/\xi] \ . \tag{3.7.7}$$

Remark 110 *From a comparison of* (3.7.7) *with the bound in* (3.7.4)*, we find that* (3.7.7) *is tighter than* (3.7.4) *for high noise.*

3.8 On the Optimization of Generalized Channel Divergences of Quantum Gaussian Channels

In this section, we address the question of computing the energy-constrained diamond norm of several channels of interest that have appeared in this dissertation. We provide a very general argument, based on some definitions and results in [153] and phrased in terms of the "generalized channel divergence" as a measure of the distinguishability of quantum

channels. We find that, among all Gaussian input states with a fixed energy constraint, the two-mode squeezed vacuum state saturating the energy constraint is an optimal state for the energy-constrained generalized channel divergence of two particular Gaussian channels. We describe these results in more detail in what follows.

We begin by recalling some developments from [153]:

Definition 111 (Generalized divergence [174, 175]) *A functional* $\mathbf{D} : \mathcal{D}(\mathcal{H}) \times \mathcal{D}(\mathcal{H}) \to \mathbb{R}$ *is a generalized divergence if it satisfies the monotonicity (data processing) inequality*

$$\mathbf{D}(\rho \| \sigma) \geq \mathbf{D}(\mathcal{N}(\rho) \| \mathcal{N}(\sigma)), \tag{3.8.1}$$

where $\mathcal{N}$ *is a quantum channel.*

Particular examples of a generalized divergence are the trace distance, quantum relative entropy, and the negative root fidelity.

We say that a generalized channel divergence possesses the direct-sum property on classical–quantum states if the following equality holds:

$$\mathbf{D}\left(\sum_x p_X(x)|x\rangle\langle x|_X \otimes \rho^x \middle\| \sum_x p_X(x)|x\rangle\langle x|_X \otimes \sigma^x\right) = \sum_x p_X(x)\mathbf{D}(\rho^x \| \sigma^x), \tag{3.8.2}$$

where p_X is a probability distribution, $\{|x\rangle\}_x$ is an orthonormal basis, and $\{\rho^x\}_x$ and $\{\sigma^x\}_x$ are sets of states. We note that this property holds for trace distance, quantum relative entropy, and the negative root fidelity.

Definition 112 (Generalized channel divergence [153]) *Given quantum channels* $\mathcal{N}_{A\to B}$ *and* $\mathcal{M}_{A\to B}$*, we define the generalized channel divergence as*

$$\mathbf{D}(\mathcal{N} \| \mathcal{M}) \equiv \sup_{\rho_{RA}} \mathbf{D}((\mathrm{id}_R \otimes \mathcal{N}_{A\to B})(\rho_{RA}) \| (\mathrm{id}_R \otimes \mathcal{M}_{A\to B})(\rho_{RA})). \tag{3.8.3}$$

In the above definition, the supremum is with respect to all mixed states and the reference system R *is allowed to be arbitrarily large. However, as a consequence of purification, data*

processing, and the Schmidt decomposition, it follows that

$$\mathbf{D}(\mathcal{N}\|\mathcal{M}) = \sup_{\psi_{RA}} \mathbf{D}((\mathrm{id}_R \otimes \mathcal{N}_{A\to B})(\psi_{RA})\|(\mathrm{id}_R \otimes \mathcal{M}_{A\to B})(\psi_{RA})), \tag{3.8.4}$$

such that the supremum can be restricted to be with respect to pure states and the reference system R isomorphic to the channel input system A.

Particular cases of the generalized channel divergence are the diamond norm of the difference of $\mathcal{N}_{A\to B}$ and $\mathcal{M}_{A\to B}$ as well as the Rényi channel divergence from [176].

Covariant quantum channels have symmetries that allow us to simplify the set of states over which we need to optimize their generalized channel divergence [177]. Let G be a finite group, and for every $g \in G$, let $g \to U_A(g)$ and $g \to V_B(g)$ be unitary representations acting on the input and output spaces of the channel, respectively. Then a quantum channel $\mathcal{N}_{A\to B}$ is covariant with respect to $\{(U_A(g), V_B(g))\}_g$ if the following relation holds for all input density operators ρ_A and group elements $g \in G$:

$$(\mathcal{N}_{A\to B} \circ \mathcal{U}_A^g)(\rho_A) = (\mathcal{V}_B^g \circ \mathcal{N}_{A\to B})(\rho_A), \tag{3.8.5}$$

where

$$\mathcal{U}_A^g(\rho_A) = U_A(g)\rho_A U_A^\dagger(g), \tag{3.8.6}$$

$$\mathcal{V}_B^g(\sigma_B) = V_B(g)\sigma_B V_B^\dagger(g). \tag{3.8.7}$$

We say that channels $\mathcal{N}_{A\to B}$ and $\mathcal{M}_{A\to B}$ are *jointly covariant* with respect to $\{(U_A(g), V_B(g))\}_{g\in G}$ if each of them is covariant with respect to $\{(U_A(g), V_B(g))\}_g$ [168, 178].

The following lemma was established in [153]:

Lemma 4 (Lemma II.3, [153]) *Let $\mathcal{N}_{A\to B}$ and $\mathcal{M}_{A\to B}$ be quantum channels, and let $\{(U_A(g), V_B(g))\}_{g\in G}$ denote unitary representations of a group G. Let ρ_A be a density*

operator, and let ϕ^{ρ}_{RA} *be a purification of* ρ_A*. Let* $\bar{\rho}_A$ *denote the group average of* ρ_A *according to a distribution* p_G*, i.e.,*

$$\bar{\rho}_A = \sum_g p_G(g)\, \mathcal{U}^g_A(\rho_A), \tag{3.8.8}$$

and let $\phi^{\bar{\rho}}_{RA}$ *be a purification of* $\bar{\rho}_A$*. If the generalized divergence possesses the direct-sum property on classical–quantum states, then the following inequality holds*

$$\begin{aligned}&\mathbf{D}(\mathcal{N}_{A\to B}(\phi^{\bar{\rho}}_{RA})\|\mathcal{M}_{A\to B}(\phi^{\bar{\rho}}_{RA}))\\ &\qquad\geq \sum_g p_G(g)\mathbf{D}\Big(\left(\mathcal{V}^{g\dagger}_B\circ\mathcal{N}_{A\to B}\circ\mathcal{U}^g_A\right)(\phi^{\rho}_{RA})\Big\|\left(\mathcal{V}^{g\dagger}_B\circ\mathcal{M}_{A\to B}\circ\mathcal{U}^g_A\right)(\phi^{\rho}_{RA})\Big).\end{aligned} \tag{3.8.9}$$

By approximation, the above lemma can be extended to continuous groups for several generalized channel divergences of interest:

Lemma 5 *Let* $\mathcal{N}_{A\to B}$ *and* $\mathcal{M}_{A\to B}$ *be quantum channels, and let* $\{(U_A(g), V_B(g))\}_{g\in G}$ *denote unitary representations of a continuous group* G*. Let* ρ_A *be a density operator, and let* ϕ^{ρ}_{RA} *be a purification of* ρ_A*. Let* $\bar{\rho}_A$ *denote the group average of* ρ_A *according to a measure* $\mu(g)$*, i.e.,*

$$\bar{\rho}_A = \int d\mu(g)\, \mathcal{U}^g_A(\rho_A), \tag{3.8.10}$$

and let $\phi^{\bar{\rho}}_{RA}$ *be a purification of* $\bar{\rho}_A$*. If the generalized divergence possesses the direct-sum property on classical–quantum states and is a Borel function, then the following inequality holds*

$$\begin{aligned}&\mathbf{D}(\mathcal{N}_{A\to B}(\phi^{\bar{\rho}}_{RA})\|\mathcal{M}_{A\to B}(\phi^{\bar{\rho}}_{RA}))\\ &\qquad\geq \int d\mu(g)\ \mathbf{D}\Big(\left(\mathcal{V}^{g\dagger}_B\circ\mathcal{N}_{A\to B}\circ\mathcal{U}^g_A\right)(\phi^{\rho}_{RA})\Big\|\left(\mathcal{V}^{g\dagger}_B\circ\mathcal{M}_{A\to B}\circ\mathcal{U}^g_A\right)(\phi^{\rho}_{RA})\Big).\end{aligned} \tag{3.8.11}$$

We can apply this lemma effectively in the context of quantum Gaussian channels. To this end, we consider an energy-constrained generalized channel divergence for $W \in [0, \infty)$ and an energy observable G as follows:

$$\mathbf{D}_{G,W}(\mathcal{N}\|\mathcal{M}) = \sup_{\psi_{RA} \,:\, \mathrm{Tr}\{G\psi_A\} \leq W} \mathbf{D}((\mathrm{id}_R \otimes \mathcal{N}_{A\to B})(\psi_{RA})\|(\mathrm{id}_R \otimes \mathcal{M}_{A\to B})(\psi_{RA})). \quad (3.8.12)$$

In what follows, we specialize this measure even further to the Gaussian energy-constrained generalized channel divergence, meaning that the optimization is constrained to be with respect to Gaussian input states:

$$\mathbf{D}^{\mathcal{G}}_{G,W}(\mathcal{N}\|\mathcal{M}) = \sup_{\psi_{RA} \,:\, \mathrm{Tr}\{G\psi_A\} \leq W,\ \psi_{RA} \in \mathcal{G}} \mathbf{D}((\mathrm{id}_R \otimes \mathcal{N}_{A\to B})(\psi_{RA})\|(\mathrm{id}_R \otimes \mathcal{M}_{A\to B})(\psi_{RA})), \quad (3.8.13)$$

where $\mathcal{G}$ denotes the set of Gaussian states. We then establish the following proposition:

Proposition 113 *Suppose that channels $\mathcal{N}_{A\to B}$ and $\mathcal{M}_{A\to B}$ are Gaussian, they each take one input mode to m output modes, and they have the following action on a single-mode, input covariance matrix V:*

$$V \to XVX^T + Y_{\mathcal{N}}, \quad (3.8.14)$$

$$V \to XVX^T + Y_{\mathcal{M}}, \quad (3.8.15)$$

where X is an $m \times 1$ matrix, $Y_{\mathcal{N}}$ and $Y_{\mathcal{M}}$ are $m \times m$ matrices such that $\mathcal{N}_{A\to B}$ and $\mathcal{M}_{A\to B}$ are legitimate Gaussian channels. Suppose furthermore they these channels are jointly phase covariant (phase-insensitive), in the sense that for all $\phi \in [0, 2\pi)$ and input density operators ρ, the following equality holds

$$\mathcal{N}_{A\to B}(e^{i\hat{n}\phi}\rho e^{-i\hat{n}\phi}) = \left(\bigotimes_{i=1}^{m} e^{i\hat{n}_i(-1)^{a_i}\phi}\right) \mathcal{N}_{A\to B}(\rho) \left(\bigotimes_{i=1}^{m} e^{-i\hat{n}_i(-1)^{a_i}\phi}\right), \quad (3.8.16)$$

$$\mathcal{M}_{A\to B}(e^{i\hat{n}\phi}\rho e^{-i\hat{n}\phi}) = \left(\bigotimes_{i=1}^{m} e^{i\hat{n}_i(-1)^{a_i}\phi}\right) \mathcal{M}_{A\to B}(\rho) \left(\bigotimes_{i=1}^{m} e^{-i\hat{n}_i(-1)^{a_i}\phi}\right), \quad (3.8.17)$$

where $a_i \in \{0,1\}$ for $i \in \{1,\ldots,m\}$ and $\hat{n}_i$ is the photon number operator for the ith mode. Then it suffices to restrict the optimization in the energy-constrained generalized channel divergence as follows:

$$\mathbf{D}_{\hat{n},N_S}(\mathcal{N}\|\mathcal{M}) = \sup_{\psi_{RA}:\mathrm{Tr}\{\hat{n}\psi_A\}=N_S} \mathbf{D}((\mathrm{id}_R \otimes \mathcal{N}_{A\to B})(\psi_{RA}) \,\|\, (\mathrm{id}_R \otimes \mathcal{M}_{A\to B})(\psi_{RA})), \quad (3.8.18)$$

where $\psi_{RA} = |\psi\rangle\langle\psi|_{RA}$ and

$$|\psi\rangle_{RA} = \sum_{n=0}^{\infty} \lambda_n |n\rangle_R |n\rangle_A, \quad (3.8.19)$$

for some $\lambda_n \in \mathbb{R}^+$ such that $\sum_{n=0}^{\infty} \lambda_n^2 = 1$ and $\sum_{n=0}^{\infty} n\lambda_n^2 = N_S$. Furthermore, the Gaussian energy-constrained generalized channel divergence is achieved by the two-mode squeezed vacuum state with parameter N_S, i.e.,

$$\mathbf{D}^{\mathcal{G}}_{\hat{n},N_S}(\mathcal{N}\|\mathcal{M}) = \mathbf{D}((\mathrm{id}_R \otimes \mathcal{N}_{A\to B})(\psi_{\mathrm{TMS}}(N_S)) \,\|\, (\mathrm{id}_R \otimes \mathcal{M}_{A\to B})(\psi_{\mathrm{TMS}}(N_S))). \quad (3.8.20)$$

Proof. This result is an application of Lemma 5 and previous developments in this dissertation. We first exploit the joint displacement covariance of the channels $\mathcal{N}_{A\to B}$ and $\mathcal{M}_{A\to B}$. That is, the fact that channels $\mathcal{N}_{A\to B}$ and $\mathcal{M}_{A\to B}$ have the same X matrix as given in (3.8.14)–(3.8.15) implies that they are jointly covariant with respect to displacements; i.e., for all input density operators ρ and unitary displacement operators $D(\alpha) \equiv \exp\left(\alpha\hat{a}^\dagger - \alpha^*\hat{a}\right)$, the following equalities hold

$$\mathcal{N}_{A\to B}(D(\alpha)\rho D(-\alpha)) = \left(\bigotimes_{i=1}^{m} D(f_i(X,\alpha))\right) \mathcal{N}_{A\to B}(\rho) \left(\bigotimes_{i=1}^{m} D(-f_i(X,\alpha))\right), \quad (3.8.21)$$

$$\mathcal{M}_{A\to B}(D(\alpha)\rho D(-\alpha)) = \left(\bigotimes_{i=1}^{m} D(f_i(X,\alpha))\right) \mathcal{M}_{A\to B}(\rho) \left(\bigotimes_{i=1}^{m} D(-f_i(X,\alpha))\right), \quad (3.8.22)$$

where f_i for $i \in \{1,\ldots,m\}$ are functions depending on the entries of the matrix X and α. Let ϕ_{RA} be an arbitrary pure state such that $\mathrm{Tr}\{\hat{n}\phi_A\} = N_1 \leq N_S$. Consider the following

additive-noise Gaussian channel acting on an input state ρ_A:

$$\mathcal{A}(\rho_A) = \int d^2\alpha \; p_{N_2}(\alpha) \; D(\alpha)\rho_A D(-\alpha), \tag{3.8.23}$$

where $p_{N_2}(\alpha) = \exp\{-|\alpha|^2/N_2\}/\pi N_2$ is a complex, centered Gaussian probability density function with variance $N_2 \equiv N_S - N_1 \geq 0$. Applying this channel to ϕ_A increases its photon number from N_1 to N_S:

$$\text{Tr}\{\hat{n}\mathcal{A}(\phi_A)\} = N_S, \tag{3.8.24}$$

which follows because

$$\begin{aligned}
\text{Tr}\{\hat{n}\mathcal{A}(\phi_A)\} &= \text{Tr}\{\hat{a}^\dagger\hat{a}\int d^2\alpha \; p_{N_2}(\alpha) \; D(\alpha)\phi_A D(-\alpha)\} && (3.8.25)\\
&= \int d^2\alpha \; p_{N_2}(\alpha)\,\text{Tr}\{D(-\alpha)\hat{a}^\dagger\hat{a}D(\alpha)\phi_A\} && (3.8.26)\\
&= \int d^2\alpha \; p_{N_2}(\alpha)\,\text{Tr}\{D(-\alpha)\hat{a}^\dagger D(\alpha)D(-\alpha)\hat{a}D(\alpha)\phi_A\} && (3.8.27)\\
&= \int d^2\alpha \; p_{N_2}(\alpha)\,\text{Tr}\{[\hat{a}^\dagger + \alpha^*][\hat{a} + \alpha]\phi_A\} && (3.8.28)\\
&= \int d^2\alpha \; p_{N_2}(\alpha)\left[\text{Tr}\{\hat{a}^\dagger\hat{a}\phi_A\} + \alpha\,\text{Tr}\{\hat{a}^\dagger\phi_A\} + \alpha^*\,\text{Tr}\{\hat{a}\phi_A\} + |\alpha|^2\,\text{Tr}\{\phi_A\}\right] && (3.8.29)\\
&= N_1 + 0 + 0 + N_2 = N_S. && (3.8.30)
\end{aligned}$$

The first three equalities use definitions, cyclicity of trace, and the fact that $D(\alpha)D(-\alpha) = I$. The fourth equality uses the well known identities (see, e.g., [68])

$$D(-\alpha)\hat{a}D(\alpha) = \hat{a} + \alpha, \qquad D(-\alpha)\hat{a}^\dagger D(\alpha) = \hat{a}^\dagger + \alpha^*. \tag{3.8.31}$$

The second-to-last equality follows because $p_{N_2}(\alpha)$ is a probability density function with mean zero and variance N_2 (we have explicitly indicated what each of the four terms evaluate to in the following line). Let φ_{RA} denote a purification of the state $\mathcal{A}(\phi_A)$. We can then exploit the joint covariance of the channels with respect to displacements, the

relation in (3.8.23), and Lemma 5 to conclude that

$$\mathbf{D}(\mathcal{N}_{A\to B}(\varphi_{RA})\|\mathcal{M}_{A\to B}(\varphi_{RA})) \geq \mathbf{D}(\mathcal{N}_{A\to B}(\phi_{RA})\|\mathcal{M}_{A\to B}(\phi_{RA})), \tag{3.8.32}$$

for all $N_1 \leq N_S$. As a consequence of this development, we find that it suffices to restrict the optimization of the energy-constrained, generalized channel divergence to pure bipartite states φ_{RA} that meet the energy constraint with equality (i.e., $\mathrm{Tr}\{\hat{n}\varphi_A\} = N_S$).

Now we exploit the joint phase covariance of the channels. Let φ_{RA} be a pure bipartite state that meets the energy constraint with equality. Consider that

$$\overline{\varphi}_A \equiv \frac{1}{2\pi}\int_0^{2\pi} d\phi\ e^{i\hat{n}\phi}\varphi_A e^{-i\hat{n}\phi} = \sum_{n=0}^{\infty} |n\rangle\langle n|\varphi_A|n\rangle\langle n|. \tag{3.8.33}$$

That is, the state after phase averaging is diagonal in the number basis, and furthermore, the resulting state $\overline{\varphi}_A$ has the same photon number N_S as φ_A because

$$\begin{aligned}
\mathrm{Tr}\{\hat{n}\overline{\varphi}_A\} &= \frac{1}{2\pi}\int_0^{2\pi} d\phi\ \ \mathrm{Tr}\{\hat{n}e^{i\hat{n}\phi}\varphi_A e^{-i\hat{n}\phi}\} && (3.8.34)\\
&= \frac{1}{2\pi}\int_0^{2\pi} d\phi\ \ \mathrm{Tr}\{e^{-i\hat{n}\phi}\hat{n}e^{i\hat{n}\phi}\varphi_A\} && (3.8.35)\\
&= \frac{1}{2\pi}\int_0^{2\pi} d\phi\ \ \mathrm{Tr}\{\hat{n}\varphi_A\} = \mathrm{Tr}\{\hat{n}\varphi_A\}. && (3.8.36)
\end{aligned}$$

Thus, $\overline{\varphi}_A = \sum_{n=0}^{\infty}\lambda_n^2|n\rangle\langle n|_A$, for some $\lambda_n \in \mathbb{R}^+$ such that $\sum_{n=0}^{\infty}\lambda_n^2 = 1$ and $\sum_{n=0}^{\infty} n\lambda_n^2 = N_S$. Let ξ_{RA} denote a pure bipartite state that purifies $\overline{\varphi}_A$. By applying Lemma 5 and the joint phase covariance relations in (3.8.16)–(3.8.17), we find that the following inequality holds

$$\mathbf{D}(\mathcal{N}_{A\to B}(\xi_{RA})\|\mathcal{M}_{A\to B}(\xi_{RA})) \geq \mathbf{D}(\mathcal{N}_{A\to B}(\varphi_{RA})\|\mathcal{M}_{A\to B}(\varphi_{RA}))\,. \tag{3.8.37}$$

Since all purifications are related by isometries acting on the purifying system R, and since

a generalized divergence is invariant under such an isometry [179], we find that

$$\mathbf{D}(\mathcal{N}_{A\to B}(\xi_{RA})\|\mathcal{M}_{A\to B}(\xi_{RA})) = \mathbf{D}(\mathcal{N}_{A\to B}(\psi_{RA})\|\mathcal{M}_{A\to B}(\psi_{RA})), \tag{3.8.38}$$

where ψ_{RA} is a state of the form in (3.8.19). This concludes the proof of (3.8.18).

To conclude (3.8.20), consider that the thermal state $\theta(N_S)$ is the only Gaussian state of a single mode that is diagonal in the number basis with photon number equal to N_S. A purification of the thermal state $\theta(N_S)$ is the two-mode squeezed vacuum $\psi_{\text{TMS}}(N_S)$ with parameter N_S. So this means that, for a fixed photon number N_S, the two-mode squeezed vacuum with parameter N_S is optimal among all Gaussian states with reduced state on the channel input having the same photon number. ■

We note here that joint phase covariance of two otherwise arbitrary channels implies that states of the form in (3.8.19) with mean photon number of their reduced states $\leq N_S$ are optimal, while joint displacement covariance of two otherwise arbitrary channels implies that states with mean photon number of their reduced states $= N_S$ are optimal. In Proposition 113, we chose to present the interesting case of Gaussian channels in which both kinds of joint covariance hold simultaneously. The aforementioned result regarding jointly phase-covariant channels was concluded in [180] for a special case by employing a different argument and considering the special case of fidelity and Chernoff-information divergences, as well as the discrimination of pure-loss channels. It is worthwhile to note that our argument is different, relying mainly on channel symmetries and data processing, and thus applies in far more general situations than those considered in [180].

Proposition 113 applies to the various settings and channels that we have considered in this dissertation for ε-degradable and ε-close degradable bosonic thermal channels. Thus, we can conclude in these situations that the Gaussian energy-constrained generalized channel divergence is achieved by the two-mode squeezed vacuum state.

Particular generalized channel divergences of interest are the energy-constrained di-

amond norm [137, 138] and the energy-constrained, channel version of the C-distance [130, 132, 133, 181], respectively defined as

$$\|\mathcal{N} - \mathcal{M}\|_{\diamond,G,W} \equiv \sup_{\psi_{RA} \,:\, \mathrm{Tr}\{G\psi_A\} \leq W} \|(\mathrm{id}_R \otimes \mathcal{N}_{A\to B})(\psi_{RA}) - (\mathrm{id}_R \otimes \mathcal{M}_{A\to B})(\psi_{RA})\|_1 \,, \tag{3.8.39}$$

$$C_{G,W}(\mathcal{N}, \mathcal{M}) \equiv \sup_{\psi_{RA} \,:\, \mathrm{Tr}\{G\psi_A\} \leq W} \sqrt{1 - F((\mathrm{id}_R \otimes \mathcal{N}_{A\to B})(\psi_{RA}), (\mathrm{id}_R \otimes \mathcal{M}_{A\to B})(\psi_{RA}))}, \tag{3.8.40}$$

where F denotes the quantum fidelity. Proposition 113 implies that the Gaussian-constrained versions of these quantities reduce to the following for channels satisfying the assumptions stated there:

$$\|\mathcal{N} - \mathcal{M}\|^{\mathcal{G}}_{\diamond,\hat{n},N_S} = \|(\mathrm{id}_R \otimes \mathcal{N}_{A\to B})(\psi_{\mathrm{TMS}}(N_S)) - (\mathrm{id}_R \otimes \mathcal{M}_{A\to B})(\psi_{\mathrm{TMS}}(N_S))\|_1 \,, \tag{3.8.41}$$

$$C^{\mathcal{G}}_{\hat{n},N_S}(\mathcal{N}, \mathcal{M}) = \sqrt{1 - F((\mathrm{id}_R \otimes \mathcal{N}_{A\to B})(\psi_{\mathrm{TMS}}(N_S)), (\mathrm{id}_R \otimes \mathcal{M}_{A\to B})(\psi_{\mathrm{TMS}}(N_S)))}. \tag{3.8.42}$$

We note that the latter quantity is readily expressed as a closed formula in terms of the Gaussian specification of the channels $\mathcal{N}_{A\to B}$ and $\mathcal{M}_{A\to B}$ in (3.8.14)–(3.8.15) and the parameter N_S by employing the general formula for the fidelity of zero-mean Gaussian states from [182]. One could also employ the formulas from [183] or [184, 185] to compute Gaussian, energy-constrained channel divergences based on Rényi relative entropy or quantum relative entropy, respectively.

The result in (3.8.18) already significantly reduces the set of states that we need to consider in computing a given energy-constrained, generalized channel divergence for channels satisfying the conditions of Proposition 113. However, it is a very interesting open question to determine whether, under the conditions given in Proposition 113, the energy-constrained generalized channel divergence is always achieved by the two-mode squeezed vacuum state (if the restriction to Gaussian input states is lifted). Divergences of interest

in applications are the trace distance, fidelity, quantum relative entropy, and Rényi relative entropies. All of these measures lead to a very interesting suite of Gaussian optimizer questions, which we leave for future work. If there is a positive answer to this question, then we would expect to see, in the low-photon-number regime, significant improvements of the ε-degradable and ε-close degradable upper bounds on the capacities of the thermal channel.

In the following remark we provide an example where the two-mode squeezed vacuum state is not optimal to distinguish two particular Gaussian channels satisfying conditions of Proposition 113 with respect to the energy-constrained channel fidelity. Thus the aforementioned suggestion does not hold for all the energy-constrained generalized channel divergences to distinguish two Gaussian channels satisfying Proposition 113.

Remark 114 *In Chapter 5 we prove that the optimal state to distinguish an identity channel $\mathcal{I}$ from an additive-noise channel $\mathcal{T}^{\xi}$ with respect the energy-constrained channel fidelity is an entangled superposition of twin-Fock states. In general, these states are non-Gaussian quantum states. Note that both $\mathcal{I}$ and $\mathcal{T}^{\xi}$ are Gaussian channels with the same X matrices and are jointly phase covariant. Thus, in general, two-mode squeezed vacuum states saturating the energy constraints are not optimal to distinguish two Gaussian channels satisfying Proposition 113. An interesting question is to determine whether a similar result holds for the energy-constrained diamond distance between two Gaussian channels in the context of the approximate degradability bounds introduced in this chapter.*

3.9 Conclusion

In this chapter, we established several bounds on the energy-constrained quantum and private capacities of single-mode, phase-insensitive bosonic Gaussian channels. The energy-constrained bounds imply bounds for the corresponding unconstrained capacities.

In particular, we began by proving several different upper bounds on the energy-constrained quantum capacity of thermal channels. We discussed the closeness of these

four upper bounds with a known lower bound. In particular, we have shown that the ε-close degradable bound works well only in the low-noise regime and that the data-processing and bottleneck upper bounds are close to a lower bound for both low and high thermal noise. We also discussed an interesting case in which the ε-degradable bound is tighter than all other upper bounds. We speculate that the ε-degradable bound can be further tightened by estimating the energy-constrained diamond distance between two particular Gaussian channels that satisfy the conditions in Proposition 113. In Chapters 4 and 5, we develop techniques to estimate the energy-constrained diamond distance and the energy-constrained channel fidelity, which can be further used in bounding the quantum and private capacities of phase-insensitive Gaussian channels. We leave this for future work.

Similarly, we established several different upper bounds on the energy-constrained private capacity of thermal channels. We have also shown an improvement in the achievable rates of private communication through quantum thermal channels by using displaced thermal states as inputs to the channel.

Additionally, we proved several different upper bounds on the energy-constrained quantum and private capacities of quantum amplifier channels. We also established the data-processing and the bottleneck upper bounds on the energy-constrained quantum and private capacities of additive-noise channels. Moreover, in Chapter 5 (see Remark 117) we briefly summarize a method for establishing an ε-close-degradable bound on capacities of additive-noise channels.

We also found that the data-processing bound can be at most 1.45 bits larger than a known lower bound on the energy-constrained quantum and private capacities of all phase-insensitive Gaussian channels. Moreover, our results establish strong limitations on any potential superadditivity of the coherent information of a thermal channel in the low-noise regime.

Since thermal noise is present in almost all communication and optical systems, our results have implications for quantum computing and quantum cryptography. The knowledge

of bounds on quantum capacity can be useful to quantify the performance of distributed quantum computation between remote locations, and private communication rates are connected to the ability to generate secret keys.

We finally used the generalized channel divergence from [153] to address the question of optimal input states for the energy-bounded diamond norm and other related divergences. In particular, we showed that for two Gaussian channels that are jointly phase and displacement covariant, the Gaussian energy-constrained generalized channel divergence is achieved by a two-mode squeezed vacuum state that saturates the energy constraint. It is an interesting open question to determine whether, among all input states, the two-mode squeezed vacuum is the optimal input state for several energy-constrained, generalized channel divergences of interest. Here, we have reduced the optimization to be as given in (3.8.18). As discussed in Remark 114, we provide a partial answer to this question by showing both numerically and analytically that the suggestion mentioned above does not hold for the task of distinguishing an additive-noise channel from an identity channel with respect to the energy-constrained sine distance.

CHAPTER 4

CHARACTERIZING THE PERFORMANCE OF CONTINUOUS-VARIABLE GAUSSIAN QUANTUM GATES

In this chapter, we study three different performance criteria to analyze how well experimental approximations simulate ideal Gaussian operations. We focus on the following notions of convergence for quantum channels: uniform and strong convergence, and uniform convergence on the set of density operators whose marginals on the channel input have bounded energy (see Section 2.5 in Chapter 2 for more details). We analyze several experimental approximations of particular Gaussian unitaries, such as displacement operators, phase rotations, beamsplitters, single-mode squeezing operators, and the SUM operation, which are sufficient to generate an arbitrary Gaussian unitary operation acting on n modes of the electromagnetic field [74].

We first prove that none of these experimental approximations converge uniformly to the ideal Gaussian processes. We then show that these experimental approximations of an ideal displacement operator, beamsplitter, phase rotation, single-mode squeezer, and SUM gate converge to the ideal unitaries in the strong sense. Since the strong convergence of a sequence of infinite-dimensional channels is equivalent to uniform convergence on the set of energy-bounded density operators [137], our results imply that these experimental approximations of an ideal displacement operator, single-mode squeezer, and SUM gate converge uniformly to the ideal unitaries on the set of energy-bounded density operators.

In order to experimentally approximate these different unitary operations, it is important to study how the uniform convergence over the set of energy-bounded operators depends on different experimental parameters. In particular, we consider the energy-constrained sine distance [93, Section 12] as a metric to bound the energy-constrained diamond distance between an ideal displacement operator and its experimental approximation. We first show that the fidelity between the ideal displacement and its experimental

approximation when acting on a fixed input state is equal to the fidelity between a pure-loss channel and an ideal channel when acting on the same input state. We then provide an analytical expression to upper bound the energy-constrained diamond distance between an ideal displacement and its experimental approximations, by using the recent result of [186]. Furthermore, we study different performance metrics to analyze how well an experimental approximation simulates a tensor product of different displacement operators.

We also establish two different lower bounds on the energy-constrained diamond distance [137, 138] between an ideal displacement operator and its experimental approximation by employing two different techniques. A first technique is based on the trace distance between the outputs of these two channels for a particular choice of the input state. In particular, we provide an analytical expression for a lower bound on the energy-constrained diamond distance for low values of the energy constraint. A second technique is to estimate the energy-constrained diamond distance by using a semidefinite program (SDP) on a truncated Hilbert space. In particular, we use an SDP from [138], which directly follows from an SDP from [187, 188] defined in the context of finite-dimensional quantum channels. Moreover, we analytically show that for a fixed value of the energy constraint and for a sufficiently high value of the truncation parameter, the energy-constrained diamond distance between two quantum channels can be estimated with an arbitrarily high accuracy by using an SDP on a truncated Hilbert space.

Similarly, we establish analytical bounds on the energy-constrained diamond distance between ideal beamsplitters, phase rotations, and their respective experimental approximations. We also study uniform convergence over the energy-bounded quantum states of some experimental approximations of both an ideal single-mode squeezing operation and a SUM gate, by considering several experimentally relevant input quantum states.

The chapter is organized as follows. We first describe experimental implementations of a displacement operator, a beamsplitter, a phase rotation, a single-mode squeezer, and a SUM gate, and then we study different notions of convergence for these gates individually.

Finally, we conclude with a brief summary and open questions.

4.1 Approximation of a Displacement Operator

In this section, we analyze convergence of the experimental implementation of a displacement operator from [70] (see also [189]) to the ideal displacement operator. As discussed in Chapter 2, for a single-mode light field, a unitary displacement operator is defined as [68]

$$D^{\alpha} \equiv \exp\Big(\alpha \hat{a}^{\dagger} - \alpha^{*} \hat{a}\Big), \tag{4.1.1}$$

where $\alpha \in \mathbb{C}$, $\hat{a} = (\hat{x} + i\hat{p})/\sqrt{2}$ is an annihilation operator, and $\hat{x}$ and $\hat{p}$ are position- and momentum-quadrature operators, respectively. The action of a displacement operator on a single-mode Gaussian state ρ can be understood as a displacement of the mean values $\langle \hat{x} \rangle_{\rho}$ and $\langle \hat{p} \rangle_{\rho}$.

We note that in this chapter we denote a displacement operator by D^{α}, while we denoted it as D_{α} in Chapter 2. We changed the notation here to accommodate the system label; i.e., D^{α}_{A} denotes a displacement operator acting on system A.

Let ρ_A be a single-mode input quantum state. We then simulate the action of D^{α} on the state ρ_A, according to [70], by employing a beamsplitter $\mathcal{B}^{\eta}_{AB}$ of transmissivity $\eta \in (0, 1)$ and an environment state prepared in a coherent state $|\beta\rangle_B$ [68], where β is chosen such that

$$\sqrt{1-\eta}\beta = \alpha \ . \tag{4.1.2}$$

We denote the channel corresponding to the experimental implementation of the displacement operator D^{α} by

$$\widetilde{\mathcal{D}}^{\eta,\beta} = \widetilde{\mathcal{D}}^{\eta, \frac{\alpha}{\sqrt{1-\eta}}}. \tag{4.1.3}$$

As described in Figure 4.1, the simulation of the ideal channel

$$\mathcal{D}^{\alpha}(\rho_A) \equiv D^{\alpha} \rho_A D^{-\alpha} \tag{4.1.4}$$

realized by the displacement operator D^{α} is given by the following transformation:

$$\widetilde{\mathcal{D}}^{\eta,\beta}(\rho_A) \equiv \mathrm{Tr}_B(\mathcal{B}^{\eta}_{AB}(\rho_A \otimes |\beta\rangle\langle\beta|_B)). \tag{4.1.5}$$

We begin by showing that the channel corresponding to the experimental implementation of a displacement operator is equivalent to a pure-loss channel followed by the ideal displacement operator. Consider that

$$\begin{aligned}
(\mathrm{Tr}_B \circ \mathcal{B}^{\eta}_{AB})(\rho_A \otimes |\beta\rangle\langle\beta|_B) &= (\mathrm{Tr}_B \circ \mathcal{B}^{\eta}_{AB} \circ \mathcal{D}^{\beta}_B)(\rho_A \otimes |0\rangle\langle 0|_B) && (4.1.6)\\
&= (\mathrm{Tr}_B \circ [\mathcal{D}^{\sqrt{1-\eta}\beta}_A \otimes \mathcal{D}^{\sqrt{\eta}\beta}_B] \circ \mathcal{B}^{\eta}_{AB})(\rho_A \otimes |0\rangle\langle 0|_B) && (4.1.7)\\
&= (\mathrm{Tr}_B \circ \mathcal{D}^{\sqrt{1-\eta}\beta}_A \circ \mathcal{B}^{\eta}_{AB})(\rho_A \otimes |0\rangle\langle 0|_B) && (4.1.8)\\
&= (\mathcal{D}^{\sqrt{1-\eta}\beta}_A \circ \mathrm{Tr}_B \circ \mathcal{B}^{\eta}_{AB})(\rho_A \otimes |0\rangle\langle 0|_B) && (4.1.9)\\
&= (\mathcal{D}^{\alpha}_A \circ \mathcal{L}^{\eta}_A)(\rho_A). && (4.1.10)
\end{aligned}$$

The first equality follows from the definition of a coherent state. The second equality follows from the following covariance of the beamsplitter unitary with respect to displacement operators [68]:

$$\mathcal{B}^{\eta}_{AB} \circ \mathcal{D}^{\beta}_B = [\mathcal{D}^{\sqrt{1-\eta}\beta}_A \otimes \mathcal{D}^{\sqrt{\eta}\beta}_B] \circ \mathcal{B}^{\eta}_{AB}\ . \tag{4.1.11}$$

The third equality follows from the cyclicity of partial trace. In the final equality we defined the pure-loss channel as $\mathcal{L}^{\eta}_A(\rho_A) = (\mathrm{Tr}_B \circ \mathcal{B}^{\eta}_{AB})(\rho_A \otimes |0\rangle\langle 0|_B)$.

Let ψ_{RA} be an arbitrary two-mode state. To compute the fidelity between the ideal displacement operator and its experimental approximation, consider that

$$F\Big(\mathcal{D}^{\alpha}_A(\psi_{RA}), (\mathcal{D}^{\alpha}_A \circ \mathcal{L}^{\eta}_A)(\psi_{RA})\Big) = F\Big(\psi_{RA}, \mathcal{L}^{\eta}_A(\psi_{RA})\Big), \tag{4.1.12}$$

where we employed the unitary invariance of the fidelity.

Therefore, analyzing the convergence of the sequence $\{\widetilde{\mathcal{D}}^{\eta,\frac{\alpha}{\sqrt{1-\eta}}}\}_{\eta\in[0,1)}$ to $\mathcal{D}^{\alpha}$ is equiva-

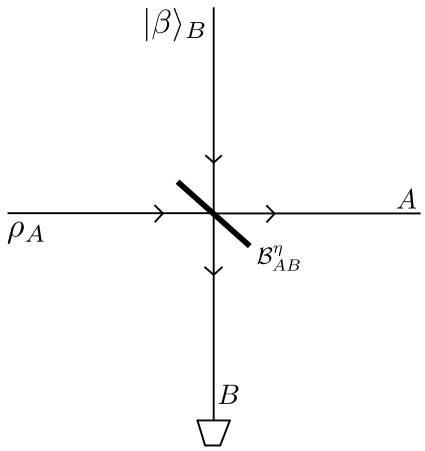

Figure 4.1: The figure plots an experimental approximation $\widetilde{\mathcal{D}}^{\eta,\frac{\alpha}{\sqrt{1-\eta}}}$ of the ideal displacement operation $\mathcal{D}^{\alpha}$ on the input state ρ_A, as introduced in [70]. $|\beta\rangle_B$ represents a coherent state in mode B, where $\alpha = \sqrt{1-\eta}\beta$. $\mathcal{B}^{\eta}_{AB}$ represents a beamsplitter channel with transmissivity η. The experimental approximation of $\mathcal{D}^{\alpha}$ corresponds to sending ρ_A and $|\beta\rangle_B$ through $\mathcal{B}^{\eta}_{AB}$, and then tracing out the mode B [70].

lent to analyzing the convergence of a sequence of pure-loss channels to an ideal channel.

4.1.1 Lack of uniform convergence

We now prove that the sequence $\{\widetilde{\mathcal{D}}^{\eta,\frac{\alpha}{\sqrt{1-\eta}}}\}_{\eta\in[0,1)}$ does not converge uniformly to $\mathcal{D}^{\alpha}$, which follows from (4.1.12) and [138, Proposition 2]. Let $|\delta\rangle$ be a pure input coherent state. Then we find that

$$F(\mathcal{D}^{\alpha}(|\delta\rangle\langle\delta|), \widetilde{\mathcal{D}}^{\eta,\frac{\alpha}{\sqrt{1-\eta}}}(|\delta\rangle\langle\delta|)) = \exp\Big[-(|\delta|^2(1-\sqrt{\eta})^2)/2\Big], \tag{4.1.13}$$

where we used (4.1.12) and the fact that $|\langle\gamma|\delta\rangle|^2 = \exp\Big(-|\gamma-\delta|^2\Big)$ for coherent states $|\gamma\rangle$ and $|\delta\rangle$. Therefore,

$$\lim_{|\delta|^2\to\infty} F(\mathcal{D}^{\alpha}(|\delta\rangle\langle\delta|), \widetilde{\mathcal{D}}^{\eta,\frac{\alpha}{\sqrt{1-\eta}}}(|\delta\rangle\langle\delta|)) = 0\ . \tag{4.1.14}$$

Let $|\phi\rangle_{RA} = |0\rangle_R |\delta\rangle_A$. Using (2.4.12), (4.1.14), and the fact that

$$\|\rho \otimes \omega - \sigma \otimes \omega\|_1 = \|\rho - \sigma\|_1 , \tag{4.1.15}$$

for density operators ρ, σ, ω, we find that

$$\lim_{|\delta|^2 \to \infty} \left\| \mathcal{I}_R \otimes \mathcal{D}_A^{\alpha}(\phi_{RA}) - \mathcal{I}_R \otimes \widetilde{\mathcal{D}}_A^{\eta, \frac{\alpha}{\sqrt{1-\eta}}}(\phi_{RA}) \right\|_1 = 2 , \tag{4.1.16}$$

which is the maximum value of the diamond distance between any two quantum channels. Therefore, the definition in (2.5.1) and the equality in (4.1.16) imply that the sequence $\{\widetilde{\mathcal{D}}^{\eta, \frac{\alpha}{\sqrt{1-\eta}}}\}_{\eta \in [0,1)}$ does not converge uniformly to the ideal displacement channel $\mathcal{D}^{\alpha}$. The equality in (4.1.16) indicates that the ideal displacement $\mathcal{D}^{\alpha}$ and its experimental approximation $\widetilde{\mathcal{D}}^{\eta, \frac{\alpha}{\sqrt{1-\eta}}}$ become perfectly distinguishable in the limit that the input state has unbounded energy. We note that the lack of uniform convergence of a sequence of pure-loss channels to another pure-loss channel was recently studied in [138, Proposition 2].

4.1.2 Strong convergence

We now argue that the sequence $\{\widetilde{\mathcal{D}}^{\eta, \frac{\alpha}{\sqrt{1-\eta}}}\}_{\eta \in [0,1)}$ converges to $\mathcal{D}^{\alpha}$ in the strong sense. Let $\chi_{\rho_A}(x, p)$ denote the Wigner characteristic function [68] for the input state ρ_A. Let $\tilde{\rho}_A^{\text{out}}$ denote the state after the action of $\widetilde{\mathcal{D}}^{\eta, \frac{\alpha}{\sqrt{1-\eta}}}$ on ρ_A:

$$\tilde{\rho}_A^{\text{out}} = \widetilde{\mathcal{D}}^{\eta, \frac{\alpha}{\sqrt{1-\eta}}}(\rho_A) . \tag{4.1.17}$$

We now find the X, Y matrices and the d vector corresponding to the Gaussian channel

$\widetilde{\mathcal{D}}^{\eta,\frac{\alpha}{\sqrt{1-\eta}}}$. By using (4.1.10), we get

$$X = \text{diag}(\sqrt{\eta}, \sqrt{\eta}) \ , \tag{4.1.18}$$

$$Y = \text{diag}(1-\eta, 1-\eta) \ , \tag{4.1.19}$$

$$d = (\sqrt{2}\text{Re}(\alpha), \sqrt{2}\text{Im}(\alpha))^{\text{T}} \ . \tag{4.1.20}$$

Then using (2.3.63), the characteristic function of $\tilde{\rho}_A^{\text{out}}$ is given by

$$\chi_{\tilde{\rho}_A^{\text{out}}}(x,p) = \chi_{\rho_A}(\sqrt{\eta}x, \sqrt{\eta}p) e^{[i\sqrt{2}(p\text{Re}(\alpha) - x\text{Im}(\alpha)) - (1/4)(x^2+p^2)(1-\eta)]} \ . \tag{4.1.21}$$

Moreover, the characteristic function after the action of an ideal displacement channel $\mathcal{D}^\alpha$ on ρ_A is given by

$$\chi_{\mathcal{D}^\alpha(\rho_A)}(x,p) = \chi_{\rho_A}(x,p) e^{[i\sqrt{2}(p\text{Re}(\alpha) - x\text{Im}(\alpha))]} \ . \tag{4.1.22}$$

Therefore, for each $\rho_A \in \mathcal{D}(\mathcal{H}_A)$, and for all $x, p \in \mathbb{R}$

$$\lim_{\eta \to 1} \chi_{\tilde{\rho}_A^{\text{out}}}(x,p) = \chi_{\mathcal{D}^\alpha(\rho_A)}(x,p) \ . \tag{4.1.23}$$

We have thus shown that the sequence of characteristic functions $\chi_{\tilde{\rho}_A^{\text{out}}}$ converges pointwise to $\chi_{\mathcal{D}^\alpha(\rho_A)}$, which implies by [141, Lemma 8] that the sequence $\{\widetilde{\mathcal{D}}^{\eta,\frac{\alpha}{\sqrt{1-\eta}}}\}_{\eta\in[0,1)}$ converges to $\mathcal{D}^\alpha$ in the strong sense.

4.1.3 Convergence in the energy-constrained diamond norm

We now discuss uniform convergence of the sequence $\{\widetilde{\mathcal{D}}^{\eta,\frac{\alpha}{\sqrt{1-\eta}}}\}_{\eta\in[0,1)}$ to $\mathcal{D}^\alpha$ on the set of density operators whose marginals on the channel input have bounded energy. As observed in [137], a sequence of quantum channels converges strongly to a quantum channel if and only if it converges uniformly on the set of density operators whose marginals on the channel input have bounded energy. Therefore, the sequence $\{\widetilde{\mathcal{D}}^{\eta,\frac{\alpha}{\sqrt{1-\eta}}}\}_{\eta\in[0,1)}$ converges

uniformly to $\mathcal{D}^{\alpha}$ if the input states have a finite energy constraint.

However, from an experimental perspective, it is important to know how the energy-constrained uniform convergence depends on experimental parameters. Using (2.4.12) and (4.1.12), we find that

$$\frac{1}{2}\left\|\mathcal{D}^{\alpha}-\widetilde{\mathcal{D}}^{\eta,\frac{\alpha}{\sqrt{1-\eta}}}\right\|_{\diamond E} \leq \sup_{\psi_{RA}:\mathrm{Tr}(H_A\psi_A)\leq E}\sqrt{1-F[\psi_{RA},\mathcal{L}_A^{\eta}(\psi_{RA})]} \tag{4.1.24}$$

$$= \sqrt{1-\left[(1-\{E\})\sqrt{\eta}^{\lfloor E\rfloor}+\{E\}\sqrt{\eta}^{\lceil E\rceil}\right]^2}\,, \tag{4.1.25}$$

where $\{E\} = E - \lfloor E\rfloor$. The equality follows from the recent result of [186] (see also the earlier result in [180]), where the energy-constrained Bures distance [139] between two pure-loss channels was calculated. From (4.1.25), it is easy to see that

$$\lim_{\eta\to 1}\frac{1}{2}\left\|\mathcal{D}^{\alpha}-\widetilde{\mathcal{D}}^{\eta,\frac{\alpha}{\sqrt{1-\eta}}}\right\|_{\diamond E}=0\,, \tag{4.1.26}$$

which justifies the energy-constrained uniform convergence of $\{\widetilde{\mathcal{D}}^{\eta,\frac{\alpha}{\sqrt{1-\eta}}}\}_{\eta\in[0,1)}$ to $\mathcal{D}^{\alpha}$. Furthermore, an optimal state ψ_{RA} that saturates the equality in (4.1.25) is

$$|\psi\rangle_{RA} = \sqrt{1-\{E\}}\,|\lfloor E\rfloor\rangle_A|\tau\rangle_R + \sqrt{\{E\}}\,|\lceil E\rceil\rangle_A\left|\tau^{\perp}\right\rangle_R\,, \tag{4.1.27}$$

which follows directly from [186]. Here $|\tau\rangle$ and $\left|\tau^{\perp}\right\rangle$ are normalized orthogonal states.

Numerical results. Next, we perform numerical evaluations to see how close the experimental approximation $\widetilde{\mathcal{D}}^{\eta,\frac{\alpha}{\sqrt{1-\eta}}}$ is to the ideal displacement channel $\mathcal{D}^{\alpha}$. We denote the energy-constrained sine distance [93, Section 12] obtained in (4.1.25) as

$$f(\eta,E) = \sqrt{1-\left[(1-\{E\})\sqrt{\eta}^{\lfloor E\rfloor}+\{E\}\sqrt{\eta}^{\lceil E\rceil}\right]^2}\,. \tag{4.1.28}$$

In Figure 4.2, we plot $f(\eta,E)$ versus η for certain values of the energy constraint E. In particular, we find that for all values of E, the experimental approximation $\widetilde{\mathcal{D}}^{\eta,\frac{\alpha}{\sqrt{1-\eta}}}$

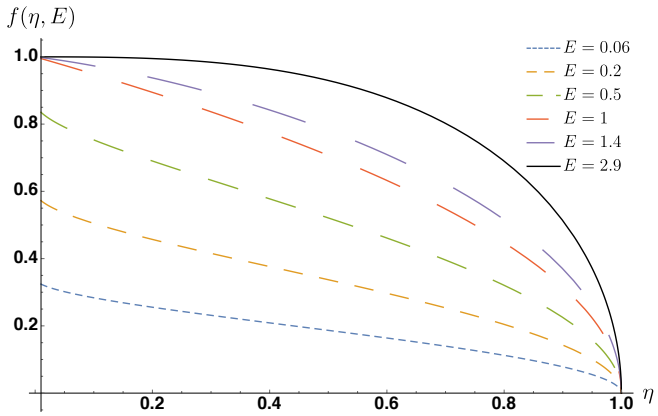

Figure 4.2: The figure plots the energy-constrained sine distance $f(\eta, E)$ (4.1.28) between an ideal displacement channel $\mathcal{D}^{\alpha}$ and its experimental approximation $\widetilde{\mathcal{D}}^{\eta,\frac{\alpha}{\sqrt{1-\eta}}}$. In the figure, we select certain values of the energy constraint E, with the choices indicated next to the figure. In all the cases, $\widetilde{\mathcal{D}}^{\eta,\frac{\alpha}{\sqrt{1-\eta}}}$ simulates $\mathcal{D}^{\alpha}$ with a high accuracy for values of $\eta \approx 1$. Moreover, for a fixed value of η, the simulation of $\mathcal{D}^{\alpha}$ is more accurate for low values of the energy constraint on input states.

simulates the ideal displacement $\mathcal{D}^{\alpha}$ with a high accuracy for $\eta \approx 1$. Moreover, for a fixed value of η, the simulation of $\mathcal{D}^{\alpha}$ is more accurate for low values of the energy constraint on input states.

In Figure 4.3, we zoom in on Figure 4.2 for high values of η. Figure 4.3 indicates that it is only for low values of E and high values of η that high accuracy in simulating $\mathcal{D}^{\alpha}$ can be achieved. Therefore, energy constraints on the input states play a critical role in simulating ideal unitary operations and determining error propagation.

We now analyze a simple case when the energy constraint E on the input density operators takes on an integer value. From (4.1.25), we find that

$$\inf_{\psi_{RA}:\mathrm{Tr}(H_A\psi_A)\leq E} F[\mathcal{D}^{\alpha}(\psi_{RA}), \widetilde{\mathcal{D}}^{\eta,\frac{\alpha}{\sqrt{1-\eta}}}(\psi_{RA})] = \eta^E \ . \tag{4.1.29}$$

Therefore, for a given energy constraint on the input states, and to implement an ideal displacement channel $\mathcal{D}^{\alpha}$ with any desired accuracy, one can find η from (4.1.25)–(4.1.29), and the corresponding β from $\sqrt{1-\eta}\beta = \alpha$. The equality in (4.1.29) illustrates just how difficult it is to achieve a good accuracy in simulating an ideal displacement channel: in

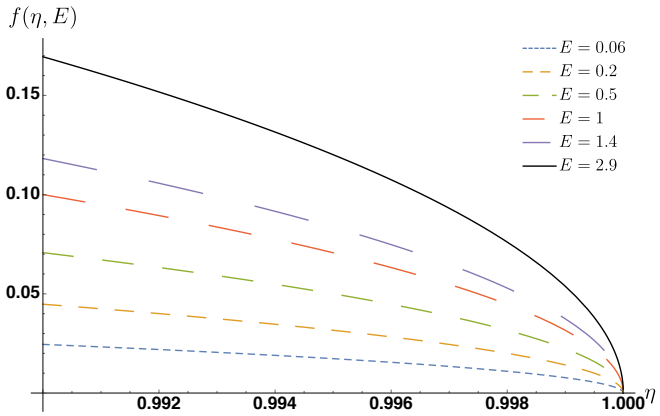

Figure 4.3: The figure plots Figure 4.2 for high values of η. The figure indicates that, only for low values of E and high values of η, high accuracy in simulating $\mathcal{D}^{\alpha}$ can be achieved.

order to achieve the same fidelity, one requires an exponential increase in η to match only a linear increase in E.

We now summarize the results from Sections 4.1.1–4.1.3. From Sections 4.1.1 and 4.1.2, it follows that the sequence $\{\widetilde{\mathcal{D}}^{\eta,\frac{\alpha}{\sqrt{1-\eta}}}\}_{\eta\in[0,1)}$ does not converge uniformly to $\mathcal{D}^{\alpha}$. Rather, convergence occurs in the strong sense. In other words, convergence of $\{\widetilde{\mathcal{D}}^{\eta,\frac{\alpha}{\sqrt{1-\eta}}}\}_{\eta\in[0,1)}$ to $\mathcal{D}^{\alpha}$ is not independent of the input state; i.e., there exists an input state for which the experimental implementation of a displacement operation has the maximum possible value of the worst-case error.

It is important to stress that, although for a fixed finite value of the energy-constraint parameter E the limit $\eta \to 1$ is necessary for the implementation of a displacement operation $\mathcal{D}^{\alpha}$ using $\{\widetilde{\mathcal{D}}^{\eta,\frac{\alpha}{\sqrt{1-\eta}}}\}_{\eta\in[0,1)}$ with a high accuracy, it also relies on the fact that $\sqrt{1-\eta}\beta = \alpha$. Due to the unitary invariance of the fidelity as shown in (4.1.12), the fidelity between $\mathcal{D}^{\alpha}$ and $\{\widetilde{\mathcal{D}}^{\eta,\frac{\alpha}{\sqrt{1-\eta}}}\}_{\eta\in[0,1)}$ becomes independent of the parameter β. However, it is implicit from $\sqrt{1-\eta}\beta = \alpha$ that $\eta \to 1$ requires $\beta \to \infty$. Although high values of β are experimentally achievable, the ideal displacement operation is achieved only in the limiting sense. This raises a further question: is it possible to implement an ideal displacement operation through a different procedure than in [70], such that a high accuracy can be achieved?

4.1.4 Convergence for a tensor product of displacements

Let us briefly discuss the various notions of convergence for experimental approximations of a tensor product of ideal displacement channels. Let $\{\mathcal{D}^{\alpha_i}\}_{i=1}^{L}$ be a set of L different displacement channels. We approximate the tensor product of these operators by a tensor product of $\{\widetilde{\mathcal{D}}^{\eta_i,\beta_i}\}_{i=1}^{L}$, such that $\sqrt{1-\eta_i}\beta_i = \alpha_i$, for $i \in \{1,\ldots,L\}$. From the same counterexample given above (coherent states with large energy), it follows directly that the sequence $\{\bigotimes_{i=1}^{L} \widetilde{\mathcal{D}}^{\eta_i,\alpha_i/\sqrt{1-\eta_i}}\}_{\eta_1,\ldots,\eta_L\in[0,1)}$ does not converge uniformly to $\bigotimes_{i=1}^{L}\mathcal{D}^{\alpha_i}$. Rather, the convergence holds in the strong sense, as a consequence of [117, Proposition 1]. Moreover, suppose that there is an average energy constraint on the input state to the tensor product of displacement operators, i.e., $\operatorname{Tr}\left(\widetilde{H}_{A^L}\psi_{A^L}\right) \leq E$, where

$$\widetilde{H}_{A^L} \equiv H_A \otimes I \otimes \cdots \otimes I + \cdots + I \otimes \cdots \otimes I \otimes H_A, \tag{4.1.30}$$

and $E \in [0,\infty)$. Let $\operatorname{Tr}(H_A\psi_{A_i}) = E_i$, where $E_i \in [0,\infty)$, $\forall i \in \{1,\ldots,L\}$.

Consider the following chain of inequalities:

$$\begin{aligned}
&\frac{1}{2}\left\|\left(\bigotimes_{i=1}^{K}\mathcal{D}^{\alpha_i}\right)(\psi_{RA^K}) - \left(\bigotimes_{i=1}^{K}\widetilde{\mathcal{D}}^{\eta_i,\alpha_i/\sqrt{1-\eta_i}}\right)(\psi_{RA^K})\right\|_1 \\
&\leq \sum_{i=1}^{K} C\left(\mathcal{L}_{A_i}^{\eta_i}(\psi_{RA_i}), \mathcal{I}_{A_i}(\psi_{RA_i})\right) \qquad (4.1.31)\\
&\leq \max_{\{E_i\}_i : \sum_i E_i \leq E} \sum_{i=1}^{K} \sqrt{1-[(1-\{E_i\})\sqrt{\eta_i}^{\lfloor E_i\rfloor} + \{E_i\}\sqrt{\eta_i}^{\lceil E_i\rceil}]^2}. \qquad (4.1.32)
\end{aligned}$$

The first inequality follows from (2.4.12) and [117, Proposition 1]. The last inequality follows from the recent result of [190], and due to the maximization over a set of energy values satisfying the input energy constraint. Since the chain of inequalities is true for all

input states satisfying the input energy constraint, the following holds

$$\frac{1}{2}\left\|\bigotimes_{i=1}^{K}\mathcal{D}^{\alpha_i}-\bigotimes_{i=1}^{K}\widetilde{\mathcal{D}}^{\eta_i,\alpha_i/\sqrt{1-\eta_i}}\right\|_{\diamond E} \leq \max_{\{E_i\}_i:\sum_i E_i\leq E}\sum_{i=1}^{K}\sqrt{1-[(1-\{E_i\})\sqrt{\eta_i}^{\lfloor E_i\rfloor}+\{E_i\}\sqrt{\eta_i}^{\lceil E_i\rceil}]^2}\ . \quad (4.1.33)$$

Therefore, $\{\bigotimes_{i=1}^{K}\widetilde{\mathcal{D}}^{\eta_i,\alpha_i/\sqrt{1-\eta_i}}\}_{\eta_1,\ldots,\eta_K\in[0,1)}$ converges uniformly to $\bigotimes_{i=1}^{K}\mathcal{D}^{\alpha_i}$ on the set of density operators whose marginals on the channel input have bounded energy.

4.1.5 Estimates of energy-constrained diamond distance

We now provide good estimates of the energy-constrained diamond distance, as defined in (2.4.17) between the ideal displacement operation $\mathcal{D}^{\alpha}$ and its experimental approximation $\widetilde{\mathcal{D}}^{\eta,\alpha/\sqrt{1-\eta}}$. In particular, we introduce two different techniques to lower bound the energy-constrained diamond distance.

A first technique is based on the trace distance between $\mathcal{I}_R\otimes\mathcal{D}^{\alpha}(\psi_{RA})$ and $\mathcal{I}_R\otimes\widetilde{\mathcal{D}}^{\eta,\alpha/\sqrt{1-\eta}}(\psi_{RA})$ for a finite energy-constraint E, i.e., $\mathrm{Tr}(\hat{n}\psi_A)\leq E$, where ψ_{RA} is given by (4.1.27). Since the energy-constrained diamond distance, as defined in (2.4.17), involves an optimization over all input states satisfying the energy constraint, we find that

$$\left\|\mathcal{I}_R\otimes\mathcal{D}^{\alpha}(\psi_{RA})-\mathcal{I}_R\otimes\widetilde{\mathcal{D}}^{\eta,\frac{\alpha}{\sqrt{1-\eta}}}(\psi_{RA})\right\|_1\leq\left\|\mathcal{D}^{\alpha}-\widetilde{\mathcal{D}}^{\eta,\frac{\alpha}{\sqrt{1-\eta}}}\right\|_{\diamond E}\ . \quad (4.1.34)$$

A second technique is based on the numerical evaluation of the energy-constrained diamond distance between $\mathcal{D}^{\alpha}$ and $\widetilde{\mathcal{D}}^{\eta,\alpha/\sqrt{1-\eta}}$ on a truncated Hilbert space. In particular, we consider input states to these quantum channels such that instead of acting on an infinite-dimensional separable Hilbert space, these states act on an $(M+1)$-dimensional Fock space. Moreover, we consider a mean photon number constraint on these states. Let $\mathcal{H}_M$ denote an $(M+1)$-dimensional Fock space. Let $\underline{\hat{n}}$ denote the following truncated

number operator:

$$\underline{\hat{n}} = \sum_{n=0}^{M} n|n\rangle\langle n| \ . \tag{4.1.35}$$

Let $\varphi_A \in \mathcal{D}(\mathcal{H}_M)$. Then the following inequality holds:

$$\text{Tr}(\underline{\hat{n}}\varphi_A) \leq E \ , \tag{4.1.36}$$

where E denotes the mean energy constraint.

We define the energy-constrained diamond distance between two quantum channels $\mathcal{N}_{A\to B}$ and $\mathcal{M}_{A\to B}$ on a truncated Hilbert space as

$$\|\mathcal{N}_{A\to B} - \mathcal{M}_{A\to B}\|_{\diamond E,M} \equiv \sup_{\phi_{RA}\in\mathcal{D}(\mathcal{H}_M^{\otimes 2}):\text{Tr}(\underline{\hat{n}}\phi_A)\leq E} \|\mathcal{N}_{A\to B}(\phi_{RA}) - \mathcal{M}_{A\to B}(\phi_{RA})\|_1 \ , \tag{4.1.37}$$

where E and M denote the mean energy constraint and the truncation parameter, respectively, and $\phi_{RA} = |\phi\rangle\langle\phi|_{RA}$ is a purification of the state ϕ_A. Moreover, it is implicit that the identity channel acts on the reference system R. Finally, note that the following identity holds:

$$\|\mathcal{N}_{A\to B} - \mathcal{M}_{A\to B}\|_{\diamond E,M} = \sup_{\phi_{RA}\in\mathcal{D}(\mathcal{H}_M^{\otimes 2}):\text{Tr}(\hat{n}\phi_A)\leq E} \|\mathcal{N}_{A\to B}(\phi_{RA}) - \mathcal{M}_{A\to B}(\phi_{RA})\|_1 \ , \tag{4.1.38}$$

where we have replaced $\underline{\hat{n}}$ with $\hat{n}$, following as a consequence of the reduced state of $\phi_{RA} \in \mathcal{D}(\mathcal{H}_M^{\otimes 2})$ on A having support only on the truncated space and from the Schmidt decomposition, implying that the reference system R need only have support as large as the input space A.

We now show that the set of density operators acting on a truncated Hilbert space with a finite mean energy constraint (yet an arbitrarily high truncation parameter) is dense in the set of density operators acting on an infinite-dimensional Hilbert space and with the same mean energy constraint. In other words, any finite mean energy state acting on an infinite-dimensional separable Hilbert space can be approximated with an arbitrary

accuracy by a state with the same finite mean energy acting on a truncated Hilbert space with a sufficiently high value of the truncation parameter. Let ρ_{RA} denote a density operator acting on an infinite-dimensional separable Hilbert space, such that $\mathrm{Tr}(\hat{n}_A \rho_{RA}) \leq E$, where $E > 0$. Let Π_A^M denote an M-dimensional projector defined as

$$\Pi_A^M = \sum_{n=0}^{M} |n\rangle\langle n| \ . \tag{4.1.39}$$

Consider the following chain of inequalities:

$$\mathrm{Tr}\Big(\Pi_A^M \rho_{RA}\Big) = \mathrm{Tr}(\rho_{RA}) - \sum_{n=M+1}^{\infty} \langle n|\rho_A|n\rangle \tag{4.1.40}$$

$$\geq 1 - \sum_{n=M+1}^{\infty} \frac{n}{M+1} \langle n|\rho_A|n\rangle \tag{4.1.41}$$

$$\geq 1 - \frac{1}{M+1}\left(\sum_{n=0}^{\infty} n\langle n|\rho_A|n\rangle \right) \tag{4.1.42}$$

$$\geq 1 - \frac{E}{M+1} \ . \tag{4.1.43}$$

The first inequality follows from the fact that $n/(M+1) \geq 1$ for all $n \in [M+1, \infty)$. The second inequality follows because $\sum_{n=0}^{M} n\langle n|\rho_A|n\rangle$ is a sum of positive numbers. The last inequality follows because $\mathrm{Tr}(\hat{n}_A \rho_A) \leq E$. We note that (4.1.43) can also be derived from the Fock cutoff lemma in [191].

Let ρ_{RA}^M denote the following truncated state

$$\rho_{RA}^M = \frac{\Pi_A^M \rho_{RA} \Pi_A^M}{\mathrm{Tr}(\Pi_A^M \rho_{RA})} \ . \tag{4.1.44}$$

The following proposition establishes a bound on the trace distance between ρ_{RA} and ρ_{RA}^M.

Proposition 115 *Let ρ_{RA} be a density operator acting on an infinite-dimensional separable Hilbert space such that $\mathrm{Tr}(\hat{n}_A \rho_{RA}) \leq E$, where $E > 0$, and $\hat{n}_A$ is the number operator as defined in* (2.3.4)*. Let ρ_{RA}^M be the M-dimensional truncation of the state ρ_{RA}, as defined in*

(4.1.44). *Then*

$$\frac{1}{2}\left\|\rho_{RA} - \rho_{RA}^{M}\right\|_1 \leq \sqrt{\frac{E}{M+1}}\ . \tag{4.1.45}$$

Proof. The proof follows directly from (4.1.43) and the gentle measurement lemma introduced in [192] and subsequently improved in [193]. ■

Proposition 116 below states that for low values of the mean energy constraint E, the energy-constrained diamond distance between two quantum channels $\mathcal{N}$ and $\mathcal{M}$ can be estimated with an arbitrarily high accuracy by using the energy-constrained diamond distance on a truncated input Hilbert space with sufficiently high values of the truncation parameter M.

Proposition 116 *Let $\mathcal{N}$ and $\mathcal{M}$ be quantum channels, and let E be the energy constraint on the input states to these channels. Let M denote the truncation parameter. Then*

$$\tfrac{1}{2}\left\|\mathcal{N}-\mathcal{M}\right\|_{\diamond E,M} \leq \tfrac{1}{2}\left\|\mathcal{N}-\mathcal{M}\right\|_{\diamond E} \leq \tfrac{1}{2}\left\|\mathcal{N}-\mathcal{M}\right\|_{\diamond E,M} + 2\sqrt{\frac{E}{M+1}}\ . \tag{4.1.46}$$

Proof. The inequality $\left\|\mathcal{N}-\mathcal{M}\right\|_{\diamond E,M} \leq \left\|\mathcal{N}-\mathcal{M}\right\|_{\diamond E}$ follows from (2.4.17) and (4.1.38).

We now prove the other inequality. Let ρ_{RA} be a density operator acting on an infinite-dimensional separable Hilbert space such that $\operatorname{Tr}(\hat{n}_A \rho_{RA}) \leq E$. Let ρ_{RA}^M be the M-dimensional truncation of the state ρ_{RA} as defined in (4.1.44). Consider the following chain of inequalities:

$$\begin{aligned}
\left\|\mathcal{N}(\rho_{RA}) - \mathcal{M}(\rho_{RA})\right\|_1 &\leq \left\|\mathcal{N}(\rho_{RA}) - \mathcal{N}(\rho_{RA}^M)\right\|_1 + \left\|\mathcal{N}(\rho_{RA}^M) - \mathcal{M}(\rho_{RA}^M)\right\|_1 \\
&\quad + \left\|\mathcal{M}(\rho_{RA}^M) - \mathcal{M}(\rho_{RA})\right\|_1 && (4.1.47)\\
&\leq 2\left\|\rho_{RA} - \rho_{RA}^M\right\|_1 + \left\|\mathcal{N}(\rho_{RA}^M) - \mathcal{M}(\rho_{RA}^M)\right\|_1 && (4.1.48)\\
&\leq 4\sqrt{\frac{E}{M+1}} + \left\|\mathcal{N}-\mathcal{M}\right\|_{\diamond E,M}\ . && (4.1.49)
\end{aligned}$$

In all the steps above, it is implicit that the identity channel acts on the reference system

R. The first inequality is the consequence of triangle inequality for the trace distance. The second inequality follows from monotonicity of the trace distance. The last inequality follows from Proposition 115 and from (4.1.37). Since the chain of inequalities holds for all input states ρ_{RA} satisfying the energy constraint, the desired result follows. ■

We now study the aforementioned two techniques in detail to characterize the performance of the simulation of an ideal displacement operator. It is evident from Figure 4.2 that for a fixed value of η, the accuracy in simulating an ideal displacement operation $\mathcal{D}^{\alpha}$ by using the protocol from [70] is reasonable only for low values of the energy constraint on input states. Therefore, we now study the simulation of $\mathcal{D}^{\alpha}$ in detail only for low values of the energy constraint.

Let $0 < E < 1$. Then

$$\frac{1}{2}\left\|\mathcal{I}_R \otimes \mathcal{D}^{\alpha}(\psi_{RA}) - \mathcal{I}_R \otimes \widetilde{\mathcal{D}}^{\eta,\frac{\alpha}{\sqrt{1-\eta}}}(\psi_{RA})\right\|_1 = \frac{1}{2}[\{E\}(1-\eta) + (1-\sqrt{\eta})\varkappa(\eta,\{E\})] \quad (4.1.50)$$

$$\equiv d_1(\eta, E)\ , \quad (4.1.51)$$

where

$$\varkappa(\eta,\{E\}) = \sqrt{\{E\}(4+\{E\}(\eta+2\sqrt{\eta}-3))}, \quad (4.1.52)$$

$\{E\} = E - \lfloor E \rfloor$, and ψ_{RA} is given by (4.1.27).

Therefore, from (4.1.34), it follows that (4.1.50) is a lower bound on the energy-constrained diamond distance between $\mathcal{D}^{\alpha}$ and $\widetilde{\mathcal{D}}^{\eta,\alpha/\sqrt{1-\eta}}$ for $0 < E < 1$, i.e.,

$$d_1(\eta, E) \leq \frac{1}{2}\left\|\mathcal{D}^{\alpha} - \widetilde{\mathcal{D}}^{\eta,\frac{\alpha}{\sqrt{1-\eta}}}\right\|_{\diamond E}\ . \quad (4.1.53)$$

We now provide a proof for (4.1.50). Let $t = \sqrt{\eta}$ and $r = \sqrt{1-\eta}$. Then the action of a pure-loss channel with transmissivity η on ψ_{RA} in (4.1.27) is given by

$$(\mathcal{I}_R \otimes \mathcal{L}_A^{\eta})(\psi_{RA}) = \mathrm{Tr}_B((\mathcal{I}_R \otimes \mathcal{B}_{AB}^{\eta})(\psi_{RA} \otimes |0\rangle\langle 0|_B)) \equiv \rho_{RA}\ . \quad (4.1.54)$$

Consider the following unitary evolution of the pure state $|\psi\rangle_{RA} \otimes |0\rangle_B$:

$$
\begin{aligned}
&(I_R \otimes \mathcal{B}^{\eta}_{AB})(|\psi\rangle_{RA} \otimes |0\rangle_B) \\
&= \mathcal{B}^{\eta}_{AB}\Big(\sqrt{\frac{1-\{E\}}{\lfloor E \rfloor !}}(\hat{a}^{\dagger}_{\mathrm{in}})^{\lfloor E \rfloor}|0\rangle_A |\tau\rangle_R |0\rangle_B + \sqrt{\frac{\{E\}}{\lceil E \rceil !}}(\hat{a}^{\dagger}_{\mathrm{in}})^{\lceil E \rceil}|0\rangle_A \left|\tau^{\perp}\right\rangle_R |0\rangle_B\Big) \qquad (4.1.55) \\
&= \sqrt{\frac{1-\{E\}}{\lfloor E \rfloor !}}(t\hat{a}^{\dagger}_{\mathrm{out}} + r\hat{b}^{\dagger}_{\mathrm{out}})^{\lfloor E \rfloor}|0\rangle_A |\tau\rangle_R |0\rangle_B + \sqrt{\frac{\{E\}}{\lceil E \rceil !}}(t\hat{a}^{\dagger}_{\mathrm{out}} + r\hat{b}^{\dagger}_{\mathrm{out}})^{\lceil E \rceil}|0\rangle_A \left|\tau^{\perp}\right\rangle_R |0\rangle_B \qquad (4.1.56) \\
&= \sqrt{1-\{E\}}\sum_{k_1}\sqrt{\binom{\lfloor E \rfloor}{k_1}}t^{k_1}r^{\lfloor E \rfloor - k_1}|k_1\rangle_A |\tau\rangle_R |\lfloor E \rfloor - k_1\rangle_B \\
&\qquad + \sqrt{\{E\}}\sum_{k_2}\sqrt{\binom{\lceil E \rceil}{k_2}}t^{k_2}r^{\lceil E \rceil - k_2}|k_2\rangle_A \left|\tau^{\perp}\right\rangle_R |\lceil E \rceil - k_2\rangle_B \ . \qquad (4.1.57)
\end{aligned}
$$

The second equality follows from the beamsplitter transformation in the Heisenberg picture (2.3.78). Then the density operator after tracing out B in (4.1.56) is given by

$$
\begin{aligned}
\rho_{RA} = &(1-\{E\})\sum_{k_1}\binom{\lfloor E \rfloor}{k_1}t^{2k_1}r^{2(\lfloor E \rfloor - k_1)}|k_1\rangle\langle k_1|_A|\tau\rangle\langle\tau|_R \\
&+ \{E\}\sum_{k_2}\binom{\lceil E \rceil}{k_2}t^{2k_2}r^{2(\lceil E \rceil - k_2)}|k_2\rangle\langle k_2|_A|\tau^{\perp}\rangle\langle\tau^{\perp}|_R \\
&+ \sqrt{(1-\{E\})\{E\}}\sum_{k_1}\sqrt{\binom{\lfloor E \rfloor}{k_1}\binom{\lceil E \rceil}{k_1+1}}t^{(2k_1+1)}r^{\lfloor E \rfloor + \lceil E \rceil - 2k_1 - 1} \\
&\times\Big(|k_1\rangle\langle k_1+1|_A|\tau\rangle\langle\tau^{\perp}|_R + |k_1+1\rangle\langle k_1|_A|\tau^{\perp}\rangle\langle\tau|_R\Big) \ .
\end{aligned} \qquad (4.1.58)
$$

On the other hand, the density operator of the state in (4.1.27) is given by

$$
\begin{aligned}
\psi_{RA} = &(1-\{E\})|\lfloor E \rfloor\rangle\langle\lfloor E \rfloor|_A|\tau\rangle\langle\tau|_R + \{E\}|\lceil E \rceil\rangle\langle\lceil E \rceil|_A|\tau^{\perp}\rangle\langle\tau^{\perp}|_R \\
&+ \sqrt{(1-\{E\})\{E\}}\Big(|\lfloor E \rfloor\rangle\langle\lceil E \rceil|_A|\tau\rangle\langle\tau^{\perp}|_R + |\lceil E \rceil\rangle\langle\lfloor E \rfloor||\tau^{\perp}\rangle\langle\tau|_R\Big) \ . \qquad (4.1.59)
\end{aligned}
$$

Let ω_{RA} denote the operator corresponding to the difference of ρ_{RA} in (4.1.58) and ψ_{RA} in (4.1.59).

$$\omega_{RA} = \rho_{RA} - \psi_{RA} \tag{4.1.60}$$

$$\begin{aligned}
&= (1-\{E\})\left[\sum_{k_1}\binom{\lfloor E\rfloor}{k_1} t^{2k_1} r^{2(\lfloor E\rfloor - k_1)} |k_1\rangle\langle k_1|_A - |\lfloor E\rfloor\rangle\langle\lfloor E\rfloor|_A\right]|\tau\rangle\langle\tau|_R \\
&\quad + \{E\}\left[\sum_{k_2}\binom{\lceil E\rceil}{k_2} t^{2k_2} r^{2(\lceil E\rceil - k_2)} |k_2\rangle\langle k_2|_A - |\lceil E\rceil\rangle\langle\lceil E\rceil|_A\right]|\tau^\perp\rangle\langle\tau^\perp|_R \\
&\quad + \sqrt{(1-\{E\})\{E\}}\left[\sum_{k_1}\sqrt{\binom{\lfloor E\rfloor}{k_1}\binom{\lceil E\rceil}{k_1+1}} t^{(2k_1+1)} r^{\lfloor E\rfloor + \lceil E\rceil - 2k_1 - 1}\right. \\
&\quad \times \Big(|k_1\rangle\langle k_1+1|_A|\tau\rangle\langle\tau^\perp|_R + |k_1+1\rangle\langle k_1|_A|\tau^\perp\rangle\langle\tau|_R\Big) \\
&\quad \left. - |\lfloor E\rfloor\rangle\langle\lceil E\rceil|_A|\tau\rangle\langle\tau^\perp|_R - |\lceil E\rceil\rangle\langle\lfloor E\rfloor||\tau^\perp\rangle\langle\tau|_R\right] .
\end{aligned} \tag{4.1.61}$$

We now find $\|\omega_{RA}\|_1$ for a simple case. Let $0 < E < 1$. Then $\lfloor E\rfloor = 0$ and $\lceil E\rceil = 1$. Let $|\tau\rangle = |0\rangle$ and $\left|\tau^\perp\right\rangle = |1\rangle$. Therefore, the operator ω_{RA} is given by

$$\begin{aligned}
\omega_{RA} &= \{E\}\left[r^2|0\rangle\langle 0|_A + t^2|1\rangle\langle 1|_A - |1\rangle\langle 1|_A\right]|1\rangle\langle 1|_R \\
&\quad + \sqrt{(1-\{E\})\{E\}}\left[(t-1)\Big(|0\rangle\langle 1|_A \otimes |0\rangle\langle 1|_R + |1\rangle\langle 0|_A \otimes |1\rangle\langle 0|_R\Big)\right] .
\end{aligned} \tag{4.1.62}$$

After expressing r and t in terms of η, the matrix representation of ω_{RA} is as follows

$$\omega_{RA} = \begin{bmatrix} 0 & 0 & 0 & -\sqrt{(1-\{E\})\{E\}}(1-\sqrt{\eta}) \\ 0 & \{E\}(1-\eta) & 0 & 0 \\ 0 & 0 & 0 & 0 \\ -\sqrt{(1-\{E\})\{E\}}(1-\sqrt{\eta}) & 0 & 0 & -\{E\}(1-\eta) \end{bmatrix} \tag{4.1.63}$$

Then $\|\omega_{RA}\|_1$ is given by [164]

$$\begin{aligned} \frac{1}{2}\|\omega_{RA}\|_1 = \frac{1}{2}\Bigg[\{E\}(1-\eta) + \frac{1}{2}\left|(\sqrt{\eta}-1)\left(\{E\}(1+\sqrt{\eta}) - \sqrt{\{E\}\Big[4+\{E\}(-3+2\sqrt{\eta}+\eta)\Big]}\right)\right| \\ + \frac{1}{2}\left|(\sqrt{\eta}-1)\left(\{E\}(1+\sqrt{\eta}) + \sqrt{\{E\}\Big[4+\{E\}(-3+2\sqrt{\eta}+\eta)\Big]}\right)\right|\Bigg]. \end{aligned} \tag{4.1.64}$$

Since

$$\{E\}(1+\sqrt{\eta}) \leq \sqrt{\{E\}\Big[4+\{E\}(-3+2\sqrt{\eta}+\eta)\Big]}\Bigg) \tag{4.1.65}$$

for all $0 < E < 1$ and $\eta \geq 0$, we get that

$$\frac{1}{2}\|\omega_{RA}\|_1 = \frac{1}{2}\left[\{E\}(1-\eta) + (1-\sqrt{\eta})\sqrt{\{E\}\Big[4+\{E\}(-3+2\sqrt{\eta}+\eta)\Big]}\right]. \tag{4.1.66}$$

A second method to obtain a lower bound on the energy-constrained diamond distance between two quantum channels $\mathcal{N}_{A\to B}$ and $\mathcal{M}_{A\to B}$ is to truncate the infinite-dimensional separable Hilbert space to a finite-dimensional Hilbert space and apply energy constraints on channel input states according to the truncated number operator, as defined in (4.1.35)–(4.1.36). In particular, we obtain the energy-constrained diamond distance between $\mathcal{N}_{A\to B}$ and $\mathcal{M}_{A\to B}$ on a truncated Hilbert space by using a semi-definite program (SDP) from [138], which is inspired from an SDP defined in the context of finite-dimensional quantum channels in [187, 188]. We use the following SDP to estimate the energy-constrained diamond

distance between two quantum channels $\mathcal{N}_{A\to B}$ and $\mathcal{M}_{A\to B}$:

$$\|\mathcal{N}-\mathcal{M}\|_{\diamond E,M}=\begin{cases}\sup & \operatorname{Tr}(W_{RB}J_{RB})\\ \text{subject to} & 0\leq W_{RB}\leq \rho_R\otimes \mathbb{I}_B,\\ & \operatorname{Tr}(\rho_R)=1,\ \rho_R\geq 0,\\ & \operatorname{Tr}(\hat{\underline{n}}\rho_R)\leq E,\end{cases} \tag{4.1.67}$$

where M is the truncation parameter, E is the mean energy-constraint parameter, and $\hat{\underline{n}}$ is given by (4.1.35). Moreover, J_{RB} denotes the operator corresponding to the difference of the Choi operators of quantum channels $\mathcal{N}$ and $\mathcal{M}$ on the truncated Hilbert space $\mathcal{H}_M$ and is defined as follows

$$J_{RB}=(\mathcal{I}_R\otimes\mathcal{N}_{A\to B})(\Gamma_{RA})-(\mathcal{I}_R\otimes\mathcal{M}_{A\to B})(\Gamma_{RA}), \tag{4.1.68}$$

where $\Gamma_{RA}=|\Gamma\rangle\langle\Gamma|_{RA}$ is the projection onto the unnormalized maximally entangled vector on the truncated Hilbert space $\mathcal{H}_M$, i.e.,

$$|\Gamma\rangle_{RA}=\sum_{n=0}^{M}|n\rangle_R|n\rangle_A\ . \tag{4.1.69}$$

For a small value of the energy-constraint parameter E, the truncation parameter M can be chosen such that the value of $\|\mathcal{N}-\mathcal{M}\|_{\diamond E,M}$ does not change significantly by increasing M further. For example, in the context of the ideal displacement operation $\mathcal{D}^\alpha$ and its experimental approximation $\widetilde{\mathcal{D}}^{\eta,\alpha/\sqrt{1-\eta}}$, we find that for $E\ll 1$, the truncation parameter $M=6$ provides a good estimate of $\left\|\mathcal{D}^\alpha-\widetilde{\mathcal{D}}^{\eta,\frac{\alpha}{\sqrt{1-\eta}}}\right\|_{\diamond E}$. For $E\ll 1$, we define

$$d_2(\eta,E)\equiv\frac{1}{2}\left\|\mathcal{D}^\alpha-\widetilde{\mathcal{D}}^{\eta,\frac{\alpha}{\sqrt{1-\eta}}}\right\|_{\diamond E,M}\ , \tag{4.1.70}$$

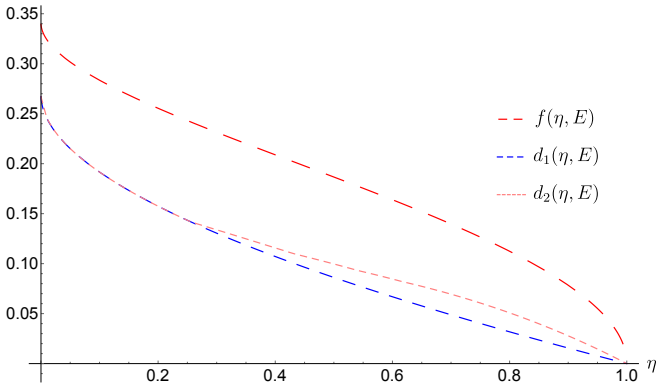

Figure 4.4: The figure depicts the lower bound $d_1(\eta, E)$ in (4.1.50), the lower bound $d_2(\eta, E)$ in (4.1.70), and the upper bound $f(\eta, E)$ in (4.1.28) for the fixed value $E = 0.06$. Here, $d_1(\eta, E)$ is the trace distance between the outputs of an ideal displacement $\mathcal{D}^{\alpha}(\psi_{RA})$ and its experimental approximation $\widetilde{\mathcal{D}}^{\eta,\alpha/\sqrt{1-\eta}}(\psi_{RA})$, when the input state ψ_{RA} is such that it optimizes the energy-constrained sine distance between $\mathcal{D}^{\alpha}$ and $\widetilde{\mathcal{D}}^{\eta,\alpha/\sqrt{1-\eta}}$ and is given by (4.1.27). Moreover, $d_2(\eta, E)$ is the energy-constrained diamond distance between $\mathcal{D}^{\alpha}$ and $\widetilde{\mathcal{D}}^{\eta,\alpha/\sqrt{1-\eta}}$ on a truncated Hilbert space with the truncation parameter $M = 6$, and $f(\eta, E)$ is the energy-constrained sine distance between $\mathcal{D}^{\alpha}$ and $\widetilde{\mathcal{D}}^{\eta,\alpha/\sqrt{1-\eta}}$. For low values of η, $d_1(\eta, E)$ is close to $d_2(\eta, E)$. The figure indicates that for a fixed value of E, high accuracy in simulating $\mathcal{D}^{\alpha}$ can be achieved only for high values of η.

for $M = 6$. From Proposition 116 it follows that

$$d_2(\eta, E) \leq \frac{1}{2} \left\| \mathcal{D}^{\alpha} - \widetilde{\mathcal{D}}^{\eta, \frac{\alpha}{\sqrt{1-\eta}}} \right\|_{\diamond E}. \tag{4.1.71}$$

Let us study in detail the case when the input states have mean energy constraint $E = 0.06$. We first calculate $d_1(\eta, E)$ by using (4.1.50) and then find $d_2(\eta, E)$, as defined in (4.1.70) by solving the corresponding SDP in (4.1.67) [164]. We then compare both $d_1(\eta, E)$ and $d_2(\eta, E)$ with the energy-constrained sine distance $f(\eta, E)$ between $\mathcal{D}^{\alpha}$ and $\widetilde{\mathcal{D}}^{\eta,\alpha/\sqrt{1-\eta}}$, as calculated in (4.1.28).

In Figure 4.4, we plot the lower bound $d_1(\eta, E)$ in (4.1.50), the lower bound $d_2(\eta, E)$ in (4.1.70), and the upper bound $f(\eta, E)$ in (4.1.28) versus η for $E = 0.06$. In particular, we find that $d_1(\eta, E)$ overlaps with $d_2(\eta, E)$ for small values of η. From numerical evaluations, we find that the value of $d_2(\eta, E)$ does not change significantly with a further increment in $M \geq 6$. These findings indicate that $d_2(\eta, E)$ is a good lower bound on the energy-

constrained diamond distance between $\mathcal{D}^{\alpha}$ and $\widetilde{\mathcal{D}}^{\eta,\alpha/\sqrt{1-\eta}}$, and furthermore, that the upper bound in Proposition 116 is loose for this case. Moreover, from Figure 4.4, it is evident that $d_1(\eta, E)$ is also a tight lower bound. Although there is a significant gap between $f(\eta, E)$ and $d_2(\eta, E)$ in Figure 4.4, the key message of our results remains the same; i.e., in order to achieve a high accuracy in simulating an ideal displacement operation $\mathcal{D}^{\alpha}$ by using the protocol from [70], the value of η should be very high and the mean energy of the input states should be very low. In summary, a good estimation of the accuracy in simulating an ideal displacement operation can be obtained from the following three methods:

1. The energy-constrained sine distance between $\mathcal{D}^{\alpha}$ and $\widetilde{\mathcal{D}}^{\eta,\alpha/\sqrt{1-\eta}}$ can be calculated from the analytical expression obtained in (4.1.28).

2. A lower bound on the energy-constrained diamond distance between $\mathcal{D}^{\alpha}$ and $\widetilde{\mathcal{D}}^{\eta,\alpha/\sqrt{1-\eta}}$ can be established by solving an SDP in (4.1.67) on a truncated Hilbert space [164] .

3. For a fixed energy range $\lfloor E \rfloor \leq E \leq \lceil E \rceil$, a lower bound on the energy-constrained diamond distance between $\mathcal{D}^{\alpha}$ and $\widetilde{\mathcal{D}}^{\eta,\alpha/\sqrt{1-\eta}}$ can be established by finding the trace distance between $\mathcal{I}_R \otimes \mathcal{D}^{\alpha}(\psi_{RA})$ and $\mathcal{I}_R \otimes \widetilde{\mathcal{D}}^{\eta,\alpha/\sqrt{1-\eta}}(\psi_{RA})$, where ψ_{RA} is given by (4.1.27). In particular, for $0 < E < 1$, an analytical expression for the trace distance is given by (4.1.50).

4.2 Approximation of a Beamsplitter

In this section, we analyze convergence of the experimental implementations of a beamsplitter transformation.

Let $\rho_{A_1A_2}$ be a two-mode input quantum state, and let $\mathcal{B}^{\eta,\phi}$ denote the beamsplitter transformation of transmissivity $\eta \in (0, 1)$ and phase $\phi \in [0, 2\pi]$ acting on mode A_1 and A_2, i.e.,

$$\mathcal{B}^{\eta,\phi}(\rho_{A_1A_2}) = U_{\text{BS}}^{\theta,\phi}(\rho_{A_1A_2})(U_{\text{BS}}^{\theta,\phi})^{\dagger}, \tag{4.2.1}$$

where $\eta = (\cos\theta)^2$.

There are at least two different ways to model the noise in implementing $\mathcal{B}^{\eta,\phi}$. A first method consists of an ideal beamsplitter preceded and followed by a tensor product of pure-loss channels with transmissivity η'. We denote the channel corresponding to the experimental implementation of the beamsplitter transformation $\mathcal{B}^{\eta,\phi}$ by $\widetilde{\mathcal{B}}^{\eta,\phi,\eta'}$, such that

$$\widetilde{\mathcal{B}}^{\eta,\phi,\eta'}(\rho_{A_1A_2}) \equiv (\mathcal{L}^{\eta'}_{A_1} \otimes \mathcal{L}^{\eta'}_{A_2}) \circ \mathcal{B}^{\eta,\phi} \circ (\mathcal{L}^{\eta'}_{A_1} \otimes \mathcal{L}^{\eta'}_{A_2})(\rho_{A_1A_2}). \tag{4.2.2}$$

This models the physical process when there is a non-zero probability of absorption of the radiation, along with reflection and transmission. We note that the beam splitter channel with transmissivity η and the channel corresponding to a tensor product of two pure-loss channels with equal transmissivity η' commute, i.e.,

$$(\mathcal{L}^{\eta'}_{A_1} \otimes \mathcal{L}^{\eta'}_{A_2}) \circ \mathcal{B}^{\eta,\phi}(\cdot) = \mathcal{B}^{\eta,\phi} \circ (\mathcal{L}^{\eta'}_{A_1} \otimes \mathcal{L}^{\eta'}_{A_2})(\cdot). \tag{4.2.3}$$

Since a concatenation of two pure-loss channels $\mathcal{L}^{\eta_1}$ and $\mathcal{L}^{\eta_2}$ is another pure-loss channel $\mathcal{L}^{\eta_1\eta_2}$ with transmissivity $\eta_1\eta_2$, we consider the following channel as an experimental approximation of the beamsplitter:

$$\widetilde{\mathcal{B}}^{\eta,\phi,\eta'}(\rho_{A_1A_2}) \equiv \mathcal{B}^{\eta,\phi} \circ (\mathcal{L}^{\eta'}_{A_1} \otimes \mathcal{L}^{\eta'}_{A_2})(\rho_{A_1A_2}), \tag{4.2.4}$$

Now let $\psi_{RA_1A_2}$ denote an arbitrary four-mode pure state, where it is understood that R is a two-mode system. From invariance of the fidelity under a unitary transformation, we find that

$$F(\mathcal{B}^{\eta,\phi}(\psi_{RA_1A_2}), \widetilde{\mathcal{B}}^{\eta,\phi,\eta'}(\psi_{RA_1A_2})) = F(\psi_{RA_1A_2}, (\mathcal{L}^{\eta'}_{A_1} \otimes \mathcal{L}^{\eta'}_{A_2})(\psi_{RA_1A_2})), \tag{4.2.5}$$

where it is implicit that the identity channel acts on the reference system R.

From arguments similar to those given in Section 4.1.1, we find that the sequence

$\{\widetilde{\mathcal{B}}^{\eta,\phi,\eta'}\}_{\eta'\in[0,1)}$ does not converge uniformly to $\mathcal{B}^{\eta,\phi}$. In particular, let $\psi_{A_1A_2} = |\delta\rangle\langle\delta|_{A_1} \otimes |0\rangle\langle 0|_{A_2}$ be a tensor product of a coherent state and a vacuum state. Then we find that

$$F(\mathcal{B}^{\eta,\phi}(\psi_{A_1A_2}), \widetilde{\mathcal{B}}^{\eta,\phi,\eta'}(\psi_{A_1A_2})) = \exp\Big[-(|\delta|^2(1-\sqrt{\eta'})^2)/2\Big] \tag{4.2.6}$$

Therefore, from arguments similar to (4.1.14) and (4.1.16), it follows that the ideal beamsplitter $\mathcal{B}^{\eta,\phi}$ and its experimental approximation $\widetilde{\mathcal{B}}^{\eta,\phi,\eta'}$ become perfectly distinguishable in the limit that the input state has unbounded energy. Hence the uniform convergence does not hold.

We now argue that the sequence converges $\{\mathcal{B}^{\eta,\phi,\eta'}\}_{\eta'\in[0,1)}$ to $\mathcal{B}^{\eta,\phi}$ in the strong sense. Let $\chi_{\rho_{A_1A_2}}(x_1,p_1,x_2,p_2)$ denote the Wigner characteristic function for the input state $\rho_{A_1A_2}$. Let $\tilde{\rho}^{\text{out}}_{A_1A_2}(\eta,\phi,\eta')$ denote the state after the action of $\widetilde{\mathcal{B}}^{\eta,\phi,\eta'}$ on $\rho_{A_1A_2}$:

$$\tilde{\rho}^{\text{out}}_{A_1A_2}(\eta,\phi,\eta') = \widetilde{\mathcal{B}}^{\eta,\phi,\eta'}(\rho_{A_1A_2})\ . \tag{4.2.7}$$

We now find the terms involved in (2.3.63) for both $\mathcal{B}^{\eta,\phi}(\rho_{A_1A_2})$ and $\rho^{\eta,\phi,\eta'}_{A_1A_2}$. The $X_{\widetilde{\mathcal{B}}^{\eta,\phi,\eta'}}$ matrix corresponding to the operation $\widetilde{\mathcal{B}}^{\eta,\phi,\eta'}$ is given by

$$X_{\widetilde{\mathcal{B}}^{\eta,\phi,\eta'}} = X_{\mathcal{B}^{\eta,\phi}} \cdot \sqrt{\eta'} I_4, \tag{4.2.8}$$

where I_4 is a four-dimensional identity matrix. Moreover, the $Y_{\widetilde{\mathcal{B}}^{\eta,\phi,\eta'}}$ matrix is given by

$$Y_{\widetilde{\mathcal{B}}^{\eta,\phi,\eta'}} = (1-\eta')I_4. \tag{4.2.9}$$

Let $r = (x_1,p_1,x_2,p_2)^{\mathrm{T}}$. Then, for each $\rho_{A_1A_2} \in \mathcal{D}(\mathcal{H}_{A_1} \otimes \mathcal{H}_{A_2})$, and for all $x_1,p_1,x_2,p_2 \in \mathbb{R}$

$$\lim_{\eta'\to 1} \chi_{\tilde{\rho}^{\text{out}}_{A_1A_2}(\eta,\phi,\eta')}(r) = \lim_{\eta'\to 1} \chi_{\rho_{A_1A_2}}(\sqrt{\eta'}\Omega^{\mathrm{T}} X^{\mathrm{T}}_{\mathcal{B}^{\eta,\phi}}\Omega r) \exp\left(-\frac{1}{4}(1-\eta')r^{\mathrm{T}} r\right) \tag{4.2.10}$$

$$= \chi_{\rho_{A_1A_2}}(\Omega^{\mathrm{T}} X^{\mathrm{T}}_{\mathcal{B}^{\eta,\phi}}\Omega r) \tag{4.2.11}$$

$$= \chi_{\mathcal{B}^{\eta,\phi}(\rho_{A_1A_2})}(r). \tag{4.2.12}$$

We have thus shown that the sequence of characteristic functions $\chi_{\tilde{\rho}^{\text{out}}_{A_1A_2}(\eta,\phi,\eta')}$ converges pointwise to $\chi_{\mathcal{B}^{\eta,\phi}(\rho_{A_1A_2})}$, which implies by [141, Lemma 8] that the sequence $\{\widetilde{\mathcal{B}}^{\eta,\phi,\eta'}\}_{\eta'\in[0,1)}$ converges to $\mathcal{B}^{\eta,\phi}$ in the strong sense.

Similar to Section 4.1.3, we investigate the dependence of convergence of the sequence of $\{\widetilde{\mathcal{B}}^{\eta,\phi,\eta'}\}_{\eta'\in[0,1)}$ to $\mathcal{B}^{\eta,\phi}$ on the experimental parameters when there is a finite energy constraint on the input states. Let $A = A_1A_2$. Consider the following chain of inequalities:

$$\frac{1}{2}\|\mathcal{B}^{\eta,\phi} - \widetilde{\mathcal{B}}^{\eta,\phi,\eta'}\|_{\diamond E} \leq \sup_{\psi_{RA}:\mathrm{Tr}(H_A\psi_A)\leq E} C(\psi_{RA}, (\mathcal{L}^{\eta'}_{A_1} \otimes \mathcal{L}^{\eta'}_{A_2})(\psi_{RA})) \tag{4.2.13}$$

$$= f(\eta', E), \tag{4.2.14}$$

where $H_A = H_{A_1} \otimes I_{A_2} + I_{A_1} \otimes H_{A_2}$ and $f(\eta', E)$ is given by (4.1.28). The first inequality follows from (2.4.12). The last inequality follows from the recent result of [186], which holds for a tensor product of loss channels with the same transmissivity. Therefore, from the analysis in Section 4.1.3, it follows that the accuracy in implementing $\mathcal{B}^{\eta,\phi}$ using $\mathcal{B}^{\eta,\phi,\eta'}$ is high only for high values of the loss parameter η' and low values of the energy constraint E.

A second experimental approximation of an ideal beamsplitter is a phenomenological model that accounts for the imprecision in implementing $\mathcal{B}^{\theta,\phi}$ with an exact value of the parameters θ and ϕ, as defined in (2.3.52). For the analysis that follows, we fix $\phi = 0$, which is typically considered in experiments. We denote the ideal beamsplitter for $\phi = 0$ by $\mathcal{B}^{\theta}$. We note that a similar analysis follows for $\phi = \pi/2$.

The channel corresponding to an experimental approximation of $\mathcal{B}^{\theta}$ is given by

$$\widetilde{\mathcal{B}}^{\theta,\sigma} \equiv \int_0^{2\pi} d\theta' \; p(\theta', \theta, \sigma, 0, 2\pi)\mathcal{B}^{\theta'}, \tag{4.2.15}$$

where $p(\theta', \theta, \sigma, a, b)$ is a truncated normal distribution with location parameter θ, scale parameter σ, truncation range in between a and b, and is given by

$$p(\theta', \theta, \sigma, a, b) = \frac{\phi((\theta' - \theta)/\sigma)}{\sigma[\Phi((b-\theta)/\sigma) - \Phi((a-\theta)/\sigma)]}, \tag{4.2.16}$$

where

$$\phi(x) = \frac{1}{\sqrt{2\pi}} \exp\Big(-x^2/2\Big), \tag{4.2.17}$$

$$\Phi(x) = \frac{1}{2}(1 + \operatorname{erf}(x/\sqrt{2})), \tag{4.2.18}$$

and $\operatorname{erf}(x)$ is the error function.

Now let $\psi_{A_1A_2} = |\alpha\rangle\langle\alpha|_{A_1} \otimes |0\rangle\langle 0|_{A_2}$ be an input state, where $|\alpha\rangle$ is a coherent state. From (4.2.15) it follows that

$$F(\mathcal{B}^{\theta}(\psi_{A_1A_2}), \widetilde{\mathcal{B}}^{\theta,\sigma}(\psi_{A_1A_2})) = \int_0^{2\pi} d\theta' \; p(\theta', \theta, \sigma, 0, 2\pi) F(\mathcal{B}^{\theta}(\psi_{A_1A_2}), \mathcal{B}^{\theta'}(\psi_{A_1A_2})). \tag{4.2.19}$$

Now consider that

$$F(\mathcal{B}^{\theta}(\psi_{A_1A_2}), \mathcal{B}^{\theta'}(\psi_{A_1A_2})) = F(\psi_{A_1A_2}, \mathcal{B}^{(-\theta)} \circ \mathcal{B}^{\theta'}(\psi_{A_1A_2})) \tag{4.2.20}$$

$$= \exp\Big[-2|\alpha|^2(\sin(\theta' - \theta))^2\Big], \tag{4.2.21}$$

which converges to zero as $|\alpha|^2 \to \infty$. Then from (4.2.19) and by an application of the dominated convergence theorem, it follows that the sequence $\{\widetilde{\mathcal{B}}^{\theta,\sigma}\}_{\sigma\in[0,\infty)}$ does not converge uniformly to the ideal beamsplitter $\mathcal{B}^{\theta}$.

We now show that convergence occurs in the strong sense. Let $\psi_{RA_1A_2}$ denote the input state. Then the following holds:

$$F(\mathcal{B}^\theta(\psi_{RA_1A_2}), \widetilde{\mathcal{B}}^{\theta,\sigma}(\psi_{RA_1A_2})) = \int_0^{2\pi} d\theta' p(\theta', \theta, \sigma, 0, 2\pi) F(\mathcal{B}^\theta(\psi_{RA_1A_2}), \mathcal{B}^{\theta'}(\psi_{RA_1A_2})) \ . \tag{4.2.22}$$

Since $\lim_{\sigma\to 0} p(\theta', \theta, \sigma) = \delta(\theta - \theta')$, it follows that

$$\lim_{\sigma\to 0} F(\mathcal{B}^\theta(\psi_{RA_1A_2}), \widetilde{\mathcal{B}}^{\theta,\sigma}(\psi_{RA_1A_2})) = 1, \tag{4.2.23}$$

which implies that the sequence $\{\widetilde{\mathcal{B}}^{\theta,\sigma}\}_{\sigma\in[0,\infty)}$ converges strongly to $\mathcal{B}^\theta$.

We now investigate convergence of the sequence $\{\widetilde{\mathcal{B}}^{\theta,\sigma}\}_{\sigma\in[0,\infty)}$ to $\mathcal{B}^\theta$ in terms of the experimental parameters when there is a finite energy constraint on the input states. Consider the following chain of inequalities:

$$\begin{aligned}
\frac{1}{2}\|\mathcal{B}^\theta - \widetilde{\mathcal{B}}^{\theta,\sigma}\|_{\diamond E} &\leq \frac{1}{2}\int_0^{2\pi} d\theta' \ p(\theta', \theta, \sigma, 0, 2\pi)\|\mathcal{B}^\theta - \mathcal{B}^{\theta'}\|_{\diamond E} && (4.2.24)\\
&= \frac{1}{2}\int_0^{2\pi} d\theta' \ p(\theta', \theta, \sigma, 0, 2\pi)\|\mathcal{I} - \mathcal{B}^{\theta'-\theta}\|_{\diamond E} && (4.2.25)\\
&\leq \int_0^{2\pi} d\theta' \ p(\theta', \theta, \sigma, 0, 2\pi) 2\sqrt{E|\theta' - \theta|} \ . && (4.2.26)
\end{aligned}$$

The first inequality follows from convexity of the trace distance. The first equality follows the unitary invariance of the trace distance. The last inequality follows from [194, Proposition 3.2].

We denote the upper bound on the energy-constrained diamond distance between $\mathcal{B}^\theta$ and $\widetilde{\mathcal{B}}^{\theta,\sigma}$, obtained in (4.2.26) by $g(\theta, \sigma, E)$:

$$g(\theta, \sigma, E) = \int_0^{2\pi} d\theta' p(\theta', \theta, \sigma, 0, 2\pi) 2\sqrt{E|\theta' - \theta|}. \tag{4.2.27}$$

In Figure 4.5, we plot $g(\theta, \sigma, E)$ versus σ for certain values of the energy constraint E and for $\theta = \pi/4$, which corresponds to the simulation of a balanced beamsplitter. In

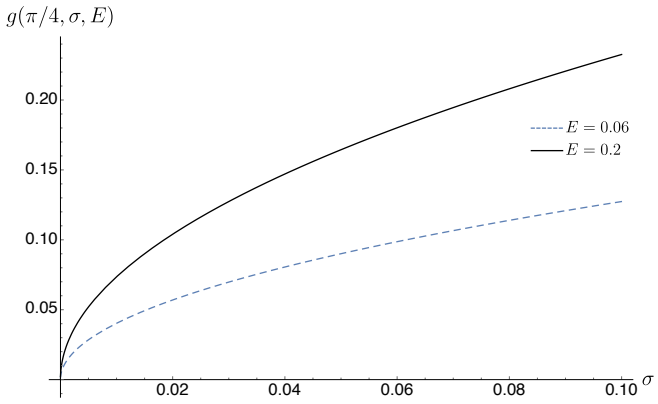

Figure 4.5: The figure depicts the upper bound $g(\theta, \sigma, E)$ in (4.2.27) for a fixed value of the beamsplitter parameter $\theta = \pi/4$ and for two different values of the energy-constraint parameter $E = 0.06$ and $E = 0.2$. Here, $g(\theta, \sigma, E)$ is an upper bound on the energy-constrained diamond distance between an ideal beamsplitter and its experimental approximation in (4.2.15). The figure indicates that for a fixed value of σ in (4.2.16), high accuracy in simulating $\mathcal{B}^\theta$ can be achieved only for low values of the energy-constraint parameter E.

particular, we find that for all values of E, the experimental approximation $\widetilde{\mathcal{B}}^{\theta,\sigma}$ simulates the ideal beamsplitter $\mathcal{B}^\theta$ with a high accuracy for $\sigma \approx 0$. Moreover, for a fixed value of σ, the simulation of $\mathcal{B}^\theta$ is more accurate for low values of the energy constraint on input states.

4.3 Approximation of a Phase Rotation

In this section, we analyze convergence of the experimental implementation of a phase rotation. In general, the unitary operator corresponding to the phase rotation is given by

$$U_{\mathrm{PR}}^{\phi} = \exp(i\hat{n}\phi), \tag{4.3.1}$$

where $\hat{n}$ denotes the number operator.

Similar to Section 4.2, there are at least two ways to model the noise in implementing the unitary channel $\mathcal{U}_{\mathrm{PR}}^{\phi}(\cdot) \equiv U_{\mathrm{PR}}^{\phi}(\cdot)(U_{\mathrm{PR}}^{\phi})^\dagger$. A first model consists of sending the input state through a pure-loss channel, followed by the ideal phase rotation. This models the case when some photons are lost in the medium used to implement the phase rotation. We denote the channel corresponding to such an approximation of the ideal phase rotation by

$\widetilde{\mathcal{U}}_{\mathrm{PR}}^{\phi,\eta}$, such that

$$\widetilde{\mathcal{U}}_{\mathrm{PR}}^{\phi,\eta}(\rho) \equiv (\mathcal{U}_{\mathrm{PR}}^{\phi} \circ \mathcal{L}^{\eta})(\rho) \ . \tag{4.3.2}$$

Now let ψ_{RA} denote an arbitrary two-mode pure state. Then from unitary invariance of fidelity, we find that

$$F(\mathcal{U}_{\mathrm{PR}}^{\phi}(\psi_{RA}), \widetilde{\mathcal{U}}_{\mathrm{PR}}^{\phi,\eta}(\psi_{RA})) = F(\psi_{RA}, \mathcal{L}_{A}^{\eta}(\psi_{RA})), \tag{4.3.3}$$

where it is implicit that the identity channel acts on the reference system R. Therefore, analyzing the convergence of the sequence $\{\widetilde{\mathcal{U}}_{\mathrm{PR}}^{\phi,\eta}\}_{\eta\in[0,1)}$ to $\mathcal{U}_{\mathrm{PR}}^{\phi}$ is equivalent to analyzing the convergence of a sequence of pure-loss channels to an identity channel. We note that the same result holds for an ideal displacement unitary and its experimental approximation, as shown in (4.1.12). Therefore, from the results in Section 4.1, it follows directly that the sequence $\{\widetilde{\mathcal{U}}_{\mathrm{PR}}^{\phi,\eta}\}_{\eta\in[0,1)}$ does not converge uniformly to $\mathcal{U}_{\mathrm{PR}}^{\phi}$. Rather the convergence holds in the strong sense. Moreover, the dependence of an estimate of the energy-constrained diamond distance between $\widetilde{\mathcal{U}}_{\mathrm{PR}}^{\phi,\eta}$ and $\mathcal{U}_{\mathrm{PR}}^{\phi}$ is given by (4.1.25). From the analysis in Section 4.1.3, we conclude that only for low values of the energy constraint E on input states and high values of η, i.e., low values of the loss, high accuracy in simulating $\mathcal{U}_{\mathrm{PR}}^{\phi}$ can be achieved.

We now consider a phenomenological model to approximate the ideal phase rotation $\mathcal{U}_{\mathrm{PR}}^{\phi}$. In particular, instead of $\mathcal{U}_{\mathrm{PR}}^{\phi}$, the following channel is applied:

$$\widetilde{\mathcal{U}}^{\phi,\sigma} \equiv \int_{0}^{2\pi} d\phi' \ p(\phi', \phi, \sigma, 0, 2\pi)\mathcal{U}^{\phi'}, \tag{4.3.4}$$

where $p(\phi', \phi, \sigma, 0, 2\pi)$ is a truncated normal distribution with location parameter ϕ and scale parameter σ, as defined in (4.2.16).

Let $|\alpha\rangle$ be an input coherent state. Then from unitary invariance of fidelity it follows

that

$$F(\mathcal{U}^{\phi}(|\alpha\rangle\langle\alpha|),\mathcal{U}^{\phi'}(|\alpha\rangle\langle\alpha|)) = F(|\alpha\rangle\langle\alpha|,\mathcal{U}^{\phi'-\phi}(|\alpha\rangle\langle\alpha|)) \tag{4.3.5}$$

$$= \exp\Big(-2|\alpha|^2(\sin(\phi'-\phi))^2\Big), \tag{4.3.6}$$

which converges to zero as $|\alpha|^2 \to \infty$. Therefore, by an application of the dominated convergence theorem, it follows that the sequence $\{\widetilde{\mathcal{U}}^{\phi,\sigma}\}_{\sigma\in[0,\infty)}$ does not converge uniformly to the ideal phase rotation $\mathcal{U}^{\phi}$.

The strong convergence of $\{\widetilde{\mathcal{U}}^{\phi,\sigma}\}_{\sigma\in[0,\infty)}$ to $\mathcal{U}^{\phi}$ follows from arguments similar those given in (4.2.22) and (4.2.23).

We now provide an estimate of the energy-constrained diamond distance between $\widetilde{\mathcal{U}}^{\phi,\sigma}$ and $\mathcal{U}^{\phi}$. Consider the following chain of inequalities:

$$\frac{1}{2}\|\mathcal{U}^{\phi}-\widetilde{\mathcal{U}}^{\phi,\sigma}\|_{\diamond E} \leq \frac{1}{2}\int_0^{2\pi} d\phi'\ p(\phi',\phi,\sigma,0,2\pi)\|\mathcal{I}-\mathcal{U}^{\phi'-\phi}\|_{\diamond E} \tag{4.3.7}$$

$$\leq \int_0^{2\pi} d\phi'\ p(\phi',\phi,\sigma,0,2\pi)2\sqrt{E|\phi'-\phi|}\ . \tag{4.3.8}$$

The first inequality follows from convexity and unitary invariance of the trace distance. The last inequality follows from [194, Proposition 3.2]. Since the upper bound in (4.3.8) is exactly same as the upper bound in (4.2.26), we conclude that only for low values of both the energy constraint E and the scale parameter σ in (4.2.16), high accuracy in simulating $\mathcal{U}^{\phi}_{\mathrm{PR}}$ using $\widetilde{\mathcal{U}}^{\phi,\sigma}$ can be achieved.

4.4 Approximation of a Single-Mode Squeezer

In this section, we analyze the convergence of the experimental implementation of a measurement-induced single-mode squeezer from [71] to the ideal single-mode squeezer. We follow the definition of an ideal single-mode squeezer as in (2.3.56) for $\xi = r$.

Let ρ_A be an input quantum state, and let $\hat{x}_A$ and $\hat{p}_A$ denote the position- and momentum-quadrature operators for mode A, respectively. As described in Figure 4.6,

the simulation from [71] of $\mathcal{S}^r(\rho_A) = S(r)\rho_A S(-r)$, such that $e^{-r} = \sqrt{\eta}$, is given by the following transformation of the mode operators:

$$\hat{x}_A \to \sqrt{\eta}\hat{x}_A + \sqrt{1-\eta}\; e^{-r_E}\hat{x}_E^0 \;, \tag{4.4.1}$$

$$\hat{p}_A \to \frac{1}{\sqrt{\eta}}\hat{p}_A \;, \tag{4.4.2}$$

where $\hat{x}_E^0$ is the position-quadrature operator corresponding to the vacuum state and r_E is the squeezing parameter corresponding to the squeezed vacuum state. We denote the channel corresponding to the experimental implementation of an ideal single-mode squeezer by $\widetilde{\mathcal{S}}^{\eta,r_E} = \widetilde{\mathcal{S}}^{e^{-2r},r_E}$. Furthermore, by applying the inverse $\mathcal{S}^{-r}$ of the ideal single-mode squeezer $\mathcal{S}^r$ on the output of $\widetilde{\mathcal{S}}^{e^{-2r},r_E}$, we arrive at the following transformation:

$$\hat{x}_{\text{out}} = \hat{x}_A + \frac{\sqrt{1-\eta}}{\sqrt{\eta}}\; e^{-r_E}\hat{x}_E^0 \;, \tag{4.4.3}$$

$$\hat{p}_{\text{out}} = \hat{p}_A \;. \tag{4.4.4}$$

We denote the channel induced by the transformation in (4.4.3)–(4.4.4) by Ξ^{η,r_E}. Since all the elements involved in the transformation are Gaussian, the channel Ξ^{η,r_E} can be described by its action on the mean and covariance matrix of the input state ρ_A. In particular, there are two 2×2 real matrices, the scaling matrix $X_{\Xi^{\eta,r_E}}$ and the noise matrix $Y_{\Xi^{\eta,r_E}}$, which characterize the Gaussian channel Ξ^{η,r_E} completely (background on Gaussian channels can be found in the appendices). It is easy to check that the action of Ξ^{η,r_E} does not change the mean vector of ρ_A. Therefore, the scaling matrix $X_{\Xi^{\eta,r_E}} = I_2$, where I_2 is a two-dimensional identity matrix. Moreover, the expectation value of the anticommutator $\{\hat{x}_A, \hat{x}_E^0\}$ is equal to zero, which further implies that the noise matrix $Y_{\Xi^{\eta,r_E}}$ has the following form: $Y_{\Xi^{\eta,r_E}} = \text{diag}\left((1-\eta)e^{-2r_E}/\eta, 0\right)$.

Let us study the channel Ξ^{η,r_E} in further detail. As observed in [195], all single-mode bosonic Gaussian channels can be categorized into six different canonical forms. In

particular, the canonical form Φ_{B_1} has the following $X_{\Phi_{B_1}}$ and $Y_{\Phi_{B_1}}$ matrices [195]:

$$X_{\Phi_{B_1}} = I_2, \qquad Y_{\Phi_{B_1}} = \text{diag}(0, 1). \tag{4.4.5}$$

We now show that the channel Ξ^{η,r_E} is unitarily equivalent to the canonical form Φ_{B_1} [195]. Let ρ be a quantum state with the covariance matrix V_ρ. Then the symplectic matrix $\sigma_x = \begin{bmatrix} 0 & 1 \\ 1 & 0 \end{bmatrix}$ transforms the covariance matrix V_ρ as follows: $V'_\rho = \sigma_x V_\rho \sigma_x$. We then apply the symplectic transformation corresponding to the symplectic matrix $\mathcal{K} = \text{diag}(\varsigma, 1/\varsigma)$, where $\varsigma = \sqrt{(1-\eta)}e^{-r_E}/\sqrt{\eta}$, on the covariance matrix V'_ρ. The transformed covariance matrix is given by $V''_\rho = \mathcal{K} V'_\rho \mathcal{K}$. We now apply the canonical form Φ_{B_1} on the transformed state, and get the following transformation of the covariance matrix V''_ρ: $V'''_\rho = V''_\rho + Y_{\Phi_{B_1}}$. We then apply the symplectic transformation corresponding to the symplectic matrix $\mathcal{K}^{-1}$ followed by σ_x on V'''_ρ, and get the following final covariance matrix V_ρ^{final}:

$$\begin{aligned} V_\rho^{\text{final}} &= \sigma_x \mathcal{K}^{-1} V''_\rho \mathcal{K}^{-1} \sigma_x + \sigma_x \mathcal{K}^{-1} Y_{\Phi_{B_1}} \mathcal{K}^{-1} \sigma_x & (4.4.6) \\ &= V_\rho + \text{diag}(\varsigma^2, 0) & (4.4.7) \\ &= V_\rho + \text{diag}\left((1-\eta)e^{-2r_E}/\eta, 0\right) \ , & (4.4.8) \end{aligned}$$

which implies that the overall transformation is the same as the action of the channel Ξ^{η,r_E} on the state ρ. Therefore, we have shown that the Gaussian channel Ξ^{η,r_E} is unitarily equivalent by Gaussian input and output unitaries to the canonical form Φ_{B_1}. This gives a physical interpretation to channels in the class Φ_{B_1}, in terms of the measurement-induced squeezing approximation from [71].

4.4.1 Lack of uniform convergence

We now prove that the sequence $\{\widetilde{\mathcal{S}}^{e^{-2r},r_E}\}_{r_E\in[0,\infty)}$ does not converge uniformly to the ideal single-mode squeezer $\mathcal{S}^r$. Let $|z\rangle$ be a squeezed-vacuum input state with the covariance matrix $V_{|z\rangle\langle z|} = \text{diag}(z, 1/z)$ and mean vector $\mu_{|z\rangle\langle z|} = (0,0)^{\text{T}}$, where $z \in [0, \infty)$.

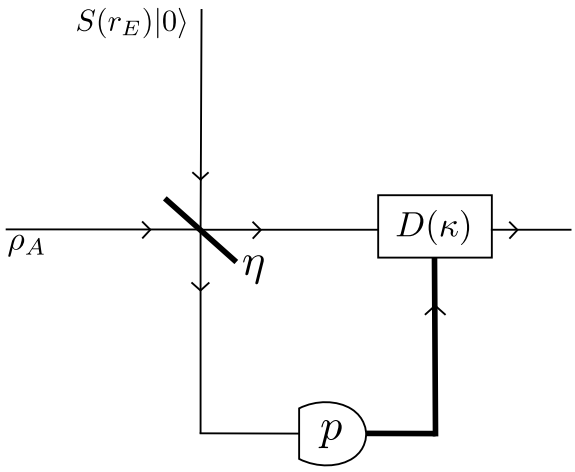

Figure 4.6: The figure plots an experimental approximation of the ideal single-mode squeezing unitary $S(r)$ on the input state ρ_A, such that $e^{-r} = \sqrt{\eta}$. $S(r_E)\left|0\right\rangle_E$ represents a squeezed vacuum state in the mode E. The experimental approximation of an ideal single-mode squeezing operation corresponds to the following transformations: sending ρ_A and $S(r_E)\left|0\right\rangle_E$ through a beamsplitter with transmissivity η followed by a measurement of the momentum quadrature in mode E. Then a feed forward operation corresponding to the measurement outcome p followed by a displacement operator $D(\kappa)$ on mode A [71], where $\kappa = -i\sqrt{(1-\eta)/(2\eta)}p$.

Then under the action of Ξ^{η,r_E}, the covariance matrix $V_{|z\rangle\langle z|}$ transforms as follows:

$$V^{\text{out}}_{|z\rangle\langle z|} = \text{diag}\Big(z + (1-\eta)e^{-2r_E}/\eta, 0\Big). \tag{4.4.9}$$

We can use these expressions in the Uhlmann fidelity formula for single-mode Gaussian states [196, 197]. By using the unitary invariance of fidelity, we find that

$$F(\mathcal{S}^r(|z\rangle\langle z|), \widetilde{\mathcal{S}}^{e^{-2r},r_E}(|z\rangle\langle z|)) = F(|z\rangle\langle z|, \Xi^{\eta,r_E}(|z\rangle\langle z|)). \tag{4.4.10}$$

Moreover, we find that [164]

$$F(|z\rangle\langle z|, \Xi^{\eta,r_E}(|z\rangle\langle z|)) = \sqrt{\frac{2z}{2z + (e^{2r}-1)e^{-2r_E}}}\ . \tag{4.4.11}$$

Therefore, for fixed r_E

$$\lim_{z\to 0} F(\mathcal{S}^r(|z\rangle\langle z|), \widetilde{\mathcal{S}}^{e^{-2r},r_E}(|z\rangle\langle z|)) = 0 \ , \tag{4.4.12}$$

which implies that the sequence $\{\widetilde{\mathcal{S}}^{e^{-2r},r_E}\}_{r_E\in[0,\infty)}$ does not converge uniformly to the ideal single-mode squeezer transformation $\mathcal{S}^r$.

The reasoning behind (4.4.12) can be intuitively explained as follows: the channel Ξ^{η,r_E} adds noise to the $\hat{x}$ quadrature only. Therefore, it can be discriminated from an identity channel by using an input state that has vanishing noise in the $\hat{x}$ quadrature operator. Since an infinitely squeezed vacuum state (infinitely squeezed in the position quadrature) satisfies such a condition, then (4.4.12) follows.

4.4.2 Strong convergence

We now argue that the sequence $\{\widetilde{\mathcal{S}}^{e^{-2r},r_E}\}_{r_E\in[0,\infty)}$ converges to $\mathcal{S}^r$ in the strong sense. Let $\chi_{\rho_A}(x,p)$ denote the Wigner characteristic function of the input state ρ_A. Let $\tilde{\rho}_A^{\text{out}}$ denote the state after the action of $\widetilde{\mathcal{S}}^{e^{-2r},r_E}$ on ρ_A: $\tilde{\rho}_A^{\text{out}} = \widetilde{\mathcal{S}}^{e^{-2r},r_E}(\rho_A)$. Then the characteristic function of $\tilde{\rho}_A^{\text{out}}$ is given by

$$\chi_{\tilde{\rho}_A^{\text{out}}}(x,p) = \chi_{\rho_A}(e^r x, e^{-r}p)e^{-\frac{1}{4}(e^{2r}-1)p^2 e^{-2r_E}} \ . \tag{4.4.13}$$

Moreover, the characteristic function of $\mathcal{S}^r(\rho_A)$ is given by

$$\chi_{\mathcal{S}^r(\rho_A)}(x,p) = \chi_{\rho}(e^r x, e^{-r}p) \ . \tag{4.4.14}$$

Therefore, for each $\rho_A \in \mathcal{D}(\mathcal{H}_A)$, and for all $x, p \in \mathbb{R}$

$$\lim_{r_E\to\infty} \chi_{\tilde{\rho}_A^{\text{out}}}(x,p) = \chi_{\mathcal{S}^r(\rho_A)}(x,p) \ . \tag{4.4.15}$$

Therefore, we have shown that the sequence of characteristic functions $\chi_{\tilde{\rho}_A^{\text{out}}}(x,p)$ converges pointwise to $\chi_{\mathcal{S}^r(\rho_A)}(x,p)$, which implies that the sequence $\{\widetilde{\mathcal{S}}^{e^{-2r},r_E}\}_{r_E\in[0,\infty)}$ converges strongly to $\mathcal{S}^r$ [141, Lemma 8].

As described in Figure 4.6, the simulation of an ideal single-mode unitary consists of an ideal displacement. We now briefly discuss the case when the displacement operator involved in the simulation of $\mathcal{S}^r$ is not ideal. By using the counterexample from before, we find that convergence of the simulation of a single-mode squeezing operation to an ideal single-mode squeezing operation is not uniform. From (4.1.23), (4.4.15), and [117, Proposition 2], it follows that convergence holds in the strong sense.

Furthermore, the strong convergence of the sequence $\{\widetilde{\mathcal{S}}^{e^{-2r},r_E}\}_{r_E\in[0,\infty)}$ to $\mathcal{S}^r$ implies that the experimental approximations of an ideal single-mode squeezer, as described in Figure 4.6, simulate the desired unitary operation uniformly on the set density operators whose marginals on the channel input have bounded energy [137]. However, as discussed previously, from an experimental perspective, it is important to know how this convergence depends on experimental parameters. We now consider experimentally relevant input Gaussian states with energy constraints, such as single-mode squeezed states, coherent states, and two-mode squeezed vacuum states. For any fixed finite value of the energy constraint, we find that, among these Gaussian states, inputting a two-mode squeezed vacuum state provides the largest value of the sine distance between the ideal single-mode squeezer and its experimental approximation.

4.4.3 Estimates of the energy-constrained diamond norm

Let us study in detail the case when the input state is the two-mode squeezed vacuum state with parameter N, as defined in (2.3.34). The fidelity between $\mathcal{S}^r(\psi_{\text{TMS}}(N))$ and $\widetilde{\mathcal{S}}^{e^{-2r},r_E}(\psi_{\text{TMS}}(N))$ is given by [164]

$$F(\mathcal{S}^r(\psi_{\text{TMS}}(N)),\widetilde{\mathcal{S}}^{e^{-2r},r_E}(\psi_{\text{TMS}}(N))) = \frac{1}{\sqrt{1+(N+1/2)(e^{2r}-1)e^{-2r_E}}}\,. \tag{4.4.16}$$

Next, we perform numerical evaluations to see how close the experimental approximation $\widetilde{\mathcal{S}}^{e^{-2r},r_E}$ is to the ideal squeezing operation $\mathcal{S}^r$ for a fixed input quantum state $\psi_{\text{TMS}}(N)$. Fix the squeezing parameter $r = 0.46$, which corresponds to the squeezing strength 4 dB. We use the relation $10\log_{10}(\exp(2r)) \approx 8.686r$ to convert the squeezing parameter r to units of dB. Let $g(r_E, N)$ denote the sine distance between $\mathcal{S}^r(\psi_{\text{TMS}}(N))$ and $\widetilde{\mathcal{S}}^{e^{-2r},r_E}(\psi_{\text{TMS}}(N))$:

$$g(r_E, N) = \sqrt{1 - \frac{1}{\sqrt{1 + (N + 1/2)(e^{0.92} - 1)e^{-2r_E}}}}\,, \tag{4.4.17}$$

where we used (4.4.16).

In Figure 4.7, we plot $g(r_E, N)$ in (4.4.17) versus the offline squeezing strength r_E for certain values of the input mean photon number N. In particular, we find that the simulation of $\mathcal{S}^r$ is more accurate for low values of the energy constraint on the input states. The figure indicates that an offline squeezing strength of 15 dB, which is what is currently experimentally achievable [198], is not sufficient to simulate an ideal squeezing operation with squeezing strength 4 dB, with a high accuracy, by using the measurement-induced protocol from [71].

We further investigate the strength of the offline squeezing required to simulate the ideal squeezing operator with high accuracy. In Figure 4.8, we plot Figure 4.7 for high values of the squeezing parameter r_E. The figure indicates that for the low input mean photon number $N \approx 0.06$, approximately 26 dB offline squeezing strength is required to achieve a reasonable accuracy ($\approx 97\%$).

4.5 Approximation of a SUM Gate

In this section, we analyze the convergence of experimental approximations of a measurement-induced SUM gate from [71] to the ideal SUM gate. We follow the definition of an ideal SUM gate as in (2.3.58).

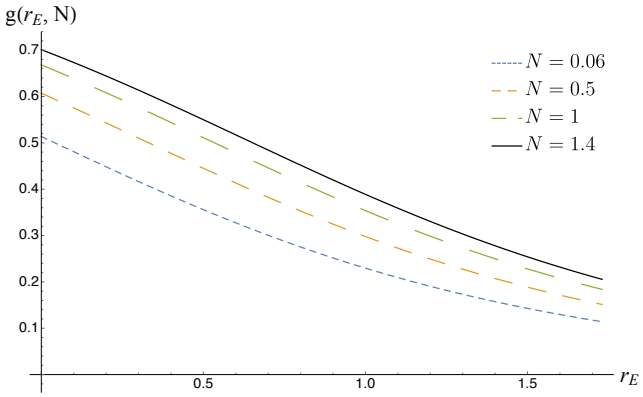

Figure 4.7: The figure plots the sine distance $g(r_E, N)$ in (4.4.17) between an ideal single-mode squeezer $\mathcal{S}^r$ with 4 dB squeezing strength and its experimental approximation $\widetilde{S}^{e^{-2r},r_E}$ when the input state is the two-mode squeezed vacuum state with parameter N, as defined in (2.3.34). In the figure, we select certain values of the mean-photon number N of the channel input, with the choices indicated next to the figure. For a fixed value of r_E, the simulation of $\mathcal{S}^r$ is more accurate for low values of the energy constraint on input states. The figure indicates that an offline squeezing strength of 15 dB, which is what is currently experimentally achievable [198], is not sufficient to simulate an ideal squeezing operation with squeezing strength 4 dB, with a high accuracy, by using the protocol from [71].

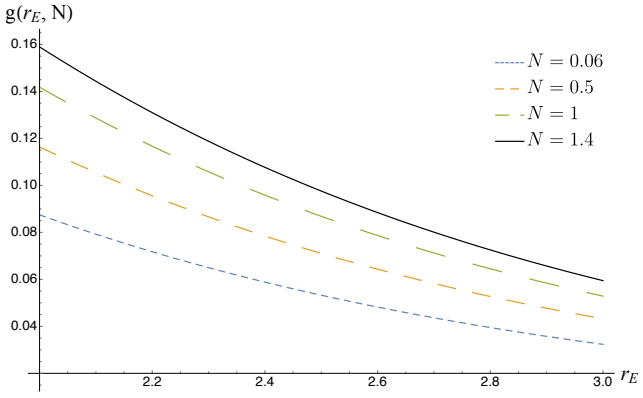

Figure 4.8: The figure plots $g(r_E, N)$ in (4.4.17) for high values of the offline squeezing parameter r_E. The figure indicates that only for high values of the offline squeezing parameter r_E and low values of N, high accuracy in simulating $\mathcal{S}^r$ with 4 dB squeezing strength can be achieved.

Let ρ_{12}^{in} denote a two-mode input quantum state. Then the action of the ideal SUM^G gate on the mode operators $\hat{x}_1$, $\hat{x}_2$, $\hat{p}_1$, and $\hat{p}_2$ of ρ_{12}^{in} is given by

$$\hat{x}_1^{\text{in}} \to \hat{x}_1^{\text{in}} \ , \tag{4.5.1}$$

$$\hat{p}_1^{\text{in}} \to \hat{p}_1^{\text{in}} - G\hat{p}_2^{\text{in}} \ , \tag{4.5.2}$$

$$\hat{x}_2^{\text{in}} \to \hat{x}_2^{\text{in}} + G\hat{x}_1^{\text{in}} \ , \tag{4.5.3}$$

$$\hat{p}_2^{\text{in}} \to \hat{p}_2^{\text{in}} \ . \tag{4.5.4}$$

On the other hand, as described in Figure 4.9, the simulation of $\text{SUM}^G(\rho_{12}^{\text{in}})$ from [71] is given by the following transformation of the mode operators $\hat{x}_1$, $\hat{x}_2$, $\hat{p}_1$, and $\hat{p}_2$ of ρ_{12}^{in}:

$$\hat{x}_1^{\text{in}} \to \hat{x}_1^{\text{in}} - \sqrt{\frac{1-R}{1+R}} e^{-r_A} \hat{x}_A^0 \ , \tag{4.5.5}$$

$$\hat{p}_1^{\text{in}} \to \hat{p}_1^{\text{in}} - G\hat{p}_2^{\text{in}} + \sqrt{\frac{R(1-R)}{1+R}} e^{-r_B} \hat{p}_B^0 \ , \tag{4.5.6}$$

$$\hat{x}_2^{\text{in}} \to \hat{x}_2^{\text{in}} + G\hat{x}_1^{\text{in}} + \sqrt{\frac{R(1-R)}{1+R}} e^{-r_A} \hat{x}_A^0 \ , \tag{4.5.7}$$

$$\hat{p}_2^{\text{in}} \to \hat{p}_2^{\text{in}} + \sqrt{\frac{1-R}{1+R}} e^{-r_B} \hat{p}_B^0 \ , \tag{4.5.8}$$

where $G = 1/\sqrt{R} - \sqrt{R}$, r_A and r_B denote the squeezing parameter corresponding to the modes A and B, respectively, and $0 < R \leq 1$. We denote the channel corresponding to the experimental implementation of an ideal SUM^G by $\widetilde{\text{SUM}}^{r_A, r_B, R}$. Furthermore, by applying the inverse of SUM^G on the output of $\widetilde{\text{SUM}}^{r_A, r_B, R}$, we get the following transformation of

the mode operators:

$$\hat{x}_1^{\text{out}} = \hat{x}_1^{\text{in}} - \sqrt{\frac{1-R}{1+R}} e^{-r_A} \hat{x}_A^0 \ , \tag{4.5.9}$$

$$\hat{p}_1^{\text{out}} = \hat{p}_1^{\text{in}} + \sqrt{\frac{1-R}{R(1+R)}} e^{-r_B} \hat{p}_B^0 \ , \tag{4.5.10}$$

$$\hat{x}_2^{\text{out}} = \hat{x}_2^{\text{in}} + \sqrt{\frac{1-R}{R(1+R)}} e^{-r_A} \hat{x}_A^0 \ , \tag{4.5.11}$$

$$\hat{p}_2^{\text{out}} = \hat{p}_2^{\text{in}} + \sqrt{\frac{1-R}{1+R}} e^{-r_B} \hat{p}_B^0 \ . \tag{4.5.12}$$

We denote the channel induced by this overall transformation by $\Lambda^{r_A,r_B,R}$. Since all the elements involved in the transformation are Gaussian, the channel $\Lambda^{r_A,r_B,R}$ can be described by its action on the mean vector and covariance matrix of the input state ρ_{12}^{in}. We now find two 4×4 real matrices $X_{\Lambda^{r_A,r_B,R}}$ and $Y_{\Lambda^{r_A,r_B,R}}$, which characterize the Gaussian channel $\Lambda^{r_A,r_B,R}$ completely (background on Gaussian channels can be found in the appendices). From the aforementioned equations, it is clear that the mean vector of ρ_{12}^{in} is invariant under the action of the channel $\Lambda^{r_A,r_B,R}$. Therefore, the scaling matrix $X_{\Lambda^{r_A,r_B,R}} = I_4$, where I_4 is a four-dimensional identity matrix. Moreover, the noise matrix $Y_{\Lambda^{r_A,r_B,R}}$ has the following form:

$$Y_{\Lambda^{r_A,r_B,R}} = \begin{bmatrix} \alpha(r_A) & 0 & -\frac{\alpha(r_A)}{\sqrt{R}} & 0 \\ 0 & \frac{\beta(r_B)}{R} & 0 & \frac{\beta(r_B)}{\sqrt{R}} \\ -\frac{\alpha(r_A)}{\sqrt{R}} & 0 & \frac{\alpha(r_A)}{R} & 0 \\ 0 & \frac{\beta(r_B)}{\sqrt{R}} & 0 & \beta(r_B) \end{bmatrix} , \tag{4.5.13}$$

where

$$\alpha(r_A) = [(1-R)e^{-2r_A}]/(1+R), \tag{4.5.14}$$

$$\beta(r_B) = [(1-R)e^{-2r_B}]/(1+R). \tag{4.5.15}$$

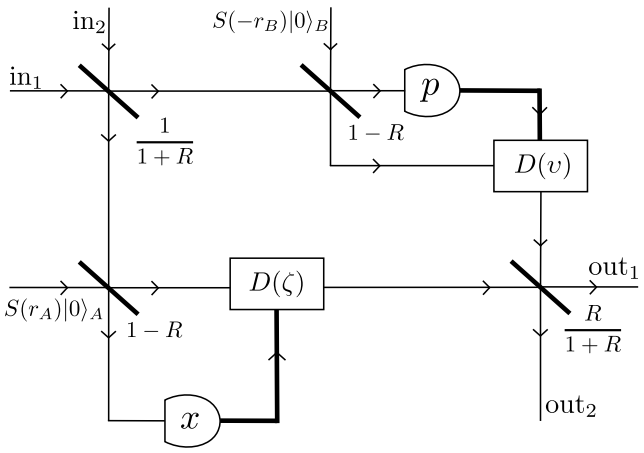

Figure 4.9: The figure plots an experimental approximation of the ideal SUM gate ($\text{SUM}^G = \exp(-i\, G\hat{x}_1 \otimes \hat{p}_2)$, where $G = 1/\sqrt{R} - \sqrt{R}$, and $0 < R \leq 1$) on a two-mode input quantum state. The circuit consists of a sequence of passive transformations, off-line squeezed vacuum states, homodyne measurements, feed-forward operations, and displacement unitaries [71]. $D(\zeta)$ and $D(\upsilon)$ denote displacement unitaries with $\zeta = -\sqrt{1-R}x/\sqrt{2R}$ and $\upsilon = -\sqrt{1-R}p/\sqrt{2R}$, respectively.

4.5.1 Lack of uniform convergence

We now prove that the sequence $\{\widetilde{\text{SUM}}^{r_A,r_B,R}\}_{r_A,r_B\in[0,\infty)}$ does not converge uniformly to the ideal SUM^G gate. Let $|\psi\rangle_{12} = |z\rangle_1 |z\rangle_2$, where $|z\rangle$ denotes a single-mode squeezed-vacuum state with the covariance matrix $V_{|z\rangle\langle z|} = \text{diag}(z, 1/z)$, where $z \in [0,\infty)$. The covariance matrix of ψ_{12} is $V_{\psi_{12}} = \text{diag}(z, 1/z, z, 1/z)$, and its mean vector is $\mu_{\psi_{12}} = (0,0,0,0)^{\text{T}}$. Under the action of $\Lambda^{r_A,r_B,R}$, the covariance matrix $V_{\psi_{12}}$ transforms as follows:

$$V_{\psi_{12}}^{\text{out}} = \begin{bmatrix} z+\alpha(r_A) & 0 & -\frac{\alpha(r_A)}{\sqrt{R}} & 0 \\ 0 & \frac{1}{z}+\frac{\beta(r_B)}{R} & 0 & \frac{\beta(r_B)}{\sqrt{R}} \\ -\frac{\alpha(r_A)}{\sqrt{R}} & 0 & z+\frac{\alpha(r_A)}{R} & 0 \\ 0 & \frac{\beta(r_B)}{\sqrt{R}} & 0 & \frac{1}{z}+\beta(r_B) \end{bmatrix}.$$

We now use these expressions in the Uhlmann fidelity formula for two-mode Gaussian states [166]. By using the unitary invariance of fidelity, we find that

$$F(\text{SUM}^G(\psi_{12}), \widetilde{\text{SUM}}^{r_A,r_B,R}(\psi_{12})) = F(\psi_{12}, \Lambda^{r_A,r_B,R}(\psi_{12})). \tag{4.5.16}$$

Moreover, we find that [164]

$$F(\psi_{12}, \Lambda^{r_A,r_B,R}(\psi_{12})) = \frac{2\sqrt{z}R}{\sqrt{(2zR + (1-R)e^{-2r_A})(2R + z(1-R)e^{-2r_B})}}. \tag{4.5.17}$$

Therefore, for fixed r_A, r_B

$$\lim_{z\to 0} F(\mathrm{SUM}^G(\psi_{12}), \widetilde{\mathrm{SUM}}^{r_A,r_B,R}(\psi_{12})) = 0 \ , \tag{4.5.18}$$

which implies that the sequence $\{\widetilde{\mathrm{SUM}}^{r_A,r_B,R}\}_{r_A,r_B\in[0,\infty)}$ does not converge uniformly to the ideal SUM^G gate.

4.5.2 Strong convergence

We now argue that the sequence $\{\widetilde{\mathrm{SUM}}^{r_A,r_B,R}\}_{r_A,r_B\in[0,\infty)}$ converges to the SUM^G gate in the strong sense. Let ρ_{12}^{in} denote the input state. Let $\chi_{\mathrm{SUM}^G(\rho_{12}^{\mathrm{in}})}(x_1, p_1, x_2, p_2)$ denote the characteristic function of the state $\mathrm{SUM}^G(\rho_{12}^{\mathrm{in}})$. Let $\tilde{\rho}_{12}^{\mathrm{out}}$ denote the state after the action of $\widetilde{\mathrm{SUM}}^{r_A,r_B,R}$ on ρ_{12}: $\tilde{\rho}_{12}^{\mathrm{out}} = \widetilde{\mathrm{SUM}}^{r_A,r_B,R}(\rho_{12})$. Then the characteristic function of $\tilde{\rho}_{12}^{\mathrm{out}}$ is given by

$$\chi_{\tilde{\rho}_{12}^{\mathrm{out}}}(x_1, p_1, x_2, p_2) = \chi_{\mathrm{SUM}^G(\rho_{12}^{\mathrm{in}})}(x_1, p_1, x_2, p_2)\times \exp\left(\frac{R-1}{4(1+R)}[(p_1 - \sqrt{R}p_2)^2 e^{-2r_A} + (\sqrt{R}x_1 + x_2)^2 e^{-2r_B}]\right).$$

Therefore, for each $\rho_{12}^{\mathrm{in}} \in \mathcal{D}(\mathcal{H}_1 \otimes \mathcal{H}_2)$, and for all $x_1, p_1, x_2, p_2 \in \mathbb{R}$

$$\lim_{r_A,r_B\to\infty} \chi_{\tilde{\rho}_{12}^{\mathrm{out}}}(x_1, p_1, x_2, p_2) = \chi_{\mathrm{SUM}^G(\rho_{12}^{\mathrm{in}})}(x_1, p_1, x_2, p_2), \tag{4.5.19}$$

which implies that $\{\widetilde{\mathrm{SUM}}^{r_A,r_B,R}\}_{r_A,r_B\in[0,\infty)}$ converges strongly to the SUM^G gate.

4.5.3 Unideal displacements

As described in Figure 4.9, the simulation of an ideal SUM gate consists of two ideal displacements. We now briefly discuss the case when these displacement operators are not ideal. From the counterexamples given previously, we find that convergence of the simulation of a SUM gate to an ideal SUM gate is not uniform. By using the triangle inequality for sine distance, (4.1.23), (4.5.19), and [117, Proposition 2], the convergence holds in the strong sense. Moreover, the strong convergence of the sequence $\{\widetilde{\mathrm{SUM}}^{r_A,r_B,R}\}_{r_A,r_B\in[0,\infty)}$ to the SUM^G gate implies that the experimental approximations of an ideal SUM gate simulate the desired unitary operation uniformly on the set of density operators whose marginals on the channel input have bounded energy [137].

4.5.4 Estimates of the energy-constrained diamond norm

Similar to Section 4.4, we investigate the dependence of the convergence of the sequence $\{\widetilde{\mathrm{SUM}}^{r_A,r_B,R}\}_{r_A,r_B\in[0,\infty)}$ to the SUM^G gate on the experimental parameters when there is a finite energy constraint on the input states. Since the SUM^G gate acts on two modes, we consider several experimentally relevant quantum states with energy constraints, such as a tensor product of two coherent states, a tensor product of two single-mode squeezed states, a two-mode squeezed vacuum state, and a tensor product of two two-mode squeezed vacuum states. For a fixed finite value of the energy constraint, we find that a tensor product of two two-mode squeezed vacuum states provides the largest value of the sine distance between the ideal SUM gate and its experimental approximation.

We now discuss in detail the case when the input state is a tensor product of two two-mode squeezed vacuum states with parameter N, as defined in (2.3.34). For $G = 1/\sqrt{R} - \sqrt{R}$, and $0 < R \leq 1$, the fidelity between $\mathrm{SUM}^G(\psi_{\mathrm{TMS}}^{\otimes 2}(N))$ and $\widetilde{\mathrm{SUM}}^{r_A,r_B,R}(\psi_{\mathrm{TMS}}^{\otimes 2}(N))$ is

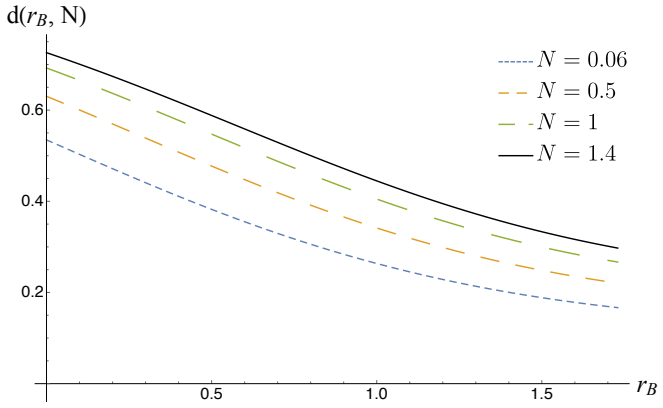

Figure 4.10: The figure plots the sine distance $d(r_B, N)$ in (4.5.21) between an ideal SUM^G gate with the interaction gain $G = 1$ and its experimental approximation $\widetilde{\text{SUM}}^{r_A,r_B,R}$ with $r_A = 1.726$ and $R = (\sqrt{5}-1)^2/4$, when the input state is a tensor product of two two-mode squeezed vacuum states with parameter N, as defined in (2.3.34). In the figure, we select certain values of the mean-photon number N of the channel input, with the choices indicated next to the figure. For a fixed value of r_B, the simulation of SUM^G is more accurate for low values of the energy constraint on input states. The figure indicates that an offline squeezing strength of 15 dB, which is what is currently experimentally achievable [198], is not sufficient to simulate an ideal SUM^G gate for $G = 1$, with a high accuracy, by using the protocol from [71].

given by [164]

$$F\left(\widetilde{\text{SUM}}^{r_A,r_B,R}(\psi_{\text{TMS}}^{\otimes 2}(N)), \text{SUM}^G(\psi_{\text{TMS}}^{\otimes 2}(N))\right) = \frac{2Re^{r_A+r_B}}{\sqrt{(\kappa(N,R)-2e^{2r_A}R)(\kappa(N,R)-2e^{2r_B}R)}}, \tag{4.5.20}$$

where $\kappa(N,R) = (-1+R)(1+2N)$.

We now perform numerical evaluations to see how close the experimental approximation $\widetilde{\text{SUM}}^{r_A,r_B,R}$ is to the ideal SUM^G gate for a fixed input state $\psi_{\text{TMS}}^{\otimes 2}(N)$. From (4.5.21), it is evident that the sine distance between $\text{SUM}^G(\psi_{\text{TMS}}^{\otimes 2}(N))$ and $\widetilde{\text{SUM}}^{r_A,r_B,R}(\psi_{\text{TMS}}^{\otimes 2}(N))$ is symmetric in r_A and r_B. Therefore, we fix $r_A = 1.726$, which corresponds to the currently experimentally achievable maximum squeezing ($\approx$ 15dB) [198]. We also fix the gain parameter $G = 1$, which implies that $R = (\sqrt{5}-1)^2/4$.

Let $d(r_B, N)$ denote the sine distance between $\text{SUM}^G(\psi_{\text{TMS}}^{\otimes 2}(N))$ and $\widetilde{\text{SUM}}^{r_A,r_B,R}(\psi_{\text{TMS}}^{\otimes 2}(N))$

for $R = (\sqrt{5}-1)^2/4$ and $r_A = 1.726$:

$$d(r_B, N) = \sqrt{1 - \frac{2Re^{r_A+r_B}}{\sqrt{(\kappa(N,R) - 2e^{2r_A}R)(\kappa(N,R) - 2e^{2r_B}R)}}}, \tag{4.5.21}$$

where we used (4.5.20).

In Figure 4.10, we plot $d(r_B, N)$ in (4.5.21) versus the offline squeezing strength r_B for certain values of the input mean photon number N. Similar to the results in Sections 4.1 and 4.4, we find that the simulation of SUM^G is more accurate for low values of the energy constraint on input states. Moreover, even with a low mean photon number $N = 0.06$ of the input states and with the currently experimentally achievable offline squeezing strength of 15 dB, only approximately 83% accuracy in simulating the ideal SUM^G gate for $G = 1$ can be achieved.

It is an open question to establish analytical bounds to quantify the performance of these experimental approximations of a SUM gate with respect to an energy-constrained distance measure.

4.6 Approximation of One- and Two-Mode Gaussian Unitaries

In this section, we show that a sequence of one-mode Gaussian channels does not converge uniformly to a one-mode Gaussian unitary. The same is true for the two-mode case. However, convergence occurs in the strong sense.

We begin by defining a set of matrices that characterizes all n-mode Gaussian channels. Let $\mathcal{G}^{X,Y}$ denote an n-mode Gaussian channel, which is completely characterized by two $2n \times 2n$ real matrices X and Y. For $\mathcal{G}^{X,Y}$ to be a physical channel, the X and Y matrices must be such that

$$Y + i\Omega \geq iX\Omega X^T, \qquad Y = Y^T. \tag{4.6.1}$$

Let S_n denote a set of a pair of matrices X and Y that satisfy (4.6.1), i.e.,

$$S_n = \{(X, Y) : Y + i\Omega \geq iX\Omega X^T, Y = Y^T\}, \tag{4.6.2}$$

where n in the subscript of S_n indicates that the set S_n consists of a pair of $2n \times 2n$ real matrices.

Let $\mathcal{U}_{A\to B}$ denote a single-mode Gaussian unitary transformation. Suppose that an experimental approximation of $\mathcal{U}_{A\to B}$ is a single-mode Gaussian channel $\widetilde{\mathcal{U}}^{X,Y}_{A\to B}$, which is completely characterized by two 2×2 real matrices X and Y. We now show that the sequence $\{\widetilde{\mathcal{U}}^{X,Y}\}_{(X,Y)\in S_1}$ does not converge uniformly to $\mathcal{U}$, where S_1 is given by (4.6.2) for $n = 1$. Let $\psi_{RA}(\bar{n})$ denote a two-mode squeezed vacuum state with parameter $\bar{n}$, as defined in (2.3.34). Let $\mathcal{G}^{\tilde{X},\tilde{Y}}_{A\to B} = \mathcal{U}^{-1} \circ \widetilde{\mathcal{U}}^{X,Y}_{A\to B}$ denote the overall Gaussian channel. Let

$$\tilde{X} = \begin{bmatrix} x_{11} & x_{12} \\ x_{21} & x_{22} \end{bmatrix}, \tilde{Y} = \begin{bmatrix} y_{11} & y_{12} \\ y_{12} & y_{22} \end{bmatrix}. \tag{4.6.3}$$

Then from the unitary invariance of fidelity, we find that

$$F(\mathcal{U}_{A\to B}(\psi_{RA}(\bar{n})), \widetilde{\mathcal{U}}^{X,Y}_{A\to B}(\psi_{RA}(\bar{n}))) = F(\psi_{RA}(\bar{n}), \mathcal{G}^{\tilde{X},\tilde{Y}}_{A\to B}(\psi_{RA}(\bar{n}))), \tag{4.6.4}$$

where it is implicit that an identity channel acts on the reference system R.

By expanding $F(\mathcal{U}_{A\to B}(\psi_{RA}(\bar{n})), \widetilde{\mathcal{U}}^{X,Y}_{A\to B}(\psi_{RA}(\bar{n})))$ about $\bar{n} = \infty$, we find that [164]

$$F(\mathcal{U}_{A\to B}(\psi_{RA}(\bar{n})), \widetilde{\mathcal{U}}^{X,Y}_{A\to B}(\psi_{RA}(\bar{n}))) = \frac{1}{(-1 + x_{11} + x_{12}x_{21} + x_{22} - x_{11}x_{22})\bar{n}^2} + O(1/\bar{n})^3. \tag{4.6.5}$$

Therefore,

$$\lim_{\bar{n}\to\infty} F(\mathcal{U}_{A\to B}(\psi_{RA}(\bar{n})), \widetilde{\mathcal{U}}^{X,Y}_{A\to B}(\psi_{RA}(\bar{n}))) = 0. \tag{4.6.6}$$

Using (2.4.12) and (4.6.6), we find that

$$\lim_{\bar{n}\to\infty} \|\mathcal{U}_{A\to B} - \widetilde{\mathcal{U}}^{X,Y}_{A\to B}\|_{\diamond} = 2, \tag{4.6.7}$$

which implies that the sequence $\{\widetilde{\mathcal{U}}^{X,Y}\}_{(X,Y)\in S_1}$ does not converge uniformly to the ideal single-mode Gaussian unitary transformation $\mathcal{U}_{A\to B}$.

Similarly, it can be shown that a sequence of two-mode Gaussian channels does not converge uniformly to an ideal two-mode Gaussian unitary transformation [164].

On the other hand, as a consequence of [117, Proposition 1], the convergence holds in the strong sense for both the one- and two-mode case, and in fact for the general n-mode case.

4.7 Conclusion

In this chapter, using different performance metrics we analyzed how well an ideal displacement operator, an ideal single-mode squeezer, and an ideal SUM gate can be simulated experimentally. In particular, we proved that none of these experimental approximations converge uniformly to the ideal Gaussian processes. Rather, convergence occurs in the strong sense.

We also discussed the notion of uniform convergence on the set of density operators whose marginals on the channel input have bounded energy, which is the most relevant from an experimental perspective, given that experiments are generally energy sensitive. In particular, we reduced the problem of distinguishing an ideal displacement operator from its experimental approximation to the problem of distinguishing a pure-loss channel from an ideal channel. We provided an analytic expression for the energy-constrained sine distance between an ideal displacement unitary and its approximation in terms of experimental parameters, by using the result of [186]. Moreover, we established two different lower bounds on the energy-constrained diamond distance between an ideal displacement operator and its experimental approximation for low values of the energy constraint on

input states. These bounds could be used to determine the requirements needed to implement a displacement operator to any desired accuracy. The displacement operator is ubiquitous in quantum optics and plays a critical role in CV quantum teleportation, CV quantum error correction and quantum computation, and quantum metrology. Therefore, quantification of the accuracy in simulating a displacement operator is important for several practical applications.

We then introduced two different methods to model the noise or loss in implementing both beamsplitters and phase rotations. For these models, we established analytical bounds on the energy-constrained diamond distance between these ideal gates and their experimental approximations. These bounds are relevant for characterizing the performance of any experiment consisting of beamsplitters and phase rotations.

Similarly, we discussed the notion of uniform convergence on the set of density operators whose marginals on the channel input have bounded energy for experimental approximations of both the single-mode squeezing unitary and the SUM gate. We considered several experimentally relevant input quantum states and studied how close these experimental approximations are to the ideal quantum processes. It is an interesting open question to determine the optimal value of energy-constrained distance measures and the corresponding optimal state to completely characterize these experimental approximations of the ideal quantum processes.

In this chapter, homodyne measurements involved in simulating a single-mode squeezer and a SUM gate were considered ideal. We expect that the well-known experimental approximation of homodyne detection converges strongly to ideal homodyne detection, based on the calculation of [199, Appendix K], and we also expect that the experimental approximation will not converge uniformly. However, it is an open question to determine the optimal value of energy-constrained distance measures and corresponding optimal states when homodyne measurements involved in these simulations are not ideal. Another interesting direction is to use these results to study the error propagation in an experiment

based on quantum optical elements.

CHAPTER 5

OPTIMAL TESTS FOR CONTINUOUS-VARIABLE QUANTUM TELEPORTATION AND PHOTODETECTORS

This chapter presents applications of energy-constrained distance measures to determine optimal tests for benchmarking continuous-variable (CV) teleportation and photodetectors. Our first main contribution is the reduction of the problem of estimating the energy-constrained channel fidelity between ideal teleportation and its experimental implementation to a quadratic program over an infinite number of variables. We then define a truncated version of this quadratic program and prove that it is a convex optimization problem. We numerically solve it using a MATLAB package, which employs the interior-point method [200]. We also provide analytical solutions by invoking the Karush-Kuhn-Tucker (KKT) conditions [86, 87]. We then argue that these solutions to the truncated versions of quadratic programs also optimize the energy-constrained channel fidelity defined over an infinite-dimensional, separable Hilbert space, i.e., without any truncation.

One of our main findings is that among all pure bipartite states, an entangled superposition of twin-Fock states saturating the energy constraint is optimal for distinguishing ideal CV teleportation from its experimental implementation. Our results thus provide an experimental strategy to verify whether an *unconditional* experimental teleportation with high accuracy is possible [76]. Here, by unconditional teleportation, we imply that teleportation of any unknown, energy-constrained state should be feasible. We also discuss why previous proposals based on the teleportation of coherent states or other commonly used states are not suitable for quantifying the performance of unconditional teleportation.

We then provide a solution to the energy-constrained diamond distance between a photodetector and its experimental approximation. We model the noisy version of a photodetector as a pure-loss channel followed by an ideal photodetector. We will prove that number-diagonal states optimize the energy-constrained diamond distance and show that

entanglement is not required for the optimal distinguishability of the ideal photodetector from its experimental implementation.

The rest of the chapter is organized as follows. We present our results on an optimal test for CV teleportation in Section 5.1. We next present results on an optimal test for photodetectors in Section 5.2. Finally, we conclude and summarize open problems in Section 5.3.

5.1 Continuous-Variable Quantum Teleportation

In this section, we characterize the performance of continuous-variable (CV) quantum teleportation in terms of the energy-constrained channel fidelity between ideal CV teleportation and its experimental approximation, the latter being the protocol from [37].

Let A denote the input mode. Ideal CV teleportation induces an identity channel on input states, which we denote by $\mathcal{I}_{A\to B}$. On the other hand, an experimental implementation of CV teleportation realizes an additive-noise channel $\mathcal{T}^{\xi}_{A\to B}$ with the variance parameter ξ, as defined in (2.3.85), which quantifies unideal squeezing and unideal detection in the teleportation protocol [37].

The energy-constrained channel fidelity between the identity channel and an additive-noise channel with parameter ξ is given by:

$$F_E(\mathcal{I}_{A\to B}, \mathcal{T}^{\xi}_{A\to B}) \equiv \inf_{\rho_{RA}:\mathrm{Tr}(\hat{n}_A\rho_A)\leq E} F(\rho_{RA}, \mathcal{T}^{\xi}_{A}(\rho_{RA})), \tag{5.1.1}$$

where $\rho_{RA} = \mathcal{D}(\mathcal{H}_{RA})$, $\rho_A = \mathrm{Tr}(\rho_{RA})$, and $\hat{n} = \sum_{n=0}^{\infty} n|n\rangle\langle n|$.

From joint concavity of root fidelity and monotonicity of the square function, the optimization in (5.1.1) can be reduced to pure states satisfying the energy constraint as follows:

$$F_E(\mathcal{I}_{A}, \mathcal{T}^{\xi}_{A}) \equiv \inf_{\phi_{RA}:\mathrm{Tr}(\hat{n}_A\phi_A)\leq E} F(\phi_{RA}, \mathcal{T}^{\xi}_{A}(\phi_{RA})), \tag{5.1.2}$$

where ϕ_{RA} is a pure state and R is a single-mode reference system.

We now argue that the optimization in (5.1.2) can be further restricted to pure states

that are entangled superpositions of twin-Fock states, satisfying the energy constraint. Let $\phi_A = \mathrm{Tr}_R(\phi_{RA})$. Consider the following phase averaging of ϕ_A:

$$\psi_A \equiv \frac{1}{2\pi}\int_0^{2\pi} d\theta\ e^{i\hat{n}\theta}\phi_A e^{-i\hat{n}\theta} \tag{5.1.3}$$

$$= \sum_{n=0}^{\infty} |n\rangle\langle n|\phi_A|n\rangle\langle n| \tag{5.1.4}$$

$$= \sum_{n=0}^{\infty} \lambda_n^2 |n\rangle\langle n|_A, \tag{5.1.5}$$

where $\lambda_n^2 \equiv \langle n|\phi_A|n\rangle$.

Then from isometric invariance and monotonicity of fidelity, and from the joint phase covariance of $\mathcal{I}_A$ and $\mathcal{T}_A^{\xi}$, it follows that (see e.g., [93, 153])

$$F(\psi_{RA}, (\mathcal{I}_R \otimes \mathcal{T}_A^{\xi})(\psi_{RA})) \leq F(\phi_{RA}, (\mathcal{I}_R \otimes \mathcal{T}_A^{\xi})(\phi_{RA})), \tag{5.1.6}$$

where $\psi_{RA} = |\psi\rangle\langle\psi|_{RA}$ is a purification of ψ_A in (5.1.5).

Since the phase averaging operation does not change the mean photon number, we get that $\mathrm{Tr}(\hat{n}\psi_A) = \mathrm{Tr}(\hat{n}\phi_A)$ [93]. Thus, combining (5.1.2) and (5.1.6) further reduces the optimization in (5.1.2) as follows:

$$F_E(\mathcal{I}_A, \mathcal{T}_A^{\xi}) = \inf_{\psi_{RA}:\mathrm{Tr}(\hat{n}_A\psi_A)\leq E} F(\psi_{RA}, \mathcal{T}_A^{\xi}(\psi_{RA})), \tag{5.1.7}$$

where

$$|\psi\rangle_{RA} = \sum_{n=0}^{\infty} \lambda_n |n\rangle_R |n\rangle_A, \tag{5.1.8}$$

for some $\lambda_n \in \mathbb{R}^+$ such that $\sum_{n=0}^{\infty} \lambda_n^2 = 1$ and $\sum_{n=0}^{\infty} \lambda_n^2 n \leq E$. As discussed in Chapter 2, we call $|\psi\rangle_{RA}$ in (5.1.8) an entangled superposition of twin-Fock states.

We now show that the optimization in (5.1.7) can be formulated as a quadratic program (see [201] for a review on quadratic programs). Note that the adjoint of a quantum-limited

amplifier channel $\mathcal{A}^{1/\eta}$ is related to a pure-loss channel $\mathcal{L}^{\eta}$ in the following sense [202]:

$$(\mathcal{A}^{1/\eta})^{\dagger} = \eta \mathcal{L}^{\eta}. \tag{5.1.9}$$

Then we get

$$\begin{aligned} F(\psi_{RA}, \mathcal{T}_A^{\xi}(\psi_{RA})) &= \operatorname{Tr}\Big(\psi_{RA} \mathcal{T}_A^{\xi}(\psi_{RA})\Big) && (5.1.10)\\ &= \operatorname{Tr}\Big(\psi_{RA} (\mathcal{A}^{1/\eta} \circ \mathcal{L}^{\eta})(\psi_{RA})\Big) && (5.1.11)\\ &= \eta \operatorname{Tr}\Big((\mathcal{L}^{\eta}(\psi_{RA}))^2\Big) && (5.1.12)\\ &= \eta \operatorname{Tr}\Big((\mathcal{L}^{1-\eta}(\psi_A))^2\Big), && (5.1.13) \end{aligned}$$

where

$$\psi_A = \sum_{n=0}^{\infty} \lambda_n^2 |n\rangle\langle n|_A. \tag{5.1.14}$$

The third equality follows from (5.1.9) and the last equality holds because the marginals of a pure bipartite state have the same purity, where the purity of a state ρ is defined as $\operatorname{Tr}(\rho^2)$.

To simplify (5.1.13) further, we recall that the action of a pure-loss channel $\mathcal{L}^{1-\eta}$ on ψ_A above is as follows:

$$\mathcal{L}_A^{1-\eta}(\psi_A) = \sum_{n=0}^{\infty} \lambda_n^2 \sum_{k=0}^{n} \binom{n}{k} (1-\eta)^k \eta^{n-k} |k\rangle\langle k|_A. \tag{5.1.15}$$

Let $p_n \equiv \lambda_n^2$ and $p \equiv (p_0, p_1, \dots)$. Then by using (5.1.15) in (5.1.13), we find that

$$\begin{aligned} F(\psi_{RA}, \mathcal{T}_A^{\xi}(\psi_{RA})) &= \sum_{n,m=0}^{\infty} p_n p_m \sum_{k=0}^{\min\{n,m\}} \binom{n}{k} \binom{m}{k} \frac{\xi^{2k}}{(1+\xi)^{n+m+1}} && (5.1.16)\\ &\equiv f(p) && (5.1.17) \end{aligned}$$

where we used

$$\eta = 1/(1+\xi)\ . \tag{5.1.18}$$

Henceforth, we denote $F(\psi_{RA}, \mathcal{T}^{\xi}_{A\to B}(\psi_{RA}))$ as $f(p)$, as indicated in (5.1.17).

Therefore, the problem of estimating the energy-constrained channel fidelity between ideal CV teleportation and its experimental implementation reduces to the following quadratic optimization problem:

$$F_E(\mathcal{I}_A, \mathcal{T}^{\xi}_A) = \begin{cases} \inf_p & f(p) \\ \text{subject to} & \sum_{n=0}^{\infty} np_n \leq E, \\ & p_n \geq 0, \forall n \in \mathbb{Z}^{\geq 0}, \\ & \sum_{n=0}^{\infty} p_n = 1. \end{cases} \tag{5.1.19}$$

Solutions to quadratic programs can be obtained numerically by using a MATLAB package that employs the interior-point method [200]. Moreover, analytical solutions can be calculated by invoking the Karush-Kuhn-Tucker (KKT) conditions [86,87]. However, these methods are suitable for solving optimization problems over a finite number of variables. Therefore, we first define a truncated version of the energy-constrained channel fidelity between two quantum channels, which is equivalent to a quadratic program over a finite number of variables for the task of distinguishing the identity channel from an additive-noise channel. We argue below that for finite E and high values of the truncation parameter, it is sufficient to find solutions on a truncated Hilbert space.

Energy-constrained channel fidelity over a truncated Hilbert space. Let M denote the truncation parameter, and let $\mathcal{H}_M$ denote an $(M+1)$-dimensional Fock space $\{|0\rangle, |1\rangle, \ldots, |M\rangle\}$. Let $\omega_A \in \mathcal{D}(\mathcal{H}_M)$. We define the energy-constrained channel fidelity

between two quantum channels $\mathcal{N}_{A\to B}$ and $\mathcal{M}_{A\to B}$ on a truncated Hilbert space as

$$F_{E,M}(\mathcal{N}_{A\to B},\mathcal{M}_{A\to B}) \equiv \inf_{\substack{\omega_{RA}\in\mathcal{D}(\mathcal{H}_R\otimes\mathcal{H}_M):\\ \operatorname{Tr}(\hat{n}\omega_A)\leq E}} F(\mathcal{N}(\omega_{RA}),\mathcal{M}(\omega_{RA})), \tag{5.1.20}$$

where ω_{RA} is an extension of ω_A. Moreover, it is implicit that the identity channel acts on the reference system R. Similar to the previous case, it suffices to optimize over pure bipartite states of systems R and A, with system R isomorphic to system A, so that the dimension of R can be set to $M+1$.

Since the optimization in (5.1.20) is over a truncated space instead of an infinite-dimensional separable Hilbert space, we get

$$F_E(\mathcal{N}_{A\to B},\mathcal{M}_{A\to B}) \leq F_{E,M}(\mathcal{N}_{A\to B},\mathcal{M}_{A\to B}) \ . \tag{5.1.21}$$

We now establish a lower bound on $F_E(\mathcal{N}_{A\to B},\mathcal{M}_{A\to B})$ in terms of $F_{E,M}(\mathcal{N}_{A\to B},\mathcal{M}_{A\to B})$, which combining with (5.1.21) will imply that solutions to (5.1.19) can be obtained by solving a quadratic program on a truncated Hilbert space. For completeness we first argue that the set of density operators acting on a truncated Hilbert space with a finite mean energy constraint is dense in the set of density operators acting on an infinite-dimensional Hilbert space and with the same mean energy constraint [92]. Let ρ_{RA} denote a density operator acting on an infinite-dimensional separable Hilbert space, such that $\operatorname{Tr}(\hat{n}_A\rho_{RA}) \leq E$, where $E>0$. Let Π_A^M denote an $(M+1)$-dimensional projector defined as

$$\Pi_A^M = \sum_{n=0}^{M} |n\rangle\langle n| \ . \tag{5.1.22}$$

Then from (4.1.43), it follows that

$$\operatorname{Tr}\Big(\Pi_A^M\rho_{RA}\Big) \geq 1 - \frac{E}{M+1}. \tag{5.1.23}$$

Let ρ_{RA}^{M} denote the following truncated state:

$$\rho_{RA}^{M} = \frac{\Pi_{A}^{M} \rho_{RA} \Pi_{A}^{M}}{\mathrm{Tr}(\Pi_{A}^{M} \rho_{RA})}. \tag{5.1.24}$$

Then by invoking the gentle measurement lemma [192, 193], we get

$$F(\rho_{RA}, \rho_{RA}^{M}) \geq 1 - \frac{E}{M+1}, \tag{5.1.25}$$

which implies that the fidelity between the truncated state ρ_{RA}^{M} and ρ_{RA} is close to one for low values of E and high values of the truncation parameter M.

We define the energy-constrained sine distance between two channels $\mathcal{N}_{A\to B}$ and $\mathcal{M}_{A\to B}$ on a truncated Hilbert space as follows:

$$C_{E,M}(\mathcal{N}_{A\to B}, \mathcal{M}_{A\to B}) \equiv \sup_{\varphi_{RA} \in \mathcal{D}(\mathcal{H}_{M}^{\otimes 2}) : \mathrm{Tr}(\hat{n}\varphi_{A}) \leq E} \sqrt{1 - F(\mathcal{N}(\varphi_{RA}), \mathcal{M}(\varphi_{RA}))}\ . \tag{5.1.26}$$

Then from (5.1.23), (5.1.25), and arguments similar to those used in Section 4.1.5, we establish the following inequalities:

$$C_{E,M}(\mathcal{N}_{A\to B}, \mathcal{M}_{A\to B}) \leq C_{E}(\mathcal{N}_{A\to B}, \mathcal{M}_{A\to B}) \leq 2\sqrt{\frac{E}{M+1}} + C_{E,M}(\mathcal{N}_{A\to B}, \mathcal{M}_{A\to B}). \tag{5.1.27}$$

Finally, by squaring the inequality on the right side and from a simple rearrangement, we get

$$F_{E}(\mathcal{N}_{A\to B}, \mathcal{M}_{A\to B}) \geq 1 - \left(2\sqrt{\frac{E}{M+1}} + \sqrt{1 - F_{E,M}(\mathcal{N}_{A\to B}, \mathcal{M}_{A\to B})} \right)^{2}, \tag{5.1.28}$$

which leads to the desired result by combining with (5.1.21)

$$1 - \left(2\sqrt{\frac{E}{M+1}} + \sqrt{1 - F_{E,M}(\mathcal{N}_{A\to B}, \mathcal{M}_{A\to B})} \right)^2 \leq F_E(\mathcal{N}_{A\to B}, \mathcal{M}_{A\to B}) \leq F_{E,M}(\mathcal{N}_{A\to B}, \mathcal{M}_{A\to B}) \ , \quad (5.1.29)$$

In other words, for low values of the mean energy constraint E, the energy-constrained channel fidelity between two quantum channels $\mathcal{N}$ and $\mathcal{M}$ can be estimated with arbitrary accuracy by using the energy-constrained channel fidelity on a truncated input Hilbert space with sufficiently high values of the truncation parameter M.

Quadratic program on a truncated Hilbert space. For low values of E and high values of M, solutions to the quadratic program in (5.1.19) can be obtained by solving the following quadratic program:

$$F_{E,M}(\mathcal{I}_A, \mathcal{T}_A^{\xi}) = \begin{cases} \inf_p & f_M(p) \equiv \sum_{n,m=0}^{M} p_n p_m \sum_{k=0}^{\min\{n,m\}} \binom{n}{k}\binom{m}{k} \frac{\xi^{2k}}{(1+\xi)^{n+m+1}} \\ \text{subject to} & \sum_{n=0}^{M} n p_n \leq E, \\ & p_n \geq 0, \ \forall n \in \{0, \ldots, M\}, \\ & \sum_{n=0}^{M} p_n = 1. \end{cases} \quad (5.1.30)$$

where $p = (p_0, p_1, \ldots, p_M)$ and $F_{E,M}(\mathcal{I}_A, \mathcal{T}_A^{\xi})$ is given by (5.1.20).

It is easy to check that (5.1.30) is equivalent to the primal optimization problem in (2.9.1).

Convexity of the objective function. We now present the argument of [203] that the function $f_M(p)$ in (5.1.30) is convex in p. The Hessian matrix corresponding to the objective

function $f_M(p)$ is given by

$$A(\xi) = 2\sum_{n,m=0}^{M}\sum_{k=0}^{\min\{n,m\}}\binom{n}{k}\binom{m}{k}\frac{\xi^{2k}}{1+\xi}\left(\frac{1}{1+\xi}\right)^{n+m}|n\rangle\langle m| \tag{5.1.31}$$

$$= 2\sum_{k=0}^{M}\frac{\xi^{2k}}{1+\xi}\left[\sum_{n=0}^{M}\binom{n}{k}\frac{1}{(1+\xi)^n}|n\rangle\right]\left[\sum_{m=0}^{M}\binom{m}{k}\frac{1}{(1+\xi)^m}\langle m|\right] \tag{5.1.32}$$

$$= 2\sum_{k=0}^{M}\frac{\xi^{2k}}{1+\xi}|\Upsilon\rangle\langle\Upsilon|, \tag{5.1.33}$$

where

$$|\Upsilon\rangle = \sum_{n=0}^{M}\binom{n}{k}\frac{1}{(1+\xi)^n}|n\rangle \ . \tag{5.1.34}$$

Thus we get

$$\langle\Phi|A(\xi)|\Phi\rangle = 2\sum_{k=0}^{M}\frac{\xi^{2k}}{1+\xi}|\langle\Phi|\Upsilon\rangle|^2 \geq 0 \ , \tag{5.1.35}$$

which implies that the objective function $f_M(p)$ in (5.1.30) is convex in p. Since the aforementioned proof holds for any value of the truncation parameter M, it further implies that the objective function $f(p)$ in (5.1.19) is also convex.

Convexity of Lagrangian. Finally, note that the inequality constraints in (5.1.19) are linear, which implies that the Lagrangian

$$L(p,\mu,\beta,\gamma) = f(p) + \mu\left(\sum_n np_n - E\right) - \sum_n \beta_n p_n + \gamma\left(\sum_n p_n - 1\right) \tag{5.1.36}$$

is also convex in p, where we introduced the dual variables μ, γ, and β_n, for $n \in \mathbb{Z}^{\geq 0}$, similar to those in (2.9.2). Convexity of the Lagrangian further ensures that an optimal point obtained from either numerical or analytical methods is the global optimal point.

Numerical results. In Figure 5.1, we plot solutions of the quadratic program in (5.1.30) for different values of the energy-constraint parameter E, with the choices indicated next to the figure. As shown in Figure 5.1, for a fixed value of the noise parameter ξ, the accuracy in implementing CV teleportation decreases as the energy constraint on the input states

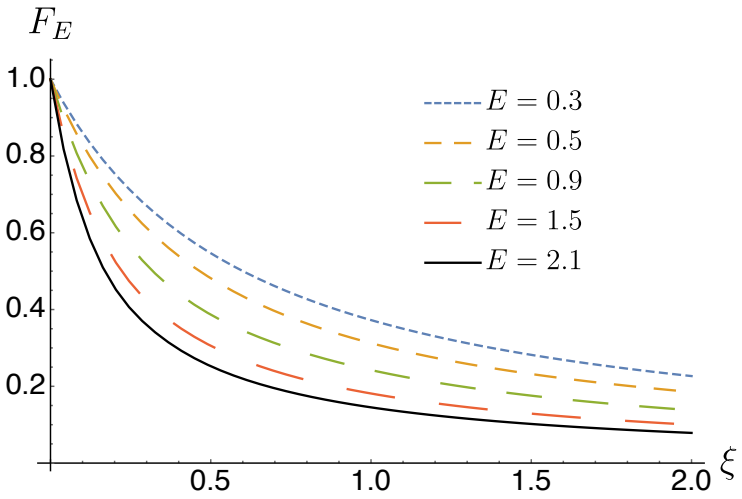

Figure 5.1: The figure plots the energy-constrained channel fidelity $F_{E,M}(\mathcal{I}, \mathcal{T}^{\xi})$ between ideal teleportation and its experimental implementation versus the noise parameter ξ. Here, we denote $F_{E,M}(\mathcal{I}, \mathcal{T}^{\xi})$ by F_E for simplicity. In the figure, we select certain values of the mean-photon energy E of the channel input, with the choices indicated in the figure legend. For a fixed value of E, we solve the optimization program in (5.1.30) for $M = 50$. The figure indicates that for a fixed value of the noise parameter ξ, the simulation of CV teleportation is more accurate as the energy constraint on the input states decreases.

increases.

Analytical results. Using the KKT conditions, we can obtain analytical solutions to the optimization problem (5.1.19). For arbitrary values of $E \geq 0$ and $\xi \geq 0$, the analytical form of the solution can be obtained by first solving the problem numerically for high values of the truncation parameter M, which provides information about non-zero elements in the optimal probability vector p^*. Using that information, the KKT conditions can then be solved analytically.

We now provide solutions to (5.1.19) for several examples.

Example 1. Let $E = 0.6$ and $\xi = 0.25$. We first numerically find the optimal solution to (5.1.30) using the MATLAB package for quadratic programming [165]. Furthermore, we find numerically that for this case, the optimal value f^* of the objective function and the corresponding optimal solution p^* do not change for values of the truncation parameter from $M = 1$ to $M = 50$. We provide reasoning for this result by analytically solving the

quadratic program by invoking the KKT conditions.

We now analytically find primal and dual feasible points that satisfy the KKT conditions and hence the optimal solution to (5.1.19) for $E = 0.6$ and $\xi = 0.25$. We begin by presenting the KKT conditions for the optimization problem in (5.1.19).

$$\begin{aligned}
&\text{Stationarity} && \partial_p L(p, \mu, \beta, \gamma)|_{p=p^*} = 0 \\
&\text{Primal feasibility} && \textstyle\sum_n np_n^* - E \leq 0 \\
& && p_n^* \geq 0, \forall n \in \mathbb{Z}^{\geq 0} \\
& && \textstyle\sum_n p_n^* = 1 \\
&\text{Dual feasibility} && \mu \geq 0 \\
& && \beta_n \geq 0, \forall n \in \mathbb{Z}^{\geq 0} \\
&\text{Complementary slackness} && \mu \left(\textstyle\sum_n np_n^* - E\right) = 0 \\
& && \beta_n p_n^* = 0, \forall n \in \mathbb{Z}^{\geq 0}
\end{aligned} \tag{5.1.37}$$

We find a set $(\tilde{p}, \tilde{\mu}, \tilde{\beta}, \tilde{\gamma})$ that satisfies the KKT conditions, which further implies that $\tilde{p} = p^*$ and $f^* = f(p^*)$, where $f(p)$ is defined in (5.1.19). Let $\tilde{p}_n = 0, \forall n \geq 2$. Let us suppose that the mean energy constraint is saturated, i.e., $\tilde{p}_1 = E$, which satisfies one of the complementary slackness conditions. To satisfy $\beta_n \tilde{p}_n = 0$, for $n = 0, 1$, we set $\beta_0 = \beta_1 = 0$. From the primal feasibility condition, we get $\tilde{p}_0 = 1 - \tilde{p}_1 = 1 - E$. All we need to show now is that $\mu \geq 0$ and $\beta_n \geq 0, \forall n \geq 2$. Combining all these facts will imply that the KKT conditions are satisfied. First, to simplify the calculation, we define

$$G(n, m, \xi) = \sum_{k=0}^{\min\{n,m\}} \binom{n}{k} \binom{m}{k} \frac{\xi^{2k}}{(1+\xi)^{n+m+1}} \ . \tag{5.1.38}$$

Then from the stationarity condition $\tilde{p}_0$ and $\tilde{p}_1$, we get the following linear system of

equations:

$$2G(0,0,\xi)\tilde{p}_0 + 2G(1,0,\xi)\tilde{p}_1 + \gamma = 0, \tag{5.1.39}$$

$$2G(0,1,\xi)\tilde{p}_0 + 2G(1,1,\xi)\tilde{p}_1 + \mu + \gamma = 0. \tag{5.1.40}$$

By solving for μ and γ, we find [165]

$$\mu = \frac{2\xi(1-(2E-1)\xi)}{(1+\xi)^3} > 0\ , \tag{5.1.41}$$

$$\gamma = -\frac{2(1+(1-E)\xi)}{(1+\xi)^2}, \tag{5.1.42}$$

for $E = 0.6$ and $\xi = 0.25$.

Since $\mu > 0$, in order to satisfy all the KKT conditions for (5.1.19), we only need to show that $\beta_n \geq 0$, $\forall n \geq 2$. From the stationarity condition for $\tilde{p}_n$ we get

$$\beta_n = 2G(0,n,\xi)\tilde{p}_0 + 2G(1,n,\xi)\tilde{p}_1 + n\mu + \gamma\ . \tag{5.1.43}$$

The only negative term in (5.1.43) is γ. For this example we get $\mu = 0.2432$ and $\gamma = -1.408$. Since $-\gamma/\mu = 5.79$, we get $n\mu \geq -\gamma$, $\forall n \geq 6$. This further implies that $\beta_n \geq 0$, $\forall n \geq 6$. Moreover, we solve for β_2, β_3, β_4, and β_5 using (5.1.43) and find their values to be $0.041, 0.1160, 0.2202$, and 0.348, respectively [165]. Thus we get $\beta_n \geq 0, \forall n \geq 2$. This completes the proof.

Since all the KKT conditions are satisfied and since $f(p)$ is a convex function, we conclude that $\tilde{p}$ is the optimal solution, i.e., $\tilde{p} = p^* = (1-E, E, 0, \ldots, 0)$ and the optimal objective function value is given by

$$f^* = f(p^*) = \frac{1+\xi(2+\xi-2E(1+(1-E)\xi))}{(1+\xi)^3} = 0.6310, \tag{5.1.44}$$

for $E = 0.6$ and $\xi = 0.25$, which is equal to the optimal value obtained numerically. Furthermore, for this case, the optimal state corresponding to the channel fidelity between the ideal teleportation and its experimental approximation is given by

$$|\psi\rangle_{RA} = \sqrt{1-E}\,|0\rangle_A\,|0\rangle_R + \sqrt{E}\,|1\rangle_A\,|1\rangle_R \ . \tag{5.1.45}$$

Example 2. Let us consider the case when $E = 1.2$ and $\xi = 2/3$. Numerically, we find that the optimal solution has $\tilde{p}_n = 0, \forall n$, except for $n = 0, 1, 2$. To satisfy the complementary slackness condition, we set $\beta_0 = \beta_1 = \beta_2 = 0$. Similar to the previous case, we assume that the energy constraint is satisfied, i.e., $\tilde{p}_1 + 2\tilde{p}_2 = E$. By invoking the stationarity conditions for $\tilde{p}_0, \tilde{p}_1$, and $\tilde{p}_2$, and the primal feasibility condition and by solving the linear system of equations, we get that [165]

$$\tilde{p}_0 = \frac{\xi(5\xi + 3E(1-\xi) - 2) - 1}{6\xi^2} > 0, \tag{5.1.46}$$

$$\tilde{p}_1 = \frac{1 + \xi(2 - 3E + \xi)}{3\xi^2} \geq 0, \tag{5.1.47}$$

$$\tilde{p}_2 = \frac{(1+\xi)(\xi(3E-1) - 1)}{6\xi^2} > 0, \tag{5.1.48}$$

$$\mu = \frac{\xi(1 + (1-E)\xi)}{(1+\xi)^3} > 0, \tag{5.1.49}$$

$$\gamma = -\frac{5 + (5 - 3E)\xi}{3(1+\xi)^2}, \tag{5.1.50}$$

for $E = 1.2$ and $\xi = 2/3$. Moreover, similar to the previous case, we find that $\beta_n \geq 0, \forall n \geq 3$ [165].

Since all the KKT conditions are satisfied and since $f(p)$ is a convex function, we conclude that $\tilde{p}$ is the optimal solution, i.e., $\tilde{p} = p^*$. Moreover, the optimal objective function is given by

$$f^* = f(p^*) = \frac{5 + 5\xi(2+\xi) - 3E\xi(2 + (2-E)\xi)}{6(1+\xi)^3} \ , \tag{5.1.51}$$

and the corresponding optimal state to distinguish the ideal teleportation channel from its experimental approximation is

$$|\psi\rangle_{RA} = \sqrt{\tilde{p}_0}\,|0\rangle_A\,|0\rangle_R + \sqrt{\tilde{p}_1}\,|1\rangle_A\,|1\rangle_R + \sqrt{\tilde{p}_2}\,|2\rangle_A\,|2\rangle_R\,. \tag{5.1.52}$$

Example 3. We provide an analytical solution for another interesting example when ξ is close to zero, which corresponds to the case of the additive-noise channel converging to the ideal teleportation channel. This example is experimentally relevant, as the goal of an approximate teleportation protocol is to converge to the ideal teleportation channel. In such a scenario we argue that

$$|\psi\rangle_{RA} = \sqrt{1-\{E\}}\,|\lfloor E\rfloor\rangle_A\,|\lfloor E\rfloor\rangle_R + \sqrt{\{E\}}\,|\lceil E\rceil\rangle_A\,|\lceil E\rceil\rangle_R \tag{5.1.53}$$

is the optimal state for the optimization problem in (5.1.1), where $\{E\} = E - \lfloor E\rfloor$. Moreover, the minimum fidelity in (5.1.1) is given by

$$F_E(\mathcal{I}_A, \mathcal{T}_A^{\xi}) = (1-\{E\})^2 G(\lfloor E\rfloor, \lfloor E\rfloor, \xi) + 2\{E\}(1-\{E\})G(\lfloor E\rfloor, \lceil E\rceil, \xi) + (\{E\})^2 G(\lceil E\rceil, \lceil E\rceil, \xi), \tag{5.1.54}$$

where $G(n, m, \xi)$ is defined in (5.1.38).

Since the marginal of the state $|\psi\rangle_{RA}$ in (5.1.53) has energy $\mathrm{Tr}(\hat{n}\psi_A) = E$, one of the complementary slackness conditions is satisfied. Let us suppose that $p_n^* = 0, \forall n$, except for $n = \lfloor E\rfloor$ and $\lceil E\rceil$. Therefore, $p^*_{\lfloor E\rfloor} = 1 - \{E\}$ and $p^*_{\lceil E\rceil} = \{E\}$, which implies that $\beta_{\lfloor E\rfloor} = \beta_{\lceil E\rceil} = 0$, to satisfy the other complementary slackness conditions. Similar to the previous examples, we need to solve the following linear system of equations and show that

$\mu \geq 0$ when ξ is close to zero:

$$2p^*_{\lfloor E \rfloor} G(\lfloor E \rfloor, \lfloor E \rfloor, \xi) + 2p^*_{\lceil E \rceil} G(\lfloor E \rfloor, \lceil E \rceil, \xi) + \lfloor E \rfloor \mu + \gamma = 0, \tag{5.1.55}$$

$$2p^*_{\lceil E \rceil} G(\lceil E \rceil, \lceil E \rceil, \xi) + 2p^*_{\lfloor E \rfloor} G(\lfloor E \rfloor, \lceil E \rceil, \xi) + \lceil E \rceil \mu + \gamma = 0. \tag{5.1.56}$$

By solving for μ, we get

$$\mu = 2\left(p^*_{\lfloor E \rfloor}(G(\lfloor E \rfloor, \lfloor E \rfloor, \xi) - G(\lfloor E \rfloor, \lceil E \rceil, \xi)) + p^*_{\lceil E \rceil}(G(\lfloor E \rfloor, \lceil E \rceil, \xi) - G(\lceil E \rceil, \lceil E \rceil, \xi))\right), \tag{5.1.57}$$

$$\approx 2\xi + O(\xi^2)\ , \tag{5.1.58}$$

which implies that the leading order term $2\xi \geq 0$ for any finite value of the energy constraint E. Similarly, we find that

$$\beta_n \approx (\lfloor E \rfloor - n)(\lceil E \rceil - n)\xi^2 + O(\xi^3), \forall n, \tag{5.1.59}$$

where again the leading term implies that $\beta_n \geq 0$ when ξ is close to zero. By combining everything, we conclude that all the KKT conditions are satisfied. Hence, for ξ close to zero, the state in (5.1.53) is optimal for the task of distinguishing the ideal teleportation channel from its experimental approximation when there is a finite energy constraint on the input states to the channels.

Finally, we consider several experimentally relevant quantum states with energy constraints, such as coherent states and the two-mode squeezed vacuum state (TMSV).

Example 4. Let $|\alpha\rangle$ denote a coherent state and let $E = |\alpha|^2$. We note that the covariance matrix of a coherent state is a two-dimensional identity matrix, which under an additive-noise channel $\mathcal{T}^\xi$ becomes $V_{\mathcal{T}^\xi(|\alpha\rangle\langle\alpha|)} = \mathrm{diag}(1 + 2\xi)$. Then the fidelity between $|\alpha\rangle$ and

$\mathcal{T}^{\xi}(|\alpha\rangle\langle\alpha|)$ is given by [68]

$$F(|\alpha\rangle\langle\alpha|, \mathcal{T}^{\xi}(|\alpha\rangle\langle\alpha|)) = \frac{2}{\sqrt{\text{Det}(\text{diag}(2(1+\xi)))}} = \frac{1}{1+\xi}. \tag{5.1.60}$$

Example 5. Let $|\psi_{\text{TMS}}(E)\rangle$ denote a two-mode squeezed vacuum state, defined as in (5.1.8) with $\lambda_n = \frac{E^{n/2}}{(E+1)^{(n+1)/2}}$. The covariance matrix of a two-mode squeezed vacuum state is given by

$$V_{\psi_{\text{TMS}}(\bar{n})} = \begin{bmatrix} (2\bar{n}+1)I_2 & 2\sqrt{\bar{n}(\bar{n}+1)}\sigma_z \\ 2\sqrt{\bar{n}(\bar{n}+1)}\sigma_z & (2\bar{n}+1)I_2 \end{bmatrix}, \tag{5.1.61}$$

which under the additive-noise channel with parameter ξ transforms as

$$V_{\mathcal{T}^{\xi}(\psi_{\text{TMS}}(\bar{n}))} = \begin{bmatrix} (2\bar{n}+1)I_2 & 2\sqrt{\bar{n}(\bar{n}+1)}\sigma_z \\ 2\sqrt{\bar{n}(\bar{n}+1)}\sigma_z & (2\bar{n}+2\xi+1)I_2 \end{bmatrix}. \tag{5.1.62}$$

Then the fidelity between $\psi_{\text{TMS}}(\bar{n})$ and $\mathcal{T}^{\xi}(\psi_{\text{TMS}}(\bar{n}))$ is given by [68]

$$F(\psi_{\text{TMS}}(\bar{n}), \mathcal{T}^{\xi}(\psi_{\text{TMS}}(\bar{n}))) = \frac{4}{\sqrt{\text{Det}(V_{\psi_{\text{TMS}}(\bar{n})} + V_{\mathcal{T}^{\xi}(\psi_{\text{TMS}}(\bar{n}))})}} = \frac{1}{1+(2\bar{n}+1)\xi}\ . \tag{5.1.63}$$

In Figure 5.2, we plot the fidelity between the identity channel and an additive-noise channel for several input states versus ξ for $E = 1.9$. We first numerically estimate the energy-constrained channel fidelity between $\mathcal{I}$ and $\mathcal{T}^{\xi}$ for $E = 1.9$, which is plotted as red dots in Figure 5.2. In order to estimate the channel fidelity on a truncated Hilbert space, we set the truncation parameter $M = 50$. Blue and black dashed curves correspond to fidelity in (5.1.60) and (5.1.63), respectively. Figure 5.2 indicates that for a fixed value of E, coherent states and two-mode squeezed vacuum states are not optimal tests for the performance of CV quantum teleportation. Interestingly, however, the TMSV is pretty close to being an optimal test for CV teleportation.

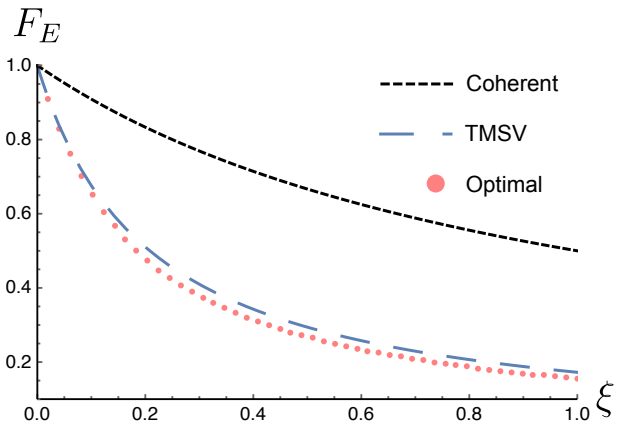

Figure 5.2: The figure plots the fidelity between the identity channel $\mathcal{I}$ and the additive-noise channel $\mathcal{T}^{\xi}$ versus the additive noise parameter ξ, for different input states, with the choices indicated in the figure legend. We set the energy-constraint parameter value to $E = 1.9$. Red dots plot the energy-constrained channel fidelity between $\mathcal{I}$ and $\mathcal{T}^{\xi}$. The black-dashed curve represents $F(|\alpha\rangle\langle\alpha|, \mathcal{T}^{\xi}(|\alpha\rangle\langle\alpha|))$ as in (5.1.60), and the blue-dashed curve represents $F(\psi_{\text{TMS}}(E), \mathcal{T}^{\xi}(\psi_{\text{TMS}}(E))$ as in (5.1.63).

Remark 117 *As discussed above, for a given additive-noise channel $\mathcal{T}^{\xi}$ with a fixed noise parameter ξ, one can find the energy-constrained channel fidelity between $\mathcal{T}^{\xi}$ and an identity channel by solving quadratic program on a truncated Hilbert space in* (5.1.30) *and by invoking KKT conditions in* (5.1). *Since an identity channel is trivially a degradable channel, from* (57) *it follows that the additive noise channel is an ε-close-degradable channel with $\varepsilon = \sqrt{1 - F_E(\mathcal{I}, \mathcal{T}^{\xi})}$, where $F_E(\mathcal{I}, \mathcal{T}^{\xi})$ is given by* (5.1.19). *Then upper bounds on quantum and private capacities of $\mathcal{T}^{\xi}$ can be established directly from Theorems 69 and 72, respectively.*

5.2 Approximation of a Photodetector

In this section, we characterize the performance of an experimental approximation of an ideal photodetector. A simple way to model the noise in photodetection is to account for the loss of photons [204]. Let $\mathcal{L}^{\eta}$ denote a pure-loss channel with transmissivity $\eta \in [0, 1)$ and let $\widetilde{\mathcal{P}}^{\eta}$ denote the experimental approximation of $\mathcal{P}$. Then we define the action of $\widetilde{\mathcal{P}}^{\eta}$

on a density operator ρ as follows:

$$\widetilde{\mathcal{P}}^{\eta}(\rho) \equiv \mathcal{P} \circ \mathcal{L}^{\eta}(\rho) \ , \tag{5.2.1}$$

where $\mathcal{P}$ is defined in (2.3.90).

Energy-constrained diamond distance between $\mathcal{P}$ and $\widetilde{\mathcal{P}}^{\eta}$. We now evaluate the energy-constrained diamond distance between $\widetilde{\mathcal{P}}^{\eta}$ and $\mathcal{P}$. We first summarize the main results and subsequently provide detailed proof steps.

Employing the joint phase covariance of $\mathcal{P}$ and $\widetilde{\mathcal{P}}^{\eta}$, it follows that among all pure states, entangled superpositions of twin-Fock states, as defined in (5.1.8), are optimal to distinguish $\mathcal{P}$ from $\widetilde{\mathcal{P}}$ with respect to the energy-constrained diamond distance.

Let $\{E\} \equiv E - \lfloor E \rfloor$. Then from the direct-sum property of the trace distance on classical-quantum states and convexity of the function $x \to \eta^x$, where $\eta \in [0, 1)$, we find that

$$\frac{1}{2}\|\mathcal{P} - \widetilde{\mathcal{P}}^{\eta}\|_{\diamond E} = 1 - \left[(1 - \{E\})\eta^{\lfloor E \rfloor} + \{E\}\eta^{\lceil E \rceil}\right] \ . \tag{5.2.2}$$

Moreover, a state that optimizes the energy-constrained diamond distance in (5.2.2) is given by the following mixed number state:

$$\psi_A = (1 - \{E\})|\lfloor E \rfloor\rangle\langle\lfloor E \rfloor|_A + \{E\}|\lceil E \rceil\rangle\langle\lceil E \rceil|_A. \tag{5.2.3}$$

From (5.2.3) it follows that entanglement is not necessary to attain the optimal distinguishability of the ideal photodetector $\mathcal{P}$ from its experimental approximation $\widetilde{\mathcal{P}}^{\eta}$. We now provide a detailed proof.

Proof of (5.2.2) **and** (5.2.3)**.** Our goal is to estimate the trace distance between $(\mathcal{I}_R \otimes \mathcal{P}_A)(\psi_{RA})$ and $(\mathcal{I}_R \otimes \widetilde{\mathcal{P}}^{\eta}_A)(\psi_{RA})$, where ψ_{RA} is given by (5.1.8).

Let

$$g(n, m, \eta) = \sqrt{\binom{n}{k}\binom{m}{k}\eta^{n+m-2k}(1-\eta)^{2k}} \ . \tag{5.2.4}$$

Consider the following chain of equalities:

$$
\begin{aligned}
&\left\|(\mathcal{I}_R \otimes \mathcal{P}_A)(\psi_{RA}) - (\mathcal{I}_R \otimes \widetilde{\mathcal{P}}^{\eta}_A)(\psi_{RA})\right\|_1 \\
&= \|(\mathcal{I}_R \otimes \mathcal{P}_A)(\psi_{RA}) - (\mathcal{I}_R \otimes (\mathcal{P}_A \circ \mathcal{L}^{\eta}_A))(\psi_{RA})\|_1 && (5.2.5)\\
&= \left\| \sum_{n,m=0}^{\infty} \lambda_m \lambda_n |n\rangle\langle m|_R \otimes \left[\mathcal{P}(|n\rangle\langle m|_A) - \sum_{k=0}^{\min\{n,m\}} g(n,m,\eta) \mathcal{P}(|n-k\rangle\langle m-k|_A) \right] \right\|_1 && (5.2.6)\\
&= \left\| \sum_{n=0}^{\infty} \lambda_n^2 |n\rangle\langle n|_R \otimes \left[|n\rangle\langle n|_A - \sum_{k=0}^{n} \binom{n}{k} \eta^k (1-\eta)^{n-k} |k\rangle\langle k|_A \right] \right\|_1 && (5.2.7)\\
&= \sum_{n=0}^{\infty} \lambda_n^2 \left\| |n\rangle\langle n|_A - \sum_{k=0}^{n} \binom{n}{k} \eta^k (1-\eta)^{n-k} |k\rangle\langle k|_A \right\|_1 && (5.2.8)\\
&= \sum_{n=0}^{\infty} \lambda_n^2 \left[\sum_{k=0}^{n-1} \binom{n}{k} \eta^k (1-\eta)^{n-k} + 1 - \eta^n \right] && (5.2.9)\\
&= 2\left(1 - \sum_{n=0}^{\infty} \lambda_n^2 \eta^n\right) \ . && (5.2.10)
\end{aligned}
$$

The second equality follows from the action of a pure-loss channel on a number state. The third equality follows from (2.3.90). The fourth equality is a consequence of the direct-sum property the trace distance on classical-quantum states. The rest of the steps follow from basic algebraic manipulations.

Therefore, the energy-constrained diamond distance between $\mathcal{P}$ and $\widetilde{\mathcal{P}}^{\eta}$ reduces to the following optimization problem:

$$
\frac{1}{2}\|\mathcal{P} - \widetilde{\mathcal{P}}^{\eta}\|_{\diamond E} = \max_{\{\lambda_n^2\}_n : \sum_n \lambda_n^2 = 1, \sum_n n\lambda_n^2 \leq E} \left(1 - \sum_{n=0}^{\infty} \lambda_n^2 \eta^n\right) \ . \tag{5.2.11}
$$

The optimization in (5.2.11) can be solved by following a method introduced in [186]. We provide a proof for completeness. Suppose that $\sum_n n\lambda_n^2 = F$, $A_l = \sum_{n=0}^{\lfloor F \rfloor} \lambda_n^2$, $A_u =$

$\sum_{n=\lceil F\rceil}^{\infty}\lambda_n^2$, $F_l=\sum_{n=0}^{\lfloor F\rfloor}(\lambda_n^2/A_l)n$, and $F_u=\sum_{n=\lceil E\rceil}^{\infty}(\lambda_n^2/A_u)n$. Then it follows that

$$A_l+A_u=1, \tag{5.2.12}$$

$$F=A_lF_l+A_uF_u, \tag{5.2.13}$$

$$F_l\leq\lfloor F\rfloor, \tag{5.2.14}$$

$$F_u\geq\lceil F\rceil. \tag{5.2.15}$$

Consider the following chain of inequalities:

$$\sum_{n=0}^{\infty}\lambda_n^2\eta^n=A_l\sum_{n=0}^{\lfloor F\rfloor}\frac{\lambda_n^2}{A_l}\eta^n+A_u\sum_{n=\lceil F\rceil}^{\infty}\frac{\lambda_n^2}{A_u}\eta^n \tag{5.2.16}$$

$$\geq A_l\eta^{F_l}+A_u\eta^{F_u} \tag{5.2.17}$$

$$\geq\lambda_{\lfloor F\rfloor}^2\eta^{\lfloor F\rfloor}+\lambda_{\lceil F\rceil}^2\eta^{\lceil F\rceil} \tag{5.2.18}$$

$$=(1-\{F\})\eta^{\lfloor F\rfloor}+\{F\}\eta^{\lceil F\rceil}. \tag{5.2.19}$$

where the first inequality follows from the convexity of the function $x\rightarrow\eta^x$. The last inequality follows from the fact that the chord joining $(\lfloor F\rfloor,\eta^{\lfloor F\rfloor})$ and $(\lceil F\rceil,\eta^{\lceil F\rceil})$ is below the chord joining (A_l,η^{F_l}) and (A_u,η^{F_u}) due to the convexity of the function. Moreover, the energy of the initial state can be satisfied by taking $F_l=\lfloor F\rfloor$ and $F_u=\lceil F\rceil$, and the corresponding probability elements are given by $\lambda_{\lfloor F\rfloor}^2=1-\{F\}$ and $\lambda_{\lceil F\rceil}^2=\{F\}$.

Since (5.2.19) monotonically decreases with F, it implies that the solution to the optimization problem in (5.2.11) is given by a state that saturates the energy constraint. Therefore, the optimal state is given by (5.2.3). This completes the proof of (5.2.2).

Numerical results. Next, we perform numerical evaluations to analyze the accuracy in

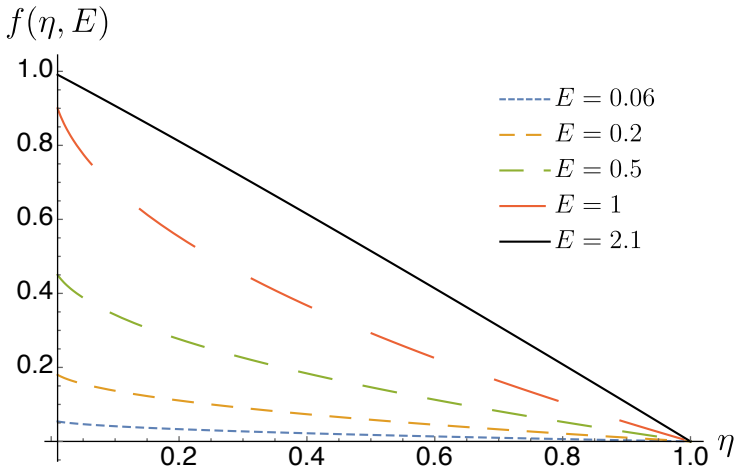

Figure 5.3: The figure plots the energy-constrained diamond distance $f(\eta, E)$ (5.2.20) between the ideal photodetector $\mathcal{P}$ and its experimental approximation $\widetilde{\mathcal{P}}^{\eta}$. In the figure, we select certain values of the energy constraint E, with the choices indicated next to the figure. In all the cases, $\widetilde{\mathcal{P}}^{\eta}$ simulates $\mathcal{P}$ with a high accuracy for values of $\eta \approx 1$. Moreover, for a fixed value of η, the simulation of $\mathcal{P}$ is more accurate for low values of the energy constraint on input states.

implementing $\mathcal{P}$ using $\widetilde{\mathcal{P}}^{\eta}$. Let

$$f(\eta, E) \equiv 1 - \left[(1 - \{E\})\eta^{\lfloor E \rfloor} + \{E\}\eta^{\lceil E \rceil}\right]. \tag{5.2.20}$$

In Figure 5.3, we plot $f(\eta, E)$ versus η for certain values of the energy constraint E. In particular, we find that for all values of E, the experimental approximation $\widetilde{\mathcal{P}}^{\eta}$ simulates the ideal photodetector $\mathcal{P}$ with a high accuracy for $\eta \approx 1$. Moreover, for a fixed value of η, the simulation of $\mathcal{P}$ is more accurate for low values of the energy constraint on input states.

Distinguishability of two noisy photodetectors. The next natural question to ask is how distinguishable one noisy photodetector is from another noisy photodetector. In particular, we now consider a task of distinguishing two noisy photodetectors $\widetilde{\mathcal{P}}^{\eta_1}$ and $\widetilde{\mathcal{P}}^{\eta_2}$, and calculate the energy-constrained sine distance between them. We provide a summary of the results below and subsequently provide proof details.

Since $\widetilde{\mathcal{P}}^{\eta_1}$ and $\widetilde{\mathcal{P}}^{\eta_2}$ are jointly phase covariant, pure states of the form in (5.1.8) are

optimal to distinguish them with respect to the energy-constrained sine distance. We then find that

$$C_E(\widetilde{\mathcal{P}}^{\eta_1}, \widetilde{\mathcal{P}}^{\eta_2}) = \sqrt{1 - [(1 - \{E\})\mu^{\lfloor E \rfloor} + \{E\}\mu^{\lceil E \rceil}]^2}\,, \tag{5.2.21}$$

where $\{E\} \equiv E - \lfloor E \rfloor$ and $\mu \equiv \sqrt{\eta_1 \eta_2} + \sqrt{(1-\eta_1)(1-\eta_2)}$. Moreover, the state that optimizes the energy-constrained sine distance in (5.2.21) is given by (5.2.3), which again implies that entanglement is not necessary for the optimal distinguishability of two noisy photodetectors.

Proof for (5.2.21). First note that the output of a noisy photodetector $\widetilde{\mathcal{P}}^{\eta}$ when the input state is ψ_{RA} in (5.1.8) is given by

$$\widetilde{\mathcal{P}}^{\eta}(\psi_{RA}) = (\mathcal{P} \circ \mathcal{L}^{\eta})(\psi_{RA}) \tag{5.2.22}$$

$$= \sum_{n} \sum_{k=0}^{n} \beta(\lambda_n, \eta, k) |n\rangle\langle n|_R \otimes |k\rangle\langle k|_A, \tag{5.2.23}$$

where

$$\beta(\lambda_n, \eta, k) = \lambda_n^2 \binom{n}{k} \eta_1^k (1-\eta_1)^{n-k} \tag{5.2.24}$$

are the eigenvalues of $\widetilde{\mathcal{P}}^{\eta}(\psi_{RA})$. Therefore, the fidelity between $\widetilde{\mathcal{P}}^{\eta_1}(\psi_{RA})$ and $\widetilde{\mathcal{P}}^{\eta_2}(\psi_{RA})$ is

given by

$$F(\widetilde{\mathcal{P}}^{\eta_1}(\psi_{RA}),\widetilde{\mathcal{P}}^{\eta_2}(\psi_{RA})) = \left[\mathrm{Tr}\left(\sqrt{\sqrt{\widetilde{\mathcal{P}}^{\eta_1}(\psi_{RA})}\widetilde{\mathcal{P}}^{\eta_2}(\psi_{RA})\sqrt{\widetilde{\mathcal{P}}^{\eta_1}(\psi_{RA})}}\right)\right]^2 \tag{5.2.25}$$

$$= \left[\sum_n \sum_{k=0}^{n} \sqrt{\beta(\lambda_n,\eta_1,k)\beta(\lambda_n,\eta_2,k)}\right]^2 \tag{5.2.26}$$

$$= \left[\sum_n \lambda_n^2 \sum_{k=0}^{n} \binom{n}{k} \sqrt{\eta_1\eta_2}^k \Big[(1-\eta_1)(1-\eta_2)\Big]^{n-k}\right]^2 \tag{5.2.27}$$

$$= \left[\sum_n \lambda_n^2 \Big(\sqrt{\eta_1\eta_2} + \sqrt{(1-\eta_1)(1-\eta_2)}\Big)^n\right]^2 \tag{5.2.28}$$

$$= \left[\sum_n \lambda_n^2 \mu^n\right]^2, \tag{5.2.29}$$

where

$$\mu = \sqrt{\eta_1\eta_2} + \sqrt{(1-\eta_1)(1-\eta_2)}. \tag{5.2.30}$$

Then from [190], we find that the energy-constrained sine distance between $\widetilde{\mathcal{P}}^{\eta_1}$ and $\widetilde{\mathcal{P}}^{\eta_2}$ is given by

$$C_E(\widetilde{\mathcal{P}}^{\eta_1},\widetilde{\mathcal{P}}^{\eta_2}) = \sqrt{1-\left[(1-\{E\})\mu^{\lfloor E\rfloor} + \{E\}\mu^{\lceil E\rceil}\right]^2}\,, \tag{5.2.31}$$

where $\{E\} = E - \lfloor E\rfloor$. Moreover, the state that optimizes the energy-constrained sine distance in (5.2.21) is given by (5.2.3), which proves that entanglement is not necessary for the optimal distinguishability of two noisy photodetectors.

5.3 Conclusion

In this chapter, using energy-constrained distinguishability measures, we quantified the accuracy in implementing continuous-variable (CV) quantum teleportation and a photodetector.

CV teleportation. We proposed an optimal test to characterize the performance of CV

teleportation in terms of the energy-constrained channel fidelity between ideal CV teleportation and its experimental approximation. We reduced the optimization problem of estimating the energy-constrained channel fidelity to a quadratic program with inequality constraints. Since, in general, optimization over an infinite number of variables is not possible, we defined the energy-constrained channel fidelity on a truncated Hilbert space, which reduces to a truncated version of the quadratic program with inequality constraints. We then showed that the objective function of the quadratic program is convex. As a consequence of the linearity of the inequality constraints and the convexity of the objective function, we found analytical solutions to the quadratic program by invoking the Karush–Kuhn–Tucker conditions. We then proved that these solutions to the energy-constrained channel fidelity on a truncated Hilbert space also optimize the energy-constrained channel fidelity defined over an infinite-dimensional separable Hilbert space.

Prior to our results, the accuracy in implementing CV teleportation was quantified by considering several input states, such as ensembles of coherent states, squeezed states, cat states, etc. We showed that instead, entangled superpositions of twin-Fock states are optimal to characterize the performance of CV teleportation. Thus, our result provides a benchmark for teleporting an unknown, energy-constrained state using CV quantum teleportation. Another interesting metric to quantify the accuracy in simulating ideal CV teleportation is the energy-constrained diamond distance between ideal CV teleportation and its experimental approximation. We leave the calculation of this quantity for future work.

Photodetectors. In this chapter, we also analytically calculated the energy-constrained diamond distance between the ideal photodetector and its experimental approximation. We modeled the noise in the experimental approximation of a photodetector as a pure-loss channel. Our main result here is that entanglement with a reference system is not required to quantify the accuracy in implementing a photodetector and the optimal input state is a mixture of photon number states. It is an interesting open question to determine the opti-

mal value of the energy-constrained distance measures when the noise in a photodetector is modeled as a thermal noise channel.

CHAPTER 6

CONCLUSION AND OPEN QUESTIONS

In this dissertation, we extensively studied several applications of energy-constrained distinguishability measures. Our results apply broadly to communication and computation tasks using continuous-variable quantum resources. In particular, we established several upper bounds on the quantum and private capacities of phase-insensitive, bosonic Gaussian channels. We described the importance of energy-constrained distinguishability measures by showing that bounds based on the approximate degradability of quantum channels can be tighter than all other upper bounds on capacities. We then studied applications of energy-constrained distance measures in assessing the performance of continuous-variable Gaussian logic gates. As a final application of energy-constrained distinguishability measures, we solved an open problem related to benchmarking CV quantum teleportation. We proved that the optimal state to distinguish ideal teleportation from its experimental approximation with respect to the energy-constrained channel fidelity is an entangled superposition of twin-Fock states. Thus our results quantify the worst-case error in teleporting a quantum state using CV quantum resources.

Below we summarize our results and several open problems.

Optimal rate of communication. In Chapter 3 we established several upper bounds on the ultimate rate of quantum and private communication using thermal, amplifier, and additive-noise channels. In particular, two upper bounds are based on the approximate degradability of quantum channels. These bounds depend on the energy-constrained distance between two particular Gaussian channels. Therefore, tighter bounds on capacities can be established by finding better estimates of the energy-constrained diamond distance between particular Gaussian channels. We now summarize open problems in the context of communication using bosonic Gaussian resources:

- As discussed in Chapters 3–5, in general, estimating the energy-constrained channel

divergences is a computationally challenging problem. Although we have developed numerical and analytical techniques in Chapters 4 and 5 to find good estimates of energy-constrained sine and diamond distances, it is not straightforward to apply these techniques to find approximate-degradable upper bounds on capacities. It is an interesting open question to further tighten approximate-degradable bounds on capacities of phase-insensitive Gaussian channels.

- Other ways to establish bounds on capacities of non-degradable quantum channels is to use notions of approximate anti-degradability, approximate entanglement-breakability, and approximate covariance (see [98] for a review on these techniques). Bounds based on these techniques also rely on the energy-constrained channel divergences between two particular Gaussian channels. Thus it is interesting to study these techniques for bounding capacities of CV Gaussian channels.

- In Chapter 3 we considered the communication setting where an infinite number of channel uses was allowed. It is an interesting open question to develop the notion of communication over bosonic Gaussian channels with energy constraints such that only a finite number of channel uses is allowed.

Continuous-variable quantum logic gates. In Chapter 4, we studied several notions of convergence for quantum channels. We then estimated the energy-constrained sine distance between ideal Gaussian unitaries and their experimental implementations. Our results imply that as the energy constraint on the input states to the channels increases, the accuracy in experimentally implementing a Gaussian unitary transformation decreases. There are several open research questions on this topic, summarized below.

- There are limitations to problems that can be solved using methods introduced in this dissertation. For example, we could estimate the energy-constrained sine distance between an ideal displacement and its experimental implementation. On the other

hand, it is still an open question to determine the energy-constrained sine distance between the ideal online squeezing operation and its experimental implementation. Similarly, we could only estimate the distance between an ideal SUM gate and its experimental implementation for a particular input state. Hence the problem of estimating the energy-constrained sine or diamond distance between the ideal SUM gate and its experimental implementation is still open.

- Other Gaussian operations of interest are homodyne and heterodyne measurements. It is an open problem to estimate the accuracy in implementing these operations.

- In Chapter 4, we studied only optical implementations of several Gaussian unitaries. It will be interesting to perform a similar study to quantify the accuracy in implementing Gaussian operations on other platforms such as vibrational modes of trapped ions [205] and microwave circuits [206].

- Another interesting direction is to use these results to study the error propagation in an experiment based on Gaussian unitaries.

- In this dissertation, we invoked properties of Gaussian unitaries and channels in order to solve the optimization involved in several energy-constrained channel divergences. It is an open problem to develop techniques to study the accuracy in implementing non-Gaussian unitaries.

Continuous-variable quantum teleportation. In Chapter 5, we proposed an optimal test to assess the performance of CV teleportation. In particular, we developed numerical and analytical methods to evaluate the energy-constrained channel fidelity between ideal CV teleportation and its experimental implementation. We now list some open problems related to CV teleportation:

- Is it possible to evaluate the energy-constrained diamond distance between CV teleportation and its experimental implementation? Using solutions of the quadratic

program in (5.1.19) and from (2.4.20), we get bounds on the energy-constrained diamond distance between CV teleportation and its experimental implementation. Results of a similar spirit appeared recently in [91].

- How does the accuracy in implementing CV teleportation affect other applications where CV teleportation is used, such as error correction, quantum networks, and quantum key distribution?

Optimization problems. In this dissertation, we solved several optimization problems.

- As summarized in Remark 79, any energy-constrained optimization problem – with optimization over quantum states – based on quantum channels would have thermal-state input saturating the energy constraint as an optimal input state if the following conditions hold: 1) The objective function being optimized is invariant with respect to local unitaries and concave in the input state. 2) The channel is phase and displacement covariant. It will be interesting to find further applications of this result.

- Similarly, in Section 3.8, we solved a general Gaussian optimization problem, where we showed that for two Gaussian channels that are jointly phase and displacement covariant, the Gaussian energy-constrained generalized channel divergence is achieved by a two-mode squeezed vacuum state that saturates the energy constraint. An interesting question to answer is for which Gaussian channels the two-mode squeezed vacuum state that saturates the energy constraint is an optimal state among all states for several energy-constrained, generalized channel divergences.

- In Chapter 4 (see Eq. (4.1.67)), we presented a semidefinite program to estimate the energy-constrained diamond distance between two channels on a truncated infinite-dimensional separable Hilbert space. Similarly, in Chapter 5 (see Eq. (5.1.30)) we estimated the energy-constrained channel fidelity between two particular Gaussian channels by first solving a quadratic program on a truncated Hilbert space and then

by invoking KKT conditions. It will be interesting to find further examples where these techniques can be directly used.

REFERENCES

[1] Michael A. Nielsen and Isaac L. Chuang. *Quantum Computation and Quantum Information: 10th Anniversary Edition*. Cambridge University Press, Cambridge, UK, 2010.

[2] Daniel R. Simon. On the power of quantum computation. *SIAM Journal on Computing*, 26(5):1474–1483, October 1997.

[3] Peter W. Shor. Polynomial-time algorithms for prime factorization and discrete logarithms on a quantum computer. *SIAM Review*, 41(2):303–332, 1999.

[4] Michel Boyer, Gilles Brassard, Peter Høyer, and Alain Tapp. Tight bounds on quantum searching. *Fortschritte der Physik: Progress of Physics*, 46(4-5):493–505, April 1999. arXiv:quant-ph/9605034.

[5] Dave Wecker, Matthew B. Hastings, Nathan Wiebe, Bryan K. Clark, Chetan Nayak, and Matthias Troyer. Solving strongly correlated electron models on a quantum computer. *Physical Review A*, 92:062318, December 2015. arXiv:1506.05135.

[6] Dave Wecker, Bela Bauer, Bryan K. Clark, Matthew B. Hastings, and Matthias Troyer. Gate-count estimates for performing quantum chemistry on small quantum computers. *Physical Review A*, 90:022305, August 2014. arXiv:1312.1695.

[7] Stephen P. Jordan, Keith SM Lee, and John Preskill. Quantum algorithms for quantum field theories. *Science*, 336(6085):1130–1133, June 2012. arXiv:1111.3633.

[8] Mark M. Wilde. *Quantum Information Theory*. Cambridge University Press, 2nd edition, 2017. arXiv:1106.1445v7.

[9] Charles H. Bennett and Gilles Brassard. Quantum cryptography: Public key distribution and coin tossing. *Theoretical Computer Science*, 560(1):7–11, December 2020. arXiv:2003.06557.

[10] Peter W. Shor and John Preskill. Simple proof of security of the bb84 quantum key distribution protocol. *Physical Review Letters*, 85:441–444, July 2000. arXiv:quant-ph/0003004.

[11] Charles H. Bennett, Gilles Brassard, Claude Crépeau, Richard Jozsa, Asher Peres, and William K. Wootters. Teleporting an unknown quantum state via dual classical and Einstein-Podolsky-Rosen channels. *Physical Review Letters*, 70(13):1895, March 1993.

[12] Michael A. Nielsen, Emanuel Knill, and Raymond Laflamme. Complete quantum teleportation using nuclear magnetic resonance. *Nature*, 396(6706):52–55, November 1998. arXiv:quant-ph/9811020.

[13] Olivier Landry, J. A. W. van Houwelingen, Alexios Beveratos, Hugo Zbinden, and Nicolas Gisin. Quantum teleportation over the Swisscom telecommunication network. *Journal of the Optical Society of America B*, 24(2):398–403, February 2007. arXiv:quant-ph/0605010.

[14] Xiao-Song Ma, Thomas Herbst, Thomas Scheidl, Daqing Wang, Sebastian Kropatschek, William Naylor, Bernhard Wittmann, Alexandra Mech, Johannes Kofler, Elena Anisimova, et al. Quantum teleportation over 143 kilometres using active feed-forward. *Nature*, 489(7415):269–273, September 2012. arXiv:1205.3909.

[15] Xiao-Hui Bao, Xiao-Fan Xu, Che-Ming Li, Zhen-Sheng Yuan, Chao-Yang Lu, and Jian-Wei Pan. Quantum teleportation between remote atomic-ensemble quantum memories. *Proceedings of the National Academy of Sciences*, 109(50):20347–20351, December 2012. arXiv:1211.2892.

[16] Shuntaro Takeda, Takahiro Mizuta, Maria Fuwa, Peter Van Loock, and Akira Furusawa. Deterministic quantum teleportation of photonic quantum bits by a hybrid technique. *Nature*, 500(7462):315–318, August 2013. arXiv:1402.4895.

[17] Christian Nölleke, Andreas Neuzner, Andreas Reiserer, Carolin Hahn, Gerhard Rempe, and Stephan Ritter. Efficient teleportation between remote single-atom quantum memories. *Physical Review Letters*, 110(14):140403, April 2013. arXiv:1212.3127.

[18] Benjamin J. Metcalf, Justin B. Spring, Peter C. Humphreys, Nicholas Thomas-Peter, Marco Barbieri, W. Steven Kolthammer, Xian-Min Jin, Nathan K. Langford, Dmytro Kundys, James C. Gates, et al. Quantum teleportation on a photonic chip. *Nature Photonics*, 8(10):770–774, September 2014. arXiv:1409.4267.

[19] Wolfgang Pfaff, Bas J. Hensen, Hannes Bernien, Suzanne B. van Dam, Machiel S. Blok, Tim H. Taminiau, Marijn J. Tiggelman, Raymond N. Schouten, Matthew Markham, Daniel J. Twitchen, et al. Unconditional quantum teleportation between distant solid-state quantum bits. *Science*, 345(6196):532–535, August 2014. arXiv:1404.4369.

[20] Xi-Lin Wang, Xin-Dong Cai, Zu-En Su, Ming-Cheng Chen, Dian Wu, Li Li, Nai-Le Liu, Chao-Yang Lu, and Jian-Wei Pan. Quantum teleportation of multiple degrees of freedom of a single photon. *Nature*, 518(7540):516–519, February 2015. arXiv:1409.7769.

[21] Stefano Pirandola, Jens Eisert, Christian Weedbrook, Akira Furusawa, and Samuel L. Braunstein. Advances in quantum teleportation. *Nature Photonics*, 9(10):641–652, September 2015. arXiv:1505.07831.

[22] Ji-Gang Ren, Ping Xu, Hai-Lin Yong, Liang Zhang, Sheng-Kai Liao, Juan Yin, Wei-Yue Liu, Wen-Qi Cai, Meng Yang, Li Li, et al. Ground-to-satellite quantum teleportation. *Nature*, 549(7670):70–73, August 2017. arXiv:1707.00934.

[23] Isaac L. Chuang and Yoshihisa Yamamoto. A simple quantum computer. *Physical Review A*, 52(5):3489, November 1995. arXiv:quant-ph/9505011.

[24] Emanuel Knill, Raymond Laflamme, and Gerard J. Milburn. A scheme for efficient quantum computation with linear optics. *Nature*, 409:46–52, January 2001. arXiv:quant-ph/0006088.

[25] Daniel Gottesman, Alexei Kitaev, and John Preskill. Encoding a qubit in an oscillator. *Physical Review A*, 64(1):012310, June 2001. arXiv:quant-ph/0008040.

[26] Pieter Kok, William J. Munro, Kae Nemoto, Timothy C. Ralph, Jonathan P. Dowling, and Gerard J. Milburn. Linear optical quantum computing with photonic qubits. *Reviews of Modern Physics*, 79(1):135, January 2007. arXiv:quant-ph/0512071.

[27] Seth Lloyd and Samuel L. Braunstein. Quantum computation over continuous variables. *Physical Review Letters*, 82(8):1784–1787, February 1999. arXiv:quant-ph/9810082.

[28] Seth Lloyd. *Hybrid Quantum computing. In: Braunstein S.L., Pati A.K. (eds) Quantum Information with Continuous Variables*. Springer, Dordrecht, 2003.

[29] Peter Van Loock. Optical hybrid approaches to quantum information. *Laser & Photonics Reviews*, 5:167, February 2011. arXiv:1002.4788.

[30] Akira Furusawa and Peter Van Loock. *Quantum Teleportation and Entanglement: A Hybrid Approach to Optical Quantum Information Processing*. Wiley-VCH, May 2011.

[31] Valerio Scarani, Helle Bechmann-Pasquinucci, Nicolas J. Cerf, Miloslav Dušek, Norbert Lütkenhaus, and Momtchil Peev. The security of practical quantum key distribution. *Reviews of Modern Physics*, 81:1301–1350, September 2009. arXiv:0802.4155.

[32] Lev Vaidman. Teleportation of quantum states. *Physical Review A*, 49(2):1473–1476, February 1994. arXiv:hep-th/9305062.

[33] Susana F. Huelga, Martin B. Plenio, and Joan A. Vaccaro. Remote control of restricted sets of operations: Teleportation of angles. *Physical Review A*, 65(4):042316, April 2002. arXiv:quant-ph/0107110.

[34] Susana F. Huelga, Joan A. Vaccaro, Anthony Chefles, and Martin B. Plenio. Quantum remote control: Teleportation of unitary operations. *Physical Review A*, 63(4):042303, March 2001. arXiv:quant-ph/0005061.

[35] Satoshi Ishizaka and Tohya Hiroshima. Asymptotic teleportation scheme as a universal programmable quantum processor. *Physical Review Letters*, 101(24):240501, December 2008. arXiv:0807.4568.

[36] Satoshi Ishizaka and Tohya Hiroshima. Quantum teleportation scheme by selecting one of multiple output ports. *Physical Review A*, 79(4):042306, April 2009. arXiv:0901.2975.

[37] Samuel L. Braunstein and H. J. Kimble. Teleportation of continuous quantum variables. *Physical Review Letters*, 80(4):869, January 1998.

[38] Seth Lloyd. Capacity of the noisy quantum channel. *Physical Review A*, 55(3):1613–1622, March 1997. arXiv:quant-ph/9604015.

[39] Peter W. Shor. The quantum channel capacity and coherent information. In *lecture notes, MSRI Workshop on Quantum Computation*, 2002.

[40] Ning Cai, Andreas Winter, and Raymond W. Yeung. Quantum privacy and quantum wiretap channels. *Problems of Information Transmission*, 40(4):318–336, October 2004.

[41] Igor Devetak. The private classical capacity and quantum capacity of a quantum channel. *IEEE Transactions on Information Theory*, 51(1):44–55, January 2005. arXiv:quant-ph/0304127.

[42] Igor Devetak and Peter W. Shor. The capacity of a quantum channel for simultaneous transmission of classical and quantum information. *Communications in Mathematical Physics*, 256(2):287–303, June 2005. arXiv:quant-ph/0311131.

[43] Graeme Smith. Private classical capacity with a symmetric side channel and its application to quantum cryptography. *Physical Review A*, 78(2):022306, August 2008. arXiv:0705.3838.

[44] David P. DiVincenzo, Peter W. Shor, and John A. Smolin. Quantum-channel capacity of very noisy channels. *Physical Review A*, 57(2):830–839, February 1998. arXiv:quant-ph/9706061.

[45] Graeme Smith and John A. Smolin. Degenerate quantum codes for Pauli channels. *Physical Review Letters*, 98(3):030501, January 2007. arXiv:quant-ph/0604107.

[46] Graeme Smith, Joseph M. Renes, and John A. Smolin. Structured codes improve the Bennett-Brassard-84 quantum key rate. *Physical Review Letters*, 100(17):170502, April 2008. arXiv:quant-ph/0607018.

[47] Toby Cubitt, David Elkouss, William Matthews, Maris Ozols, David Pérez-García, and Sergii Strelchuk. Unbounded number of channel uses are required to see quantum capacity. *Nature Communications*, 6:7739, March 2015. arXiv:1408.5115.

[48] David Elkouss and Sergii Strelchuk. Superadditivity of private information for any number of uses of the channel. *Physical Review Letters*, 115(4):040501, July 2015. arXiv:1502.05326.

[49] Graeme Smith and Jon Yard. Quantum communication with zero-capacity channels. *Science*, 321(5897):1812–1815, September 2008. arXiv:0807.4935.

[50] Graeme Smith, John A. Smolin, and Jon Yard. Quantum communication with Gaussian channels of zero quantum capacity. *Nature Photonics*, 5:624–627, August 2011. arXiv:1102.4580.

[51] Carlton M. Caves. Quantum limits on noise in linear amplifiers. *Physical Review D*, 26(8):1817, October 1982.

[52] Horace Yuen and Jeffrey H. Shapiro. Optical communication with two-photon coherent states–Part I: Quantum-state propagation and quantum-noise. *IEEE Transactions on Information Theory*, 24(6):657–668, November 1978.

[53] Jeffrey H. Shapiro. The quantum theory of optical communications. *IEEE Journal of Selected Topics in Quantum Electronics*, 15(6):1547–1569, November 2009.

[54] Filip Rozpedek, Kenneth Goodenough, Jeremy Ribeiro, Norbert Kalb, Valentina Caprara Vivoli, Andreas Reiserer, Ronald Hanson, Stephanie Wehner, and David Elkouss. Parameter regimes for a single sequential quantum repeater. *Quantum Science and Technology*, 3:034002, April 2018. arXiv:1705.00043v2.

[55] Ryo Namiki and Takuya Hirano. Practical limitation for continuous-variable quantum cryptography using coherent states. *Physical Review Letters*, 92(11):117901, March 2004. arXiv:quant-ph/0403115.

[56] Jérôme Lodewyck, Thierry Debuisschert, Rosa Tualle-Brouri, and Philippe Grangier. Controlling excess noise in fiber-optics continuous-variable quantum key distribution. *Physical Review A*, 72(5):050303, November 2005. arXiv:quant-ph/0511104.

[57] Aashish A. Clerk, Michel H. Devoret, Steven M. Girvin, Florian Marquardt, and Robert J. Schoelkopf. Introduction to quantum noise, measurement, and amplification. *Reviews of Modern Physics*, 82(2):1155, April 2010. arXiv:0810.4729.

[58] Gerald T. Moore. Quantum theory of the electromagneticfield in a variable-length one-dimensional cavity. *Journal of Mathematical Physics*, 11(9):2679–2691, September 1970.

[59] William G. Unruh. Notes on black-hole evaporation. *Physical Review D*, 14(4):870, August 1976.

[60] Stephen W. Hawking. Black holes in general relativity. *Communications in Mathematical Physics*, 25(2):152–166, June 1972.

[61] Michael J. W. Hall. Gaussian noise and quantum-optical communication. *Physical Review A*, 50(4):3295, October 1994.

[62] Mark M. Wilde and Haoyu Qi. Energy-constrained private and quantum capacities of quantum channels. *IEEE Transactions on Information Theory*, 64(12):7802–7827, December 2018. arXiv:1609.01997.

[63] Saikat Guha, Jeffrey H. Shapiro, and Baris I. Erkmen. Capacity of the bosonic wiretap channel and the entropy photon-number inequality. In *Proceedings of the IEEE International Symposium on Information Theory*, pages 91–95, Toronto, Ontario, Canada, 2008. IEEE. arXiv:0801.0841.

[64] Mark M. Wilde, Patrick Hayden, and Saikat Guha. Quantum trade-off coding for bosonic communication. *Physical Review A*, 86(6):062306, December 2012. arXiv:1105.0119.

[65] Haoyu Qi and Mark M. Wilde. Capacities of quantum amplifier channels. *Physical Review A*, 95(1):012339, January 2017. arXiv:1605.04922.

[66] David Sutter, Volkher B. Scholz, Andreas Winter, and Renato Renner. Approximate degradable quantum channels. *IEEE Transactions on Information Theory*, 63(12):7832–7844, December 2017. arXiv:1412.0980.

[67] Samuel L. Braunstein and Peter Van Loock. Quantum information with continuous variables. *Reviews of Modern Physics*, 77(2):513–577, June 2005. arXiv:quant-ph/0410100.

[68] Alessio Serafini. *Quantum Continuous Variables: A Primer of Theoretical Methods*. CRC Press, 2017.

[69] Seckin Sefi and Peter Van Loock. How to decompose arbitrary continuous-variable quantum operations. *Physical Review Letters*, 117(17):170501, October 2011. arXiv:1010.0326.

[70] Matteo G. A. Paris. Displacement operator by beamsplitter. *Physics Letters A*, 217(2-3):78–80, April 1996.

[71] Radim Filip, Petr Marek, and Ulrik L. Andersen. Measurement-induced continuous-variable quantum information. *Physical Review A*, 71(4):042308, April 2005.

[72] Jun-ichi Yoshikawa, Toshiki Hayashi, Takayuki Akiyama, Nobuyuki Takei, Alexander Huck, Ulrik L. Andersen, and Akira Furusawa. Demonstration of deterministic and high fidelity squeezing of quantum information. *Physical Review A*, 76(6):060301(R), December 2007. arXiv:quant-ph/0702049.

[73] Jun-ichi Yoshikawa, Yoshichika Miwa, Alexander Huck, Ulrik L. Andersen, Peter Van Loock, and Akira Furusawa. Demonstration of a quantum nondemolition sum gate. *Physical Review Letters*, 101(25):250501, December 2008. arXiv:0808.0551.

[74] Stephen D. Bartlett, Barry C. Sanders, Samuel L. Braunstein, and Kae Nemoto. Efficient classical simulation of continuous variable quantum information processes. *Physical Review Letters*, 88(9):097904, March 2002. arXiv:quant-ph/0109047.

[75] Sze M. Tan. Confirming entanglement in continuous variable quantum teleportation. *Physical Review A*, 60(4):2752–2758, October 1999.

[76] Samuel L. Braunstein, Christopher A. Fuchs, and H. Jeff Kimble. Criteria for continuous-variable quantum teleportation. *Journal of Modern Optics*, 47(2-3):267–278, July 2000. arXiv:quant-ph/9910030.

[77] P. van Loock and Samuel L. Braunstein. Unconditional teleportation of continuous-variable entanglement. *Physical Review A*, 61(1):010302, December 1999. arXiv:quant-ph/9906075.

[78] Samuel L. Braunstein, Christopher A. Fuchs, H. Jeff Kimble, and Peter van Loock. Quantum versus classical domains for teleportation with continuous variables. *Physical Review A*, 64(2):022321, July 2001. arXiv:quant-ph/0012001.

[79] Frédéric Grosshans and Philippe Grangier. Quantum cloning and teleportation criteria for continuous quantum variables. *Physical Review A*, 64(1):010301, June 2001. arXiv:quant-ph/0012121.

[80] Tyler J. Johnson, Stephen D. Bartlett, and Barry C. Sanders. Continuous-variable quantum teleportation of entanglement. *Physical Review A*, 66(4):042326, October 2002. arXiv:quant-ph/0204011.

[81] Klemens Hammerer, Michael M. Wolf, Eugene Simon Polzik, and J. Ignacio Cirac. Quantum benchmark for storage and transmission of coherent states. *Physical Review Letters*, 94(15):150503, April 2005. arXiv:quant-ph/0409109.

[82] Gerardo Adesso and Giulio Chiribella. Quantum benchmark for teleportation and storage of squeezed states. *Physical Review Letters*, 100(17):170503, April 2008. arXiv:0711.3608.

[83] Noriyuki Lee, Hugo Benichi, Yuishi Takeno, Shuntaro Takeda, James Webb, Elanor Huntington, and Akira Furusawa. Teleportation of nonclassical wave packets of light. *Science*, 332(6027):330–333, April 2011. arXiv:1205.6253.

[84] Giulio Chiribella and Gerardo Adesso. Quantum benchmarks for pure single-mode Gaussian states. *Physical Review Letters*, 112(1):010501, January 2014. arXiv:1308.2146.

[85] Kaushik P. Seshadreesan, Jonathan P. Dowling, and Girish S. Agarwal. Non-Gaussian entangled states and quantum teleportation of Schrödinger-cat states. *Physica Scripta*, 90(7):074029, June 2015. arXiv:1306.3168.

[86] William Karush. Minima of functions of several variables with inequalities as side conditions. In *Traces and Emergence of Nonlinear Programming*, pages 217–245. Springer, 2014.

[87] Harold W. Kuhn and Albert W. Tucker. Nonlinear programming. In *Proceedings of the Second Berkeley Symposium on Mathematical Statistics and Probability*, pages 481–492, Berkeley, California, 1951. University of California Press.

[88] Wolfgang P. Schleich. *Quantum Optics in Phase Space*. Wiley-VCH Verlag, Berlin, Germany, 2001.

[89] Alexander S. Holevo. *Quantum Systems, Channels, Information*. de Gruyter Studies in Mathematical Physics (Book 16). de Gruyter, November 2012.

[90] Kunal Sharma, Barry C. Sanders, and Mark M. Wilde. Optimal tests for continuous-variable quantum teleportation and photodetectors. December 2020. arXiv:2012.02754.

[91] Ludovico Lami. Quantum data hiding with continuous variable systems. February 2021. arXiv:2102.01100

[92] Kunal Sharma and Mark M. Wilde. Characterizing the performance of continuous-variable Gaussian quantum gates. *Physical Review Research*, 2(1):013126, February 2020. arXiv:1810.12335.

[93] Kunal Sharma, Mark M. Wilde, Sushovit Adhikari, and Masahiro Takeoka. Bounding the energy-constrained quantum and private capacities of phase-insensitive bosonic Gaussian channels. *New Journal of Physics*, 20:063025, June 2018. arXiv:1708.07257.

[94] Zoë Holmes, Kunal Sharma, M. Cerezo, and Patrick J. Coles. Connecting ansatz expressibility to gradient magnitudes and barren plateaus. January 2021. arXiv:2101.02138.

[95] Daiqin Su, Robert Israel, Kunal Sharma, Haoyu Qi, Ish Dhand, and Kamil Brádler. Error mitigation on a near-term quantum photonic device. August 2020. arXiv:2008.06670.

[96] Samson Wang, Enrico Fontana, Marco Cerezo, Kunal Sharma, Akira Sone, Lukasz Cincio, and Patrick J. Coles. Noise-induced barren plateaus in variational quantum algorithms. February 2021. arXiv:2007.14384.

[97] Kunal Sharma, M. Cerezo, Zoë Holmes, Lukasz Cincio, Andrew Sornborger, and Patrick J. Coles. Reformulation of the no-free-lunch theorem for entangled data sets. July 2020. arXiv:2007.04900.

[98] Sumeet Khatri, Kunal Sharma, and Mark M. Wilde. Information-theoretic aspects of the generalized amplitude-damping channel. *Physical Review A*, 102(1):012401, July 2020. arXiv:1903.07747.

[99] Kunal Sharma, Marco Cerezo, Lukasz Cincio, and Patrick J. Coles. Trainability of dissipative perceptron-based quantum neural networks. May 2020. arXiv:2005.12458.

[100] Kunal Sharma, Sumeet Khatri, Marco Cerezo, and Patrick J. Coles. Noise resilience of variational quantum compiling. *New Journal of Physics*, 22(4):043006, April 2020. arXiv:1908.04416.

[101] M. Cerezo, Kunal Sharma, Andrew Arrasmith, and Patrick J. Coles. Variational quantum state eigensolver. April 2020. arXiv:2004.01372.

[102] Kunal Sharma, Eyuri Wakakuwa, and Mark M. Wilde. Conditional quantum one-time pad. *Physical Review Letters*, 124(5):050503, February 2020. arXiv:1703.02903.

[103] Haoyu Qi, Kunal Sharma, and Mark M. Wilde. Entanglement-assisted private communication over quantum broadcast channels. *Journal of Physics A: Mathematical and Theoretical*, 51(37):374001, September 2018. arXiv:1803.03976.

[104] Teiko Heinosaari and Mário Ziman. *The Mathematical Language of Quantum Theory: From Uncertainty to Entanglement*. Cambridge University Press, 2011.

[105] Mark M. Wilde. Gaussian quantum information. 2019. Lecture notes.

[106] Alfred Wehrl. Three theorems about entropy and convergence of density matrices. *Reports on Mathematical Physics*, 10(2):159–163, October 1976.

[107] Valentina Baccetti and Matt Visser. Infinite Shannon entropy. *Journal of Statistical Mechanics: Theory and Experiment*, 2013(04):P04010, April 2013. arXiv:1212.5630.

[108] Harold Falk. Inequalities of J. W. Gibbs. *American Journal of Physics*, 38(7):858–869, July 1970.

[109] Göran Lindblad. Entropy, information and quantum measurements. *Communications in Mathematical Physics*, 33(4):305–322, December 1973.

[110] Göran Lindblad. Completely positive maps and entropy inequalities. *Communications in Mathematical Physics*, 40(2):147–151, June 1975.

[111] Benjamin Schumacher and Michael A. Nielsen. Quantum data processing and error correction. *Physical Review A*, 54(4):2629–2635, October 1996. arXiv:quant-ph/9604022.

[112] Alexander S. Holevo and Maksim E. Shirokov. Mutual and coherent information for infinite-dimensional quantum channels. *Problems of Information Transmission*, 46(3):201–218, September 2010. arXiv:1004.2495.

[113] Anna A. Kuznetsova. Conditional entropy for infinite-dimensional quantum systems. *Theory of Probability & Its Applications*, 55(4):709–717, November 2011. arXiv:1004.4519.

[114] Andreas Winter. Tight uniform continuity bounds for quantum entropies: conditional entropy, relative entropy distance and energy constraints. *Communications in Mathematical Physics*, 347(1):291–313, October 2016. arXiv:1507.07775.

[115] R. Simon, N. Mukunda, and Biswadeb Dutta. Quantum-noise matrix for multimode systems: $U(n)$ invariance, squeezing, and normal forms. *Physical Review A*, 49(3):1567–1583, March 1994.

[116] Albert Einstein, Boris Podolsky, and Nathan Rosen. Can quantum-mechanical description of physical reality be considered complete? *Physical Review*, 47(10):777, May 1935.

[117] Mark M. Wilde. Strong and uniform convergence in the teleportation simulation of bosonic Gaussian channels. *Physical Review A*, 97(6):062305, June 2018. arXiv:1712.00145.

[118] Alexander I. Lvovsky. *Photonics: Scientific Foundations, Technology and Applications*, volume 1, chapter Squeezed light, pages 121–163. John Wiley and Sons, Inc., 2015. arXiv:1401.4118.

[119] Carlton M. Caves. Quantum mechanical noise in an interferometer. *Physical Review D*, 23(8):1693–1708, April 1981.

[120] Samuel L. Braunstein. Error correction with continuous quantum variables. *Physical Review Letters*, 80(18):4084, May 1998. arXiv:quant-ph/9711049.

[121] Seth Lloyd and Jean-Jacques E. Slotine. Analog quantum error correction. *Physical Review Letters*, 80(18):4088, May 1998. arXiv:quant-ph/9711021.

[122] Mark M. Wilde, Hari Krovi, and Todd A. Brun. Coherent communication with continuous quantum variables. *Physical Review A*, 75(6):060303(R), June 2007. arXiv:quant-ph/0612170.

[123] Mark M. Wilde, Todd A. Brun, Jonathan P. Dowling, and Hwang Lee. Coherent communication with linear optics. *Physical Review A*, 77(2):022321, February 2008. arXiv:0709.3852.

[124] Filippo Caruso, Jens Eisert, Vittorio Giovannetti, and Alexander S. Holevo. Multimode bosonic Gaussian channels. *New Journal of Physics*, 10(8):083030, August 2008. arXiv:0804.0511.

[125] Michal Horodecki, Peter W. Shor, and Mary Beth Ruskai. Entanglement breaking channels. *Reviews in Mathematical Physics*, 15(6):629–641, 2003. arXiv:quant-ph/0302031.

[126] Alexander S. Holevo. Entanglement-breaking channels in infinite dimensions. *Problems of Information Transmission*, 44(3):171–184, September 2008. arXiv:0802.0235.

[127] Filippo Caruso, Vittorio Giovannetti, and Alexander S. Holevo. One-mode bosonic Gaussian channels: a full weak-degradability classification. *New Journal of Physics*, 8(12):310, December 2006. arXiv:quant-ph/0609013.

[128] Raul Garcia-Patron, Carlos Navarrete-Benlloch, Seth Lloyd, Jeffrey H. Shapiro, and Nicolas J. Cerf. Majorization theory approach to the Gaussian channel minimum entropy conjecture. *Physical Review Letters*, 108(11):110505, March 2012. arXiv:1111.1986.

[129] Armin Uhlmann. The "transition probability" in the state space of a *-algebra. *Reports on Mathematical Physics*, 9(2):273–279, April 1976.

[130] Alexey E. Rastegin. Relative error of state-dependent cloning. *Physical Review A*, 66(4):042304, October 2002.

[131] Alexey E. Rastegin. A lower bound on the relative error of mixed-state cloning and related operations. *Journal of Optics B: Quantum and Semiclassical Optics*, 5(6):S647–S650, October 2003. arXiv:quant-ph/0208159.

[132] Alexey E. Rastegin. Sine distance for quantum states. February 2006. arXiv:quant-ph/0602112.

[133] Alexei Gilchrist, Nathan K. Langford, and Michael A. Nielsen. Distance measures to compare real and ideal quantum processes. *Physical Review A*, 71(6):062310, June 2005. arXiv:quant-ph/0408063v2.

[134] Christopher A. Fuchs and Jeroen van de Graaf. Cryptographic distinguishability measures for quantum mechanical states. *IEEE Transactions on Information Theory*, 45(4):1216–1227, May 1998. arXiv:quant-ph/9712042.

[135] Robert T. Powers and Erling Størmer. Free states of the canonical anticommutation relations. *Communications in Mathematical Physics*, 16(1):1–33, March 1970.

[136] Alexei Y. Kitaev. Quantum computations: algorithms and error correction. *Russian Mathematical Surveys*, 52(6):1191–1249, December 1997.

[137] Maxim E. Shirokov. Energy-constrained diamond norms and their use in quantum information theory. *Problems of Information Transmission*, 54(1):20–33, April 2018. arXiv:1706.00361.

[138] Andreas Winter. Energy-constrained diamond norm with applications to the uniform continuity of continuous variable channel capacities. December 2017. arXiv:1712.10267.

[139] Maxim E. Shirokov. Uniform continuity bounds for information characteristics of quantum channels depending on input dimension and on input energy. *Journal of Physics A: Mathematical and Theoretical*, 52(1):014001, December 2018. arXiv:1610.08870.

[140] Maxim E. Shirokov and Alexander S. Holevo. On approximation of quantum channels. *Problems of Information Transmission*, 44(2):73–90, November 2008. arXiv:0711.2245.

[141] Ludovico Lami, Krishna Kumar Sabapathy, and Andreas Winter. All phase-space linear bosonic channels are approximately Gaussian dilatable. *New Journal of Physics*, 20:113012, November 2018. arXiv:1806.11042.

[142] Debbie Leung and Graeme Smith. Continuity of quantum channel capacities. *Communications in Mathematical Physics*, 292(1):201–215, November 2009. arXiv:0810.4931.

[143] Stephen P. Boyd and Lieven Vandenberghe. *Convex Optimization*. Cambridge University Press, 2004.

[144] Robert König and Graeme Smith. Classical capacity of quantum thermal noise channels to within 1.45 bits. *Physical Review Letters*, 110(4):040501, January 2013. arXiv:1207.0256.

[145] Michael M. Wolf and David Pérez-García. Quantum capacities of channels with small environment. *Physical Review A*, 75(1):012303, January 2007. arXiv:quant-ph/0607070.

[146] Graeme Smith and John A. Smolin. Additive extensions of a quantum channel. In *2008 IEEE Information Theory Workshop*, pages 368–372, May 2008.

[147] Alexander S. Holevo and Reinhard F. Werner. Evaluating capacities of bosonic Gaussian channels. *Physical Review A*, 63(3):032312, February 2001. arXiv:quant-ph/9912067.

[148] Matteo Rosati, Andrea Mari, and Vittorio Giovannetti. Narrow bounds for the quantum capacity of thermal attenuators. *Nature Communications*, 9(1):1–9, October 2018. arXiv:1801.04731.

[149] Kyungjoo Noh, Victor V. Albert, and Liang Jiang. Improved quantum capacity bounds of Gaussian loss channels and achievable rates with Gottesman-Kitaev-Preskill codes. *IEEE Transactions on Information Theory*, 65(4):2563–2582, October 2018. arXiv:1801.07271.

[150] Kunal Sharma, Mark M. Wilde, Sushovit Adhikari, and Masahiro Takeoka. Unpublished notes available upon request, August 2017.

[151] Noah Davis, Maksim E. Shirokov, and Mark M. Wilde. Energy-constrained two-way assisted private and quantum capacities of quantum channels. *Physical Review A*, 97:062310, June 2018. arXiv:1801.08102.

[152] Graeme Smith and John A. Smolin. An exactly solvable model for quantum communications. *Nature*, 504:263–267, December 2013. arXiv:1211.1956.

[153] Felix Leditzky, Eneet Kaur, Nilanjana Datta, and Mark M. Wilde. Approaches for approximate additivity of the Holevo information of quantum channels. *Physical Review A*, 97(1):012332, January 2018. arXiv:1709.01111.

[154] Robert Alicki. Isotropic quantum spin channels and additivity questions. February 2004. arXiv:quant-ph/0402080.

[155] Alexander S. Holevo. The entropy gain of infinite-dimensional quantum evolutions. *Doklady Mathematics*, 82(2):730–731, October 2010. arXiv:1003.5765.

[156] Alexander S. Holevo. Entropy gain and the Choi-Jamiolkowski correspondence for infinite-dimensional quantum evolutions. *Theoretical and Mathematical Physics*, 166(1):123–138, January 2011.

[157] Alexander S. Holevo. The entropy gain of quantum channels. In *2011 IEEE International Symposium on Information Theory Proceedings*, pages 289–292, July 2011.

[158] Elliott H. Lieb and Mary Beth Ruskai. Proof of the strong subadditivity of quantum-mechanical entropy. *Journal of Mathematical Physics*, 14(12):1938–1941, December 1973.

[159] Elliott H. Lieb and Mary Beth Ruskai. A fundamental property of quantum-mechanical entropy. *Physical Review Letters*, 30(10):434–436, March 1973.

[160] Michael M. Wolf, David Pérez-García, and Geza Giedke. Quantum capacities of bosonic channels. *Physical Review Letters*, 98(13):130501, March 2007. arXiv:quant-ph/0606132.

[161] Stefano Pirandola, Riccardo Laurenza, Carlo Ottaviani, and Leonardo Banchi. Fundamental limits of repeaterless quantum communications. *Nature Communications*, 8:15043, February 2017. arXiv:1510.08863v5.

[162] Mark M. Wilde, Marco Tomamichel, and Mario Berta. Converse bounds for private communication over quantum channels. *IEEE Transactions on Information Theory*, 63(3):1792–1817, March 2017. arXiv:1602.08898.

[163] Mathematica files are available in the source files of arXiv:1708.07257.

[164] Mathematica files are available in the source files of arXiv:1810.12335.

[165] Mathematica files are available in the source files of arXiv:2012.02754.

[166] Paulina Marian and Tudor A. Marian. Uhlmann fidelity between two-mode Gaussian states. *Physical Review A*, 86(2):022340, August 2012. arXiv:1111.7067.

[167] Jens Eisert and Michael M. Wolf. *Quantum Information with Continuous Variables of Atoms and Light*, chapter Gaussian Quantum Channels, pages 23–42. World Scientific, February 2007. arXiv:quant-ph/0505151.

[168] Masahiro Takeoka and Mark M. Wilde. Optimal estimation and discrimination of excess noise in thermal and amplifier channels. November 2016. arXiv:1611.09165.

[169] Felix Leditzky, Debbie Leung, and Graeme Smith. Quantum and private capacities of low-noise channels. *Physical Review Letters*, 120:160503, April 2018. arXiv:1705.04335.

[170] Renato Renner, Nicolas Gisin, and Barbara Kraus. Information-theoretic security proof for quantum-key-distribution protocols. *Physical Review A*, 72(1):012332, July 2005. arXiv:quant-ph/0502064.

[171] Filippo Caruso and Vittorio Giovannetti. Degradability of bosonic Gaussian channels. *Physical Review A*, 74(6):062307, December 2006. arXiv:quant-ph/0603257.

[172] Vittorio Giovannetti, Saikat Guha, Seth Lloyd, Lorenzo Maccone, and Jeffrey H. Shapiro. Minimum output entropy of bosonic channels: A conjecture. *Physical Review A*, 70(3):032315, September 2004. arXiv:quant-ph/0404005.

[173] Maksim E. Shirokov. Uniform finite-dimensional approximation of basic capacities of energy-constrained channels. *Quantum Information Processing*, 17:322, October 2018. arXiv:1707.05641.

[174] Naresh Sharma and Naqueeb Ahmad Warsi. Fundamental bound on the reliability of quantum information transmission. *Physical Review Letters*, 110(8):080501, February 2013. arXiv:1205.1712.

[175] Mark M. Wilde, Andreas Winter, and Dong Yang. Strong converse for the classical capacity of entanglement-breaking and Hadamard channels via a sandwiched Rényi relative entropy. *Communications in Mathematical Physics*, 331(2):593–622, October 2014. arXiv:1306.1586.

[176] Tom Cooney, Milan Mosonyi, and Mark M. Wilde. Strong converse exponents for a quantum channel discrimination problem and quantum-feedback-assisted communication. *Communications in Mathematical Physics*, 344(3):797–829, June 2016. arXiv:1408.3373.

[177] Alexander S. Holevo. Remarks on the classical capacity of quantum channel. December 2002. quant-ph/0212025.

[178] Siddhartha Das and Mark M. Wilde. Quantum reading capacity: General definition and bounds. *IEEE Transactions on Information Theory*, 65(11):7566–7583, March 2017. arXiv:1703.03706v2.

[179] Marco Tomamichel, Mark M. Wilde, and Andreas Winter. Strong converse rates for quantum communication. *IEEE Transactions on Information Theory*, 63(1):715–727, January 2017. arXiv:1406.2946.

[180] Ranjith Nair. Discriminating quantum-optical beam-splitter channels with number-diagonal signal states: Applications to quantum reading and target detection. *Physical Review A*, 84(3):032312, September 2011. arXiv:1105.4063.

[181] Alexey E. Rastegin. A lower bound on the relative error of mixed-state cloning and related operations. *Journal of Optics B: Quantum and Semiclassical Optics*, 5(6):S647, December 2003. arXiv:quant-ph/0208159.

[182] Gh.-S. Paraoanu and Horia Scutaru. Fidelity for multimode thermal squeezed states. *Physical Review A*, 61(2):022306, January 2000. arXiv:quant-ph/9907068.

[183] Kaushik P. Seshadreesan, Ludovico Lami, and Mark M. Wilde. Rényi relative entropies of quantum Gaussian states. *Rényi relative entropies of quantum Gaussian states*, 59:072204, July 2018. arXiv:1706.09885.

[184] Xiao-yu Chen. Gaussian relative entropy of entanglement. *Physical Review A*, 71(6):062320, June 2005. arXiv:quant-ph/0402109.

[185] Ole Krueger. *Quantum Information Theory with Gaussian Systems*. PhD thesis, Technische Universität Braunschweig, April 2006. Available at `https://publikationsserver.tu-braunschweig.de/receive/dbbs_mods_00020741`.

[186] Ranjith Nair. Quantum-limited loss sensing: Multiparameter estimation and Bures distance between loss channels. *Physical Review Letters*, 121(23):230801, December 2018. arXiv:1804.02211.

[187] John Watrous. Semidefinite programs for completely bounded norms. *Theory of Computing*, 5(11):217–238, November 2009. arXiv:0901.4709.

[188] John Watrous. Simpler semidefinite programs for completely bounded norms. *Chicago Journal of Theoretical Computer Science*, 2013(08):1–19, July 2013. arXiv:1207.5726.

[189] Giacomo Mauro D'Ariano and Massimiliano Federico Sacchi. Two-mode heterodyne phase detection. *Physical Review A*, 52(6):R4309(R), December 1995. arXiv:quant-ph/0109145.

[190] Ranjith Nair. Quantum-limited loss sensing: Multiparameter estimation and Bures distance between loss channels. *Physical Review Letters*, 121(23):230801, December 2018. arXiv:1804.02211.

[191] Nathan Killoran and Norbert Lütkenhaus. Strong quantitative benchmarking of quantum optical devices. *Physical Review A*, 83(5):052320, May 2011. arXiv:1102.3233.

[192] Andreas Winter. Coding theorem and strong converse for quantum channels. *IEEE Transactions on Information Theory*, 45(7):2481–2485, November 1999. arXiv:1409.2536.

[193] Tomohiro Ogawa and Hiroshi Nagaoka. Making good codes for classical-quantum channel coding via quantum hypothesis testing. *IEEE Transactions on Information Theory*, 53(6):2261–2266, June 2007.

[194] Simon Becker and Nilanjana Datta. Convergence rates for quantum evolution and entropic continuity bounds in infinite dimensions. *Communications in Mathematical Physics*, 374(2):823–871 October 2020. arXiv:1810.00863.

[195] Alexander S. Holevo. One-mode quantum Gaussian channels: structure and quantum capacity. *Problems of Information Transmission*, 43(1):1–11, March 2007. arXiv:quant-ph/0607051.

[196] Horia Scutaru. Fidelity for displaced squeezed thermal states and the oscillator semigroup. *Journal of Physics A: Mathematical and General*, 31(15):3659–3663, 1998. arXiv:quant-ph/9708013.

[197] Gh.-S. Paraoanu and Horia Scutaru. Bures distance between two displaced thermal states. *Physical Review A*, 58(2):869, August 1998. arXiv:quant-ph/9703051.

[198] Henning Vahlbruch, Moritz Mehmet, Karsten Danzmann, and Roman Schnabel. Detection of 15 db squeezed states of light and their application for the absolute calibration of photoelectric quantum efficiency. *Physical Review Letters*, 117(11):110801, September 2016.

[199] Wolfgang P. Schleich. *Quantum optics in phase space*. Wiley-VCH Verlag, Berlin, 2001.

[200] Panos M. Pardalos and Mauricio G. C. Resende. Interior point methods for global optimization. In *Interior Point Methods of Mathematical Programming*, pages 467–500. Springer, 1996.

[201] Jorge Nocedal and Stephen Wright. *Numerical optimization*. Springer Science & Business Media, 2006.

[202] J. Solomon Ivan, Krishna Kumar Sabapathy, and Rajiah Simon. Operator-sum representation for bosonic Gaussian channels. *Physical Review A*, 84(4):042311, October 2011. arXiv:1012.4266.

[203] Ludovico Lami, December 2020. Email correspondence.

[204] Rodney Loudon. *The Quantum Theory of Light*. Oxford Science Publications. Oxford University Press, 3rd edition, September 2000.

[205] Luis Ortiz-Gutiérrez, Bruna Gabrielly, Luis F Muñoz, Kainã T Pereira, Jefferson G Filgueiras, and Alessandro S Villar. Continuous variables quantum computation over the vibrational modes of a single trapped ion. *Optics Communications*, 397:166–174, August 2017. arXiv:1603.00065.

[206] Timo Hillmann, Fernando Quijandría, Göran Johansson, Alessandro Ferraro, Simone Gasparinetti, and Giulia Ferrini. Universal gate set for continuous-variable quantum computation with microwave circuits. *Physical Review Letters*, 125(16):160501, October 2020. arXiv:2002.01402.

VITA

Kunal Sharma was born in the year 1993. After attending schools in Jaipur, Rajasthan, in 2011, he joined the Indian Institute of Science Education and Research Bhopal to pursue a BS-MS Dual Degree Programme in Physics. He received his BS-MS degree on May 30, 2016. Subsequently, he joined Louisiana State University to pursue his doctoral studies at the Quantum Science and Technology group with Dr. Mark M. Wilde as his advisor. During his Ph.D., he also worked at the Los Alamos National Laboratory as a graduate research assistant from June-August 2019 and January-August 2020. He plans to graduate in May 2021. He has been awarded the QuICS Hartree Fellowship and will join the University of Maryland as a postdoctoral fellow in Fall 2021.